CARDIFF UNIVERSITY

PRIFYSGOL CAERDYDD

Investigation of high temperature enhanced hydrogen formation in mineral amended sediment slurries, as a potential novel deep biosphere energy source

Cathal David Linnane

Submitted in partial fulfilment of the requirements for the degree of Doctor of Philosophy (PhD)

UMI Number: U585199

UMI

Dissertation Publishing

ProQuest

Acknowledgements

Abstract

The deep biosphere has been estimated to be the largest prokaryotic habitat on Earth. However, what energy sources sustain these prokaryotes at depth and over geological timescales, remote from photosynthetic energy supply, is unclear. Hydrogen generation from basalt weathering has been controversially suggested as a potential deep terrestrial energy source, although other minerals were thought to be unimportant, as they did not generate H_2 under abiotic conditions.

In this study these experiments were repeated but in the presence of sedimentary prokaryotes using a range of minerals, with differing iron concentrations at a range of temperatures (4-105°C) and under anoxic conditions. Results showed that at certain temperatures high levels of H_2 were produced from several minerals (600-1650 μmol l^{-1}). This was associated with high levels of acetate formation (~5000-1000 μmol l^{-1}). Substantial CH_4 (100-600 μmol l^{-1}) was also produced. Sulphate reduction proceeded between ~ 50-85°C, which no removal at higher temperatures, similar to hot oil reservoirs. The amounts of these compounds produced varied depending on mineral composition. The presence of iron in minerals was found not to be necessary to facilitate the production of H_2 as previously thought. Under sterile conditions little H_2 or other products were formed. This shows that H_2 generation from minerals was a microbially mediated process and was consistent with the presence of considerable prokaryotic cell numbers (range 4.3 x 10^7 to 5.1 x 10^8 cells ml^{-1}) in these experiments. Prokaryotic cell numbers decrease with increases in temperature, similar to the predicted decrease in numbers with depth in the sub seafloor biosphere (e.g. 99°C 6.67 x 10^5 cells ml^{-1}). Sequential ramping experiments to 155°C, demonstrated that prokaryotic activity in the biotic zone <120°C, increased the formation of products such as H_2 (x34) and low weight molecular acids (acetate x2.3) in the abiotic zone >120°C. This has implications for hydrous pyrolysis experiments, which are used to simulate high temperature diagenesis. This increases the sources of potential energy, which may migrate upward to feed the base of the deep biosphere. The prokaryotic community present was assessed using 16S rRNA gene analysis (PCR-DGGE). Communities varied with mineral type and included thermophilic methanogens and acetate oxidisers, iron-reducers and *Deltaproteobacteria*, *Thermoplasmatales,* as well as uncultured bacterial and archaeal sequences. Clone libraries indicate that the archaeal community is similar to proposed HyperSliMe communities, dominated by *Thermococcales* related species at high temperature ~80-95°C. Fresh grinding of minerals enhanced activity, which has implications for the rate of energy supply in the subsurface. A mechanochemical process based on the interaction of Si radicals, which is enhanced by the presence of prokaryotes, perhaps through microbial weathering, is hypothesised to be involved in H_2 generation. But the interaction of other mineral constituents such as Fe, Al and Ti may also play a role.

We found minerals stimulated prokaryotic activity up to at least 100 days. Interestingly, the carbon isotope values for the CH_4 produced covered a wide range of values (-42 to -78‰), including depleted values that could be misinterpreted as being indicative of an abiotic origin. These results extend the range of minerals that could be potential "dark energy" sources in the subsurface and provide details of the prokaryotes and processes that such energy sources could stimulate.

Table of contents

Table of contents

Table of contents

Chapter 6

Chapter 7

Table of Figures

Chapter 4

Chapter 7

Table of tables

Table of tables

Chapter 1

Introduction

1.1 Introduction

This chapter provides a review of the deep subsurface biosphere, major metabolic processes, an overall view of hydrogen generation in the subsurface with an introduction to subsurface lithoautotrophic microbial ecosystems (SLiMES).

1.2 The subsurface biosphere

Prokaryotes in sub-seafloor sediments are thought to make up about 70% of the global prokaryotic biomass (Whitman et al., 1998). This is not surprising, when one considers that oceans cover ~70% of the earth's surface and the high amounts of particulate organic matter in the sub-seafloor. It is estimated that between 5 and 10 billion tons of particulate organic matter is constantly sinking in the world's ocean which accumulates as sediment (Jorgensen, 1983). The vast amount of this organic matter is degraded by near surface microbial activity. However, over geological time the accumulation of the remainder results in the largest global reservoir of organic carbon; 15000×10^8g C (Hedges and Keil, 1995). Despite these considerations it is only relatively recently that the existence of a deep biosphere in the marine subsurface has comprehensively been proven (Parkes et al., 1994; Wellsbury et al., 2002). The deep sub sea floor biosphere extends to at least 1626 mbsf, into sediments that are 111 My old with a temperature range of 60-100°C (Roussel et al., 2008). Prokaryotic cell numbers decrease with depth from concentrations of ~ 10^9 cm^{-3}, in near surface sediments, to ~3 x10^6 cm^{-3} at 500 mbsf (Fig 1.1).

Prokaryotic cell distributions in deep sediments from 17 ODP/IODP Legs worldwide.

- Deep bacteria ubiquitous.

- Water depth to 5867 m.

- Sediment depth 1626 mbsf.

- Low to high OM (~0.4 -6.8%).

- Low to high Temperature (2- ~150°C-hydrothermal).

- Ancient deposits (~111 mya)

- Many environments bacteria continuously decrease with depth.

- Biomass to 500m, globally equals ~10% of surface biosphere carbon, with both higher (~30%) and lower estimates (minimum based on detectable living cells.

Fig 1.1 Distribution of prokaryotic cells in sub-seafloor sediments located worldwide. The solid line is the regression line and the dotted lines either side are the 95% prediction limits. ODP Ocean Drilling Program, OM organic matter (After Parkes *et al.*, 1994)

Organic matter becomes increasingly recalcitrant during burial making it increasingly difficult to utilise as a substrate for microorganisms. Hence metabolic activity decreases with depth and metabolic rates can be 10^3-10^5 times lower in the subsurface than in the organic rich near surface sediment (Lovley and Chapelle, 1995). Energy supply is a problem for microbes at depth, as the most favourable electron acceptors are used sequentially in a predictable cascade, confining less energy generating reactions to the subsurface , such as those based on CO_2. In broad terms, the progression of terminal electron acceptors begins with O_2 near the surface, followed with increasing depth by NO_3^-, NO_2^-, Mn (IV), Fe (III), SO_4^{2-} and finally CO_2. This thermodynamically predicted progression, is determined from values of the standard Gibbs free energies of reaction (ΔG_r°), and is typically paralleled by a microbial metabolic succession (Stumm and

Morgan, 1996). This redox couple cascade is shown diagrammatically in Fig 1.2 (Telling et al., 2004)

Electron donors
E(V)

Electron acceptors
E(V)

- 0.4 H_2
        Acetate
- 0.2 CH_4
        H_2S
0.0 Fe^{2+}
+ 0.2
+ 0.4 NH_4^+
        NO_2^-
        Mn^{2+}
+ 0.6
+ 0.8

- 0.4
CO_2
SO_4^{2-} - 0.2
FeOOH   0.0
              + 0.2
NO_3^- + 0.4
MnO_2
              + 0.6
$2NO_3^-$
O_2 + 0.8
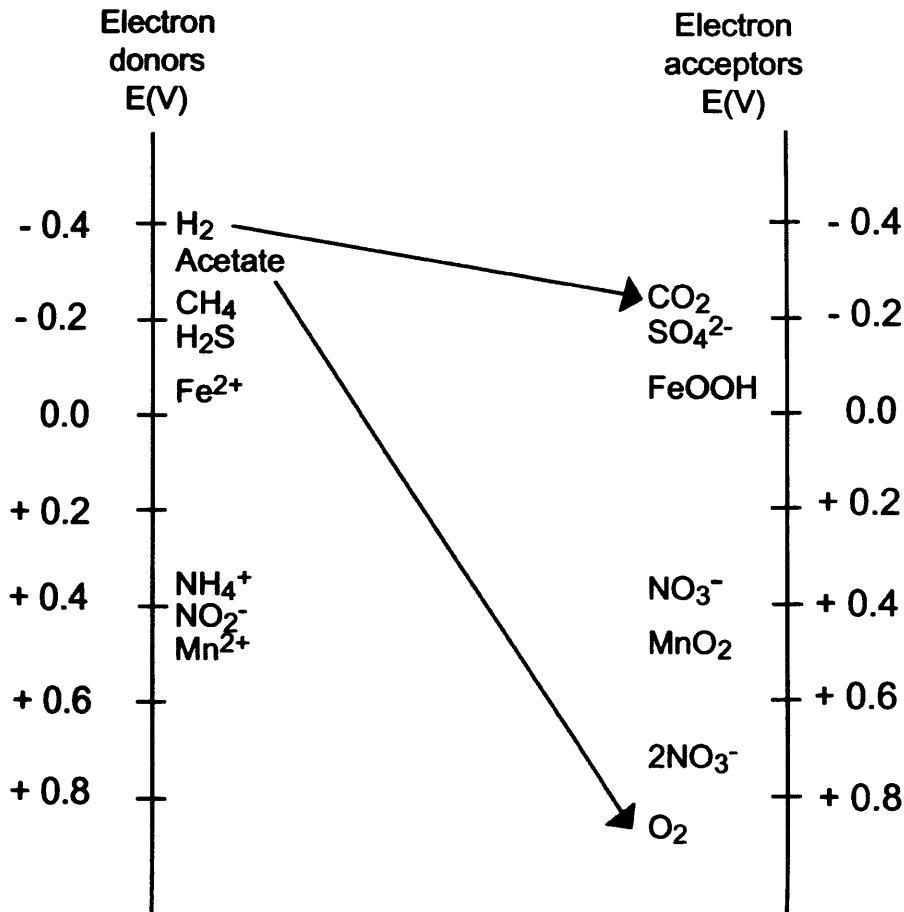
Fig 1.2. The electron tower. The strongest reductants are at the top, and strongest oxidants at the bottom of the diagram. Coupled reactions between electron donors having more negative Eo' with electron acceptors possessing more positive Eo' are exergonic and may provide sufficient energy to support bacterial metabolism. In the example cited in the text, oxidation of acetate with oxygen has a steep negative gradient, and hence a high free-energy yield. The oxidation of hydrogen with carbon dioxide (methanogenesis or acetogenesis) has a shallower gradient and consequently, a lower free-energy yield.

The Gibbs free energy (ΔG^O) is the amount of energy obtained from a given metabolic reaction. It is worth noting that the predicted succession of reactions is based on the thermodynamic properties under standard state and not conditions that exist in the

natural environment (25°C and 1 bar). The energy yield from a reaction depend on temperature, pressure and chemical concentrations & composition, and are therefore sample and site specific, and may deviate from the proposed succession. However, an idealised pore water profile is shown in Fig 1.3, which serves as a general model for metabolic activity in subsurface sediments.
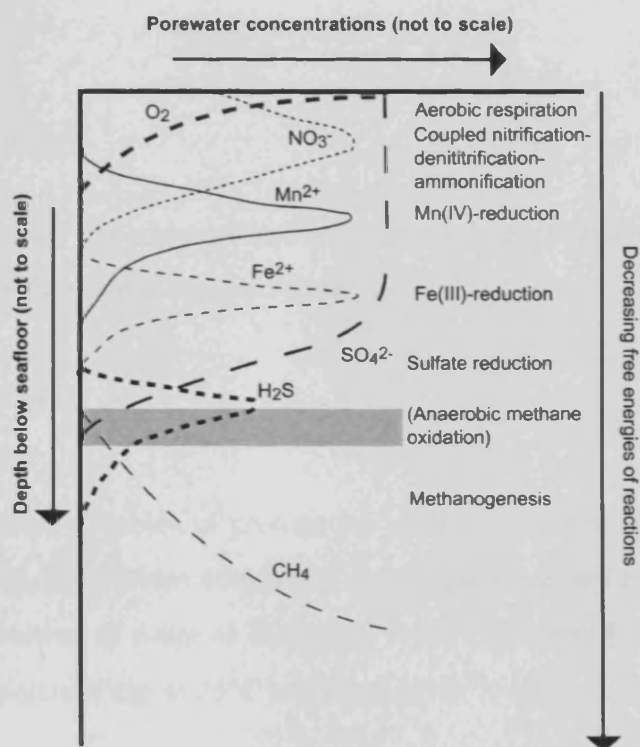
Fig 1.3 Porewater profiles in an idealised marine sediment. In the sequence, oxygen is consumed first, followed by nitrate, Mn(IV)-oxides, Fe(III)-oxides, sulfate and finally CO_2, creating a zonation of reactants and products. The sequence is determined by the free energy yield of the various redox reactions. Aerobic ammonia oxidation (nitrification) and anaerobic methane oxidation (shaded zone) are also shown. Depth is not to scale from (Telling et al., 2004).

In order to show the changes that can occur theoretically with temperature using standard half reactions (Amend and Teske, 2005) provide theoretical values for microbial metabolisms at various temperatures by, using $p\varepsilon^{o'}$ which donates $p\varepsilon^{o}$ at neutral pH. Values for this table were computed from the standard redox potentials (E_h^{o}) first by using (ΔG^{o}_r) which is the free energy change of the reaction under standard conditions.

$$E_h^o = \frac{-\Delta G_r^o}{nF}$$

n represents the number of moles of electrons in reaction r and F denotes the Faraday constant (96,485 coulomb mol 1^{-1}). E_h^o was then converted to the negative logarithm of electron activity ($p\varepsilon^o$)

$$p\varepsilon^o = \frac{FE_h^o}{2.303RT}$$

where R and T denote the gas constant and temperature in K. Furthermore valves were modified to neutral pH (biological standard state) by

$$p\varepsilon^{o'} = p\varepsilon^o + \frac{nh}{2} \log Kw$$

nH stands for the number of moles of protons per mole of electrons in the half reaction and Kw represents the equilibrium constant at the temperature and pressure of interest for the dissociation reaction of water as $H_2O \rightarrow H^+ + OH^-$. It should be noted that neutral pH changes with temperature e.g. at 25°C and 1 bar pH is 7, while at 100°C neutral pH is 6.13.

Table 1.1 $p\varepsilon^{o'}$ as a function for selected half reactions in microbial metabolisms

Reaction		25°C	50°C	100°C	150°C
I	$O_2(aq)+4H^++4e^-\rightarrow 2H_2O$	14.50	13.23	11.12	9.42
II	$NO_3^- +6H^++5e^-\rightarrow 1/2N_2(aq)+3H_2O$	12.32	11.26	9.53	8.18
III	$NO_2^- +8H^++6e^-\rightarrow NH_4^++2H_2O$	5.90	5.29	4.28	3.45
IV	$NO_3^- +2H^++2e^-\rightarrow NO_2^- +H_2O$	6.88	6.27	5.24	4.39
V	$Fe_2O_3(s)+6H^++2e^-\rightarrow 2Fe^{2+}+3H_2O$	-7.94	-8.03	-8.37	-8.85
VI	$SO_4^{2-}+10H^++8e^-\rightarrow H_2S(aq)+4H_2O$	-3.67	-3.39	-2.99	-2.70
VII	$CO_2(aq)+8H^++8e^-\rightarrow CH_4(aq)+2H_2O$ -	-4.31	-4.09	-3.81	-3.65
VIII	$S^0(s)+2H^++2e^-\rightarrow H_2S(aq)$	-4.55	-4.17	-3.60	-3.19
IX	$2CO_2(aq)+8H^++8e^-\rightarrow CH_3COOH(aq)+2H_2O$	-4.83	-4.58	-4.31	-4.16
X	$6CO_2(aq)+24H^++24e^-\rightarrow C_6H_{12}O_6(aq)+6H_2O$	-6.83	-6.46	-6.02	-5.75
XI	$H^++e^-\rightarrow 1/2H_2(aq)$	-8.55	-7.94	-6.98	-6.26

It can be seen from Table 1.1 that several of the reactions are sensitive to temperature. Several reactions including sulphate reduction, autotrophic methanogenesis and homoacetogenesis decrease only slightly with temperature. Although the general redox couples remain the same several couples can change in order with temperature. For example the CO_2/CH_4 couple drops below that of the S^o/H_2S couple between 50 and 100°C. Theoretical considerations like these should be kept in mind when dealing with subsurface reactions that involve increases in temperature with depth. However, they are just that, theoretical and may not always apply, due to different conditions *in situ* e.g. reactant concentrations, chemical / mineralogical composition.

Anaerobic metabolisms often proceed in syntrophic association where the degradation of a substrate by one species is made thermodynamically possible through the removal of end products by another species (Schink, 1997). It has previously been belived that that biological systems conserve energy in discrete amounts with a minimum biochemically convertible energy of -20 kj mol^{-1} (Schink, 1997). Meaning that decay of matter in the subsurface would stop before this minimum free energy is reached. However this seems not to be the case in syntrophic association involving the degradation of substrate by one species and removal by another it was found through experimentation with co-culture that syntrophic relationships can metabolise near thermodynamic equilibrium ($\Delta G^` \approx 0$ kj mol^{-1}) (Jackson and McInerney, 2002). Previous studies have reached the conclusion that most subsurface cells must be adapted to extremely low energy or are dead or dormant (D'Hondt et al., 2002a), this however only was considered in the presence of sulphate reducers and methanogens.

1.3 Major subsurface metabolisms

The following sections introduce the major subsurface metabolisms in order of idealised occurrence in the subsurface.

1.3.1 Denitrification and ammonification (Fig 1.4)

Denitrification, is a dissimilatory process in which nitrate rather than oxygen is used as electron acceptor by microorganisms. Respiratory reduction of nitrate (denitrification) is recognized as the most important process converting biologically available (fixed) nitrogen to N_2 (also anammox section 1.3.2). In current N cycle models, a major proportion of global marine denitrification (50–70%) (Gruber and Sarmiento, 1997; Codispoti et al., 2001) is assumed to take place on the sea floor, particularly in organic rich continental margin sediments. During denitrification, dissolved NO_3- is reduced to N_2 gas through a series of intermediates (NO_2-, NO, and N_2O) which can be catalysed by various genera of bacteria e.g. *Pseudomonas* spp, the following reactions outline the process (Knowles, 1982)

$$NO_3^- + 2H^+ + 2e^- \rightarrow NO_2^- + H_2O \qquad \textbf{Eq 1.1}$$

$$NO_2^- + 2H^+ + e^- \rightarrow NO + H_2O \qquad \textbf{Eq 1.2}$$

$$2NO + 2H^+ + 2e^- \rightarrow N_2O + H_2O \qquad \textbf{Eq 1.3}$$

$$N_2O + 2H^+ + 2e^- \rightarrow N_2 + H_2O \qquad \textbf{Eq 1.4}$$
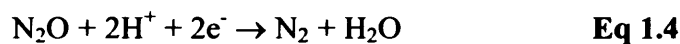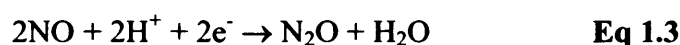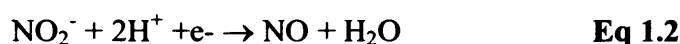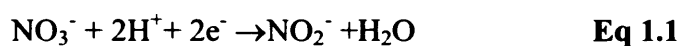
Each step in the above reaction is catalysed, by a specific enzyme. If the succession of reactions stops at any step, this liberates the product of that reaction into the environment. These reactions are carried out by a diverse range of facultatively anaerobic bacteria under anaerobic or low O_2 conditions (Jeter and Ingraham, 1996). Nitrate ammonification and denitrification share the same initial step Eq 1.1, which uses the iron-molybdenum containing nitrate reductase enzyme, whose synthesis is suppressed by O_2. Species such

as *Escherichia coli* or *Staphylococcus carnosus* at this stage either excrete the NO_2^- or reduce it further to NH_4^- (Neubauer and Gotz, 1996)
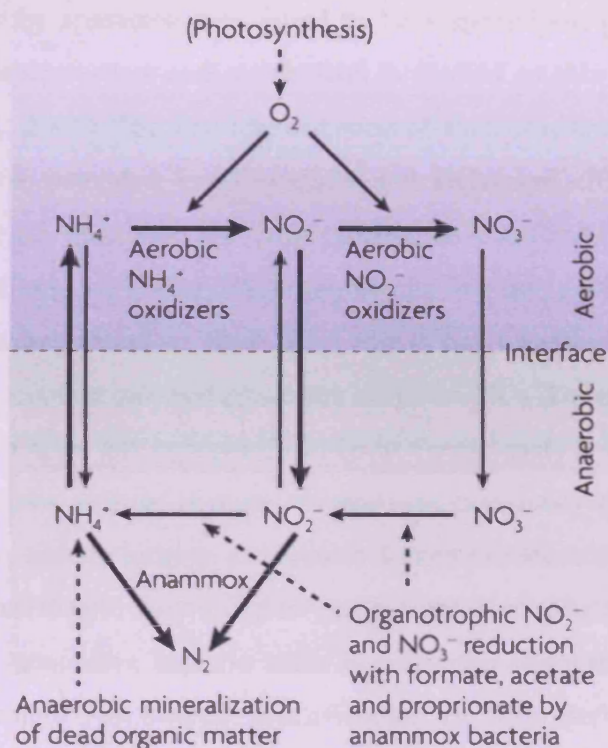
Fig 1.4 Interaction competition among aerobic and anaerobic nitrifers and Denitrifiers from (Kuenen, 2008)

1.3.2 Anaerobic ammonium oxidation (anammox)

Co-occurring with denitrifraction anaerobic ammonium oxidation (anammox) is now also considered a key part in the marine nitrogen cycle. Anammox can be coupled to NO_2^- reduction to produce N_2, Eq 1.5. Anammox involves hydrazine as an intermediate and forms N_2 by a one to one combination of nitrogen from two sources (Strous et al., 1999a; Jetten et al., 2005).

$$NO_2^- + NH_4^+ \rightarrow N_2 + 2H_2O \quad \textbf{Eq 1.5}$$
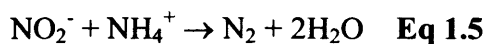
The discovery of anammox and its linkage to nitrate is relatively recent (Mulder et al., 1995) although the occurrence of this processes in nature has been hypothesised for quite some time (Broda, 1977) it was deemed one of the "missing" reactions. The organism directly responsible for anammox was found to be a specialised group of prokaryotes belonging to the *Plantomycetes* and metabolism is limited to this group (Strous et al., 1999b; Schmid et al., 2005). The first identification of anaerobic ammonium oxidation in marine sediments was provided by (Thamdrup and Dalsgaard, 2002; Kuypers et al., 2003). Anammox type reactions are now thought to contribute significantly to the production of N_2 along with denitrification in the marine environment. In marine sediments NO_3^- is more abundant than NO_2^- and it has previously been thought that anammox must rely on other external processes to reduce NO_3^- (Dalsgaard and Thamdrup, 2002). However, this does not necessarily have to be the case, it is now clear that the metabolism of anammox species is more diverse than previously thought, they can use organic acids such as acetate/formate as electron donors to reduce nitrate and nitrite thus allowing them to outcompete heterotrophic denitrifiers. The reduction of nitrate (NO_3^-) can be achieved by anammox bacteria such as *Kuenenia stuttgartiensis*, however this does not proceed through conventional denitrification via N_2O. Rather reduction of NO_3^- to NH_4^- occurs via dissimilatory nitrate and nitrite reduction which can subsequently convert nitrite and NH_4^- to N_2 by the standard anammox reaction Eq 1.5 (Kartal et al., 2007). This allows anammox bacteria to join in the competition for nitrate in marine sediments, where NO_3^- is substantially higher than NO_2^- (Jaffe, 2000).

1.3.3 Dissimilatory metal reduction

Metals have long been known as key components in proteins used for transferring electrons to key acceptors in microbial metabolisms e.g. O_2 and SO_4^{2-}. It is only relatively recently that metals have been proven to be used as external terminal electron acceptors themselves, capable of supporting microbial metabolisms this is called dissimilatory metal reduction. Here we concentrate on the use of iron (Fe^{3+}) as it is the most studied in

the natural environment, iron is also the 4th most abundant element in the earths crust and is therefore readily available for microbial interaction. Mn(IV) reduction will also be mentioned. It is also worth mentioning that other metals such as U, Se, Cr have also been studied in relation to microbial activity. (See (Lovley, 1993) for a review).

Iron is often the most abundant electron acceptor in many sedimentary environments and microbial reactions involving the reduction of Fe(III) minerals have been shown to be the primary reductive process in non-sulphidogenic sediments (Lovley, 2000). Microbial activity of this kind involving both Fe(III) and Mn(IV) may account for the majority of the oxidation of organic matter in sediments, and has previously been shown to be responsible for 50-80% of oxidation in near coastal sediments in Denmark and Norway (Canfield et al., 1993a; Canfield et al., 1993b) and close to 80% in Atlantic coastal sediments (Aller, 1990). Microbes from both the *Archaea* and *Bacteria* can exploit this energetically favourable redox potential. One of the first bacteria studied in pure culture involved in Fe(III) reduction was *Geobacter metallireducens* which can gain energy from the coupling of Fe(III) reduction to the oxidation of H_2 (Lovley et al., 1993b). Since then several hyperthermophilic *Archaea,* and sulphate reducers have all shown the ability to reduce Fe(III) (Lovley, 2004).

Dissimilatory Fe(III) reduction is more energetically favourable with the use of poorly crystalline Fe(III) oxide minerals such as ferric hydroxide e.g. goethite (FeOOH) functioning as electron acceptors and these are the preferred solid phase ferric iron for Fe reducing prokaryotes (Lovley and Philips, 1987). However, iron oxides in marine sediments predominately exist as the harder less thermodynamically favourable crystalline oxides such as hematite (Fe_2O_3) and magnetite (Fe_3O_4). Some studies using laboratory experiment have shown that some Fe reducing microbes e.g. *Shewanella putrefaciens,* strain CN32 are capable of obtaining the same energy yield from the crystalline and the poorly crystalline minerals, resulting in the formation of biogenic Fe(II) minerals such as siderite/vivanite (Kostka et al., 1996; Roden and Zachara, 1996; Fredrickson et al., 1998). These studies environmental relevance have been criticised, due to being conducted under too high nutrient concentrations which bear little resemblance to actual environmental conditions *in situ* (Glasauer et al., 2003; Lovley, 2004). Other

studies have shown that microbes can generate enough energy for survival by reducing the Fe(III) component in smectite clays (Kostka et al., 2002). *G. metallireducans* was also found to reduce goethite beyond the amorphous Fe(III) oxide content, which is an indication of microbial reduction of crystalline Fe(III) oxide in the environment (Weber et al., 2006b). Iron (III) minerals are insoluble at pH values greater than 4. Therefore it has been proposed that direct contact between the bacteria and the iron oxide is necessary for the use of that mineral as the terminal electron acceptor. Some theories have been put forward as mechanisms of how this can be achieved. Most of this work has been done using either *Geobacter* spp. or *Shewanella* spp. *Geobacter* spp were found to form flagella or pili thus being able to attach directly to the oxide (Childers et al., 2002). These pili function as conducts transferring electrons to insoluble Fe(III) oxides and maybe other terminal electron acceptors (Reguera et al., 2005). These nanowires are not exclusive to *Geobacter* species and certain species of *Shewanella* may also produce them under harsh electron limited conditions (Gorby et al., 2006).

Extracellular electron shuttles such as humic acids and certain antibiotics, have also been proposed as a means of solving the problem of direct attachment, these shuttles can be exploited as mediators to complete the transfer of electrons to the solid oxide (Lovley et al., 1996; Newman and Kolter, 2000; Turick et al., 2002). Using a combination of abiotic and biotic processes, the bacteria oxidize an electron donor coupled to the reduction of the soluble electron shuttle. The shuttle donates electrons abiotically to the oxide (Turick et al., 2002). Fig 1.5 shows a diagram of use of electron transfer by microbes using both shuttles and nanowires, taken from (Weber et al., 2006a)
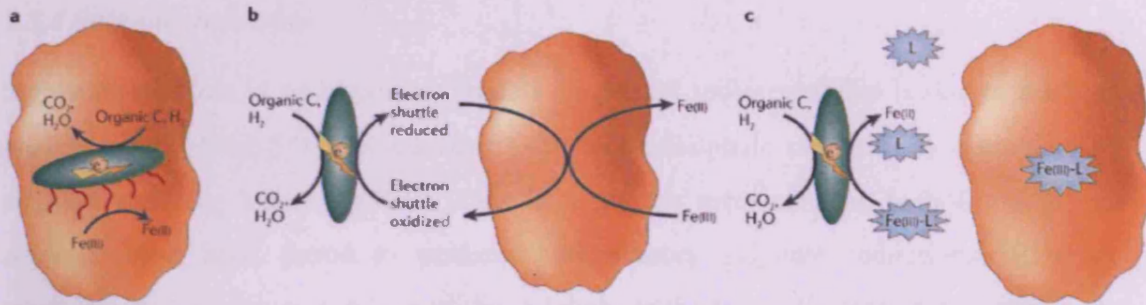
Fig 1.5 Three primary strategies have been proposed to facilitate the electron transfer between microorganisms and solid Fe(III) oxide surfaces. a | In *Geobacter* spp. direct contact with the oxide surface is required. The production of 'nanowires', conductive extracellular appendages, facilitates electron transfer by functioning as an electrical conduit to the Fe(III) oxide surface. b | An endogenously or exogenously produced electron shuttle mediates electron transfer to solid-phase Fe(III) oxides. c | The production of complexing ligands as in the case of *Geothrix* sp. aids in the dissolution of the solid-phase Fe(III) oxide providing a soluble Fe(III) form more readily available to the microorganism. Although these strategies have only been demonstrated for Fe(III)-reducing microorganisms, similar strategies might be used by Fe(II)-oxidizing microorganisms that are utilizing solid-phase Fe(II) electron donors. From (Weber et al., 2006a)

Oxidation of Fe(II) anaeorbically is less well studied, and has been coupled to nitrate reduction in marine sediments where it has been found to occur in certain hydrothermal systems and deep sea sediments (Straub et al., 1996; Edwards et al., 2003). In pure culture it has only been demonstrated in *Ferroglobus placidus* and a *Beta proteobacteria* (Hafenbradl et al., 1996; Weber et al., 2006c)

Although substantial amounts are known about the role of Fe reduction it is still only in it infancy. The physiology of Fe(III) reduction and Fe(II) oxidation is unknown a terminal Fe(III) reductase has yet to be identified, but it is clear that these type of reactions play a major role in biogeochemical cycles.

1.3.4 Sulphate reduction

Sulphate reduction is an important process in marine sediments; this is due to the high concentration of the SO_4^{2-} in seawater (~29 mM). Sulphate reduction is controlled by sulphate reducing bacteria (SRB). This is a generic term used as both *Bacteria* and *Archaea* have been found to perform dissimilatory sulphate reduction. SRBs are anaerobic microorganisms, which utilise sulphate as the terminal electron acceptor in the degradation of organic compounds, resulting in the production of sulphide. Rates of sulphate reduction can vary in marine sediments from picomole per cubic centimetres per day in deep sediments, to many thousand nanomoler per cubic centimetre per day in near surface sediments (Canfield and Teske, 1996). It has been estimated that sulphate reduction can account for more than 50% of the organic carbon mineralization in marine sediments (Jorgensen, 1982). Physiologically metabolisms employed by SRB are diverse a large diversity of sulphate reducers have been found.

Using molecular microbiological techniques sulphate reducers can be grouped into seven phylogenetic lineages which span both the *Bacteria* (5) and the *Archaea* (2). Archaeal sulphate reducers fall into the *Euryarchaeota* (*Archaeoglobus, e.g Archaeoglobus profundus* (Burggraf et al., 1990)) and the *Crenarchaeota* (*Thermocladium* (Itoh et al., 1998) and *Caldirvirga* (Itoh et al., 1999)). The majority of sulphate reducers fall within the bacteria with 23 genera within the *Delta proteobacteria* (e.g. *Desulfovibrio* spp and *Desulfobacteraceae*). The remaining groups are within the *Clostridia* (e.g. *Desulfosporosinus, Desulfotomaculum*) and 3 lineages which contain only thermophiles *Nitrospirae, Thermodesulfobiaceae*, and *Thermodesulfobacteria* . See Fig 1.6 for a phylogenetic tree for all described sulphate reducing species.

Two major metabolic groups have been identified in the sulphate reducers, which depends on their ability to oxidise acetate, group one incompletely oxidises compounds such as lactate, propionate and formate to acetate, while group two completely oxidises acetate all the way to CO_2 (Widdel, 1988). Many SRBs are also able to grow chemolithoautotrophically by using H_2 as an electron donor. Table 1.2 show common sulphate reducing reactions found in subsurface sediments.

12	Desulfobulbaceae
32	Desulfobacteraceae
	Desulfobacterium anilini (AJ237601)
	Desulfarculus baarsii (AF418174)
8	Syntrophobacteraceae
	Desulfomonile limimaris (AF282177)
	Desulfomonile tiedjei (AM086646)
47	*Desulfovibrio* spp.
	Desulfonatronum lacustre (AF418171)
	Desulfonatronum thiodismutans (AF373920)
	Desulfonatronum cooperativum (AY725424)
	Desulfonatronovibrio hydrogenovorans (X99234)
7	*Desulfomicrobium* spp.
	Desulfocaldus terraneus (AY464939)
6	*Desulfohalobium* spp.

Deltaproteobacteria

Bacteria

Thermodesulfovibrio islandicus (X96726)
Thermodesulfovibrio yellowstonii (AB231858) — Nitrospirae

Desulfosporomusa polytropa (AJ006605)
Desulfosporosinus orientis (AJ493052)
Desulfosporosinus youngii (DQ117470)
Desulfosporosinus meridiei (AF076247)

18 — *Desulfotomaculum* spp. — Clostridia

Thermodesulfobium narugense (AB077817) — Thermodesulfobiaceae

Thermodesulfobacterium hveragerdense (X96725)
Thermodesulfobacterium thermophilum (AF334601)
Thermodesulfobacterium commune (AF418169)
Thermodesulfobacterium hydrogeniphilum (AF332514)
Thermodesulfatator indicus (AF393376) — Thermodesulfobacteria

Archaeoglobus profundus (AF297529)
Archaeoglobus veneficus (AF418181)
Archaeoglobus lithotrophicus (AJ299218) — Euryarchaeota

Thermocladium modestius (AB005296)
Caldivirga maquilingensis (AB013926) — Crenarchaeota

Archaea

0.10

Fig 1.6 Phylogenetic tree based on nearly complete 16S ribosomal RNA gene sequence of described sulphate-reducing bacterial species (Muyzer and Stams, 2008)

14

Table 1.2 Sulphate reducing reactions. from (Muyzer and Stams, 2008)

Sulphate reducing reactions	$\Delta G^{\circ\prime}*$ (KJ/reaction)
$4H_2 + SO_4^{2-} + H^+ \rightarrow HS^- + 4H_2O$	-151.9
$Acetate^- + SO_4^{2-} \rightarrow 2HCO_3^- + HS^-$	-47.6
$Propionate^- + 0.75\ SO_4^{2-} \rightarrow Acetate^- + HCO_3^- + 0.75HS^- + 0.25H^+$	-37.7
$Butyrate^- + 0.5SO_4^{2-} \rightarrow 2Acetate^- + 0.5\ HS^- + 0.5H^+$	-27.8
$Lactate^- + 0.5SO_4^{2-} \rightarrow Acetate^- + HCO_3^- + 0.5HS^-$	-80.2

*Calculated from (Thauer et al., 1977)

As mentioned above a huge range of sulphate reducers have been described although acetate and hydrogen is the most common in the marine environment. The diversity of substrate utilisation is large, sulphate reducers have been found to use the following substrates, amino acids (Baena et al., 1998), methanol (Nanninga and Gottschal, 1987; Nazina et al., 1987), carbon monoxide (Henstra et al., 2007), methanethiol (Tanimoto and Bak, 1994), sugars (Sass et al., 2002), long chain alkanes (Aeckersberg et al., 1998) and alkenes (Grossi et al., 2007).

The energetics of sulphate reduction is as follows, the sulphate ion is very stable, therefore before reduction can take place, sulphate must be activated by the enzyme ATP-sulphurylase. This reaction involves the attachment of sulphate to a phosphate group of ATP (formation of adensine phosphosulfate APS). Pyrophosphate is also released as a result of this reaction and is hydrolysed by the enzyme pyrophosphatase to 2-phosphate. ATP is then reduced to sulphite by APS reductase, which releases adenosine monophosphate. Once sulphite is formed it is further reduced to H_2S by a series of intermediate reactions these intermediates, which may include thiosulphate and other sulphur compounds, can be excreted from the cell, into the surrounding environment becoming available for use by chemolithotrophs.

Some members of the sulphate reducing bacteria are able to gain energy through disproportionation reactions. This involves using sulphur compounds of intermediate oxidation state. Disproportiontion refers to the splitting of a compound in two, one which is more oxidised and one which is more reduced than the original compound. Substrates include, sulphite Eq 1.6, thiosulphate Eq.1.7 and sulphur Eq.1.8 being converted into

both sulphide and sulphate (Bak and Cypionka, 1987; Bak and Pfennig, 1987; Thamdrup et al., 1993; Lovley and Phillips, 1994; Bottcher et al., 2005).

$$4SO_3^{2-} + 2H^+ \rightarrow 3SO_4^{2-} + H_2S \qquad \textbf{Eq 1.6}$$

$$S_2O_3^{2-} + H_2O \rightarrow SO_4^{2-} + H_2S \qquad \textbf{Eq 1.7}$$

$$4S^0 + 4H_2O \rightarrow SO_4^{2-} + 3H_2S + 2H^+ \quad \textbf{Eq 1.8}$$
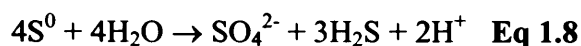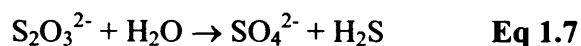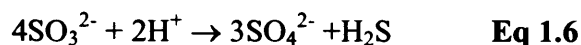
Disproportion of reaction 1.8 is often linked to formation of sulphide minerals, it is only when the H_2S is oxidised and incorporated into these minerals that the reaction becomes suitably energy yielding for microbial metabolism (Thamdrup et al., 1993).

Sulphate reducers do not necessarily have to use sulphate as a terminal electron acceptor, other compounds that can be used for growth include reduction of nitrate to nitrite and the use of inorganic compounds such as Fe(III), arsenate (As(VI) or chromate (Cr(VI) (Lovley et al., 1993a; Lovley and Philips, 1994; Macy et al., 2000). In the marine environment dimethlysulphoxide has been found to be used (Jonkers et al., 1996).

Sulphate reducers have been found in all marine environments including sediments (Parkes et al., 1993; Webster et al., 2006) and hydrothermal systems (Jorgensen et al., 1992; Teske et al., 2002). Sulphate reducers are also found in freshwater sediments (Sass et al., 1998), where sulphate concentrations are low and are thought to play a major role in fermentation. The gene *dsr*A/B is a genetic marker for sulphate reducers and specific primers targeting this can be used as a means of estimating the numbers of sulphate reducers in subsurface samples.

1.3.5 Methanogenesis

Methane production in marine sediments is very significant and is estimated at between 75-320 Tg year^{-1} (Valentine, 2002). Methane is an end product of the degradation of organic matter under anoxic conditions when inorganic oxidants such as nitrate, ferric iron or sulphate are depleted. Methanogens are a group of *Archaea* that derive energy from the production of methane. They are relatively physiologically diverse, and can be divided into 3 groups according to their substrate usage these are CO_2, acetate, and

methyl-group utilising (H_2, CO_2, acetate, formate, methanol, methylamines and CO) (Boone et al., 1993; Thauer, 1998; Thaur, 1998; Garcia et al., 2000; Ferry and Kastead, 2007).

Most methanogens are hydrogenotrophs and can reduce CO_2 to CH_4 by using H_2 as the primary electron donor. Many can also use formate similarly as an electron donor. Some species have also been found to utilise some secondary alcohols such as 2-propanol and 2-butanol (Widdel, 1986; Frimmer and Widdel, 1989).Only two genera can use acetate for methanogenesis those are *Methanosarcina* and *Methanosaeta*, and only one order so far has been found to utilise methyl group containing compounds and these are limited to the order *Methanosarcinales* with the exception of *Methanosphaera* which belongs to the order *Methanobacteriales*. Five orders of methanogens have been identified by molecular analysis these are *Methanobacteriales*, *Methanococcales*, *Methanomicrobiales*, *Methanosarcinales* and *Methaopyrales*. Table 1.3 contains a list of various microbial metabolisms (excluding CO metabolism which is mentioned in the next section).

Table 1.3.Reactions and standard changes[a] in free energies for methanogenesis

Reaction	$\Delta G^{o'}$ (KJ/mol CH_4)
4 H_2+CO_2→CH_4+$2H_2O$	-135.6
4 Formate→CH_4+$3CO_2$+$2H_2O$	-130.1
2 Ethanol+CO_2→CH_4+2 Acetate	-116.3
Methanol+H_2→CH_4+H_2O	-112.5
4 Methanol→$3CH_4$+CO_2+$2H_2O$	-104.9
4 Methylamine+$2H_2O$→$3CH_4$+CO_2+$4NH_4$	-75.0
4Trimethylamine+$6H_2O$→$9CH_4$+$3CO_2$+$4NH_4$	-74.3
2 Dimethylsulfide+$2H_2O$→$3CH_4$+CO_2+H_2S	-73.8
2 Dimethylamine+$2H_2O$→$3CH_4$+CO_2+$2NH_4$	-73.2
4 2-Propanol+CO_2→CH_4+4 Acetone+$2H_2O$	-36.5
Acetate→CH_4+CO_2	-31.0

[a]: calculated from the free energy of formation of the most abundant ionic species at neutral pH. Thus, CO_2 is HCO^- +H^+ and formate is $HCOO^-$+H^+. Taken from (Garcia et al., 2000)

Anaerobic growth of methanogens on carbon monoxide is rare and is therefore not included in Table 1.3. Certain methanogens e.g *Methanosarcina acetivorans* have the ability to utilise CO for energy production. Eq 1.9

$$4CO + 5H_2O \rightarrow CH_4 + 3HCO_3^- + 3H^+ \qquad \Delta G^{\circ\prime} = -195.6 \text{ kj/mol } CH_4 \quad \textbf{Eq 1.9}$$

Even more interesting is the fact that *M. acetivorans* is able to employ the acetyl-CoA pathway as an alternative to methanogenesis, producing acetate and formate, but not hydrogen when methanogenesis cannot proceed at its maximal rate (Rother and Metcalf, 2004). Methane production in the subsurface is limited in the presence of sulphate due to the competitive nature of the substrate. Sulphate reducers are able to utilise compounds like H_2 & acetate at lower concentrations than methanogens and thus out compete them in the presence of SO_4^{2-}(Kristjansson et al., 1982; Oremland and Polcin, 1982; Lovley and Goodwin, 1988).

Hence the majority of methane production in the subsurface occurs after sulphate and compounds such as ferric iron have been removed. This is generally but may not always be the case as several studies have shown methanogenesis occurring in zones of high sulphate concentrations (D'Hondt et al., 2002b; D'Hondt et al., 2004). This may be due to the fact that the sulphate reducers and methanogens are not competing for similar (i.e non competitive) limited substrates e.g. H_2 and methanol. Carbon isotope values of CH_4 indicate that the majority of methane from near surface sediments is as the result of H_2/CO_2 methanogenesis (Whiticar et al., 1986; Whiticar, 1999). However, the role of acetoclastic methanogenesis may be greater than previously appreciated at depth, recent studies have indicated that the amounts of acetate available in the subsurface may be greater than realised (Wellsbury et al., 1997; Parkes et al., 2007).

The majority of methane produced in marine sediments, does not reach the water colum. Methane migrates upwards and is removed when it reaches the sulphate zone, through the processes of anaerobic methane oxidation AOM. The amount of methane removed varies according to sample site from 80% (Orphan et al., 2001a) to 100% (Niewohner et al., 1998). This process is coupled to sulphate reduction and is discussed in the next section.

1.3.6 Anaerobic oxidation of methane (AOM)

It has been hypothesised for many years that methane oxidation in marine sediments has been the primary sink for methane in the sulphate reduction zone (Reeburgh, 1976, 1980). The exact metabolic process of AOM is unknown this is due to the fact that the micro organisms involved have yet to be isolated (Niewohner et al., 1998; Hinrichs and Boetius, 2002). The suggested model is the use of sulphate as the terminal electron acceptor in the process according to equation 1.10 (Barnes and Goldberg, 1976). This was due to the observation that AOM peaks co-occurred with increases in sulphate reduction rates.

$$CH_4 + SO_4^{2-} \rightarrow HCO_3^- + HS^- + H_2O \qquad \textbf{Eq 1.10}$$
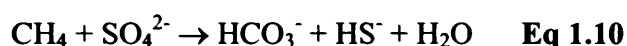
The thermodynamics of this reaction are unfavourable with only a low energy yield per reaction. It was therefore suggested that a consortium of microorganisms were involved in AOM. It was found by Hoehler et al., (1994) that AOM was possible as long as H_2 concentration is kept low they suggested that two syntrophic partners are involved, relying on interspecies hydrogen transfer, a methanogen mediating the oxidation of methane and a sulphate reducer scavenging the intermediate hydrogen.

$$CH_4 + 2H_2O \rightarrow CO_2 + 4H_2 \qquad \textbf{Eq.1.11}$$
$$SO_4^{2-} + 4H_4 + H^+ \rightarrow HS^- + 4H_2O \qquad \textbf{Eq 1.12}$$
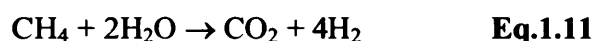
The question of whether AOM can support microbial growth has long been debated. This appears to have been answered when extremely high amounts of microbial biomass which contained aggregated methanogens through the presence of anaerobic methanotrophic archaea (ANME sequences) and sulphate reducing bacteria thought to be involved in AOM were found in sediments above marine gas hydrates (Boetius et al., 2000). The biomass of the AOM consortia was far higher than the surrounding sediment.

The use of acetate in AOM has also been hypothesised due to the 16S rRNA gene and biomass/lipids biomarker work, anaerobic methanotrophs are extremely $d^{13}C$-depleted demonstrating carbon from ^{13}C depleted CH_4, identifying species of sulphate

reducers closely related to known *Deltaproteobacteria* that oxidize acetate (Hinrichs et al., 1999; Boetius et al., 2000; Hinrichs et al., 2000; Pancost et al., 2000; Orphan et al., 2001b). Although thermodynamically the use of acetate is unattractive as concentrations would have to be lower than 2 nM (Boetius et al., 2000) and *in situ* concentrations are often in the low mM range. The use of formate is also thought possible (Sorensen et al., 2001) (use of acetate is as follows Eq 1.13 and Eq 1.14)

$$CH_4 + HCO_3^- \rightarrow CH_3COO^- + H_2O \qquad \textbf{Eq 1.13}$$

$$SO_4^{2-} + CH_3COO^- \rightarrow HS^- + 2HCO_3^- \qquad \textbf{Eq 1.14}$$
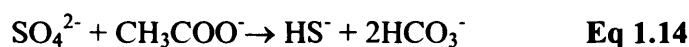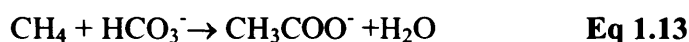
Anaerobic methane oxidation has also been coupled to denitrification (Raghoebarsing et al., 2006) in fresh water sediments. Eq 1.15 and 1.16 with a preference for nitrite over nitrate, this is thought to be a reflection of the $\Delta G^{\circ\prime}$ of each, nitrate -795 kJ mol^{-1} and nitrite -928 kJ mol^{-1} per mole of CH_4

$$5CH_4 + 8NO_3^- + 8H^+ \rightarrow 5CO_2 + 4N_2 + 14H_2O \qquad \textbf{Eq 1.15}$$

$$3CH_4 + 8NO_2^- + 8H^+ \rightarrow 3CO_2 + 4N_2 + 10H_2O \qquad \textbf{Eq 1.16}$$
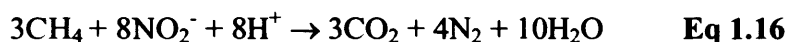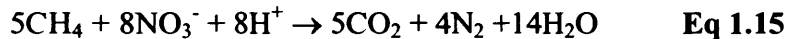
Through the use of biomarkers and 16S rRNA gene analysis, the dominating *Archaea* found in areas of active AOM in the marine environment have been closely related to the *Methanosarcinales* (ANME-2) and/or sequences that form a unique cluster (ANME-1). Although ANME-1 is distinct it is related to the *Methanomicrobiales* and *Methanosarcinales*. SRB species detected are closely related to the *Desulfosarcina / Desulfococcus* (Boetius et al., 2000; Hinrichs et al., 2000; Pancost et al., 2000; Orphan et al., 2001b) while those found in freshwater involved in denitrification bacterially are unique and distant from all other subdivisions, the *Archaea* were also quite unique, but were distantly related to ANME-2.

1.3.7 Isotope systematics of methane formation and oxidation

Through the use of ($^{13}C/^{12}C$) and (D/H $\equiv ^{2}H/^{1}H$) isotopes it is possible to track the uptake by methanogens of either CO_2 or other reduced carbon substrates e.g. acetate. The bacterial reduction of CO_2 to CH_4 is associated with a kinetic isotope effect, which discriminates against ^{13}C yielding specific values for the separation between CO_2 and CH_4 (e_c). This value varies according to the substrate used and can be plotted to show the source of CH_4 (H_2/CO_2, acetate or thermogenic origin) which is related to specific methanogenic environments e.g. marine and freshwater. The generally accepted model for usage is the Whiticar model Fig 1.7 (Whiticar et al., 1986; Whiticar, 1999)
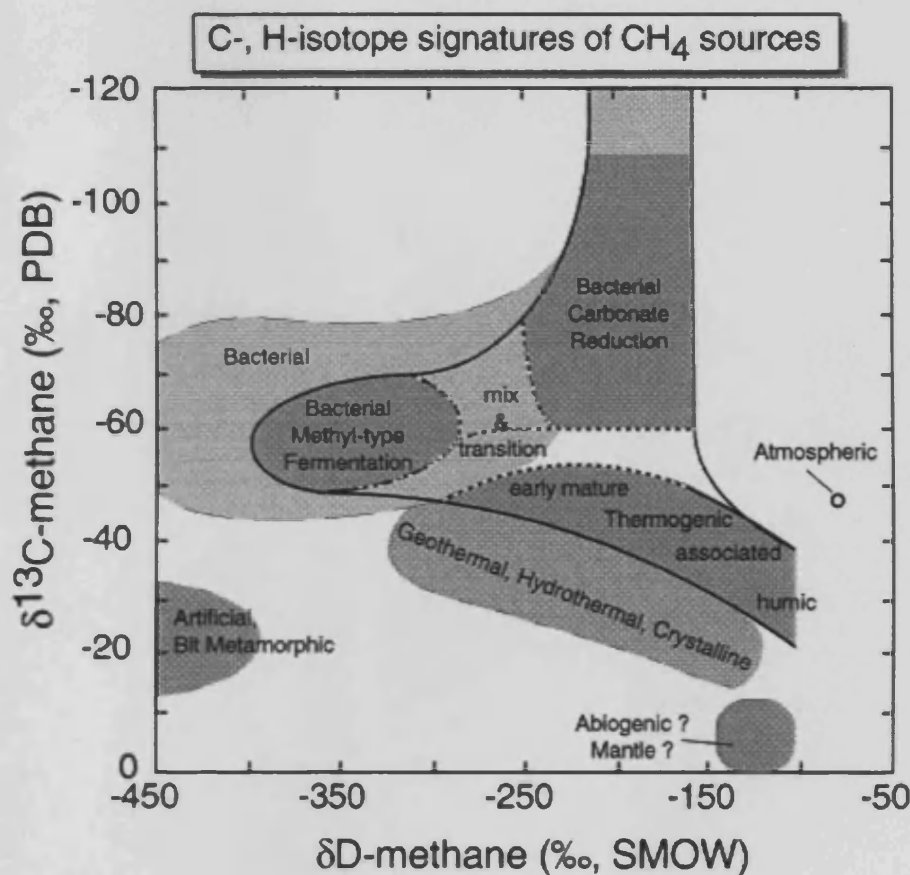
Fig 1.7 CD-diagram for classification of prokaryotic and thermogenic methane sources by combination of $\delta^{13}C_{CH4}$ and δD_{CH4} data (Whiticar, 1999)

Differentiation between thermogenic and biotic CH_4 is achieved through analysis of the $\delta^{13}C$-CH_4 values. Thermogenic methane is enriched with ^{13}C compared to prokaryotic methane and according to the model (Fig 1.7) has a range extending from -50‰ to -20‰. It is also possible to classify thermogenic methane according to source rock type and maturity level (Schoell, 1988; Whiticar, 1994). Prokaryotic methane production has a broader range of values than thermogenic. Ranging from ~ -110‰ to -50‰ (Fig 1.7). Use can also be made of the model to infer the prokaryotic pathway with the labelling if methyl-type substrates which is more common in fresh water (acetate usage) with the remainder being inferred as H_2/CO_2 (prokaryotic carbonate reduction) cut off at approximately -60‰ between both types lower than -60‰ H_2/CO_2, higher acetoclastic

1.3.8 Acetogenesis

Acetogenesis is an important process in subsurface sediments. Acetogens use the acetyl-CoA pathway for the reduction of CO_2 to the acetyl moiety of acetyl-coenzyme A, to conserve energy and assimilate CO_2 into cellular carbon (Drake, 1994). Acetogens are strictly anaerobic and similar to methanogens, H_2 is the major substrate. Acetogens are quite diverse and over 100 acetogenic species, representing 22 genera have been isolated from a large variety of environments (Drake et al., 2008). Homoacetogens produce acetate by using H_2 as an electron donor and coupling it to CO_2 reduction.

$$4H_2 + H^+ + 2HCO_3^- \rightarrow CH_3COO^- + 4H_2O \quad \Delta G^{\circ\prime} \ -104.6 \ kj/reaction \quad \textbf{Eq 1.17}$$
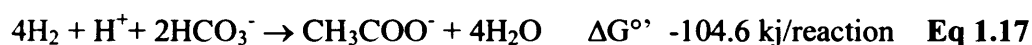
In addition to H_2 many other compounds can be used as an electron donor in acetogenesis such as amino acids, sugars and alcohols, but this entails intermediate H_2 production/consumption. Reduction of NO_3^- and $S_2O_3^{2-}$ is also possible via the usage of CO_2. All acetogens use the same pathway of CO_2 reduction namely the acety-CoA Wood-Lungdahl Pathway. This is the distinguishing feature of all acetogens. The acetyl-CoA pathway (Fig 1.8) is a reductive, linear one carbon process and thus is very different than other CO_2 cyclic fixing processes (e.g Calvin cycle) which depends upon recycled

intermediates (Wood, 1991; Wood and Ljungdahl, 1991). The acetyl-CoA pathway is a divided into two branch's. One branch reduces CO_2 to the methyl group of acetate and the other reduces CO_2 to the carbonyl group of acetate. Both compounds then merge to synthesise acetyl-CoA, which is subsequently converted to either acetate or assimilated into biomass. Acetyl-CoA synthase not only catalyzes the reduction of CO_2 to CO and the synthesis of acetyl-CoA but can also oxidises CO to CO_2. Different subunits of acetyl-CoA synthase are capable of catalyzing different reactions (Wood and Ljungdahl, 1991; Ljungdahl, 1994; Ragsdale, 1997). The conservation of energy occurs through substrate level phosphorylation and chemiosmotic processes. Four ATP are produced for each glucose that is converted to 3 acetates Fig 1.8. However substrate level phosphorylation produces no net gain in ATP. Thus growth of acetogens under these conditions is depended on chemiosmotic energy conserving processes and translocation of protons and sodium ions.
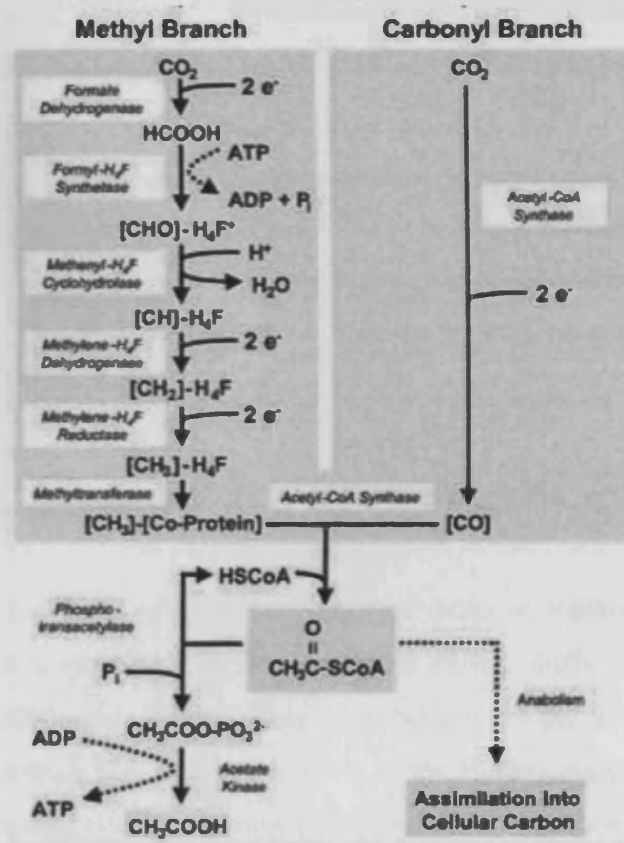
Fig 1.8 The acetyl-CoA Wood-Ljungdahl pathway, showing both branches of CO_2 reduction from (Drake et al., 2008)
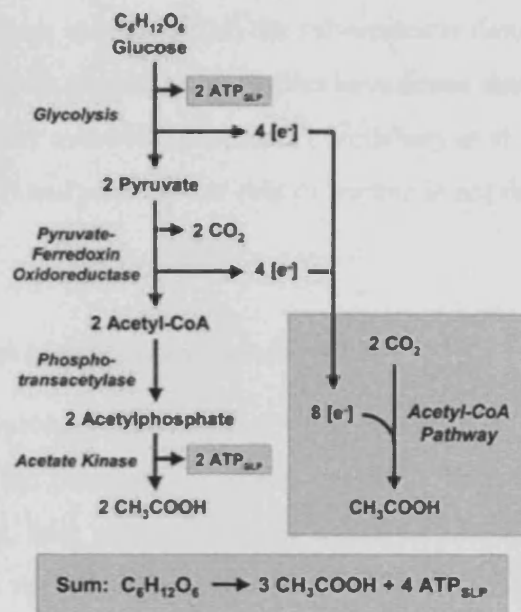
Fig 1.9 Homoacetogenic conversion of glucose to acetate.

Homoacetogenic bacteria (e.g. *Acetobacterium woodii*) are often found in association with methanogens. Homoacetogenises is the energy metabolism involving the production of acetate from either H_2 plus CO_2 or other organic compounds. Certain Homoaceogens ferment sugars such as glucose (Fig 1.9) Eq 1.18 to acetate and H_2 via a pyruvate intermediate.

$$2CH_3H_3O_3^-(\text{pyruvate}) + 2H_2O \rightarrow 2CH_3COO^- + 2CO_2 + 2H_2 \quad \Delta G^{o'} = 104 \text{ kj/reaction} \quad \textbf{Eq 1.18}$$
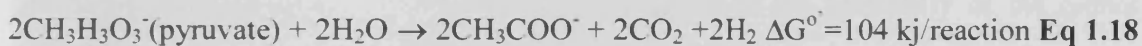
A syntrophic relationship develops between homoacetogens and methanogens both substrates of this reaction can be consumed during methanogenesis H_2 (interspecies hydrogen transfer) and acetate. This is a benefit to the acetogens, removing waste products and keeping H_2 concentration low. If the H_2 concentration is two high the above (Thiele and Zeikus, 1989) reaction (1.18) becomes thermodynamically unfavourable. Microbial acetogenesis rather than abiotic generation has been found to be the principal source of acetate generation in the marine subsurface (Chapelle and Bradley, 1996) and

normally acetogens and methanogens are in direct competition for H_2 with the exception of acetoclastic methanogens. Most methane from the subsurface is thought to come from H_2/CO_2 (Whiticar, 1999). However similar other studies have found that acetate may play a significant role in fuelling other microbial processes (Wellsbury et al., 1997; Wellsbury et al., 2002; Parkes et al., 2007) and perhaps the role of acetate is not fully appreciated in subsurface environments.

1.4 Molecular characterisation of subsurface communities

Due to the low cultivability of prokaryotes in the subsurface, molecular methods based on 16S rRNA gene analysis are the best way, currently available for the quantification of communities in the subsurface, here we give a quick overview of the main community composition of prokaryotes in the subsurface, found so far in 16S rRNA gene libraries. This is to give the reader an understanding of the amounts and phylotypes present in the subsurface, for comparison with the metabolisms mentioned previously and for reference when examining clone libraries in the upcoming results chapters. Recent reviews (Teske, 2006; Fry et al., 2008; Teske and Sorensen, 2008) have examined published clone libraries for subsurface sediments. Overall the most abundant subsurface bacterial groups are the *Gammaproteobacteria, Chloroflexi* and members of the candidate division JS1 (Webster et al., 2004) which make up 62.3% of clone libraries and are present in 62-70% of all libraries analysed. The remainder of the libraries are made up of *Alpha-,Beta-Delta* and *Epsilon proteobacteria* (7.8%, 4.9%, 3.7% 2,1%) of the remainder of the clones *Planctomycetes* are most abundant (2-26%) with the remainder novel species (Fry et al., 2008) Fig 1.10 show the diversity of clones found so far in bacterial sub-seafloor clone libraries
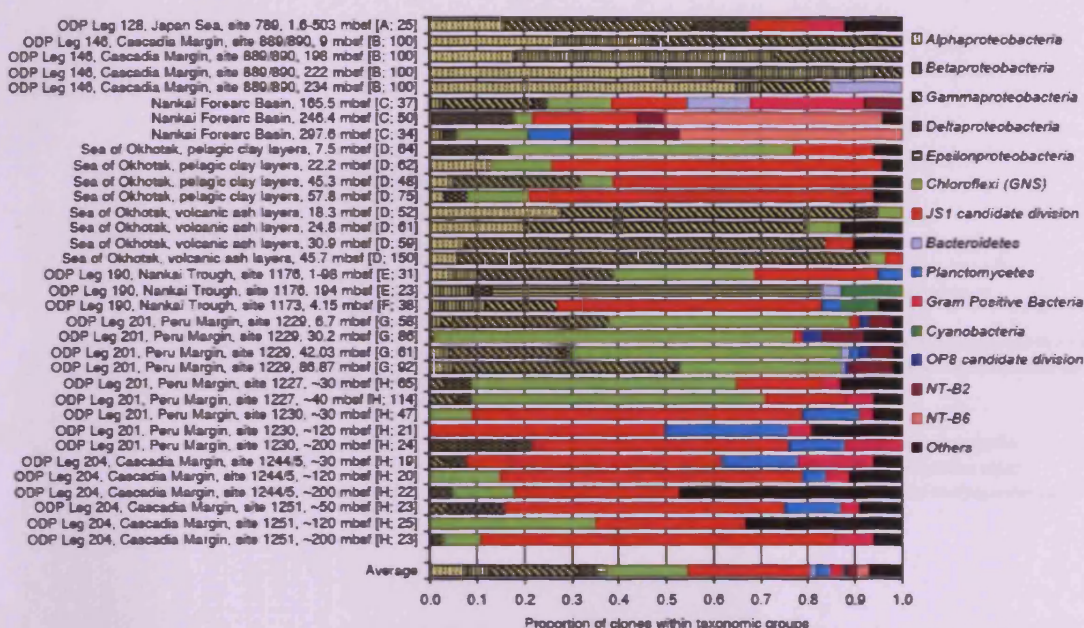
Fig 1. 10 Community composition of major taxonomic groups of Bacteria from 16S rRNA gene libraries at various sites and depths in the deep subseafloor biosphere (Fry et al., 2008)

Community composition of archaea clone libraries are dominated by the *Crenarchaeota* with 73.4% of clones belonging to the *Crenarchaeota* and 24.5 % belonging to the *Euryarchaeota* (Fry et al., 2008) The most dominate group amongst the *Crenarchaeota* fall within the *Miscellaneous Crenarchaeotic Group* (MCG) and the marine benthic group B (Teske and Sorensen, 2008) which comprised 33% and 26% of clone libraries, the next most abundant were the marine group 1 and the south African gold mine groups 8.4% and 7.6%. Thermophilic *Euryarchaeota* only account for < 8% of clones libraries. the majority of clones are related to uncultured lineages. Fig 1.11 shows the community composition of archaea from various sites in the deep subseafloor biopshere

26
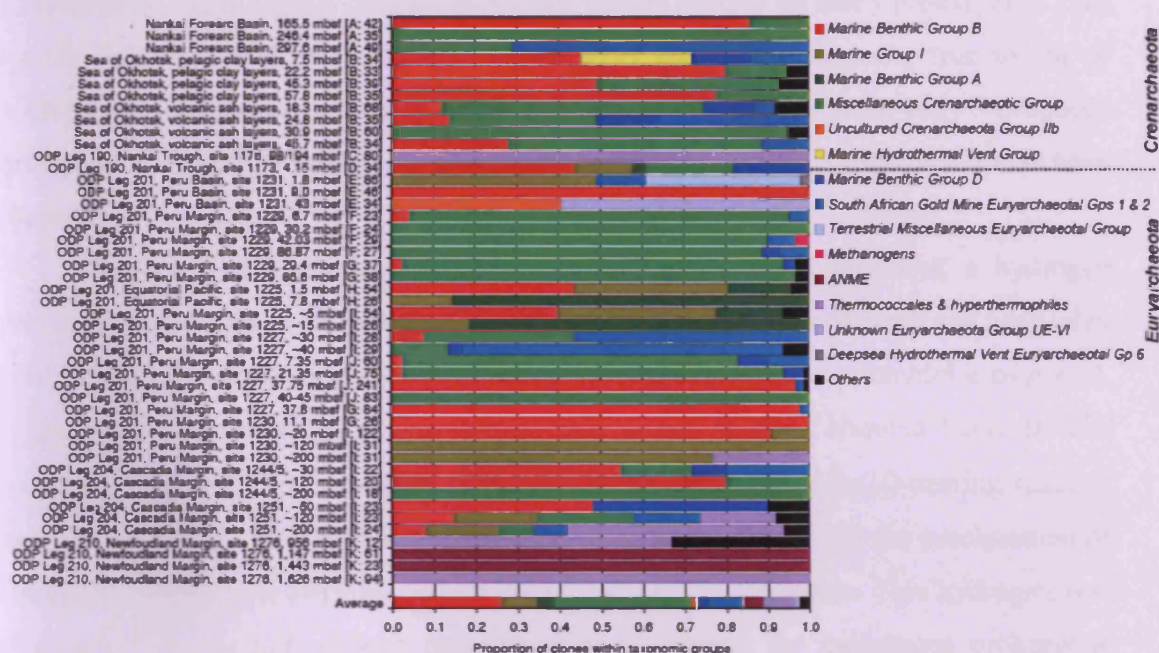
Fig 1.11 Community composition of *Archaea* 16S rRNA genes from various sites and depths in the deep subseafloor biosphere. (Fry et al., 2008)

1.5 Hydrogen driven Subsurface Lithoautrophic Microbial Ecosystems (SLiMEs)

. The possible existence of a "Deep hot biosphere" independent of photosynthetic energy supply and primary production was first hypothesised by Thomas Gold in 1992 (Gold, 1992). This involved the use of abiotically derived chemical compounds as a source of energy for subsurface microbes such compounds included H_2, CH_4 and other hydrocarbons. H_2 is a good electron donor and can be utilised by many prokaryotes. This hypothesis was ahead of its time in many ways and at the time the true extent of subsurface microbial communities was unknown and unverified. So far only 3 proposed examples of hydrogen driven communities occurring in the subsurface have been proposed.

Stevens and McKinley (Stevens and McKinley, 1995) proposed a hydrogen driven subsurface community in the Columbia river basalts. It was Stevens and McKinley who first coined the acronym SLiME (Subsurface lithoautotrophic microbial ecosystem). High concentrations of H_2 are found in ground waters in the Columbia River Basalts ($\sim$0.2-80μM). Which was proposed as the result of weathering of Fe(II)-bearing silicates at high water rock ratios, where the oxidation of ferrous silicates and the precipitation of magnetite (Fe_3O_4) and other secondary phases driving H_2 formation. This hydrogen was proposed to be in high enough concentrations to support the indigenous prokaryotic community independent of photosynthetically derived organic matter, as autotrophic populations dominated the prokaryotic community. This type of community was summed up by (Pedersen, 1997) see Fig 1.12
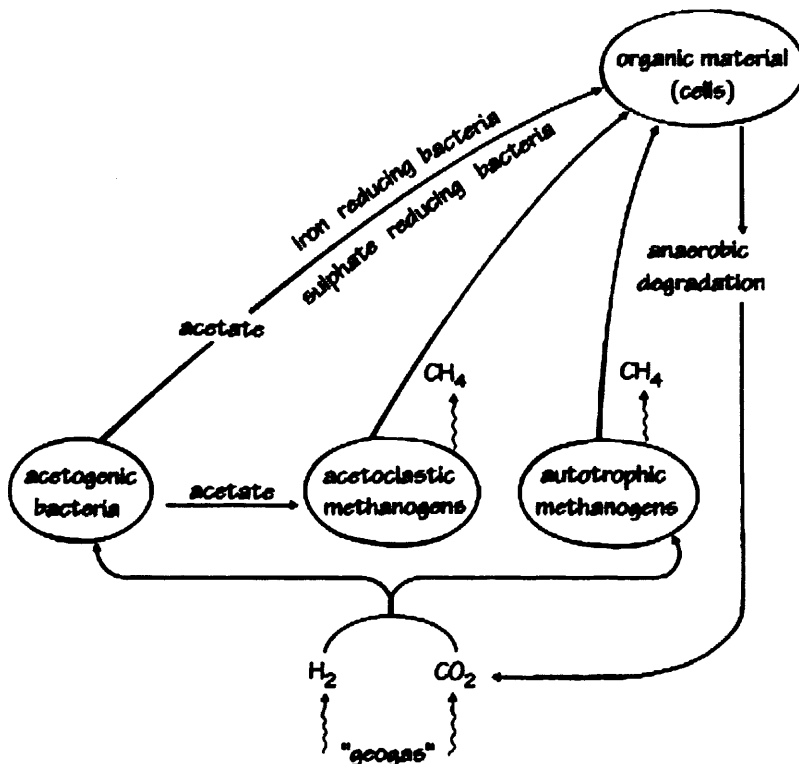
Fig 1.12 The deep hydrogen driven biosphere hypothesis, illustrated by its carbon cycle. At relevant temperature and water availability conditions, subterranean microorganisms are theoretically capable of performing a life cycle that is independent of sun driven ecosystems. Hydrogen and carbon dioxide from the deep crust of the earth or from sedimentary deposits of organic carbon can be used as energy and carbon sources. (Pedersen, 1997)

The assertion that the Columbia river Basalt aquifer (CRB) represented a community living off geochemically produced H_2 came under criticism (Anderson et al., 1998) for a number of reasons. The molecular analysis of the CRB which had previously been performed (Fry et al., 1997) showed that the microbial community composition more closely resembled that of a heterotrophic community living off organic matter than H_2. Less than 3% of the microbial community was comprised of methanogenic microorganisms. In the system that was proposed by Stevens and McKinley (1995) in which the main electron donor was H_2 (abiotically produced) and H_2/CO_2 methanogens are the primary consumers of this, its follows that these should form the majority of the community, which they did not. Also the amount of organic matter (DOM) found in the CRB (Fry et al., 1997) is 2-5 mg/l and it was noted (Anderson et al., 1998) that these

amounts of DOM have previously been enough to sustain deep pristine aquifers in which the community was found to be heterotrophic. The final line of argument against the presence of a H_2 sustained community concerns the mechanism and amount of H_2 production in laboratory experiments carried out with crushed basalt and artificial buffers (Stevens and McKinley, 1995, 2000). While a range of pH values were tested continuous H_2 was generated at an artificially low pH with the highest concentrations of H_2 produced at pH 6. Only low and unsustainable amounts were produced at pH 8. This is a major factor as basalt aquifers including the CRB are buffered at an alkaline pH (Hearn et al., 1986). The breakdown of basalt minerals at low temperature in ground water consumes H^+ and releases Ca^{2+} and HCO_3^- with the precipitation of $CaCO_3$, this combined process buffers the system at pH ~8. This vital factor makes the amounts of H_2 produced at pH 6 in laboratory experiments not relevant to processes occurring in the CRB.

The Lidy hot springs are another proposed hydrogen based subsurface community and unlike the CRB contains negligible concentrations of dissolved organic carbon <0.27 mg l^{-1} subsurface waters from the spring were 58.5°C (Chapelle et al., 2002). H_2 concentrations were 13 ± 2 nM. The community structure matches a community proposed to be driven by H_2 99% of the community were archaeal with 62 out of 65 (95%) clones, sequenced being related to methanogens. However, no methane production could be demonstrated which is unusual considering methanogens are dominant.

A HyperSLiME community which is a hyperthermophilic SLiME community is proposed in the central Indian ridge at the Kairei hydrothermal field (Takai et al., 2004). Mid oceanic ridge spreading centres are promising sites for SLiME communities due to the low levels of dissolved organic carbon (DOC) and these areas are generally sediment poor. Active geological processes may provide a readily available source of H_2. At the Kairei field the hydrothermal fluids emitted from the vents studied had high amounts of H_2 (2.5 mM) and low Mg concentrations indicated little mixing with the surrounding seawater. Serpentinization type reactions are thought to be responsible for H_2 formation Relative high concentrations of CO_2 were found (7.8-8 mM) as well as some small concentrations of CH_4 (84-199 nM). Molecular analysis showed an abundance of *Archaea* similar to the Lidy hot springs. Unlike the Lidy hot spring however, 2 groups dominated those being the *Thermococcales* and *Methanococcales*. Movement away from

vents produced a more diverse community structure with bacterial populations beginning to dominate.

1.6 Abiotic sources of Hydrogen generation in the subsurface

All SLiME communities proposed so far rely on sources of abiotically generated H_2. The following section will attempt to clarify these sources and processes. The production of hydrogen through the oxidation of Fe^{2+} bearing minerals as proposed by Stevens and McKinley (Stevens and McKinley, 1995) has already been discussed .

1.6.1 Serpentinization

The most speculated process providing H_2 as a possible microbial energy source is serpentinization of ultramafic rocks mainly composed of olivine [$(Mg, Fe)_2SiO_4$] and pyroxenes both orthopyroxenes [$(Mg,Fe)-SiO_3$] and clinopyroxenes [$Ca(Mg,Fe)Si_2O_6$] with atomic Mg/Fe ratios of ~ 9:1. Owning to differences in mineralogy and bulk chemistry the serpentinization of ultramafics which occurs in association with hydrothermal processes results in a substantially different composition of vent fluid than can be found with hydrothermal processes associated with basalt (Janecky and Seyfried, 1986; Wetzel and Shock, 2000; Allen and Seyfried, 2003)

The most common exposure of ultramafics is along axis of slow and very slow spreading ridges where the mantle is too cool to form significant basalts (Sleep et al., 2004) approximately 10% of oceanic crust is thought to form at these ridges (Dick et al., 2003). At temperatures below 300°C and with low Si(aq) concentrations these rocks react with H_2O to form hydrous Mg and Fe^{2+} silicates and hydroxides Eq 1.19

$$Fe_2SiO_4 + 5Mg_2SiO_4 + 9H_2O \rightarrow 3Mg_3Si_2O_5(OH)_4 + Mg(OH)_2 + 2Fe(OH)_2 \quad \textbf{Eq 1.19}$$
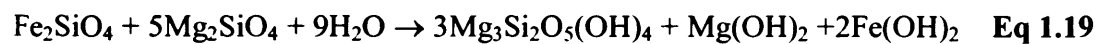
This fluid then oxidizes some of the Fe^{2+} to magnetite and liberates H_2 gas which may fuel associated biological reactions Eq 1.20

$$3Fe(OH)_2 \rightarrow Fe_3O_4 + 2H_2O + H_2 \qquad \textbf{Eq 1.20}$$
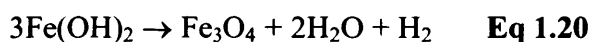
The major difference between ultramafic rocks and basalt, which enables higher concentrations of H_2 to be formed in ultramafics, is the Si concentration, low Si results in the formation of alteration minerals (e.g. serpentine), these minerals during formation tend to exclude Fe(II) which leads to the formation of magnetite and H_2 which at elevated temperatures can also lead to CH_4 formation, (which can therefore theoretically fuel H_2 and AOM utilizers). In basalt which generally has a higher concentration of Si more Fe(II) is incorporated into alteration minerals such as chlorite meaning less is converted to Fe(III), resulting in lower amounts of H_2 generation. This is somewhat unique to ultramafics, H_2 generation thus depends on the relative partitioning of Fe(II) into product minerals (Bach et al., 2004). Huge amounts of H_2 have been found associated with serpentinization at deep sea hydrothermal vent fluids (12-16 mmol/kg (Charlou et al., 2002; Kelley et al., 2005). Concentrations exceeding 100 mmol/kg have been found in some circumstances and are thought to result from the presence of certain metal alloys which catalyse hydrogen generation (Alt and Shanks, 1998). These have been reproduced in the laboratory (McCollom and Seewald, 2001).

Basalt interaction with hydrothermal fluids result in $H_2 \sim$ 0.05-1.7 μmol/kg (Von Damm, 1995). Another common product result from serpentinization is CH_4 the percentage amount of methane produced by various processes at vent fluids has yet to be determined correctly (McCollom and Seewald, 2007) but is considered to be the result of abiotic processes although it may also proceed through biotic functions. Basalt fluids are often highly enriched in H_2S leaving the oxidation of sulphur as the predominant source of metabolic energy (McCollom and Shock, 1997; Kelley et al., 2002). Ultramafics on the other hand are typically low in sulphur.

1.6.2 Pyrite formation

Other sources of water rock interactions which produce H_2 is the formation of FeS_2 from FeS (Drobner et al., 1990).This involves the formation of pyrite at 100°C with H^+ as the oxidant under anaerobic conditions. The first time this was observed it contradicted the previous hypothesis that the presence of elemental sulphur or sulphur equivalent (polysulphide or thiosulphate) was required for pyrite formation. H_2 formations was linked to pyrite formation from both amorphous FeS or with synthetic pyrrhotite by the following reactions

$$FeS + H_2S \rightarrow Fe(SH)_2 \qquad \textbf{Eq 1.21}$$

$$Fe(SH)_2 \rightarrow FeS_2 + H_2 \qquad \textbf{Eq 1.22}$$

Amounts of H_2 formed varied from 0.2 to 40 $\mu mol \ l^{-1}$ the most H_2 was evolved from reactions with amorphous FeS. Mineral products were pyrite and mackinawite (FeS_{1-x})

1.6.3 Thermal decomposition

Thermal decomposition of alkanes and carboxylic acids has been proposed as a mechanism for the production of H_2 (Seewald, 2001). Experiments were conducted at elevated temperatures of between 300-350°C in order to mimic hydrothermal conditions; reaction systems were buffered with minerals such as pyrite magnetite and hematite. The addition of these minerals seemed to stimulate previously unknown pathways. Results indicated that decomposition of n-alkanes proceeds through a series of oxidation and hydration reactions sequentially producing alkenes, alcohols, ketones and organic acids (as intermediates). These organic acids subsequently underwent decarboxylation and or oxidation reactions forming CO_2 and some short chain saturated hydrocarbons with H_2 as a product. The highest H_2 concentration achieved was 0.9 mM in the pyrite-pyrrhotote and magnetite buffered assemblage. Lower temperature aromatisation of organic matter in the presence of prokaryotes is also thought to result in the production of H_2 (Parkes et al., 2007) 20-90°C.

1.6.4 Radiolytic dissociation of water

It has been noted previously that molecular hydrogen and oxidants produced by the radiolysis of water may provide energy sources in the deep subsurface (Pedersen, 1997; Lin et al., 2005). In rocks and sediments alpha, beta, and gamma radiation which is released by the decay of various radioactive elements, mainly uranium (^{238}U), thorium (^{232}Th) and potassium (^{40}K) which are the most abundant in marine sediments (Lin et al., 2002) leads to the dissociation water molecules, producing molecular H_2. Energy from the alpha beta and gamma radiation is transferred to the water molecules leading to excitation and ionisasation. Reactive species are formed as a result such as, (e^-_{aq}). protons (H^+), hydrogen radicals ($H\bullet$) and hydroxyl radicals ($OH\bullet$) (Draganic and Draganic, 1971) These reactions are short lived and the subsequent reactions form molecular H_2 and have hydrogen peroxide H_2O_2, $OH\bullet, H^+$ and $H\bullet$ as products (Harris and Pimblott, 2002). Additional H_2 can be formed from the reaction of two $H\bullet$ or one $H\bullet$ and one e^-_{aq} and one H_2O molecule, and possibly also through the combination of two e^-_{aq} ions with two H_2O molecules (Spinks and Woods, 1990).

In marine sediments the U, TH and K concentrations are similar to those in igneous continental crust (Taylor and McLennan, 1985), but with the small grain size and higher relative porosity and abundance of water throughout the sediment, the amount of radiolysis is thought to be much higher. Studies on actual subsurface samples indicted that H_2 production by radiolysis fuelled as much as 10% of the metabolic respiration at leg 201 (site 1231) during IODP cruises drilling on the deep biosphere (Blair et al., 2007). It is also hypothesised that in ecosystems with extremely low rates of respiration such as central ocean gyre, water radiolysis may be the principal source of electron donors.

Very little is known about microbial communities in the deep sub seafloor. Even less is known about SLiMEs, which may be occurring within hydrothermal sites. The study of communities that are independent of photosynthesis could have great benefit not just in terms of expanding our understanding of "dark energy" sources (Bach and Edwards, 2003) and the origin of life on this planet and the elements necessary for life to

survive, but also could be used as analogies for proposed microbial communities occurring on other planets

Chapter 2

Materials and Methods

This chapter contains and covers the main experimental techniques used during this research project. Where adaptations and changes were made to the general procedure these have been dealt with separately in the various individual sections.

2.1 Sample Sites

Sediment from two sample sites were used in this project. The majority of the sediment used was obtained from the St John's Lake section of the Tamar estuary in Cornwall, United Kingdom.
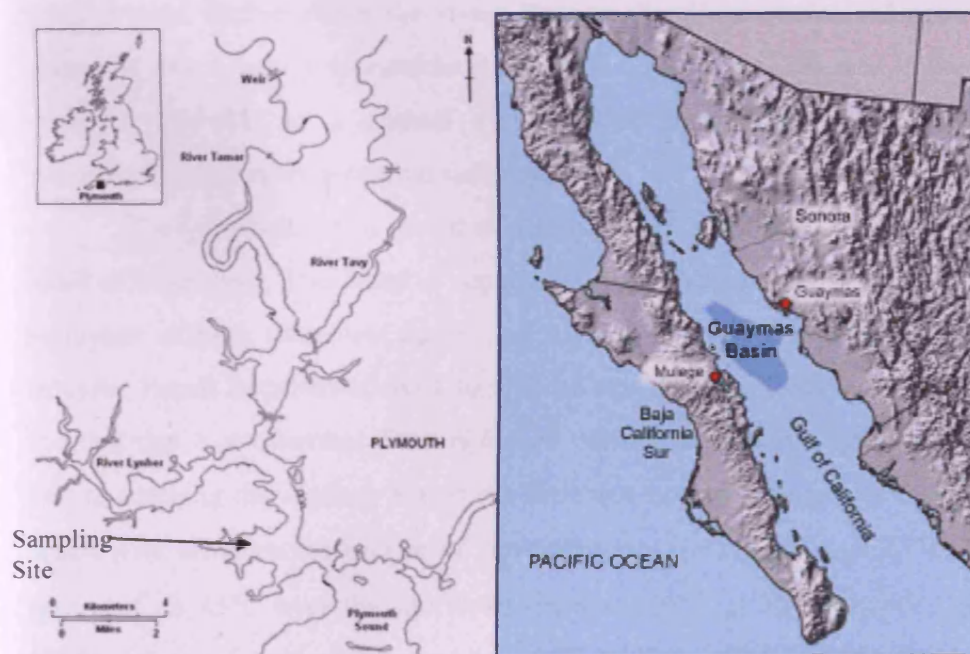
Fig 2.1 Maps of sampling sites, Tamar estuary and Guaymas Basin.

A small amount of sediment in each experiment was (as inoculum) obtained from the hydrothermally active Guaymas Basin, Gulf of California, courtesy of Andreas Teske

(University of North Carolina, Chapel Hill). These sediments came from Alvin dives 3204 which was at 27-00.764N, 111-24.558W and at a depth of 2100 m sampling into soft sediments and 3205 at 27-00.888N, 111-24.734W, at 2000 m sampling into high temperature vents and adjacent soft sediment (Woods Hole Oceanographic Institute).

2.2 Sediment Sites

The Tamar estuary is one of the most studied tidal systems in the United Kingdom (Watson et al., 1985 a, 1985 b; Stephens et al., 1992). It has also been used as a basis for various biogeochemical studies, some of which similar to this project have looked at reactions in the deep subsurface, in terms of effect that temperature increase during burial has on microbial relevant processes (Wellsbury and Parkes, 1995; Wellsbury et al., 1997; Parkes et al., 2007). The river Tamar flows from north Cornwall for approx 100 km to Plymouth sound through a catchment area of 1700 km (Miller, 1999). Samples were taken at St Johns Lake approx 3 km northwest of Plymouth sound. Pollution input is concentrated further down the river, close to the large centres of population and the sampling site is easily assessable at low tide. Lack of pollution is important as it is as close as possible to a natural system with minimal anthropogenic input and is representative of other estuarine systems.

The Guaymas Basin is part of a short series of seafloor-spreading segments in the Gulf of California. The basin is separated from adjacent deeps by long, north western-southeast striking transform faults, and divided into sub parallel northern and southern troughs. Rapid Sedimentation (1 to 5 m ka^{-1} (Fisher and Becker, 1991)) combined with the fact that hydrothermal fluid is forced through a sediment layer of 300-400 m thick before reaching the seafloor makes it a different system biologically than most other vent areas. The temperature profile of the sediment can range from 2.7°C just above the sediment, to 45°C over the first 0-10 cm and 126°C at 70 cm depth (Jorgensen et al., 1990). A large variety of thermophiles and hyperthermophiles have been found in the rich sediments of the Guaymas Basin such as the sulphate reducer *Archaeoglobus* (Burggraf et al., 1990) and hyperthermophilic methanogens such as *Methanopyrus* (Huber et al., 1989) and *Methanococcus* (Jones et al., 1983) and also members of the anaerobic

methane oxidising *Euryarchaeota* (ANME) (Teske et al., 2002) have been found to inhabit this environment.

The inclusion of Guaymas Basin inoculum was to ensure that there was a definite presence of thermophilic and hyperthermophilic organisms available for reactions during high temperature incubations (> 60°C).

2.3 Sampling

Sampling was conducted in the Tamar estuary using hand corers, all sampled cores were kept cool and transported with frozen ice packs. The cores were taken straight to the laboratory within 4 hours and stored at 4 ^{O}C until required. All Guaymas samples were sampled using the Woods hole oceanographic submersible ALVIN and were stored and shipped under anaerobic conditions in sealed Balch-type tubes, crimped with a rubber stopper. These were also stored at 4°C until required

Fig 2.2 Tamar estuary sampling

2.4 Minerals

Minerals used in this project were the following, Basalt, Hornblende, Labradorite, Hematite, Pyrite, Olivine, Olivine bombs, Pyrrohotite and Magnetite (Richard Taylor minerals, Surry, England). Also a sample of sand (silica/ quartz) was used as a control for some of the thermal gradient experiments.

39

All samples were from natural outcrop sources. The exact composition of each mineral used was determined by ICP-OES (Inductively coupled plasma, optical emission spectrometry) and by XRD (X-Ray Diffraction). Mineral composition is given in results chapter 3.

2.5 X-Ray Diffraction and ICP-OES

X-Ray diffraction was performed on samples using a Philips PW1710,XRD. Samples were crushed into a fine powder and packed inside aluminium holders, which was mounted inside the chamber of the diffractometer. Samples were run for 25 mins. The following is a brief outline of XRD. Braggs law ($n\lambda=2d\,sin\theta$) was used to distinguish the various mineral phases, where n is the order of reflection, λ is known wavelength of the X-rays, θ is the angle of incidence and d is the interplaner distance. By varying the angle of incidence, Braggs law is satisfied by different d spacings within the crystalline structure. The different angular positions and intensities can be plotted to provide a unique characteristic X-ray powder pattern, which can be used to identify the unknown crystal mineral phase. Phases were identified using the operating software in this case Philips PW1877APD

Inductively coupled plasma optical emission spectrometry (ICP-OES) was carried out in the School of Earth and Ocean Sciences, Cardiff University. Samples were fused using a Classie FLUXY fusion system, with a lithium metaborate flux before being analysed using a Jobin Yvon Ultima 2 ICP-OES.

2.6 Mineral preparation for slurry addition

Minerals were received in whole rock form from Taylor minerals and those, which were not small enough for powdering, were crushed to a course consistency using a Fritsch Jaw Crusher. Minerals were generally left in this course form until they were needed for experimental use, at which stage they were powdered using a Retsh pm 400, Agate, centrifugal ball mill. The mill pots were washed with 70% ethanol solution prior to mineral addition. Samples were powdered for 5 Min at 200 rpm. The majority of the

particles were less than 125 mm. However the mineral was not divided up into varying particle size (except for initial size comparison experiment) this was to more accurately mimic the processes occurring in the natural environment also separating particles adds more possible sources of contamination and delays the addition of mineral to master slurry. This use of freshly ground reactive surfaces was found to have a major effect on biogeochemical processes and thus any delay from grinding to addition was avoided where possible

2.7. Slurry preparation

This was based on procedures described by (Parkes et al., 2007) for similar experiments. Anoxic artificial seawater solution formed the basis of all media in slurry experiments, was identical regardless of experiment, and was initially set up in a master slurry. All chemicals used were AnalaR grade and were purchased from Sigma Aldrich or Fisher.
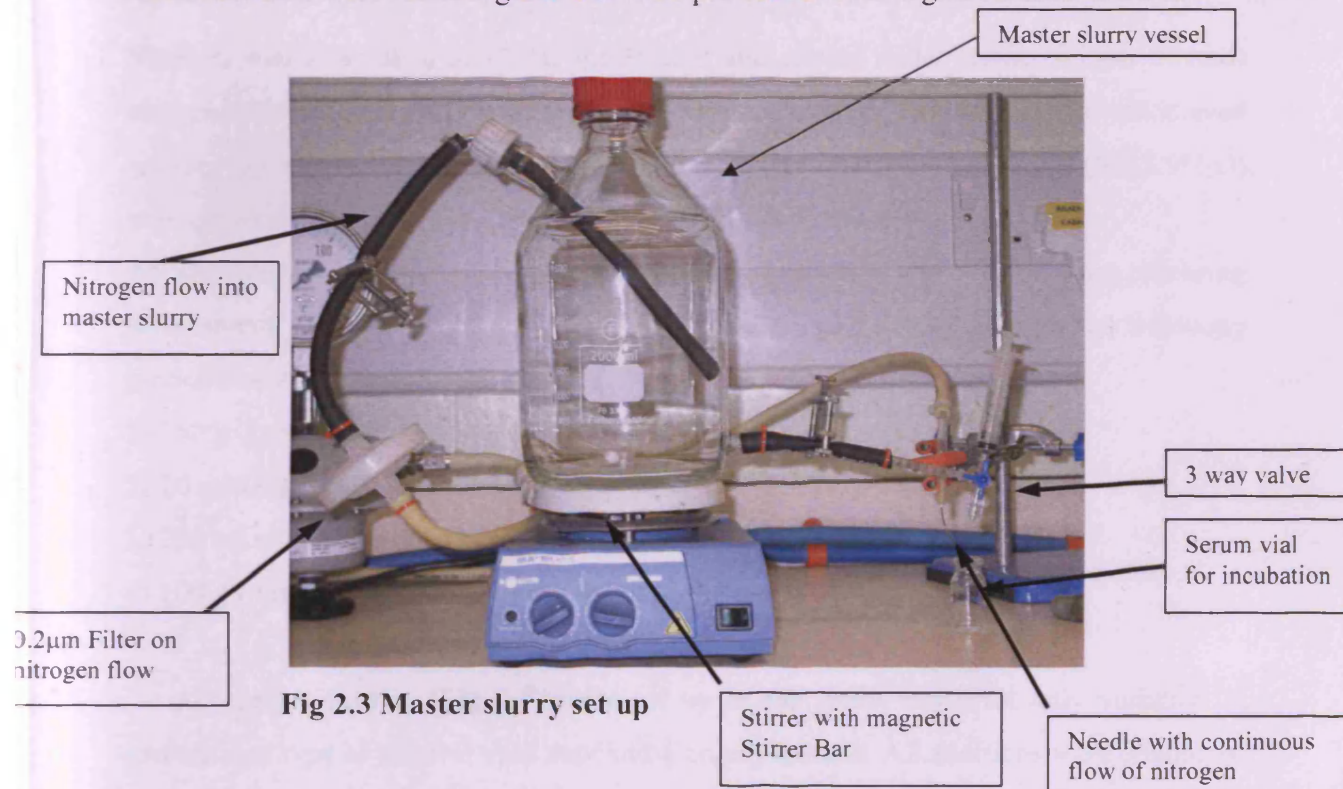
Fig 2.3 Master slurry set up

Master slurry vessel

Nitrogen flow into master slurry

3 way valve

Serum vial for incubation

0.2μm Filter on nitrogen flow

Stirrer with magnetic Stirrer Bar

Needle with continuous flow of nitrogen

Table 2.1
Recipe for anoxic artificial seawater solution.

Compound	g/L
NaCl	26.5
$MgCl_2.6H_2O$	1.28
$CaCl_2.2H_2O$	0.15
KCl	0.50
NH_4Cl	0.25
KH_2PO_4	0.20
Na_2SO_4	1.42
1M $NaHCO_3$	30.00ml

Medium was autoclaved at 121°C for 30 min and cooled under sterile (0.2μm filtered) oxygen-free nitrogen (OFN) and the pH was adjusted to 7.6 with sterile autoclaved sodium hydroxide (1M). Sterile autoclaved 12% (w/v) sulphide solution ($Na_2S.9H_2O$) was added (6ml/l) and the pH was adjusted to 7.6 where necessary.

All slurries were made according to the following procedure and contained the following components per litre. To this the following constituents were added with the following procedures to produce sediment slurry.

1) 250 g Tamar Sediment

2) 10 ml Guaymas basin sediment inoculum

3) 750 ml anoxic artificial seawater solution

4) 100 g of mineral (10 g /L in initial experiments).

All master slurries (Fig 2.3) were set up in the same way with only variation in amount and type of mineral used depending on experiment. All additions were conducted whilst gassing with OFN

1) Cooled, sterile, anoxic artificial seawater solution as above was prepared, with the 1 litre mark and 750 ml mark on the vessel measured and marked prior to autoclaving, 250 ml was removed.

2) 10 ml of Guaymas basin sediment was added, using a sterile syringe with the end removed.

3) A sterilised bag was filled with Tamar sediment pushed directly from the core, with the top 5 cm removed to leave anoxic sediment into bag.

4) 250 ml of mixed sediment was added to the anoxic artificial seawater solution.

5) This was manually mixed and stirred with a magnetic stirrer bar.

6) 10 g or 100 g of freshly ground mineral was added depending on experimental setup.

7) Slurry was mixed using a magnetic stirrer bar for 10-15 minutes

8) The master slurry was flushed with OFN before the liquid slurry was dispensed into varying reaction vessels under continuous OFN flow.

9) Amount of slurry added was controlled by a syringe attached to master slurry (Fig 2.3)

10) Headspace was flushed with nitrogen then reaction vessel was sealed and in case of serum vials crimped, then incubated at appropriate experimental temperature.

2.8 Reaction Vessels

Varying types of reaction vessels were used throughout this project depending on the experiment being conducted and due to the fact that we developed easier and better ways of incubating the vessels over the course of the project.

Type 1, initial experiments were carried out using a modified conical flask, sealed with a rubber bung (Fig 2.4). Through which a needle was placed with a 3-way valve, this was used for sampling gases and liquid sampling was done through modified sampling port at the bottom which was sealed with a Hoffman clamp. This was found to be unsatisfactory for long-term incubation as the bung was prone to failure.

Type 2, was a modified inverted 2 litre conical flask used for initial experimentation (Fig 2.5) as reported by (Parkes et al., 2007). The inverted shape enabled some compensation for changes in surface area/head space contact during repeat

sampling. Unlike type 1 it has a PTFE stopper with 2 O-rings with a 3-way valve fitted to the top. Gas sampling was through the 3 way valve and liquid sampling through a modified sampling port at the bottom. The PTFE stopper was found to be a great improvement on previous stoppers with no failures, however size and shape of vessel made it awkward to handle and sample, plus the number of replicates were limited.

Type 3, is a 100 ml Duran plugged with a PTFE stopper (Fig 2.6) liquid and gas sampling was via the 3 way valve at the top. This set up worked well and was used for the 60 ^{O} C. Incubations with varying minerals; this provided the ease of working with a smaller vessel and the safety of a PTFE stopper.

Type 4, an 8.5 ml Wheaton® serum vials (Fig 2.7), the vial was used in conjunction with a neoprene stopper and was crimped, this was used in all the thermal gradient experiments and was destructively sampled, with 6 replicates for each temperature being sampled over the given time period. This was to ensure no chance of contamination/ re-inoculation or leakage over the temperature profile. These worked very well up to temperatures of 100-105°C above that they tended to leak.

Type 5, (Fig 2.8/2.9) was a commercial pressure vessel constructed by Parr Scientific © (Moline, Illinois, USA). This was constructed to withstand temperatures up to 200°C and pressures up to 15 bar. This was used in the ramping experiment for temperatures over 100°C.

Fig 2.4. Type 1 reaction vessel (modified conical flask)

Fig 2.5. Type 2 reaction vessel (inverted modified conical flask)

Fig 2.6. Type 3 reaction vessel (PTFE stopperd duram bottle)

Fig 2.7.Type 4 reaction vessel Wheaton® serum vials
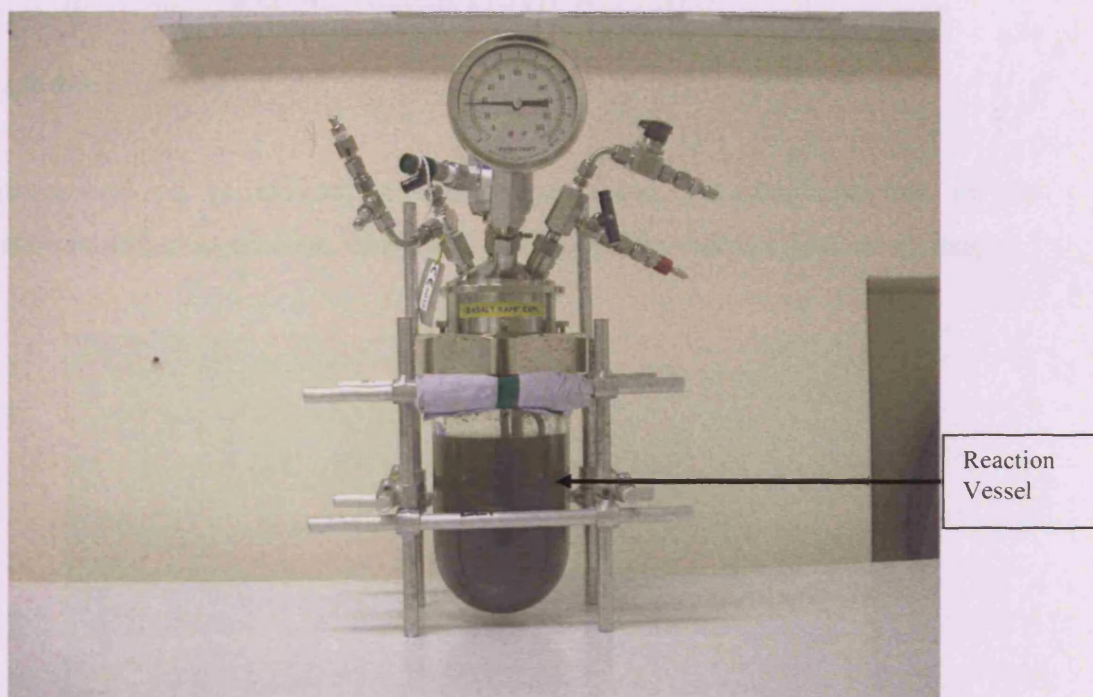
Fig 2.8. Type 5 reaction vessel (Parr Scientific pressure vessel)
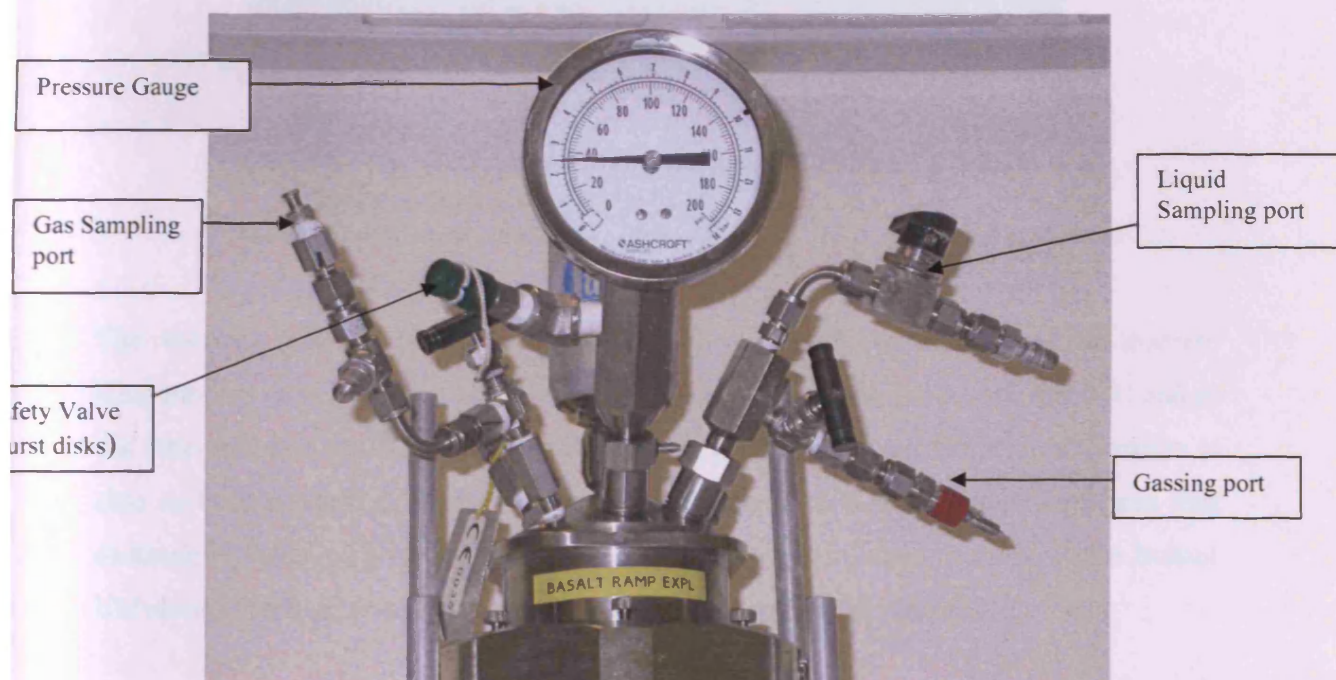
Fig 2.9. Type 5 reaction vessel close up

2.9 Incubations

Incubations were all carried out in Gallenkamp ovens with the exception of the temperature profiling experiment, which was carried out in a thermal gradient system.
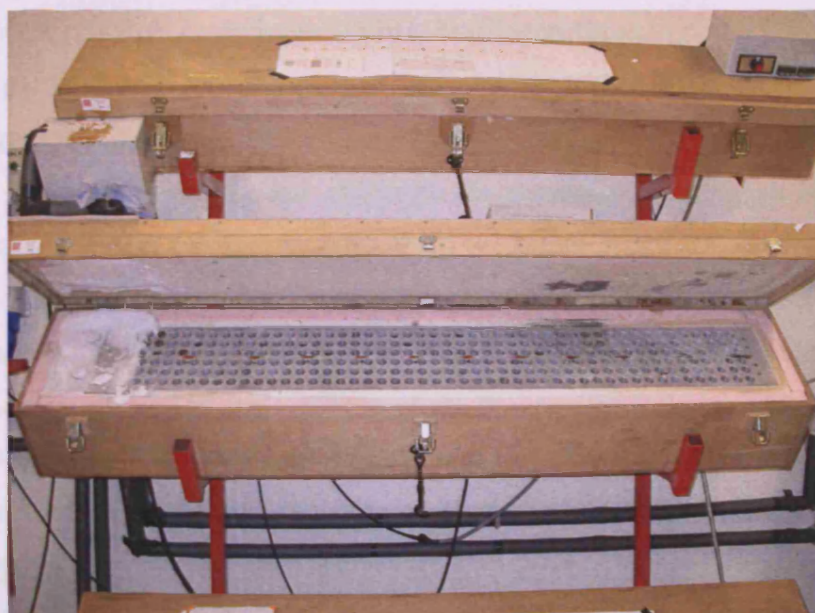
0°C   150°C

Thermal gradient set up 0 to 150°C
Fig 2.10. Thermal Gradient system

The thermal gradient system is an apparatus to replicate incubations at discrete temperatures over a defined temperature range. At one end the temperature is 0°C and at the other end it is 150°C. with sample positions every 2°C. Each temperature position is able to hold 6 samples at that temperature, which is ideal for running replicates and destructive sampling over a time course. The systems were custom made at the Bristol University, Earth Science Dept, workshops after (Isaksen et al., 1994).

2.10 Pore water analysis

Liquid for pore water analysis was removed through the liquid sampling port in each vessel; the amount removed was replaced with the same amount of nitrogen as to avoid creation of a vacuum except for destructive sampling. The sample was centrifuged using a Rotanta 460R (Hettich Zentrifugen GmbH, Tuttlingen Germany) at 1780 g for 12 min to remove particles and supernatant was used for analysis. Pore water sulphate and volatile fatty acid (acetate lactate and formate) as well as chloride and several other compounds were measured by ion exchange chromatography using an ICS-2000 ion chromatography system (Dionex®, UK) fitted with two AS15-HC 4 mm columns in series, and a Dionex® Anion Self-Regenerating Suppressor (ASRS®-ULTRA II 4-mm) unit in combination with a Dionex® DS6 heated conductivity cell. Components were separated using a potassium hydroxide gradient program as follows: a normal program run of 18 mM (14 min isocratic), 40 mM (10 min isocratic), 90 mM (6 min isocratic) 18 mM (7 min isocratic) for a total run time of 38 mins and a longer program of 6.0 mM KOH (38 min isocratic), 16.0 mM KOH min-1 to 70 mM (17 min isocratic) for more accurate determination of lactate and butyrate was also occasionally used depending on sample

Calibration used 5 standards with varying concentrations depending on concentrations of samples to be analysed i.e. high acetate or low acetate. Any calibration under 99% calibration coefficients was rejected. Cations were analysed using a Dionex® DX-120 ion chromatograph, using CS16 column 5x250 mm and a cation self-regenerating suppressor (CSRS® ultra II 4 mm). Components were separated using 38 mM Methanosulphonic acid, over a sample run time of 35 mins (isocratic) detection was via suppressed conductivity detector. This was connected to AS50 auto sampler for ease of sampling. Again 5 standards were used of varying concentration and any calibration under 99% was rejected. Calibration was linear for all samples with the exception of acetate which was quadratic at high concentrations.

2.11 Gas Analysis

Each gas sample was collected using the same method with the syringe being flushed 3 times with sample headspace before the sample was taken. The headspace was analysed by gas chromatography using a modified Perkin Elmer/Arnel Clarus 500 Natural Gas Analyser. With a configuration of flame ionisation Detector (FID) and Thermal Conductivity detector (TCD) which consists of two TCDs combined. Argon was used as the carrier gas for the TCD and helium as carrier gas for the FID. TCD was used for CO_2 and hydrogen determination and FID for methane, ethane, propane, butane and isobutene. Oven Temperature was $110^{\circ}C$ with TCD at $150^{\circ}C$ and FID at $250^{\circ}C$ air and hydrogen were used as gases to enable combustion at the FID. Calibration was by means of 3 standard gases mixtures (Scott Scientific). Detection limits for methane, ethane, propane, butane and isobutane were 0.5 ppm and hydrogen was 70 ppm, and CO_2 was 50 ppm with a sampling loop size of 100μl.

Lower levels of hydrogen were detected using a Mercury Vapour system (Peak Laboratories, Menlo park California) giving a lower detection limit of 5 ppb for Hydrogen. Carrier gas used was nitrogen and column temp was 220 $^{\circ}C$ loop size 10μl. Calibration was by means of one-shot calibration using a blended standard of 20 ppm concentration (Scott scientific).

2.12 Iron analysis

Samples for iron (II) analysis were spun in the small 8.5 ml vials used for the thermal gradient system, so as to keep the sample in anaerobic condition as long as possible, 200 μl of sample supernatant was removed through the septum by sterile syringe and immediately stored in 800 μl of 0.5M HCl. Samples were analysed after the method of (Stookey, 1970). A standard Fe (II) Solution was made using 0.05 g ferrous sulphate dissolved in 50ml of 1.2M HCl, and 0.05 ml, 0.15 ml, 0.30 ml, 0.50 ml and 0.8 ml aliquots were added to 5 ml of 0.5 M HCl and made up to 6 ml with 18MΩ Milliq water.

Aliquots (0.5 ml) of each sample and of each standard were transferred to a 5 ml ferrozine solution (0.5 g ferrozine dissolved in 500 ml of 50 mM HEPES buffer at pH 7) Colour intensity was allowed to develop for 30 mins. Colour intensity was measured using a Varian Cary 50 Probe UV Visible Spectrophotometer at 562 nm. A plot of standard absorption (minus the blank) against Fe (II) concentration had a liner response allowing the determination of the Fe (II) concentration in each sample. Calibrations that have an R^2 value of less than 0.98 were rejected.

2.13 $\delta^{13}C$ Isotope analysis

The gas was stored as a headspace in inverted crimp top Wheaton® vials by displacement of a preservative solution that consisted of 10% (w/v) KCl in deionised water adjusted to pH 1 using HCl. Stable carbon isotope analysis of CH_4 was conducted by GC combustion isotope ratio mass spectrometry using a Varian 3400® GC coupled to a Thermoelectron XP® mass spectrometer via a Gas Bench® interface. Methane was separated on a PLOT Q capillary column (0.32 mm x 30 m) and combusted to CO_2 at 1000°C in a ceramic reactor containing Cu and Pt wires. A high purity blend of 1% O_2 in helium was fed into the reactor at ~0.1 ml min^{-1} to ensure quantitative conversion of CH_4 to CO_2. The H_2O produced was removed using a Nafion® membrane. Accuracy and precision of $\delta^{13}C$-CH_4 analyses by this method were both better than ± 0.2‰ based upon replicate analysis of a BOC alpha gravimetric CH_4 standard. Stable isotope ratios are reported in the standard delta (™13) notation in units of per mil (‰) relative to Vienna Pee Dee Belemnite standard. Samples with concentrations of less than 800 ppm are below the detection limit and could not be analysed. Storage of samples in KCl lead to the loss of the ability to measure $\delta^{13}C$-CO_2 due to the buffering effect of KCl.

2.14 Acridine orange direct counts

Prokaryotic cell numbers in experiments were quantified using acridine orange counts after (Fry, 1988) with minor modifications. Acridine orange is a fluorescent dye that binds to the groove on DNA double helix, which produces a change in UV fluorescence

(orange to green). A 1ml Aliquot of shaken mixed slurry was added to 5 mls of a filtered (0.1 μm) (Whatman anotop) solution containing 2% formaldehyde and 3.5% NaCl (w/v). This was stored until sample could be counted by fluorescent microscopy. Fixed samples were vortex mixed and a quantity added to 10 ml of 2% filter sterilised (0.1 μm) formaldehyde in 3.5% in NaCl. The quantity added varied depending on cell numbers present. Acridine orange (50 μl) was added to give a final concentration of 5 mg/l. This was left for 3 mins in solution and then was filtered through a 25 mm Nucleopore black polycarbonate membrane (Osmonics inc., Minnetonka, MN, U.S.A) of 0.2 μm pore size. The filter was rinsed with a further 10 ml of solution as above. This was mounted on a slide with paraffin oil.

The mounted membrane filters were viewed under incident illumination with a Zeiss Axioskop microscope (Carl Zeiss, Oberkochen, Germany) fitted with a 50-W mercury vapour lamp, a wide-band interference filter set for blue excitation, a 100 X (numerical aperture = 1.3) Plan Neofluar objective lens, and 10 X eyepieces. The volume of sample stained and filtered were adjusted to optimize filter coverage by particles to around 70%. Sediment particles were orange/red whilst bacterial cells were bright green/blue fluorescence. Three replicate filters were prepared from each sample to minimize count variance (Kirchman et al., 1982). A minimum of 200 fields of view, or 200 prokaryotic cells were counted. The total number of bacteria and the numbers of dividing and divided cells were separately counted. The number of cells counted on opaque particles were doubled to account for cells hidden from view (Goulder, 1977). Blank membranes were regularly counted to asses any contamination and prokaryotic population size is calculated after subtraction of the any reagent blank.

Total bacterial numbers were calculated from;

$$\left(\left(\left(\frac{2C_{ON} + C_{OFF} + C_{DG} + 2C_{DD}\left(\dfrac{C_{ON}}{2C_{DD})}\ x\ (C_{DG} + \right)}{VIEW}\right) x\ A\right) - B_T\right) x\ \frac{1000}{V_{CT}}$$

D

Numbers of dividing and divided cells were calculated from the same equation with the omission of the terms "$2C_{ON} + C_{OFF}$" at the start of the equation, and the substitution of B_D for B_T.

The percentage of dividing and divided cells were calculated from the numbers of dividing and divided cells expressed as a percentage of the total bacterial cell numbers. Where total bacterial numbers approach the calculated detection limit, or numbers of cells counted approach the number of cells observed in the blanks, then this calculation becomes unreliable.

Key

C_{ON} and C_{OFF}: Number of cells counted ON and OFF particles, for the purposes of this calculation transparent particles.

C_{DG} and C_{DD}: Numbers of cells observed dividing (a cell with an invagination) and divided (two adjacent cells of identical morphology with a distinct space between them). Cells counted in these two categories are not also tallied under ON and OFF particle categories.

VIEW: The total number of fields of view observed during a cell count on a filter.

A: Filter area ratio. Total countable area of the filter divided by the area of filter observed for one field of view.

B_T and B_D: Blank correction terms for the total cell number (B_T) and the dividing and divided cell numbers (B_D). Calculated from counts of blank membranes and using the same equation with the omission of the correction term. In this instance V_{CT} will equal 10050 (10 mL of formaldehyde +50 μL of Acridine orange) and D will equal 1.

V_{CT}: Volume of formaldehyde-preserved sample that is stained (μL)

D: Dilution factor of original sample expressed as a proportion, e.g., 1 cm^3 of sediment in 9 mL of formaldehyde will give D = 0.1

2.15 Molecular analysis

2.15.1 DNA extraction

All sediment samples collected for molecular analysis were stored at -80°C until required.

The FastDNA Spin Kit for Soil (MP Biomedicals, Ohio, USA) with modifications (Webster et al., 2003) was used for DNA extraction in all cases. DNA extractions were carried out on 1 g of sediment slurry with the kit to give a final DNA solution of 50 μl. Visualization of DNA for yield and size was by agarose (1.0% w/v) gel electrophoresis with 0.5 μg ml^{-1} ethidium bromide or Syber safe (Invitrogen©, Carlsbad, Ca, USA) and compared to HyperLadder I DNA quantification marker (Bioline, London, UK). Extracted DNA solutions were stored at -80°C until required.

2.15.2 PCR reactions

PCR set-up was carried out under aseptic conditions using autoclaved and/or UV-treated plastic ware and pipettes and sterile nuclease-free molecular-grade water (Severn Biotech Ltd., Kidderminster, UK) to restrict contamination to a minimum. Positive [pure culture DNA] and negative controls (molecular-grade water) were used in all PCR amplifications, and undertaken in a DNA Engine Dyad Thermal Cycler gradient block (MJ Research, Boston, MA) with the PCR primers listed in Table 2. The 16S rRNA gene

PCR mixtures contained (total 50 μL, molecular-grade water) 0.4 pmol μL^{-1} of primers, 1 μL of sediment DNA template (1/10 dilution or 1/50 depending on sample), 1 x reaction buffer (Promega Corporation, Madison, WI), 1.5 mM MgCl$_2$, 1.5 U Biotaq DNA polymerase (Promega), 0.25 mM each dNTP, 10 μg bovine serum albumin (BSA; Promega).

Bacterial 16S rRNA genes were amplified from sediment DNA samples using primer combinations 27F-1492R or 27F-907R (Table 2.1) with the following PCR conditions. Reaction mixtures were held at 95°C for 2 min followed by 30 cycles of 94°C for 30 s, 52°C for 30 s and 72°C for 90 s plus 1 s per cycle, with a final extension step of 5 min at 72°C. Archaeal and Euryarchaeal 16S rRNA genes were amplified from sediment DNA with primer combinations 109F-958R with the following PCR reaction of 30 cycles of 98°C for 30 s 92°C for 45 s, 45°C for 45 s, 72°C for 42 s followed by an extension step of 72°C for 5 min, as described by (Newberry et al., 2004). The primer combination 109F-958R was chosen after analysis of the RDP (Ribosomal Database Project) database version 8.1 with the computer software OligoCheck (http://www.cardiff.ac.uk/biosi/research/biosoft/), because in silico results suggested that these primers could target >85% of the RDP archaeal sequences, including 16S rRNA genes from methanogenic Archaea shown to be important in subsurface marine sediments (Bidle et al., 1999; Marchesi et al., 2001; Newberry et al., 2004).

The 16S rRNA gene PCR products analysed by DGGE were re-amplified in a nested PCR reaction using the reaction mixture described above without BSA. Bacterial 16S rRNA genes were reamplified with primers 357F-518R at 95°C for 5 min followed by 10 cycles of 94°C for 30 s, 55°C for 30 s, 72°C for 60 s, and 25 cycles of 92°C for 30 s, 52°C for 30 s, 72°C for 60 s, with a final step of 10 min at 72°C. Archaeal and euryarchaeal 16S rRNA gene products were re-amplified with primers SAf and PARCH519r at 95°C for 5 min followed by 4 cycles of 94°C for 30 s ,53.5°C for 30 s 72°C for 1 min followed by 92°C for 30 s with 29 cycles of 53.5°C for 30 s and 72°C for 1 min and a final extension step of 72°C for 10 min as described (Nichols, 2003).

Table 2.2 Primers used in this study.

Target gene	Primer Name	Sequence 5'-3'	Procedure	Reference
16S rRNA Bacteria	27F	AGAGTTTGATCMTGGCTCAG	PCR	Lane (1991)
	907R	CCGTCAATTCMTTTGAGTTT	PCR	Muyzer et al.,(1998)
	1492R	GGTTACCTTGTTACGACTT	PCR	Lane (1991) Grosskopf et al (1998)
16S rRNA Archaea	109F	ACKGCTCAGTAACACGT	PCR	
	958R	YCCGGCGTTGAMTCCAATT	PCR	De Long (1992) Muyzer et al (1993)
16S rRNA Bacteria	357F-GC	GCCGCCCGCCGCGCGCGGCGGGCGGGGCG GGGGCACGGGGGGGCCTACGGGAGGCAGCAG	PCR-DGGE	
	518R	ATTACCGCGGCTGCTGG	PCR-DGGE	Muyzer et al (1993
16S rDNA Archaea	Saf-GC [B] SA1f	CGCCCGCCGCGCGCGGCGGGCGGGGCGGG GGCACGGGGGGGCCTAYGGGGCGCAGCAGG	PCR-DGGE	Nicol et al ., (2003)
	SA2f	CGCCCGCCGCGCGCGGCGGGCGGGGCGGG GGCACGGGGGGGCCTACGGGGCGCAGAGGG	PCR-DGGE	Nicols et al ., (2003
	PARCH519r	TTACCGCGGCKGCTG	PCR-DGGE	
				O'Sullivan et al.,(2008)
16S rRNA Bacterial DGGE bands	357F-GC-M13R	CAGGAAACAGCTATGACGGGCGGGGCGG GGGCACGGGGGGGCCTACGGGAGGCAGCAG	DGGE band reamplification	
	518R-AT-M13F	GTAAAACGACGGCCAGTAAATAAAATAA AAATGTAAAAAAATTACCGCGGCTGCTGG	DGGE band reamplification	O'Sullivan et al.,(2008)
16S rRNA Archaea DGGE	SAaf-GC M13R[C]	CAGGAAACAGCTATGAC<u>GGGCGGGGCGGG</u>[D] <u>GGCACGGGGGGG</u>CCTACGGGGCGCAGCAGG	DGGE band reamplification	O'Sullivan et al.,(2008)
	SAbf-GC-M13R	CAGGAAACAGCTATGAC<u>GGGCGGGGCGGG</u> <u>GGCACGGGGGGG</u>CCTATGGGGCGCAGCAGG	DGGE band reamplification	O'Sullivan et al.,(2008)
	SAcf-GC-M13R	CAGGAAACAGCTATGAC<u>GGGCGGGGCGG</u> <u>GGGCACGGGGGGG</u>CCTACGGGGCGCAGAGGG	DGGE band reamplification	O'Sullivan et al.,(2008)
	PARCH519r-AT-M13F	GTAAAACGACGGCCAG<u>TAAATAAAATA</u> <u>AAAATGTAAAAAA</u>TTACCGCGGCKGCTG	DGGE band reamplification	O'Sullivan et al.,(2008)
16S rRNA	M13F	GTAAAACGACGGCCAG	Sequencing	

A. D=G or A or T, H=A or T or C, K=G or T, M=A or C, R=A or G, W=A or T, Y= C or T.
B. Primer SAf is a mixture of SA1f and SA2f in a 2:1 molar ratio (Nicol et al., 2003)
C. Primer SAf-GC-M13R is a mixture of SAaf-GC-M13R, SAbf-GC-M13R and SAcf-GCM13R in a 1:1:1 molar ratio
D. Underlined type indicates the GC- or AT- linker

2.15.3 DGGE analysis

DGGE was carried out as described with some modifications (Webster et al., 2002; Webster et al., 2005). PCR products (c. 100 ng of each PCR product) were separated using a DCode™ Universal Mutation Detection System (Bio-Rad Laboratories, Hercules, CA, USA) and 1-mm-thick (16 x 16 cm glass plates) 8% (w/v) polyacrylamide gels (Acrylogel 2.6 solution, acrylamide: N,N'-methylenebisacrylamide; 37 : 1; BDH Laboratory Supplies, Poole, UK) with a gradient of alcrylamide denaturant between 30 and 60% and in some cases a 30 and 80% gradient (indicated in text). Gels were poured with a 50-mL volume Gradient Mixer (Fisher Scientific, Loughborough, UK) and prepared with 1 x TAE buffer (pH 8; 40 mM Tris base, 20 mM acetic acid, 1 mM EDTA). Electrophoresis was at 200 V for 5 h (with an initial 10 min at 80 V) at 60°C in 1 x TAE buffer. Polyacrylamide gels were stained with SYBRGold® (invitrogen, Carlsbad Ca, USA) nucleic acid gel stain for 30 min and viewed under UV. Gel images were captured with a Gene Genius Bio Imaging System (Syngene, Ca , USA).

Individual DGGE bands were excised by use of a sterile scalpel and washed in sterile nuclease-free molecular-grade water (Severn Biotech Ltd, Kidderminster, UK) for 10 min. Bands were air-dried and crushed in 10-20 µl molecular-grade water and incubated overnight at 4°C. The supernatant (1µl) was used as template DNA in a PCR using primers, 357F-518R (M13) or SAf-PARCH519r (M13), as described above, and PCR products were re-analysed by DGGE to confirm recovery of excised bands. PCR products of excised bands had the DNA yield quantified by 1.2% (w/v) agarose gel electrophoresis and DNA quantification marker Hyperladder I (Bioline). Sequencing reactions were performed with primer 518R-M13 or PARCH519r –M13 and an ABI PRISM 3100-Genetic Analyzer (Applied Biosystems, Foster City, CA).Partial 16S rRNA gene sequences were subjected to a blast® search in the National Centre for Biotechnology Information (NCBI) database (http://www.ncbi.nlm.nih.gov/blast/) to identify sequences with highest similarity. By Cardiff university sequencing core.
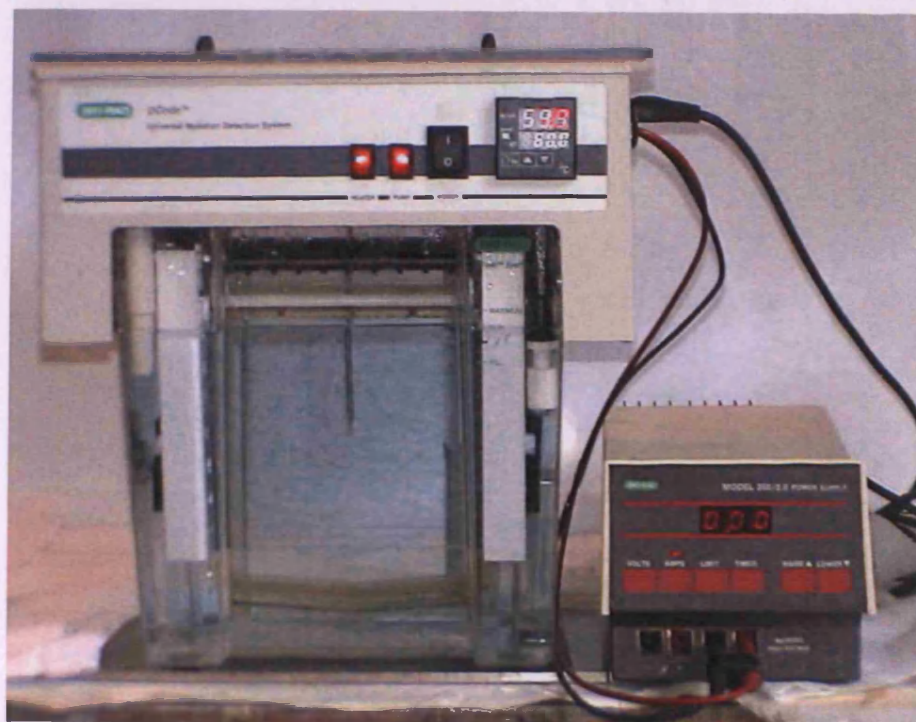
Fig 2.11 DCode™ Universal Mutation Detection System (Bio-Rad Laboratories) used to carry out DGGE analysis.

2.15.4 Cloning

All 16S rRNA gene fragments were screened by DGGE prior to cloning as recommended for deep biosphere samples (Webster et al., 2003). Only products from reactions showing the highest diversity assessed by DGGE and without PCR product in the negative controls were cloned. Each gene library was constructed from five independent PCR products that were pooled and cleaned with Microcon PCR Preps DNA Purification System (Promega Corporation) according to the manufacturer's instructions. Cloning was with pGEM-T Easy (Promega Corporation), using optimized insert: vector ratios and overnight ligation at 4°C. Libraries were screened by PCR with M13F or 16S rRNA gene primers and clones with verified inserts were randomly selected for sequencing with 27F (bacterial 16S rRNA genes), 109F (Archaeal 16S rRNA genes), and were sequenced using the ABI PRISM 3100.
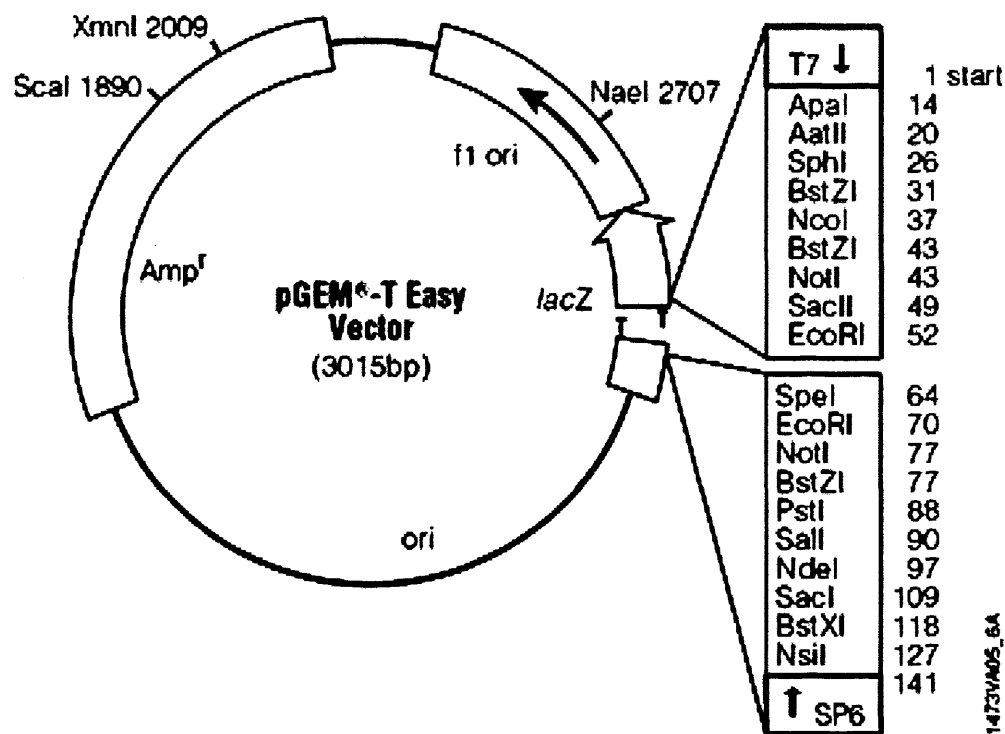
Fig 2.12 pGEM®-T Easy Vector circle map and sequence reference points.

pGEM-T Easy vector sequence reference points are for pUC/M13 Reverse Sequencing Primer binding site, 176-197 and pUC/M13 Forward Sequencing Primer binding site is 2949-2972.

2.15.5 Phylogenetic analysis

Sequence chromatographs were analysed using the chromas software package version 1.45 (http://www.technelysium.com.au/chromas.html). Closest relatives were identified by use of the NCBI database (http://www.ncbi.nlm.nih.gov/). All nucleotide sequences were aligned using ClustalX (Thompson et al., 1997) with sequences retrieved from the database. Alignments were edited manually using BioEdit Sequence Alignment Editor version 5.0.9 (Hall, 1999) and regions of ambiguous alignment removed. Guide trees were constructed using neighbour joining with the Jukes and Cantor correction algorithm in mega version 3.1 (Kumar et al., 2001) and the data bootstrapped 1000 times to assess support for nodes.

Chapter 3

Initial mineral experiments

3.1 Introduction

The initial experiments (results shown in appendix A) to determine the viability of microbially mediated hydrogen generation; by the addition of minerals to sediment slurries provided mixed results. The main aim of the initial magnetite experiments were to determine what effect temperature and particle size had on microbially driven hydrogen formation and utilisation. These initial experiments proved that processes such as acetogenesis, methanogenesis and sulphate reduction were effected by temperature and particle size, however, the effect that the mineral itself had on these processes could not be accurately determined. Therefore it was decided to broaden the range of minerals being used so as to compare our biotic experiments with previously published abiotic experiments with a range of iron minerals (Stevens and McKinley, 2000).The objective of these experiments was to demonstrate direct microbial involvement in hydrogen generation and to observe the effect of different mineral types on other relevant microbial processes such as acetogenesis methanogenesis and sulphate reduction.

3. 2 Mineral composition

Table 3.1 Minerals chosen for experimentation were the following

Mineral	Formula
Magnetite	Fe_3O_4
Hematite	Fe_2O_2
Pyrite	FeS_2
Pyrrhotite	FeS
Hornblende	$NaCa_2(Mg,Fe,Al)_5(Si,Al)_8O_{22}(OH_2)$
Ilmenite	$FeTiO_3$
Olivine	$(Mg,Fe)_2(SiO_4)$
Labradorite	$(Ca_{0.5}Na_{0.5})(Al_{0.5}Si_{0.5})AlSiO_8$
Olivine bombs (Hematisied Olivine)	$(Mg,Fe)_2(SiO_4)$
Basalt	Basalt from isle of Skye UK

Rationale for choosing the minerals selected were two fold, 1) to enable comparison with minerals studied previously under abiotic conditions (Stevens and McKinley, 2000) ,2) To investigate the effect of mineral composition by using a range of mafic and felsic mineral types. All minerals were analysed using XRD (appendix B) and ICP-OES (Table 3.2). With the exception of pyrite and pyrrhotite, where analysis was confined to XRD as analysis of high sulphur containing minerals by ICP-OES requires addition of extra flux and thus the loss of ability to detect minor compounds in the sample. Comparison of samples analysed by XRD and ICP-OES showed that the XRD analysis was consistent with major elements detected by ICP-OES.

Table 3.2. Mineral composition according to ICP-OES. In order of decreasing SiO$_2$

ICP-OES	SiO$_2$	TiO$_2$	Al$_2$O$_3$	Fe$_2$O$_3$	MnO	MgO	CaO	Na$_2$O	K$_2$O	P$_2$O$_5$	Total
Mineral	wt%	wt%	wt%	wt%	wt%	wt%	wt%	wt%	wt%	wt%	wt%
Labradorite	52.57	0.14	28.24	0.62	0.02	0.63	12.94	3.53	0.24	0.02	98.94
Hornblende	49.95	0.30	8.25	7.87	0.09	15.91	12.55	2.33	0.83	0.00	98.07
Basalt	47.50	1.61	15.52	12.62	0.17	7.45	9.91	1.96	0.23	0.13	97.11
Olivine	41.82	0.01	0.55	7.94	0.09	49.35	0.10	0.08	0.03	0.00	99.98
Olivine B	41.72	0.17	0.37	7.56	0.12	48.34	0.26	0.16	0.00	0.01	98.71
Hematite	20.53	0.79	17.76	54.12	0.04	1.81	4.94	0.29	0.90	0.23	101.41
Magnetite	2.57	0.05	1.05	99.49	0.18	0.36	0.25	0.23	0.30	0.00	104.48
Ilmenite	1.06	47.31	1.28	50.75	0.22	3.41	0.19	0.04	0.00	0.01	104.27
Silica	100.2	0.02	0.06	0.04	0	0	0.01	0.01	0.02	0	100.36

3.3 Experimental Setup

All incubations were set up according to master slurry description in Chapter 2. Initial experiments shown in appendix B were conducted in type 1 reaction vessels with 10 g/l of mineral addition. Experiments in this chapter were conducted using type 3 reaction vessels with a concentration of 100 g/l. of mineral. Minerals were reground and left for a period of 48 hrs before addition to slurry mix. At periodical intervals samples for gas, VFA, AODC and molecular analyses were taken. At each sampling event the amount of liquid or gas sampled was replaced by an equal amount of nitrogen to avoid the creation

of a vacuum. Incubation was at 60°C for 88 days except for hornblende, which had an

extra sampling point after 135 days.

3.4 Results Section
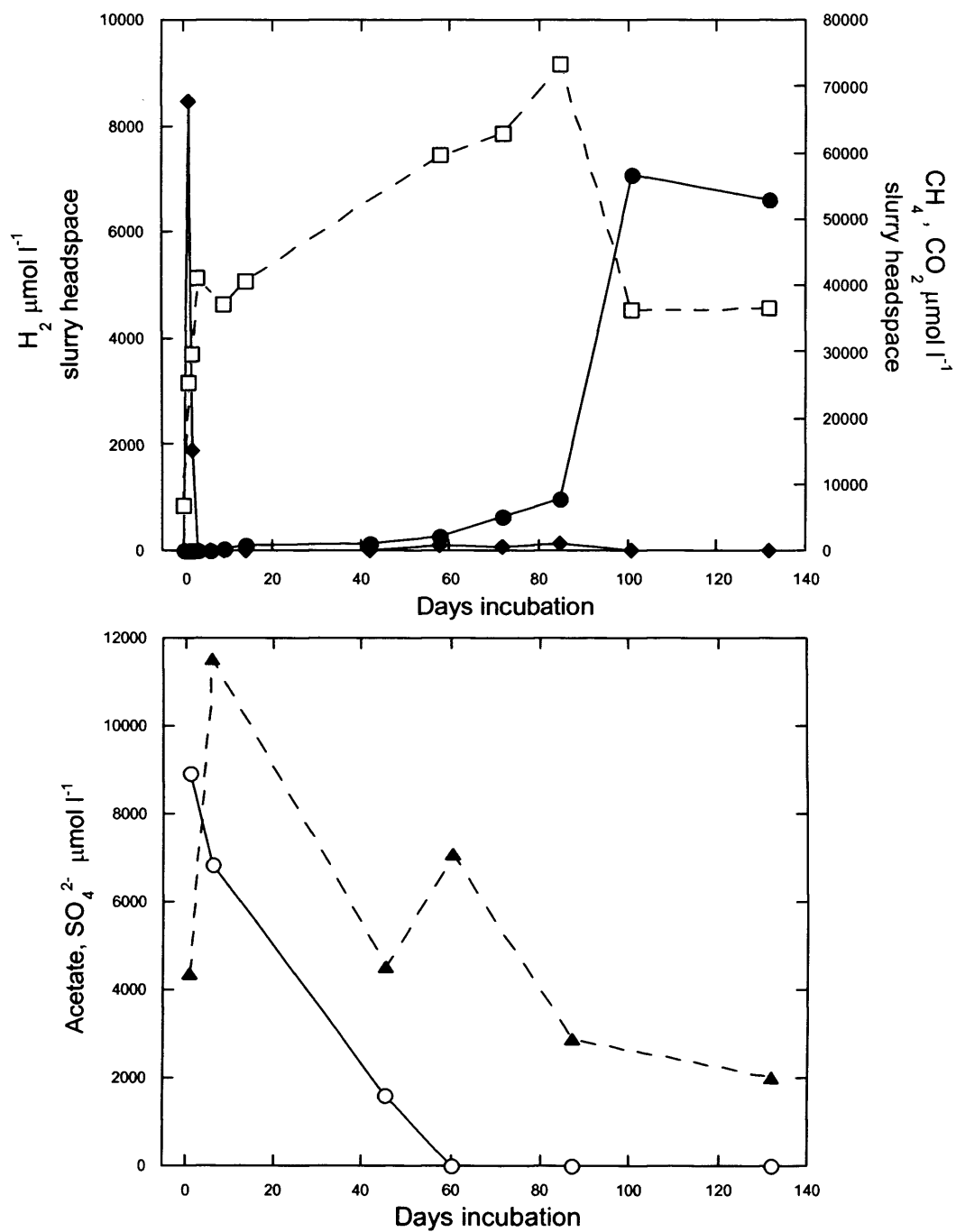
Fig 3.1. Hornblende incubation
Key: CH_4 (●), CO_2 (□), H_2 (◆), Acetate (▲) and SO_4^{2-} (○)
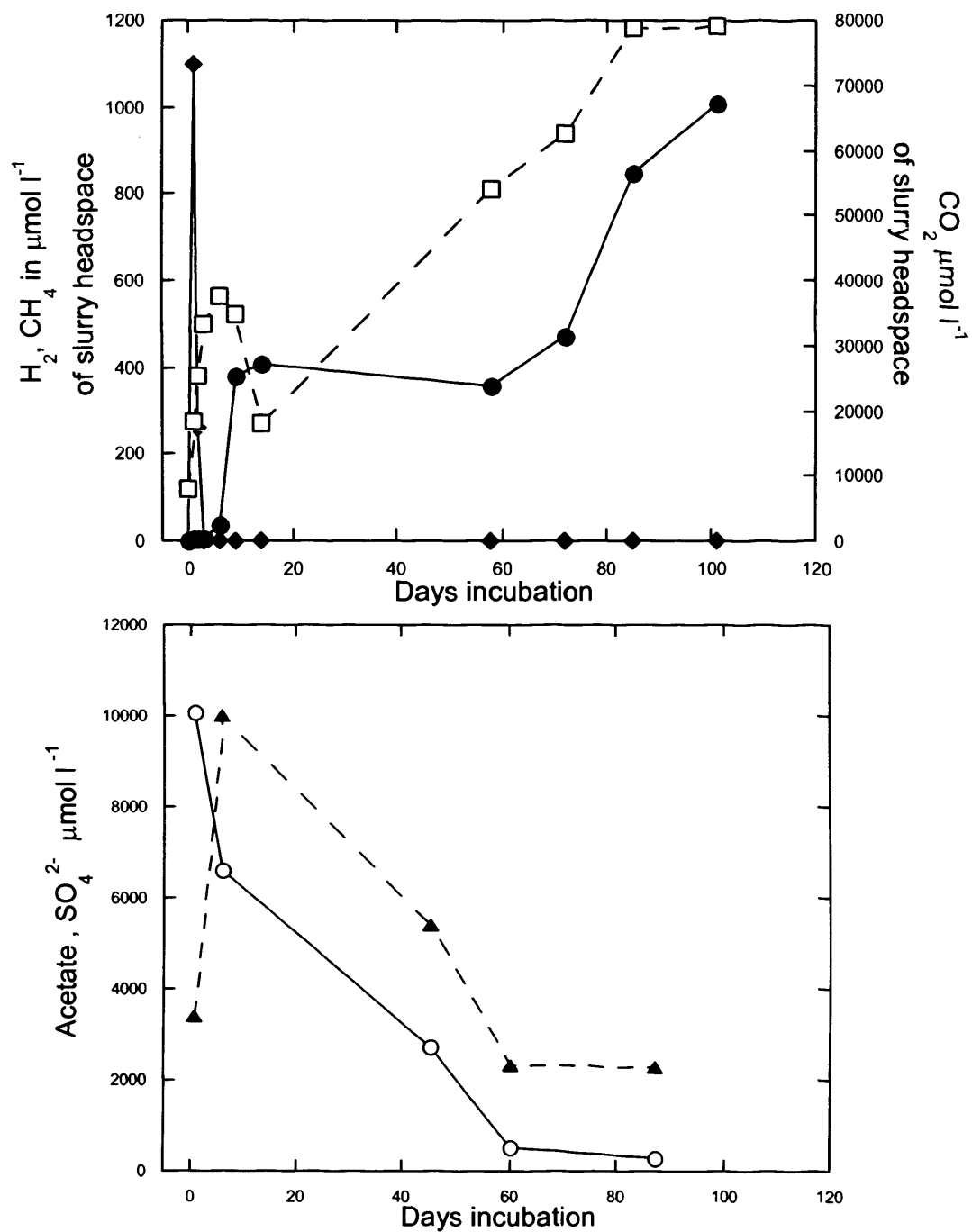
Fig3.2 Ilmenite incubation.

Key: CH_4 (●), CO_2 (□), H_2 (◆), Acetate (▲), and SO_4^{2-} (○)
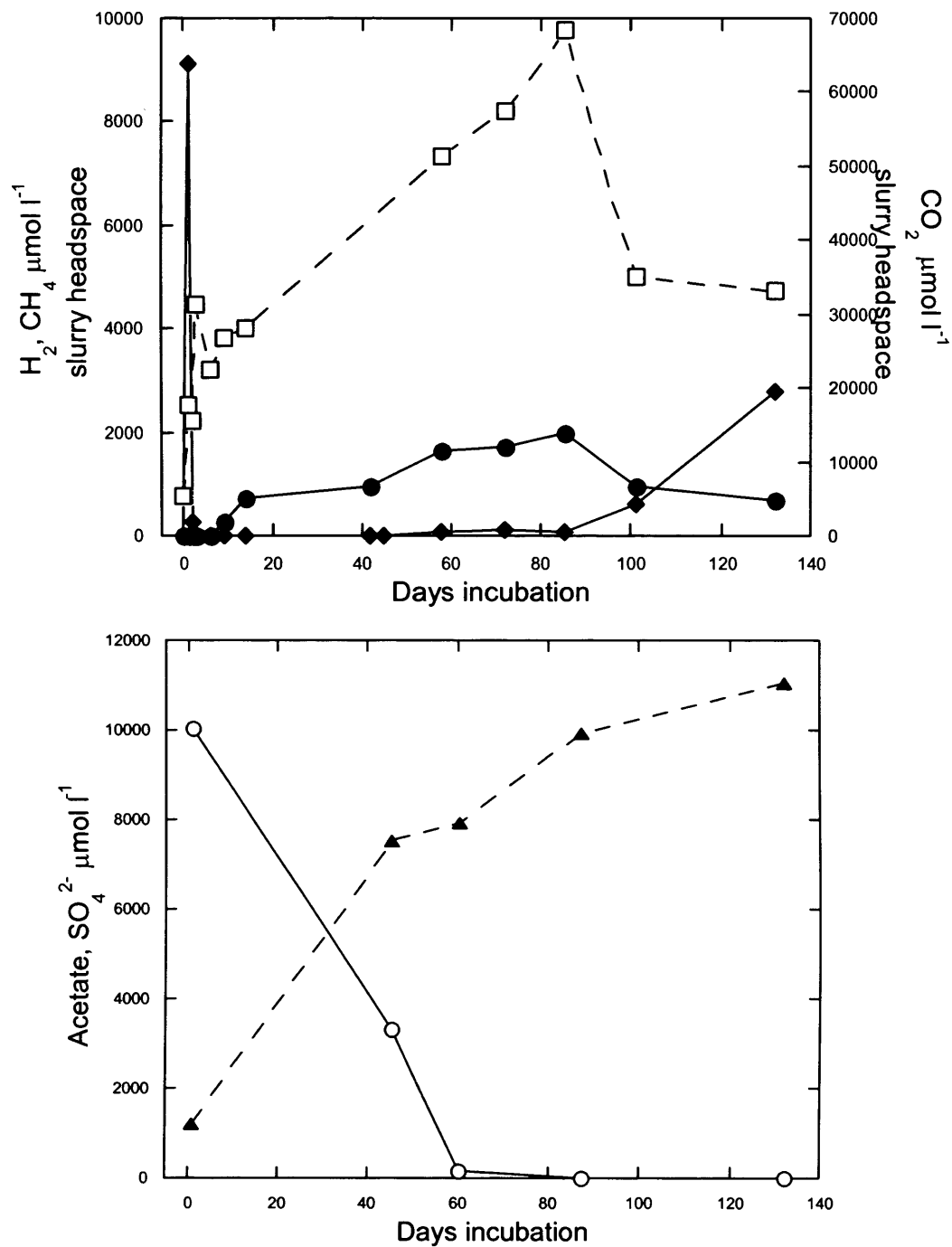
Fig 3.3 Olivine Incubation.
Key: CH_4 (●), CO_2 (□), H_2 (◆), Acetate (▲), and SO_4^{2-} (○)
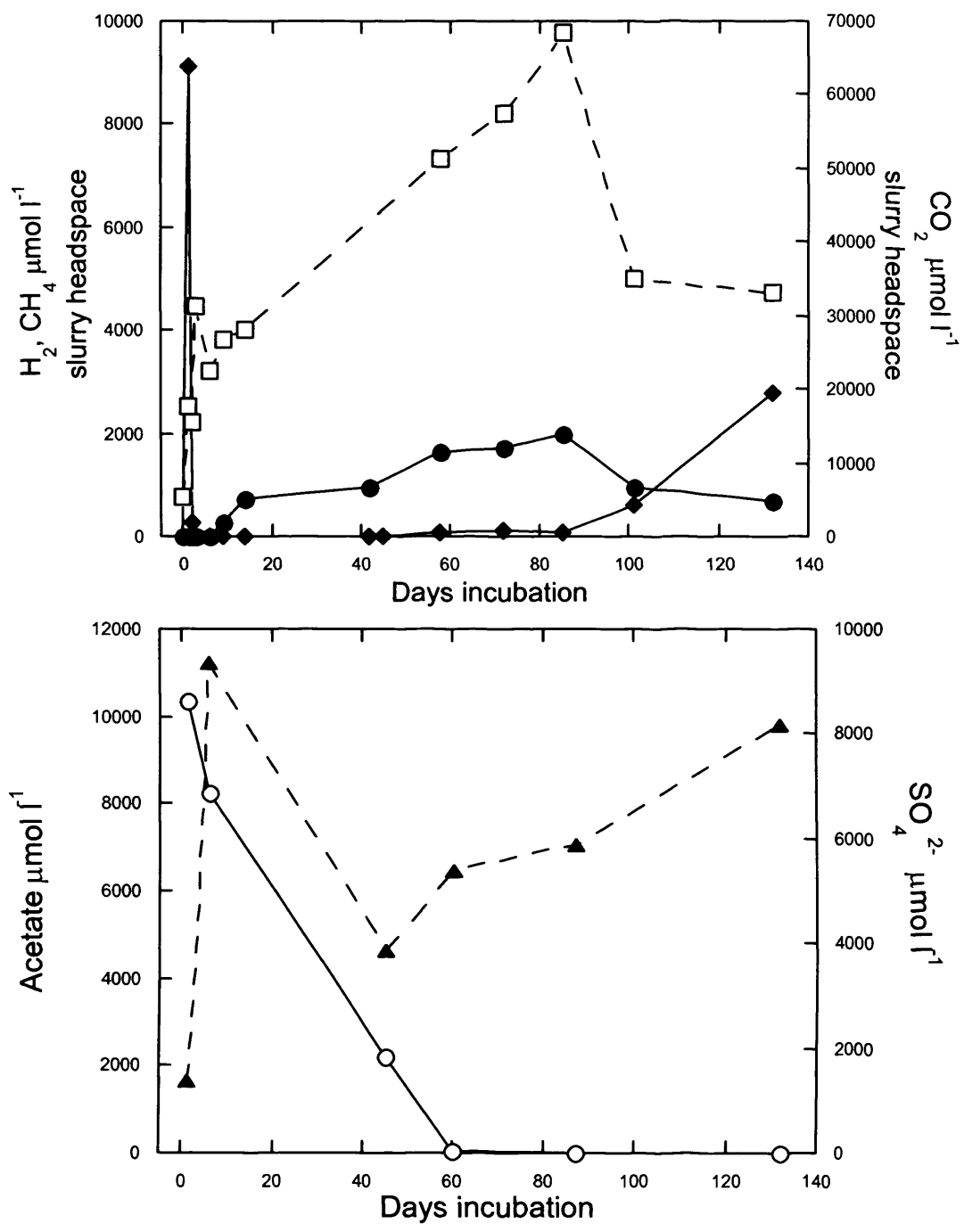
Fig 3.4 Olivine bombs incubation.
Key: CH_4 (●), CO_2 (□), H_2 (◆), Acetate (▲) and SO_4^{2-} (○)

3.5 Results: Hornblende, Ilmenite, Olivine and Olivine bombs

3.5.1 Hornblende (Fig 3.1)

Incubation with hornblende showed significant concentrations of hydrogen generated over the first 3 days (max of 8451 µmol l^{-1}). After which, hydrogen levels rapidly decrease reaching levels below detection limit by day 5. This initial hydrogen spike co-occurs with a rapid increase in carbon dioxide to 40.8 mmol l^{-1}. Once hydrogen concentrations drop below the detection limit, carbon dioxide slowly increases until day 85 reaching a maximum of 73.19 mmol l^{-1}. Before decreasing by 36.9 mmol l^{-1} to 36.29 mmol l^{-1} at day 101 and remaining stable thereafter until the termination of the experiment (132 days). This CO_2 decrease coincides with a rapid increase in methane from 7.918 mmol l^{-1} at day 85 to 56.6 mmol l^{-1} at day 101 (a 7-fold increase). Methane then remains stable from 101 to 132 days. Initially methane concentrations remained low, reaching a concentration of 1101 µmol l^{-1} after 20 days. Once sulphate depletion occurs methane starts to increase reaching a maximum concentration of 56.6 mmol l^{-1} by day 85. Sulphate concentrations have a start value of 8.94 mmol l^{-1} and show a stepwise decrease over the course of the experiment until depletion occurs at day 60. The start of sulphate removal mirrors the decrease in hydrogen at the beginning of the experiment. Acetate values show an initial rapid increase over the first 6 days from a start value of 4.3 mmol l^{-1} to 11.5 mmol l^{-1} this is then followed by a gradual decrease to 2.01 mmol l^{-1} after 132 days. A slight increase is noted around the 60-day mark, 4.5 to 7.06 mmol l^{-1} this transitory peak in acetate occurs when sulphate reduction stops and is a possible indication of previous acetate utilisation during sulphate removal.

3.5.2 Ilmenite (Fig 3.2)

During ilmenite slurry incubations, high amounts of hydrogen were formed over the first 3 days, with a maximum of 1097 µmol l^{-1} at day 2 (which is 7.7 times lower than hornblende), which decreased below the detection limit by day 5. Carbon dioxide shows a rapid initial increase to 37.5 mmol l^{-1} (day 7) decreasing to 18.1 mmol l^{-1} by day 15

before a gradual increase, to plateau at 73.9 mmol l^{-1} after 85 days. The initial drop in carbon dioxide values co-occurs with increases in methane concentrations from 35 μmol l^{-1} to 407 μmol l^{-1} between day 6 to day 14 (an 11 fold increase). Methane then remains stable until day 60 before beginning a gradual increase to 1010 μmol l^{-1} after 101 days, which is 56 times less than hornblende. Unusually methane production occurs in the presence of high sulphate concentrations and active sulphate reduction. This is unusual as sulphate reducers can out compete methanogens for competitive substrates. Occurrence of both processes may indicate that they are using differing substrates or that competitive substrates are being supplied in excess. Sulphate has a start value of 10.08 mmol l^{1} and gradually decreases over the course of the incubation however, sulphate is never fully removed reaching a minimum value of 270 μmol l^{-1} after 87 days incubation (removal of 9.8 mmol l^{-1}). Acetate values show a initial rapid increase from 3411 μmol l^{-1} (day 2) to 10 mmol l^{-1} (day 7) this is the maximum value obtained and concentrations slowly decrease to a minimum value of 2288 μmol l^{-1} after 87 days.

3.5.3 Olivine (Fig 3.3)

Olivine incubation experiment shows a rapid initial increase in hydrogen values reaching 9137 μmol l^{-1} (day 2) before dropping below the detection limit by day 4. However unlike the previous experiments, hydrogen levels slowly start to increase again around day 72 from 110 μmol l^{-1} to 2775 μmol l^{-1} after 135 days. This increase in hydrogen begins 12 days after sulphate depletion. Sulphate has a start value of 10 mmol l^{-1}, removal starts immediately until depletion at day 85. Again similar to ilmenite methane is formed during active sulphate reduction. Methane slowly increases to a maximum value of 1988 μmol l^{-1} (day 85) which is 28 times less than hornblende, decreasing then to 695 μmol l^{-1} (day 132). This decreases in methane co-occurs with an increase in hydrogen and decrease in carbon dioxide. Carbon dioxide shows an initial rapid increase coinciding with the observed initial H_2, reaching 31.34 mmol l^{-1} after 4 days. Before gradually increasing further to 68.37 mmol l^{-1} at day 85 then decreasing to 33.2 mmol l^{-1} at 132 days.

Acetate concentrations unlike ilmenite, hornblende start at a relatively low level 1184 μmol l^{-1} and continue to rise throughout the experiment, which is in contrast to the decreasing concentrations found in the hornblende and ilmenite. Final acetate concentrations were 11.02 μmol l^{-1} after 132 days.

3.5.4 Olivine bombs (Fig 3.4)

Olivine bomb addition results are not surprisingly quite similar to Olivine. As they are both chemically similar according to ICP-OES analysis (Table 3.2). Similar to all four mineral additions covered in this section an initial rapid increase in hydrogen occurs over the first 3 days reaching a maximum of 8898 μmol l^{-1} (day 2), decreasing below detection limit by day 6. Like Olivine but unlike ilmenite and hornblende detectable hydrogen reappears at day 85 increasing to 1089 μmol l^{-1} by day 132. Carbon dioxide levels increase rapidly reaching a maximum of 24.80 mmol l^{-1} by day four followed by a dip to 7864 μmol l^{-1} by day 14. CO_2 gradually increases until day 85 (62.87 mmol l^{-1}), after 85 days carbon dioxide decreases similar to olivine coinciding with a noticeable increase in hydrogen values and a decrease in methane. Methane production also co-occurs with sulphate reduction; methane gradually increases to 2409 μmol l^{-1} at day 85 decreasing after to 695 μmol l^{-1} at 132 days. Sulphate levels starts at 8.6 mmol l^{-1} and decrease gradually to 110 μmol l^{-1} at day 60 before full depletion at day 87. Acetate formation is slightly different than the olivine incubation. Initial rapid increase occurs over the first 7 days with an increase of 9.56 mmol l^{-1} to11.21 mmol l^{-1}, this decreases to 4625 μmol l^{-1} at day 46 gradually increasing again to a final value of 9801 μmol l^{-1} after 132 days.
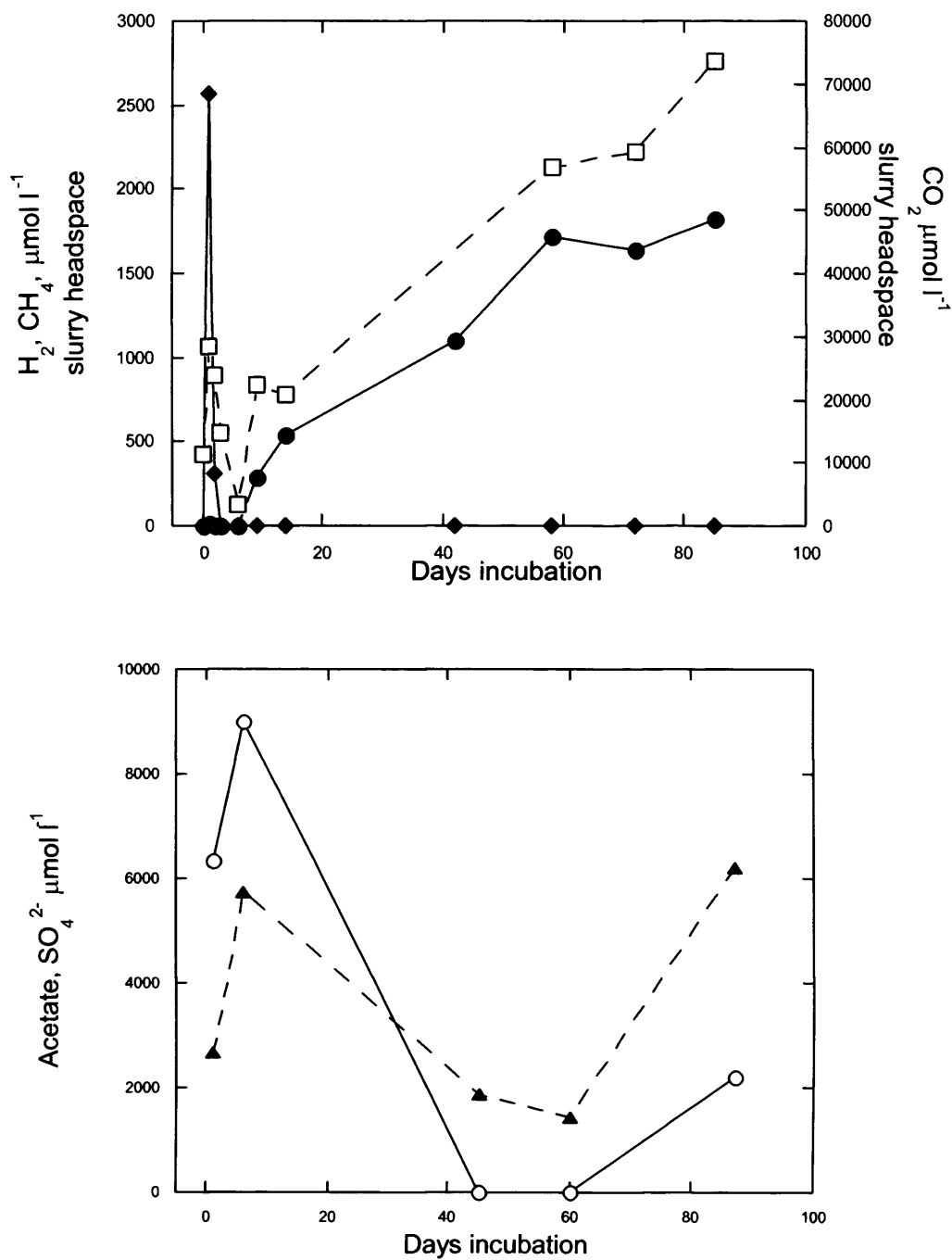
Fig 3.5. Labradorite incubation.

Key: CH_4 (●), CO_2 (□), H_2 (◆), Acetate (▲) and SO_4^{2-} (○)
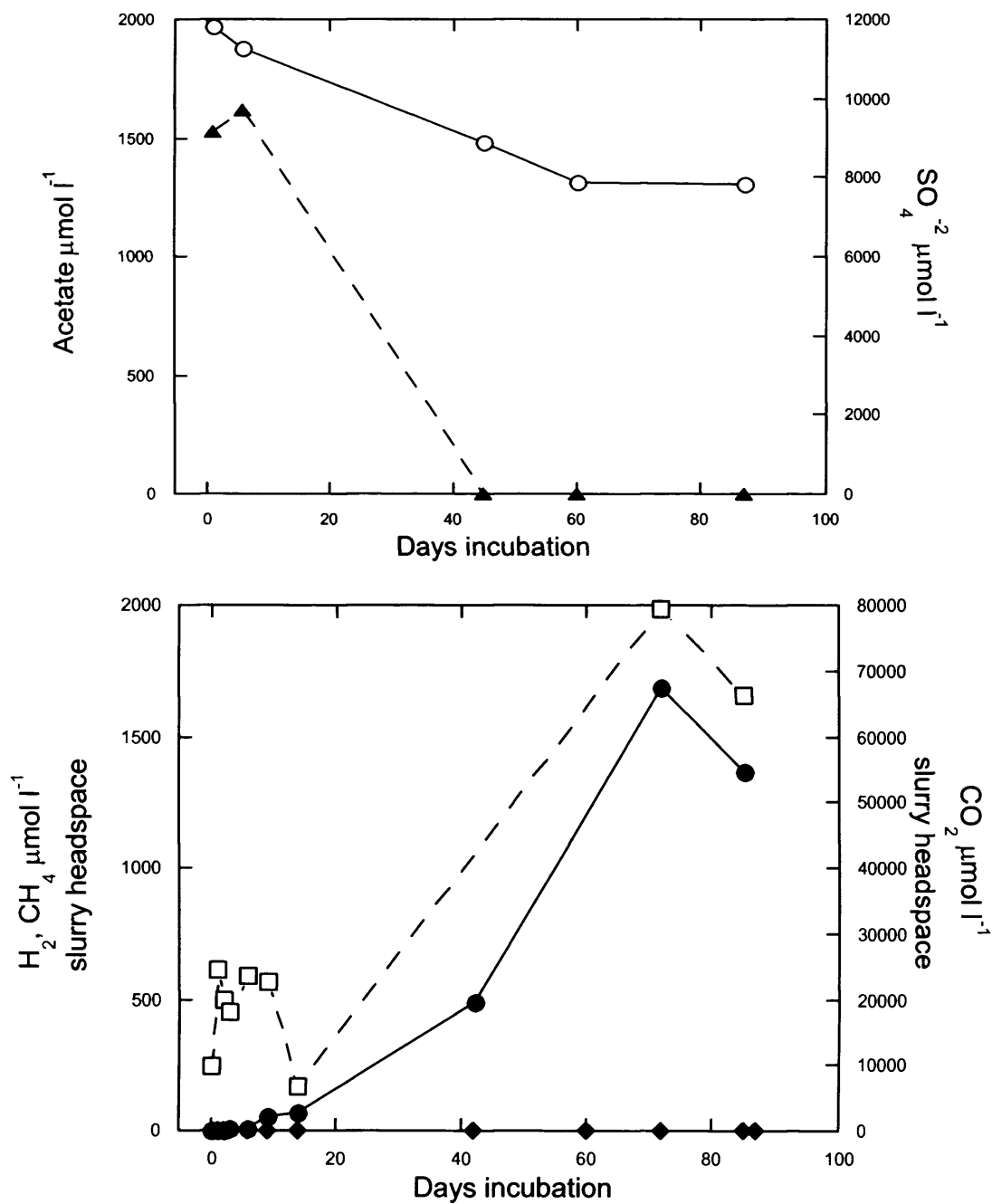
Fig 3.6. Hematite incubation.

Key: CH_4 (●), CO_2 (□), H_2 (♦), Acetate (▲) and SO_4^{2-} (○)
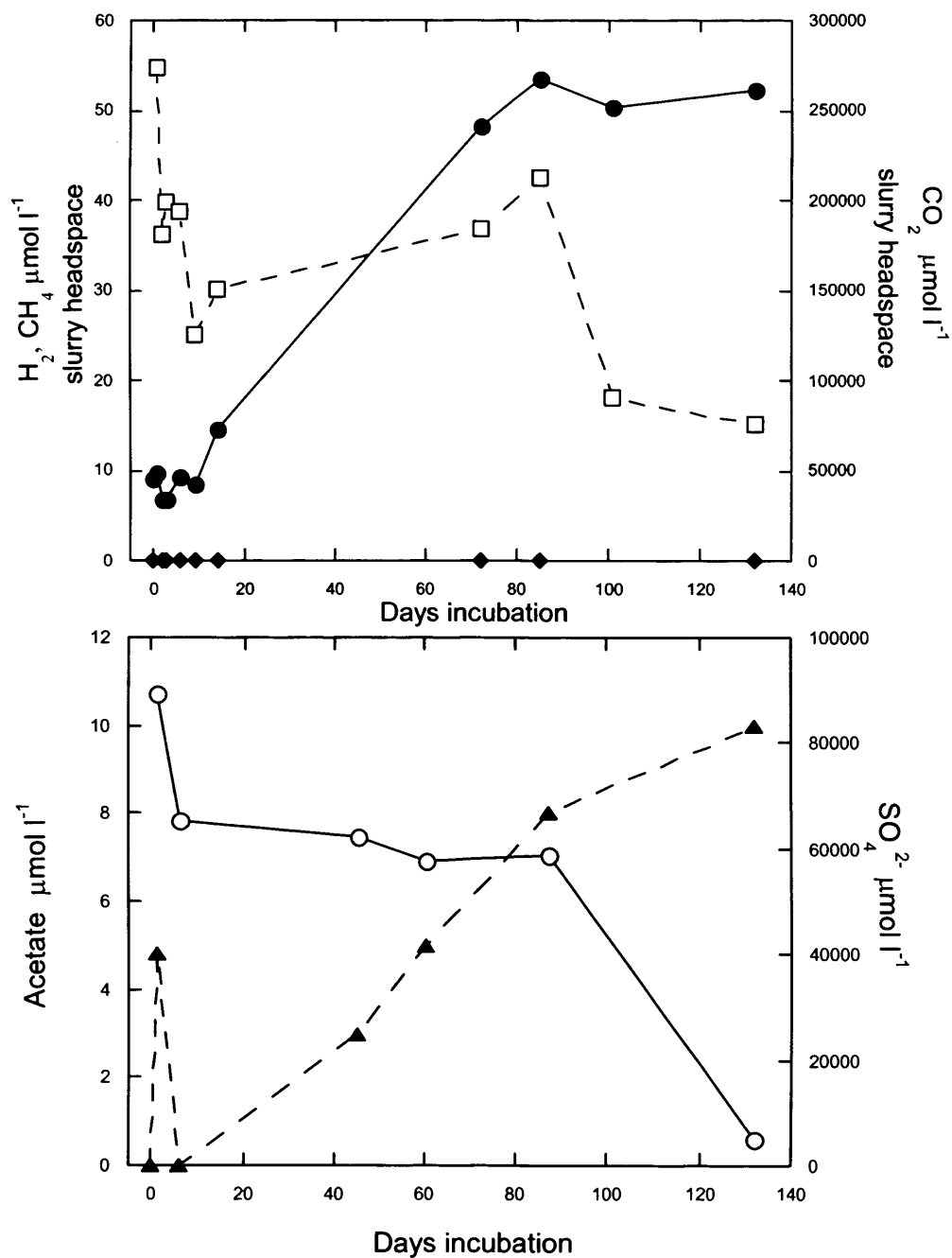
Fig 3.7 Pyrite incubation

Key: CH_4 (●), CO_2 (□), H_2 (♦), acetate (▲) and SO_4^{2-} (○)
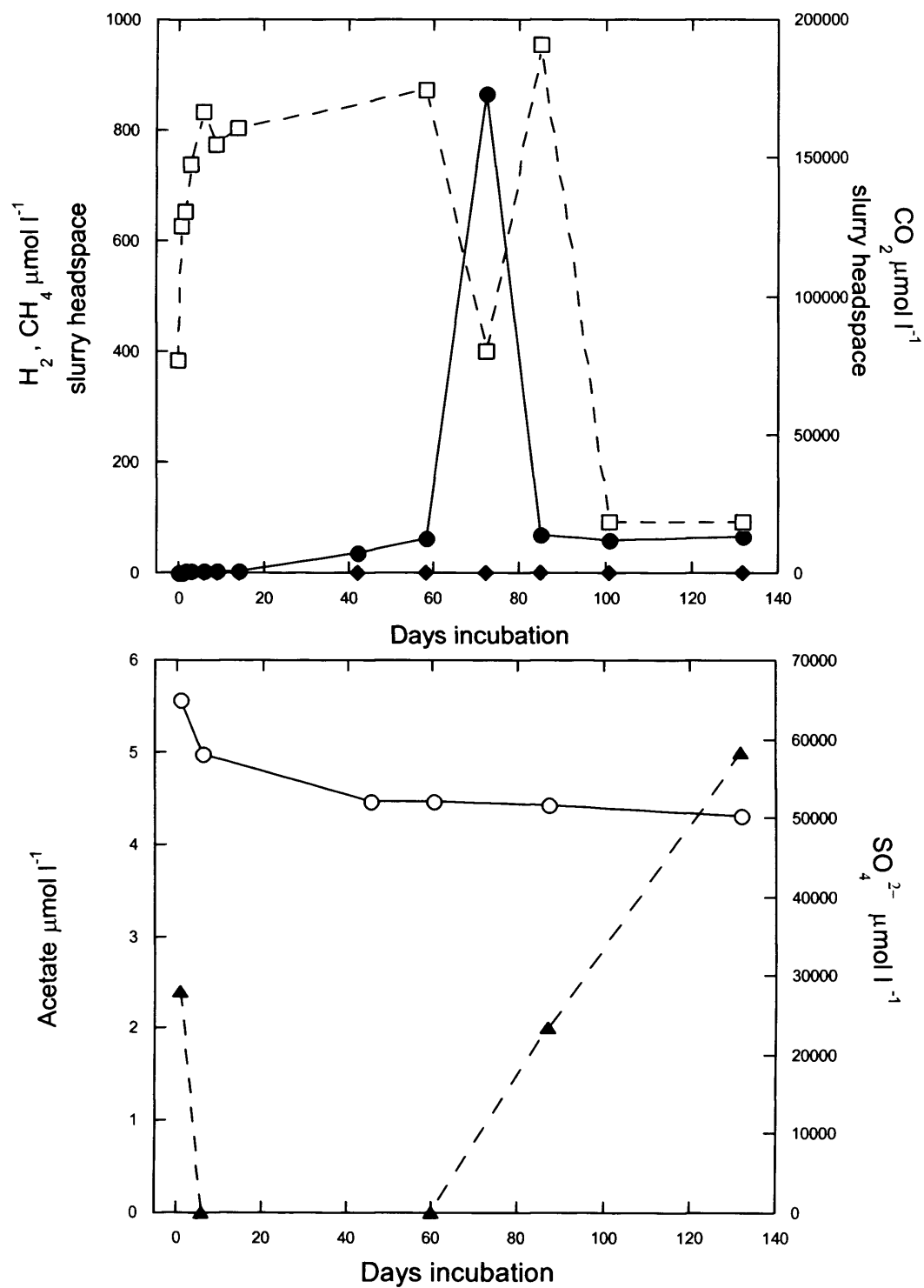
Fig 3.8. Pyrrhotite incubation.

Key: CH_4 (●), CO_2 (□), H_2 (◆), Acetate (▲) and SO_4^{2-} (○)
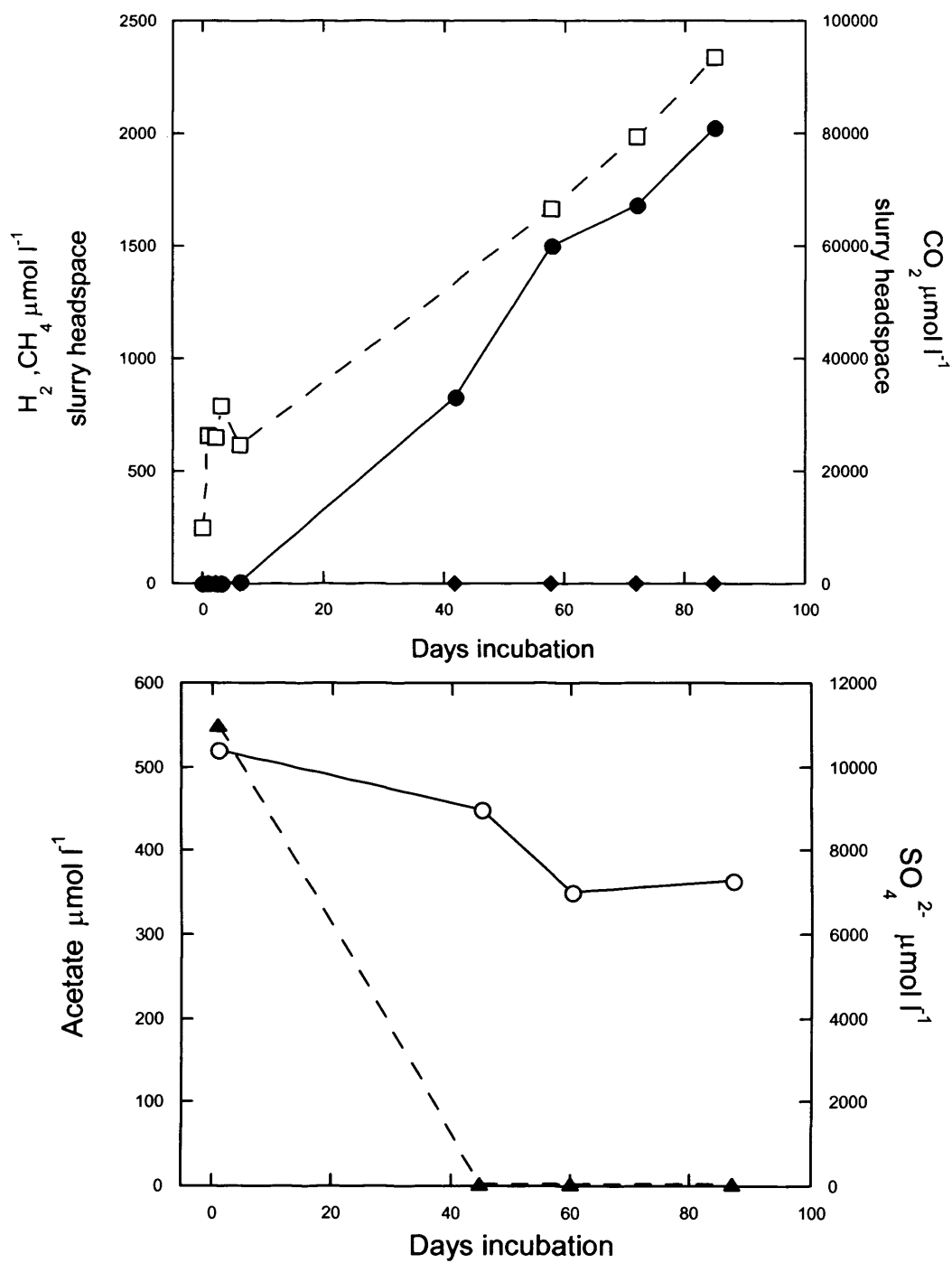
Fig 3.9 Basalt incubation.

Key: CH_4 (●), CO_2 (□), H_2 (◆), acetate (▲) and SO_4^{2-} (○).

3.4 Results: Labradorite, hematite, pyrite, pyrrhotite and basalt

3.6.1 Labradorite (Fig 3.5)

Labradorite incubation shows, initial rapid hydrogen formation (max of 2560 μmol l^{-1}) which decreases below the detection limit by day 4 and remains at this level over the course of the experiment. Carbon dioxide also shows a rapid initial peak reaching 28.2 mmol l^{-1} by day 2 then decreasing to 3.4 mmol l^{-1} at day 6. CO_2 then gradually increases throughout the remainder of the experiment to a maximum of 73.55 mmol l^{-1} after 85 days. Methanogenesis commences at day 6 when carbon dioxide is at its lowest concentration (3419 μmol l^{-1}) and methane concentrations steadily increases to a maximum of 1822 μmol l^{-1} after 85 days of incubation (31x less than hornblende). Methane production co-occurs with sulphate reduction and high sulphate concentrations. Sulphate concentrations are initially at 6350 μmol l^{-1}, unusually the second sampling point is higher (9.1 mmol l^{-1}), this second sampling point is close to the start concentrations for other incubations and perhaps the initial sulphate point is the result of some sort of sampling error. Sulphate reduction begins after this point and is depleted by day 45, much more rapidly than many of the other minerals such as ilmenite and hornblende where depletion only occurred after 60 days. However at the 87 day sampling point there is an increase in sulphate, this can happen if some O_2 was introduced into the system at the precious sampling point, however, the fact that methane and carbon dioxide levels do not change seems to rule this out. They do however stop increasing temporarily. Acetate values increase from a start value of 2655 μmol l^{-1} to 5721 μmol l^{-1} after 7 days. Then steadily decreasing until day 60 after which, time similar to sulphate, an increase occurs from 1420 μmol l^{-1} to 6214 μmol l^{-1}.

3.6.2 Hematite (Fig 3.6)

Hematite incubation was different to previous incubations. No hydrogen was detected throughout the course of the experiment and complete SO_4^{2-} removal does not occur. Also carbon dioxide levels do not initially increase as rapidly reaching a peak of

24.28 mmol l^{-1} then decreasing to 6667 μmol l^{-1} by day 14. Subsequently CO_2 levels increase again to an overall maximum of 79.42 mmol l^{-1} at 72 days before decreasing to 66.13 mmol l^{-1} after 85 days (Despite high SO_4^{2-}). Methane values start to increase at day 4 from 4 μmol l^{-1} to a maximum of 1684 μmol l^{-1} after 72 days, decreasing slightly towards the end of the experiment to a final concentration of 1368 μmol l^{-1} after 85 days. Sulphate start concentration was 11.9 mmol l^{-1}, sulphate reduction began immediately and continued until 60 days before stabilising at 7.91 mmol l^{-1}. This possibly occurs shortly after the time that acetate becomes depleted. Sulphate final concentration was 7.83 mmol l^{-1}, a removal of 3.44 mmol l^{-1}. Acetate levels increase slightly at the beginning from a start value of 1526 μmol l^{-1} to 1615 μmol l^{-1}, after 6 days of incubation. Then acetate becomes depleted by day 45.

3.6.3 Pyrite (Fig 3.7)

Pyrite mineral incubation also produced no detectable hydrogen, neither was there an initial rapid increase in carbon dioxide, as seen in other incubations e.g. ilmenite (10 mmol l^{-1} to 30 mmol l^{-1} in 6 days). However, initial concentrations were high in comparison (273 mmol l^{-1}). Carbon dioxide decreases to 125 mmol l^{-1} by day 9, (-16.4 mmol l^{-1} day). Then increases to 212.5 mmol l^{-1} by day 85, before decreasing to 75.4 mmol l^{-1} (day 132). The carbon dioxide concentration changes, seems overall to be related to the sulphate reduction profile. Methanogenesis occurs during active sulphate reduction and methane concentrations gradually increase to 53 μmol l^{-1} by day 85, plateauing for the remainder of the experiment (Day 132). The amount of methane formed is considerably less than other experiments e.g. 1684 μmol l^{-1} maximum in hematite.

Initial concentrations of sulphate in this incubation, and the pyrrhotite incubation, are very high in comparison to all other incubations (pyrite 89.4 mmol l^{-1} and pyrrhotite 65 mmol l^{-1}, compared to 11.2 mmol l^{-1} for hematite), such high levels seem to be a direct result of the crushing process. Exposure of freshly crushed pyrite surfaces to the atmosphere (O_2) may release previously oxidised compounds $S^{2-} \rightarrow SO_4^{2-}$. This can be

limited by speeding up the transfer process between crushing and slurry addition, and this problem was not as pronounced during later pyrite thermal gradient experiments. Sulphate reduction begins immediately lowering the sulphate concentration from 89.4 mmol l^{-1} to 65.1 mmol l^{-1} by day. The sulphate concentration then stabilises and remains more or less constant until day 87 (58.9 mmol l^{-1}) Rapid sulphate removal occurs between day 87 and day 132 (down to 5.1 mmol l^{-1}) . This rapid onset of sulphate reduction is contiguous with a decrease in carbon dioxide, and this was unexpected since CO_2 is a product of sulphate reduction. Total sulphate removed over the incubation period is large, 84.3 mmol l^{-1} over 132 days.

Acetate values initially peak to 4 μmol l^{-1} then dips to 0 μmol l^{-1} before increasing gradually to finish at 10 μmol l^{-1} by day 132. Acetate and methane amounts produced are low, with start concentrations for acetate much lower than previous incubations.

3.6.4 Pyrrhotite (Fig 3.8)

Similarly pyrrhotite incubation shows no measurable hydrogen production. Carbon dioxide increases rapidly initially from 76.88 mmol l^{-1} day 1 to 166.38 mmol l^{-1} after 6 days. Carbon dioxide levels then more gradually increase to 174.44 mmol l^{-1} by day 58. After this point a rapid dip occurs down to 80.16 mmol l^{-1} before increasing again to 190.87 mmol l^{-1}. This dip in CO_2 coincides with a sharp peak in methane values, potentially indicating H_2/CO_2 methanogenesis. Carbon dioxide again decreases to 18.56 mmol l^{-1} by 100 days and then remains constant. Initially methane concentrations remain low, increasing slowly from 4.5 to 63 μmol l^{-1} over the first 58 days. Then there is a peak in methane formation at day 72 to 865 μmol l^{-1}. After this methane decreases and levels of to 65 μmol l^{-1} after 132 days.

Sulphate levels are initially high starting at 65.02 mmol l^{-1}, this is again possibly due to the crushing and powdering process before addition, possibly due to S^{2-} oxidation as mentioned in the pyrite results. Sulphate reduction occurs immediately with rapid sulphate removal occurring over the first 45 days (13 mmol l^{-1}) sulphate removal then slows with only 1.6 mmol l^{-1} removed over the remaining 87 days finishing at 50.34

mmol l^{-1} (day 135). Complete sulphate removal does not occur, hence the peak in CH_4 occurs in the presence of high methane concentrations. Acetate concentrations are very low with a maximum of 5 μmol l^{-1} during the course of the experiment (day 132). An initial ~2 μmol l^{-1} occurs at the start, this decreases to 0 μmol l^{-1} by day 6 and remains at zero until after day 60 by day 87 acetate concentrations had reached 2 μmol l^{-1} and further increases to 5 μmol l^{-1}. Again the dominant process is sulphate reduction total removal of 14.67 mmol l^{-1} (0.111 mmol l^{-1}/day)

3.6.5 Basalt (Fig 3.9)

With basalt mineral addition, no hydrogen was observed during the experiment. Carbon dioxide promptly increases from 9820 μmol l^{-1} to 31.629 mmol l^{-1} by day 4. Then gradually increases during the course of the incubation reaching a maximum of 93519 μmol l^{-1} (day 85). A small dip in CO_2 concentrations occurs at day 6 (6998 μmol l^{-1}) coinciding with the onset of methane formation. Methane formation begins at day 6 and increases gradually to 2023 μmol l^{-1} (day 83). Methanogenesis occurs during active sulphate reduction. Sulphate reduction is not as rapid as in the previous two mineral incubations (pyrite and pyrrhotite). The start value for sulphate is much lower at 10.40 mmol l^{-1}. Sulphate reduction begins immediately reaching 7010 μmol l^{-1} (day 60). Sulphate is not however, completely removed as it levels and increases slightly to 7270 μmol l^{-1} (day 85). This increase at the end of a long incubation may be the result of O_2 entering into the reaction vessel (through a leak) or during sampling. However, both methane and carbon dioxide concentrations do not change making a strong argument against this. Acetate concentrations have a start value of 549 μmol l^{-1} reaching zero by day 45. Depletion of acetate precedes the cessation of sulphate reduction, by aprox a 15-day lag, but due to lack of sampling this may have been much longer.

3.7 AODC Counts

All Experiments were counted after 65 days of incubation using acridine orange direct count technique. Interestingly, the number of prokaryotes present was similar in all cases

except for the basalt experiment, which was slightly lower. This is irrespective of the differing rates of methanogenesis, sulphate reduction and acetogenesis and H_2 generation.

Table 3.3 AODC bacterial numbers of varying mineral incubations, after 65 days of incubation.

Sample	95%CL	Totals/ ml
Hornblende	0.104	2.23×10^8
Pyrohotite	0.069	2.31×10^8
Ilmenite	0.473	1.90×10^8
Hematite	0.099	1.92×10^8
Olibomb	0.0230	3.72×10^8
Basalt	0.051	4.24×10^8
Olivine	0.063	5.10×10^8
Pyrite	0.273	4.07×10^8
Labrodorite	0.048	2.45×10^8

3.8 Sterile controls

Sterile controls were run for all individual mineral experiments in order to demonstrate whether prokaryotes could influence H_2 from mineral: water reactions, that have previously been considered to be purely abiological processes. Sterilisation was carried out as described in chapter 2. Minerals were powdered and treated in the same way as the biotic experiments. Triple autoclaving was chosen due to previous experience, that in certain circumstances single autoclaving of bulk sediment was not enough to fully sterilise. This was shown by sulphate reduction occurring in initial sterile controls (data not presented in this study) after 20-30 days of incubation.

Only the graphs for the hornblende sterile incubation are being shown here with the remainder of the data presented in the appendix. This is because all the data was similar with no noticeable difference and hornblende is a good example of the overall trend.
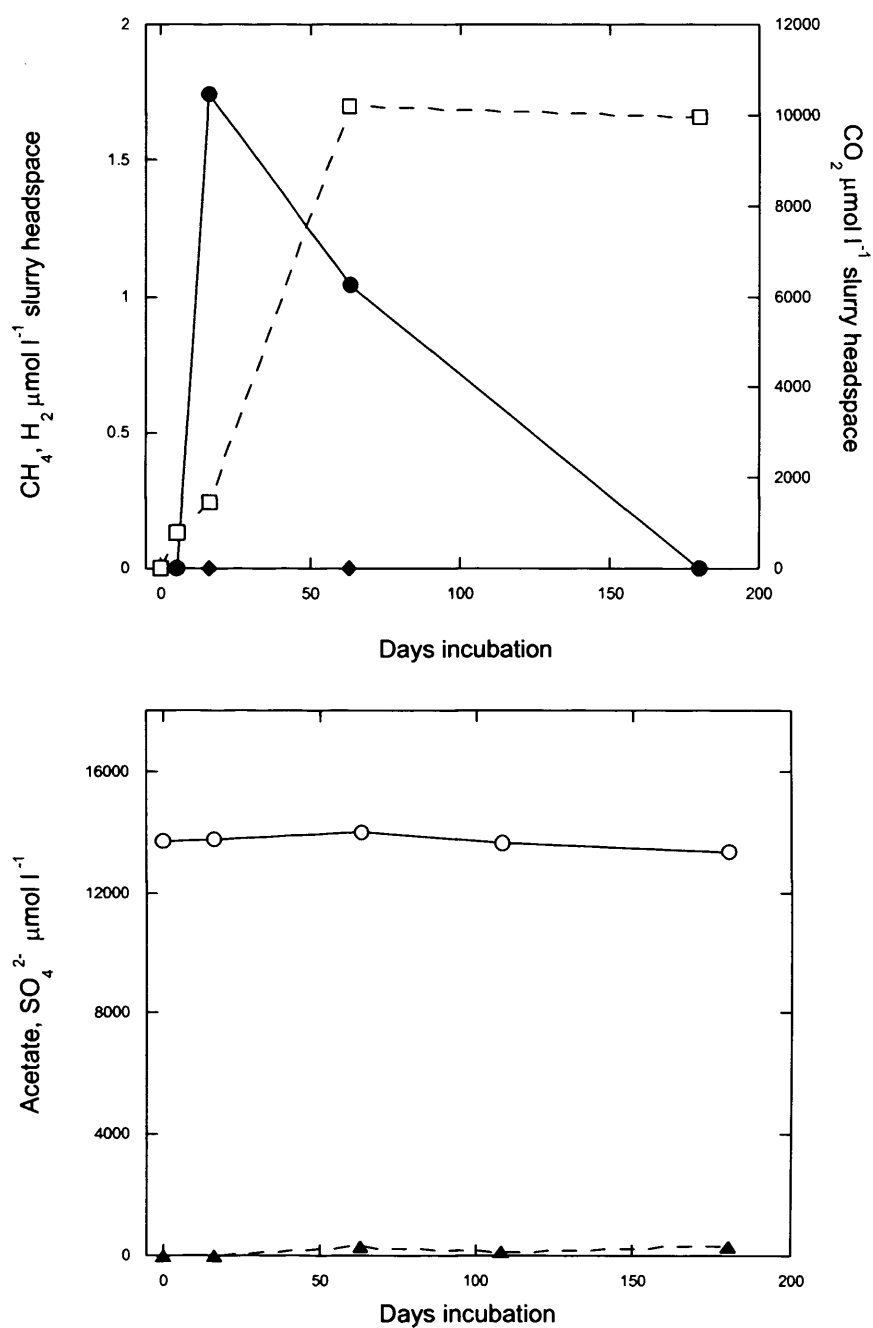
Fig 3.10 Hornblende sterile control.

Key CH_4 (●), CO_2 (□), H_2 (♦), acetate (▲) and SO_4^{2-} (○)

Hornblende sterile control results shown (Fig 3.10) were run over a longer incubation period than the any of the abiotic experiments (182 days). This was to ensure that even if abiotic reactions were slower than biotic reactions, sufficient time was provided to detect chemical changes. No hydrogen was detectable. Trace amounts of methane (1.7 μmol l^{-1}) were formed over the first 3 days before decreasing to zero after 182 days. No significant acetate formation occurred, with a concentration of 7-15 μmol l^{-1} throughout the course of the experiment. This was still higher than detected in the pyrite and Pyrrohotite experiment. No sulphate reduction takes place. There is some variability in sulphate values, however, this is within analytical error. All other sterile controls also showed no significant methane acetate or hydrogen formation and absence of sulphate reduction over 182 days incubation at 60°C.

3.9 $\delta^{13}C$-CH_4 isotope data.

Isotope $\delta^{13}C$-CH_4 analysis was performed on specific mineral incubations, in order to better understand methanogenic processes occurring during mineral incubation. Gas samples were taken from all mineral incubations. However, instrument constraints meant only samples with CH_4 concentrations in excess of 800 ppmv could be used.

Table 3.4 isotope data for selected samples

Sample	$\delta^{13}C$-CH_4 (‰)	SD (‰)	
Hornblende	-78.7	0.2	H_2/CO_2
Olivine	-46.7	2.1	
Olivine bombs	-55.3	0.1	
Basalt	-51.8	0.4	Acetate or
Hematite	-47.4	0.4	mixed
Pyrite	-57.8	1.4	
Ilmenite	-60.6	5.3	

SD= Standard Deviation.

There is a surprising range of $\delta^{13}C$-CH_4 values for the different minerals incubated under identical conditions, all were characteristic of biogenic methane formation. This difference in values is a reflection of the differing biogeochemical process occurring to produce the methane A detailed diagram of methane sources and isotopic composition is shown in Fig 1.7. Values seem to group together as follows 2 values between 40‰, which are close to, the thermogenic zone and 50‰, 3 values between 50‰ and 60‰, 2 values 60 ‰ plus. This shows that depending on the mineral under incubation a different metabolic pathway may be followed i.e. Acetoclastic methanogenesis and H_2/CO_2 being the main pathways however other substrates can be used e.g. methyl substrates such as methanol,(eg *Methanosphaera stadtmaniae*) and other CO_2 type substrates such as formate and carbon monoxide. Overall it would seem mineral composition effects substrate formation, which in turn effects substrate used for methanogenesis.

3.10 Molecular analysis

Samples were taken for molecular analysis after 80 days incubation.　　　DNA extraction was as described in Chapter 2. DNA extraction was diluted 1 in 10 for archaeal amplification and 1 in 50 for bacterial amplification this was found to give the best results in terms of ease of product amplification.

Primers used were Bacterial 27F-907R nested with 357F-518R.Archaeal 109F-958R nested with Parch –Saf. Samples were run on a 30-60% denaturing gradient gel for profiling of different sequences by DGGE.

To compare community profile in each of the samples. Bands were excised and amplified using M13F GC, followed by sequencing in the Cardiff University-sequencing core.
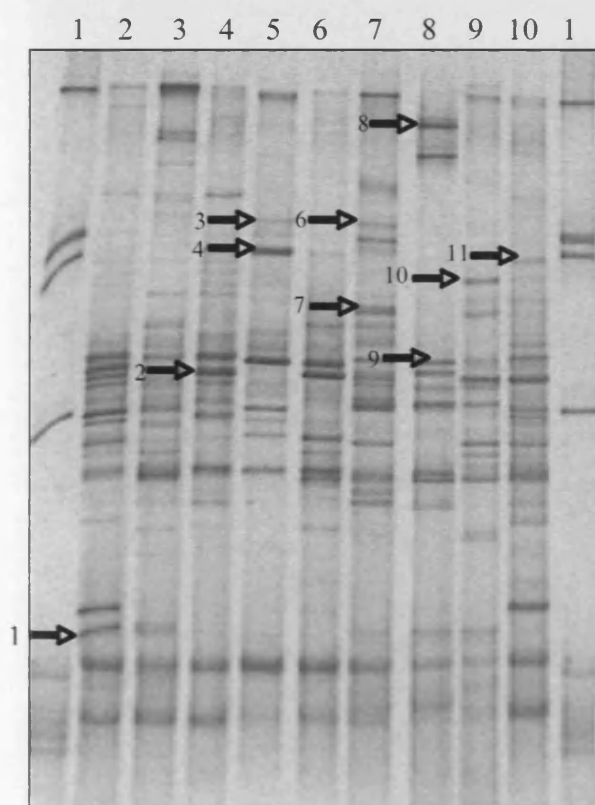
Fig 3.11 Bacterial DGGE profile　　　　**Fig 3.12 Archaeal DGGE profile**
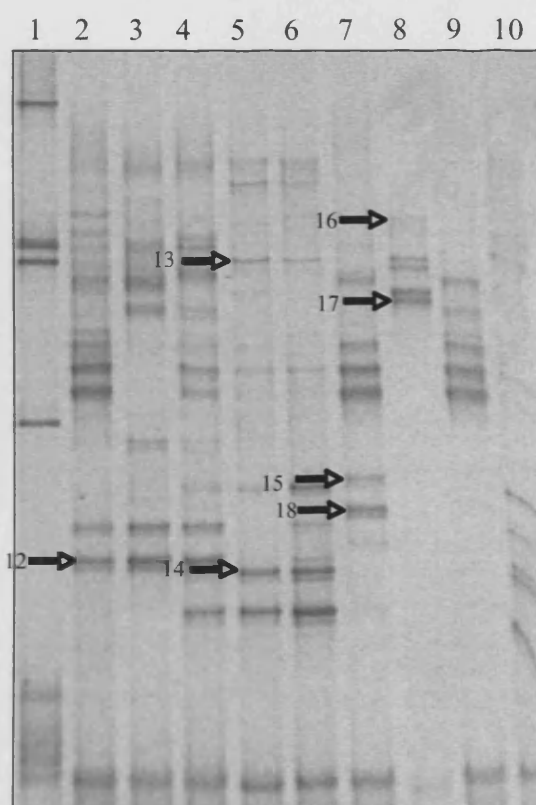
Key on following page.

Key for Figs 3.11 and 3.12
1) Marker   6) Pyrite
2) Basalt   7) Pyrrhotite
3) Olivine   8) Labradorite
4) Olivine Bombs   9) Hematite
5) Hornblende   10). Ilmenite
Numbers with arrows shows bands excised and sequenced.

The following tables shows the molecular match's of the excised bands. In both archaeal and bacterial DGGE gels. Substantially more bands were excised and sequenced than are shown here however not all were of the desired quality especially many of the bacterial sequences; all bands that are included in this study were over 100 bps. Expected Size of DGGE product was 200 bp.

Table 3.5 Bacterial sequences Fig 3.11

Number	Nearest match by Blastn search (Accession number)	Sequence Similarity (%)	Phylogenetic affiliation	Isolation environment nearest match
1	*Thermosyntropha lipolytica* (X99980)	83%	*Syntrophomonadaceae*. *Thermosyntropha*	Bioreactor co-culture With methanogen
2	Uncultured vent bacterium ML-8 (AF209003)	98%	*Candidate division OP9*	Hydrothermal Vent
3	Thermotogales bacterium Ag55 (AB260049)	83%	*Thermotogales*	Hydrothermal vent
4	Thermotogales bacterium Ag55 (AB260049)	92%	*Thermotogales*	Hydrothermal vent
5	Thermotoga thermarum (AB039769)	91%	*Thermotogales. Thermotoga.*	High temperature oil reservoir
6	Beta proteobacterium PCSC1 (AF411828)	97%	*Proteobacteria: Betaproteobacteria*	Unknown
7	Bacillus sp. OS-ac-18 (U46747)	100%	*Firmicutes*	Hot Spring
8	uncultured Methylococcaceae bacterium clone Elev_16S_1037 (EF019533)	97%	*Gammaproteobacteria: Methylococcales:*	Soil sample
9	Uncultured actinobacterium clone R61-03-00r09 (DQ316867)	98%	Actinobacteria	Microbial communities contaminated Subsurface sediments
10	Uncultured delta proteobacterium clone PA74 (AY771988)	100%	*Deltaproteobacteria*	Tidal flats (Wadden Sea)
11	Moorella sp. enrichment clone R65 (DQ533547)	100%	*Clostridia: Thermoanaerobacteriales*	Petroleum reservoir

Table 3.6 Archaeal sequences Fig 3.12

Number	Nearest match by Blastn search (Accession number)	Sequence Similarity (%)	Phylogenetic affiliation	Isolation environment of nearest match
12	Aciduliprofundum boonei strain T469 (DQ451875)	97%	*Euryarchaeota; Aciduliprofundum*	Hydrothermal vent system
13	Uncultured Thermoplasmatales archaeon clone GoM HDA-13 (AY542186)	97%	*Euryarchaeota; Thermoplasmatales*	Gulf of Mexico Gas hydrate
14	Uncultured archaeon clone: IAN1-62 (AB175594)	96%	*Euryarchaeota; Methanococcales*	hydrothermal vent field
15	Uncultured archaeon clone NAK1-a1 (DQ867048)	100%	*Methanobacteriales*	High temperature natural gas field
16	Uncultured archaeon clone SBAK-shallow-40 (DQ640171)	96%	*Thermoplasmatales*	Subsurface sediment estuarine sediment
17	Uncultured archaeon clone SBAK-shallow-40 (DQ640171)	97%	*Thermoplasmatales*	Subsurface sediment estuarine sediment
18	Uncultured archaeon clone NAK1-a1 (DQ867048)	96%	*Methanobacteriales*	High temperature natural gas field

It can be seen by visual analysis of both gels that the community structure is significantly different depending on mineral type. This is a reflection of the different rates of biogeochemical processes occurring during the incubation, such as sulphate reduction, methanogenesis, acetogenesis despite being common to all. Also it maybe that these biogeochemical reactions are catalysed by different prokaryotes depending on mineral type, or a reflection of different prokaryotes involved in additional mineral specific reactions.

The community structure within the bacterial community appears to be more complex than the archaeal, at 60°C however the effect of primer bias must be taken into account on all DGGE profiles especially towards archaea (Teske and Sorensen, 2008). Thus it appears the dominant community may be bacterial. Species diversity reflected that commonly found in the deep biosphere sediments mostly from high temperature hydrothermal environments. This gave added confidence that our approach could be taken as a true refection of prokaryotic composition of our high temperature incubations, which had been inoculated with Guaymas hydrothermal sediment. It must also be stated that 97% similarity equates to species level, 95% equals genera and less than 95% is indicative of novel genera. Sequence data from bands extracted and analysed (and

deemed to be of acceptable quality) showed *Thermotogales* related species was one of the dominant bacterial species to occur. *Thermotogales* is a branch of the *Eubacteria* consisting of only three genera: *Thermotoga*, *Thermosipho*, and *Fervidobacterium*. All of these organisms are extremophiles. Members of the *Thermotogales* are strictly anaerobic growing optimally at neutral pH. The hyperthermophilic species *T.maritima* and *T. neapolitana* grow at a maximum temperature of 90°C and an optimum around 80°C (Huber and Stetter, 1992 (a)), these are the highest growth temperatures in this order. *Thermotogales* are organotrophs, fermenting simple and complex carbohydrates with end products of acetate, ethanol, carbon dioxide and hydrogen formed when grown on glucose (Huber and Stetter, 1992 (B)). Members of the *Thermotogales* are often found in high temperature hydrothermal vents sediments and deep-sea sediments.

Other species that feature prominently are the *Firmicutes*. *Firmicutes* are Gram positive of which the *Clostridia* are a sub division. In several hydrogen producing bioreactor systems *Clostridia* were found to be the dominant species. Gram positive *proteobacteria* belonging to the *Beta, Gamma* and *Delta* divisions were also present. *Betaproteobacteria* are often associated with degradation of organic matter and are known to be facultatively anaerobic. *Gammaproteobacterial* species *Methylococcales* was also found, these are methanotrophs, which gain energy and carbon through the oxidation of methane. However, all species so far have been found to be aerobic. This sequence was only 97% related to *Methylococcales* over a 200 bp product, so it is possibly a related anaerobic species. *Deltaproteobacteria* contain the sulphate reducing bacteria and iron reducing species e.g. (*Geobacter*). Other recognised sequences were related to the *Thermosytropha,* which is a thermophilic fatty acid oxidising bacteria however the % similarity is very low 83%, so no physiological relationship can be inferred. Related sequences to the *Thermoanaerobacteriales* (100%) were also found which is a member of the *Clostridia*. Unfortunately description of the most closely related match is unpublished, however the most closely related isolated member to our sequence is *Moorella glycerini*. Which is a moderate thermophilic homoacetogen with optimum growth at 58°C and pH 6.8 (Slobodkin et al., 1997). Subsurface *Thermoanaerobacter* species have been isolated from the marine subsurface that are also capable of metal reduction. Using H_2 acetate and other compounds at optimal

temperature of approx 60°C (Roh et al., 2002) Sequences similar to candidate division OP9 were also found however very little is know about this division apart from its association with deep sea hydrothermal vent systems (possible relationship with candidate division JS1). Some of the matches had a low percentage similarity this is perhaps a reflection of the presence of novel species not so far incorporated into the BLAST database.

The Archaeal community structure appears to be not as complex as the bacterial community. A change in composition is notable with varying mineral type with methanogen species such as *Methanococcales* (found in hornblende and pyrite, unusual as methane levels are low in pyrite) *Methanococcales* contain such species as *Methanococcus jannaschii* which is a thermophile and produces methane through H_2/CO_2 methanogenesis(Jones et al., 1983) and *Methanobacteriales* (most pronounced in labradorite and pyrrhotite incubations) the most common exponent of this species is *Methanobacterium thermoautotrophicum* which is an Archaeon that grows optimally at ~65°C it is an "absolute" autotroph, requiring only CO_2, H_2 and salts for growth (Zeikus, 1972). Other archaeal species were related to the *Thermoplasmatales* and *Aciduliprofundum boonei* (found in basalt, olivine and olivine bombs). *Thermoplasmatales* (present in all, differing species but all *Thermoplasmatales* related) often associated with sulphur respiration at elevated temperatures. *Aciduliprofundum boonei* is the only isolated representative of phylogenetic DHVE2 cluster, it has been shown to be an obligate thermoacidophilic sulphur and iron reducing heterotroph, capable of growing from pH 3.3 to 5.8 and between 60 and 75°C (Reysenbach et al., 2006) perhaps this strain is capable of growing at neutral pH.

The molecular data is consistent with a thermophilic archaeal community being active in the mineral slurry experiments.

3.11 Activation of mineral surfaces versus non-activation

In previous publications (Kita et al., 1982; Stevens and McKinley, 2000) it has been indicated that the fresh grinding of minerals plays a major role in hydrogen generation. In the initial magnetite experiments (appendix A), minerals were left for approx 96 hours after grinding before addition to the master slurry. No hydrogen was generated and processes such as sulphate reduction and acetogenesis were slow by comparison to other experiments. In the previously described 60°C experiments minerals were left for approximately 16 hours before addition. An initial experiment was conducted comparing freshly re-ground minerals less than 10 minutes between grinding and addition, with minerals that had been ground and stored for 3 months (aerobically) in order to directly quantify the effect of fresh grinding on the initial stages of biotic mineral reactions. Slurries were set up and incubated at 60°C with the two varying mineral treatments. The following graphs show the results. (Fig 3.13a/3.13b)
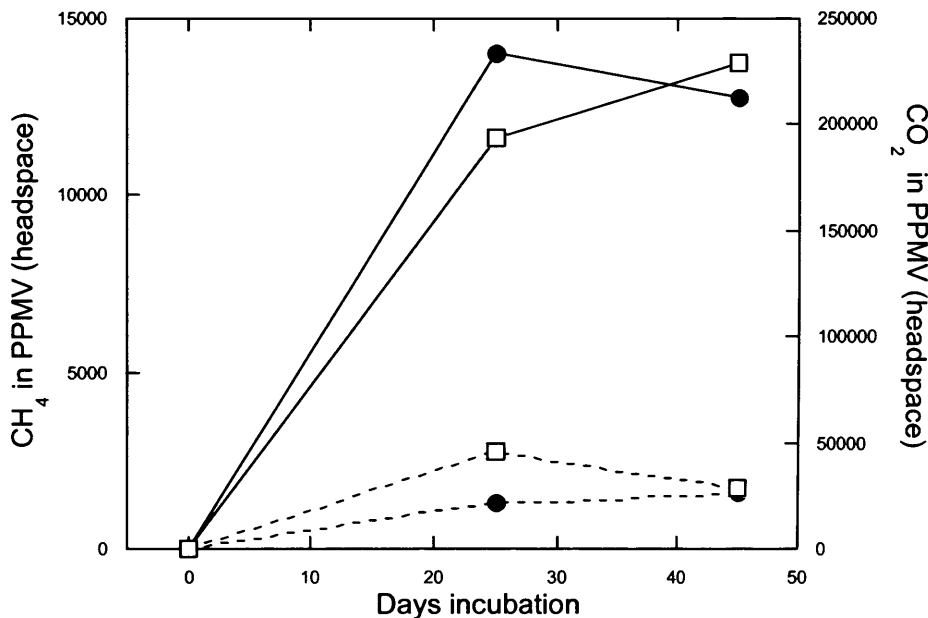
Fig 3.13 (a)Hornblende incubation fresh grinding versus no grinding, gas results
Key: CH₄ (●) CO₂ (□) dashed line no re-grinding, Solid line fresh grinding.
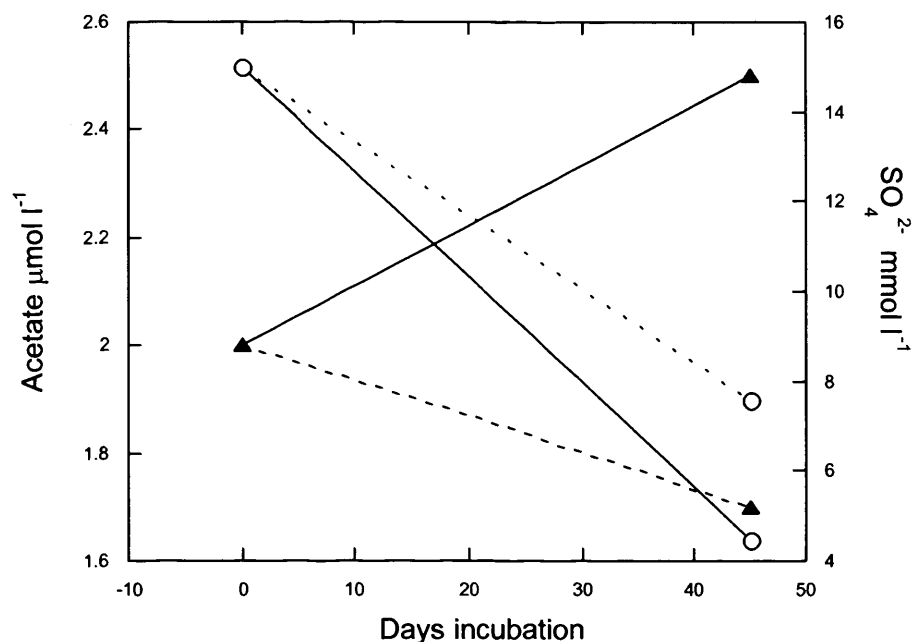
**Fig 3.13b hornblende incubation fresh grinding, versus no grinding
(B) Acetate (▲), SO_4^{2-}(O).Fresh grinding solid line, No re-grinding
dashed line.**

The two graphed results (Figs 3.13(a)/(b)) using hornblende at 60°C shows a clear grinding effect. Fresh grinding of minerals in the presence of prokaryotes substantially speeds up reactions, such as methanogenesis and sulphate reduction, as well as increasing the production of carbon dioxide. No hydrogen was detected. Gas results shows methane concentrations increase to 14017 ppmv over the first 25 days in the freshly ground slurry (FG) with the non-reground minerals (NG) reaching only 1333 ppmv. A 10.5 fold increase in methane production rates. Methane levels plateau after this with a final value of 12798 ppmv for FG minerals and 1602 ppmv for NG minerals after 45 days. Carbon dioxide levels similarly differ with a difference of 147987 ppmv after 25 days (FG 194000 ppmv, NG 46013 ppmv) final carbon dioxide levels reach 229000 ppmv and 29055 ppmv for FG and NG minerals respectively, a 7.8 fold difference in production. Gas production is between 7 and 11 times faster in slurries with freshly ground minerals than without.

Rates of sulphate removal also differed; sulphate start values were identical for both. Sulphate started at 15 mmol l^{-1} after 45 days incubation FG minerals sulphate levels were at 4.46 mmol l^{-} (10.54 mmol l^{-} removed) and NG slurries were at 7.57 mmol l^{-} (7.43 mmol l^{-1} removed). Gives you a rate of removal of 0.234 mmol l^{-1} per day for FG slurry and 0.168 mmol l^{-1} per day for NG slurry. Acetate levels start at the same concentration however acetate values increase in FG slurry from 2 μmol l^{-1} to 2.4 μmol l^{-1} and decreases to 1.75 μmol l^{-1} in NG slurry. The amount of acetate produced is very low and one should not read to much into such low levels of acetate formation and removal.

The following table shows the data for the other mineral incubations used for grinding analysis ilmenite and olivine.

Table 3. 7 Grinding experiment ilmenite and olivine results

Mineral	Days	Methane (ppm)	Carbon Dioxide (ppm)	Acetate μmol l^{-1}	Sulphate mmol l^{-1}
Ilemnite (FG)	0	0	0	1	15.01
Ilemnite (FG)	25	10272	1.96E+05	na	na
Ilemnite (FG)	45	9483	2.19E+05	5.6	4.76
Ilmenite (NG)	0	0	0	1	15.01
Ilmenite (NG)	25	1434	51691	na	na
Ilmenite (NG)	45	511	41192	1.7	6.72
Olivine (FG)	0	0	0	1	14.2
Olivine (FG)	25	9807	1.56E+05	na	na
Olivine (FG)	45	10453	2.19E+05	122	3.62
Olivine (NG)	0	0	0	1	14.2
Olivine (NG)	25	977	53678	na	Na
Olivine (NG)	45	317	36837	15	6.4

FG= Fresh grinding, NG=No grinding

Table 3.7 clearly shows the difference in rates of methanogenesis sulphate removal and acetogenesis for olivine and ilmenite. The following is an approximate difference in changes between FG and NG slurries for both mineral types:

a) Ilmenite, CH_4 FG greater by 18 fold, Carbon dioxide by 5, sulphate removal by 1.5 and acetate formation by 5.

b) Olivine, FG greater than NG for methane by 32 fold increase. Carbon dioxide by 5, Acetate formation 8. Sulphate removal 2 fold.

Grinding also affected the $\delta^{13}C$ values of the methane produced.

Table 3.8 δ^{13}C values for methane from grinding experiment.

Sample	δ^{13}C-CH$_4$	SD
	(‰)	(‰)
Olivine (FG)	-50.7	0.6
Hornblende (FG)	-57.4	0.5
Hornblende (NG)	-77.4	1.5

FG=Fresh grinding and NG= no grinding

Methane production was too low in the other samples for isotopic analysis. No results were obtained for ilmenite incubation as a failure of the reaction vessel prior to sampling caused less methane to be present than was required for analysis. The results show a marked difference in δ^{13}C-CH$_4$ values for hornblende depending on grinding or non-grinding of fresh mineral surfaces. However all values are indicative of biogenic methane formation. But the lighter values for the hornblende NG incubation would be consistent with greater CH$_4$ from H$_2$/CO$_2$. The heavier values for hornblende FG are more consistent with acetoclastic methanogenesis. Unfortunately due to limited data it is not known whether this is true for other minerals.

3.12 Inhibition experiments

Inhibition experiments were conducted to determine immediate substrates for the key anaerobic reactions of sulphate reduction and methanogenesis. This is a well-used approach in anaerobic microbial ecology and works on the following principle. Molybdate, chromate, tungstate and selenate are analogs of the sulfate ion which inhibit sulfate reduction with the approximate order of effectiveness. CrO$_4^{3-}$> MoO$_4^{2-}$= Wo$_4^{2-}$> SeO$_4^{2-}$ (Taylor and Oremland, 1979) but molybdate is the most commonly used inhibitor. Molybdate enters cells via a sulphate transport system and interferes with the formation of adenosine phosphosulfate (APS), leading to deprivation of reduced sulphur compounds for growth. It forms adenosine phospho-molybdate in the cell. Without the presence of a stable intermediate like APS, the next sequential enzymatic step cannot occur.(Eq 3.1) and substrates that would have been used by sulphate reducing bacteria accumulate.

$$APS + 2e^- \rightarrow AMP + SO_3^{2-} \textbf{(Eq 3.1)} \text{ (Oremland and Capone, 1988)}$$
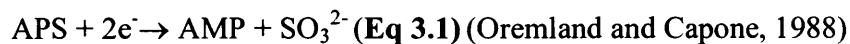
Addition of molybdate to the slurry, is at the concentration of SO_4^{2-} present.

Methane inhibition occurs by means of addition of 2-bromoethanesulfonic acid (BES) which is a structural analogue of meraptoethanesulfonic acid (which is the co-factor known as "HS-coenzyme M" (CoM)) . CoM is associated with the terminal methylation reactions involved in methanogenesis, including methyl-CoM reductase enzyme complex from which methane is evolved. Uptake of BES inhibits methanogenesis and substrates that would have been used by methanogens accumulate.

It has been found that 70μm BES blocked all methane on *Methanosarcina* sp grown on acetate. (Smith, 1978) and is Usually effective when added in excess of 0.1mM (Oremland and Capone, 1988)

A point to remember is that too long specific inhibition may cause feed back inhibition, as substrates accumulate, of the producing prokaryotes.

3.13 Sulphate inhibition of basalt mineral incubation at 60 °C

Sulphate inhibition was achieved through the addition of molybdate (MoO_4^{2-}) Addition concentration was the *in situ* concentration of sulphate at, in this case 3 mmol l^{-1} at the start of inhibition. Inhibition was started when sulphate reduction was well established. Due to time taken to analyse SO_4^{2-},removal was slightly more advanced than was ideal.
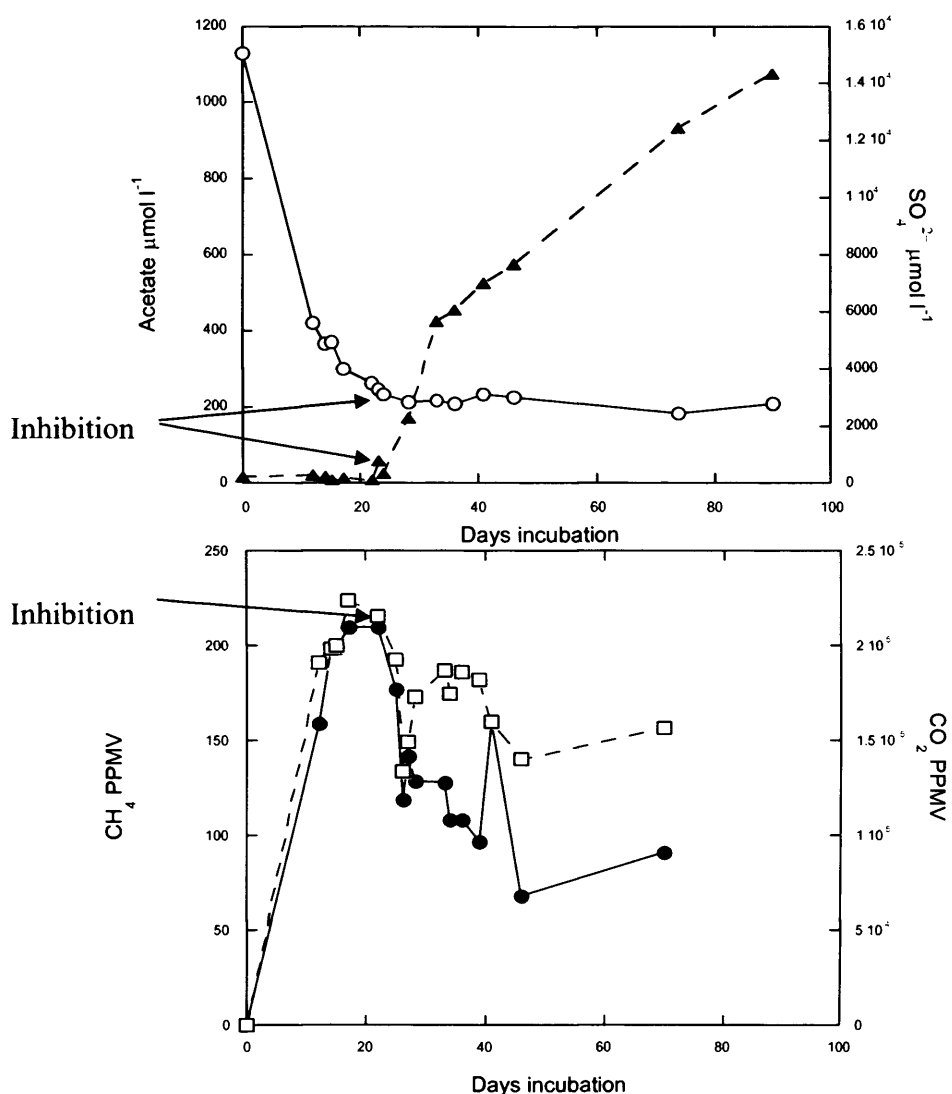
Fig 3.14 sulphate reduction inhibition in basalt mineral sediment slurries at 60°C. Key CH₄ (●) CO₂ (□), Acetate (▲), SO_4^{2-} (○). arrows indicate point of inhibition

Inhibition with molybdate was achieved, as sulphate removal and hence, sulphate reduction was inhibited. This caused a rapid increase in acetate concentrations from 24 μmol l^{-1} at 24 days to 574 μmol l^{-1} by day 54 achieving a final concentration of 1078 μmol l^{-1} at day 9. Inhibition occurred at day 24 when sulphate values were at 3.1mmol l^{-1} after 90 days sulphate values were at 2.9 mmol l^{-1} this is within analytical error. $^{-1}$ However prior to inhibition sulphate removal rates had began to slow and taking this into account the approx percentage of sulphate reduction to acetate oxidation is 25.4% as acetate, sulphate is in a ratio of 1:1. This would seem to indicate either sulphate reduction is not completely achieved using acetate or some other process is using acetate when sulphate reduction is inhibited

$$Acetate^- + SO_4^{2-}+3H^+\rightarrow 2CO_2+ H_2S + 2H_2O \quad \Delta G^{0'}= -57.2 \text{ kj/reaction}(\textbf{ Eq 3.2})$$
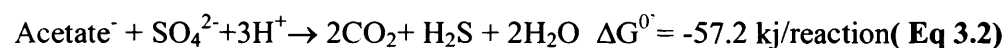
Methane and carbon dioxide concentrations that were increasing rapidly decreased equally as rapidly methane decreasing from 210 ppmv after 24 days (inhibition point) down to 91 ppmv after 90 days. CO_2 decreasing from 216000 ppmv (24 Days) to 157000ppm (90days) no hydrogen accumulation was detected.

3.14 Methane inhibition of basalt mineral incubation at 60 °C

Methane inhibition by addition of 0.1M 2-Bromoethanosulphonic acid was started after consistent methanogenesis was established.

Basalt slurry, incubation at 60°C.
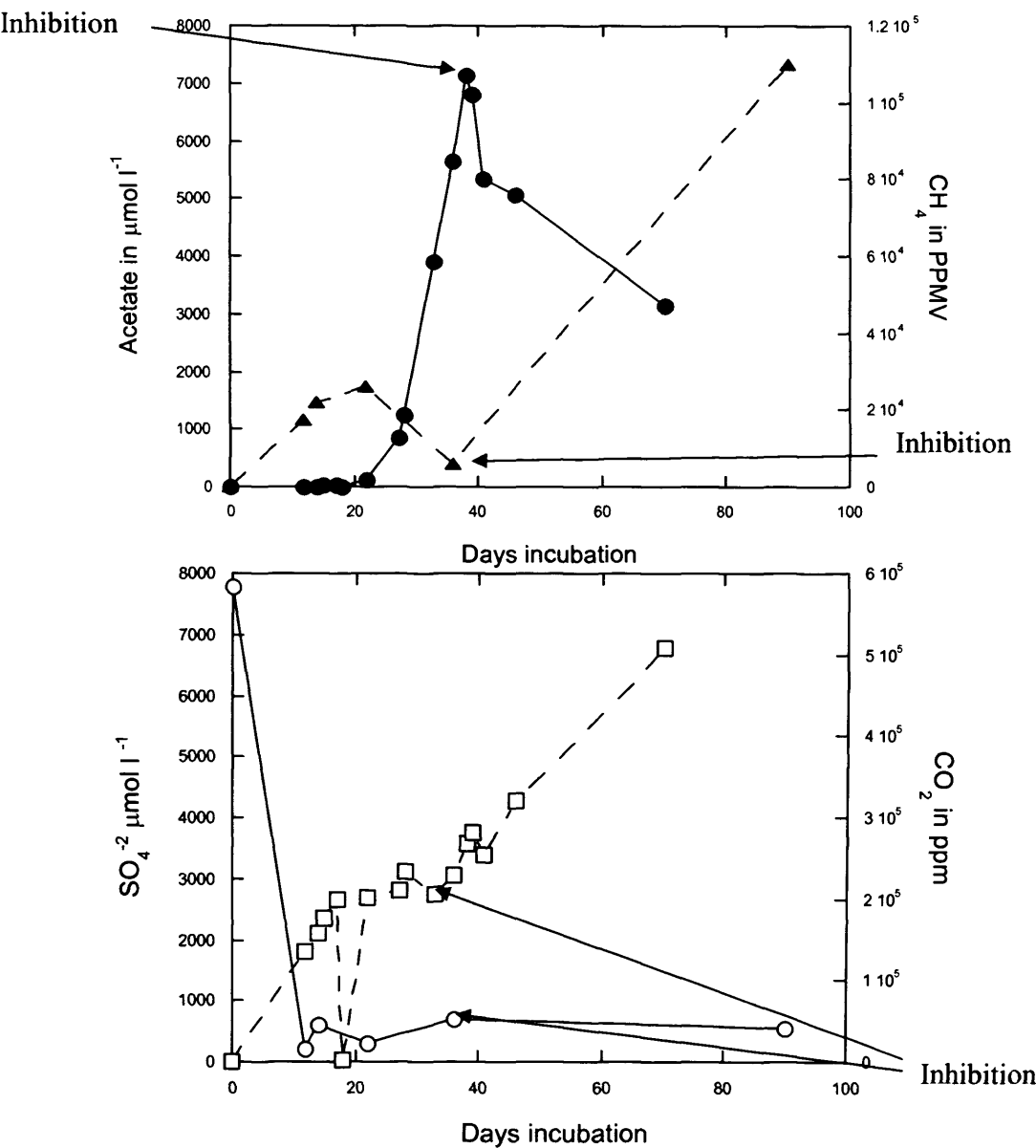
Fig 3.15 Methane inhibition, basalt incubation at 60°C:

Key: Carbon dioxide, (□),Sulphate (○) Acetate (▲) and Methane (●)

Methane inhibition was successfully achieved on addition of BES after 38 days of incubation. Methane levels at day 38 were 107090 ppmv and start to drop after addition to 47091 after 70 days. Before inhibition acetate was decreasing, but after inhibition, acetate concentrations increased from 406 μmol l^{-1} at inhibition to 7339 μmol l^{-1}. Carbon dioxide and sulphate remain the same carbon dioxide increasing and sulphate low (0.56 mmol l^{-1}). No hydrogen was detected either before or after inhibition. The lack of hydrogen liberated and increase in acetate concentrations suggests that methane production was via acetoclastic methanogenesis (Eq.3.3).

$$CH_3COO^- + H_2O \rightarrow CH_4 + HCO_3^-\ \Delta G^{0'} = -113kj/reaction \textbf{(Eq.3.3)}$$
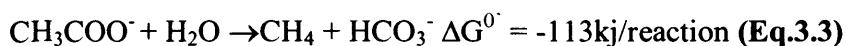
3.15 Discussion

The aim of these initial mineral experiments were numerous and were as follows. What is the effect of mineral addition and differing composition, on major biogeochemical process such as methanogenesis, acetogenesis, sulphate reduction and hydrogen generation? Is mineral H_2 generation, influenced by microbially driven processes? Is there an effect on microbial community structure with differing minerals? Is the microbial community present similar to typical environmental samples so that these incubations have a realistic bases for extrapolation to a natural environmental setting. Does physical alteration of the mineral in terms of grinding and activation of "fresh surfaces" have an effect on microbial processes? Through the use of specific inhibition experiments identify the substrate used in the major processes of sulphate reduction and methanogenesis in the presence of minerals. Can this work be extended by the use of more detailed chemical analysis, molecular genetics and an extension of the range and type of treatment of samples/minerals

Mineral addition has a clear effect on processes such as methanogenesis, acetogenesis and sulphate reduction. This effect varies according to the composition of the mineral used. Detectable hydrogen was only found in 5 of the incubations (hornblende, ilmenite, olivine, olivine bombs, and labradorite) and is used rapidly over the first 4/5 days. H_2 is not detectable for the remainder of these experiments, with the

exception of olivine and olivine bombs where some hydrogen is formed after sulphate depletion and a decrease in methane concentrations occurs, (possible indication of hydrogen use in each). No detectable hydrogen was found in basalt, hematite, pyrite and pyrrhotite (magnetite was also analysed [appendix B] and found not to produce hydrogen). Initial theories suggesting that hydrogen liberation was dependent on iron concentrations, seem not to be the case, as hematite and magnetite both produced no detectable hydrogen where as labradorite did. (Hematite Fe_2O_3 54.12%, Magnetite 99.49%, Labradorite 0.62%, Table 3.2). However, lack of detectable hydrogen does not necessarily mean hydrogen is not produced as hydrogen is rapidly and readily cataboilized by a range of anaerobic prokaryotes for many purposes such as methanogenesis acetogenesis and sulphate reduction.

Methane formation is affected by mineral type, both in terms of amount and timing of formation. Methanogenesis occurs during sulphate reduction for all minerals bar hornblende (Fig 3.1), where only after sulphate is depleted is there substantial methane formation. Methane concentrations varied with mineral, hornblende being the highest and pyrite being the lowest, this could be due to a number of factors primarily being that methane can be produced via use of hydrogen (Eq.3.4) and there was no detectable hydrogen formed with pyrite.

$$CO_2 + 4H_2 \rightarrow CH_4 + 2H_2O \; \Delta G^{O} = -131 \text{ kj/reaction } \textbf{(Eq.3.4)}$$

Sulphate levels start at a high level in the pyrite and pyrrhotite incubation. Sulphate reducing bacteria (SRBs) utilise hydrogen at a lower partial pressure than methanogens (Kristjansson et al., 1982) are capable of, thus limiting possible hydrogen availability for methane formation during pyrite incubation. In Hornblende sulphate is depleted, freeing up hydrogen for use in methanogenesis, as there is a drop in carbon dioxide concentrations (Fig 3.1) and an isotope CH_4 value of -78‰ (Table 3.4) both indicating H_2/CO_2 methane formation (Eq.3.4). The remaining incubations produced methane while sulphate was also being removed and also provide a mix of $\delta^{13}C$-CH_4 values (Table 3.4), indicating a possible mixture of methane production mechanisms, including acetoclastic methanogenesis (Eq.3.3). But acetate is also preferentially removed by sulphate reducers

in competition with methanogens (Schonheit et al., 1982). So it is surprising that both processes are occurring together unless acetate concentrations are in excess in these mineral experiments, or non-competitive substrates are being produced. Sulphate removal rates also vary with mineral; sulphate is fully depleted in four incubations, (Hornblende, olivine, olivine bombs and labradorite) and not fully depleted in the rest, hematite basalt ilmenite pyrite and pyrrhotite. The latter, pyrite and pyrrhotite, start at a much higher level than the other minerals, the overall amount of SO_4^{2-} removed far exceeds the other minerals where sulphate was fully depleted. Acetate concentrations are linked to sulphate removal rates, two processes of sulphate reduction seem to be taking place, firstly using acetate as in Eq.3.2, inhibition experiments however only document acetate utilization, sulphate reduction may also be conducted using hydrogen (Eq 3.5)

$$4H_2 + SO_4^{2-} + H^+ \rightarrow HS^- + 4H_2O \quad \Delta G^{O'} = -151.6 \text{ kj/reaction} \textbf{ (Eq.3.5)}$$

Olivine (Fig 3.3) shows acetate increasing during the course of the incubation, and once sulphate is depleted after a 10-15 day lag phase hydrogen levels increase, pointing to a possible usage of hydrogen during the initial sulphate reduction phase. However many of the incubations show an initial high acetate concentration from H_2/CO_2 acetogenesis, which is gradually used until sulphate, is depleted (hornblende Fig 3.1). In the case of basalt (Fig 3.9) once acetate is depleted sulphate removal ceases and full depletion never occurs. Acetate formation is also linked to hydrogen generation (Eq.3.6)

$$4H_2 + H^+ + 2HCO_3^- \rightarrow CH_3COO^- + 4H_2O \quad \Delta G^{O''} = -104.6 \text{ kj/reaction} \textbf{ (Eq.3.6)}$$
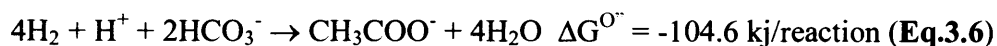
Highest concentrations of acetate were formed in slurries where initial hydrogen was detected (e.g. hornblende, ilmenite Figs 3.1, 3.2). Conclusions from this are that rates of processes such as methanogenesis, acetogenesis, sulphate reduction plus hydrogen generation and co-occurrence of competitive substrates are affected by mineral composition.

Hydrogen generation was influenced by microbial processes with little or no H_2 formation controls at 60°C (max of 3-4 μmol l^{-1}) even when running longer than the

mineral incubations themselves (Fig 3.10a), Standard AODC counts show no difference in cell numbers per ml between varying slurry incubations (Table 3.3). However, molecular genetic analysis using the 16S rRNA gene. Shows that both bacterial and archaeal community structure differs according to mineral, related mineral compositions show similar profiles (Figs 3.11, 3.12). Sequenced bands revealed majority of 16S rRNA gene sequences were related to thermophilic species found in deep marine environments such as hydrothermal vents, gas hydrates and oil reservoirs. This gave confidence that our simulations could be used to simulate deep subsurface processes.

Physical alteration of the mineral through regrinding speeds up processes. This may be due to the creation of fresh reactive surface. It is not due to particle size/ surface area effects, as the mineral that was not ground was previously powdered using the same procedure and time as the freshly ground sample. Perhaps hydrogen is generated by stimulated prokaryotic activity at reactive surfaces and under elevated temperatures.

The specific inhibition of sulphate reduction, using molybdate and methanogenesis through BES, showed that both processes in those specific basalt incubations were significantly acetate driven 25.4% in case of sulphate reduction. No hydrogen was formed during inhibition of either process. This confirmed our interpretation of the basalt mineral incubation (Fig 3.9) where it was assumed that acetate depletion was the limiting factor that caused sulphate removal to cease after 60 days incubation.

This series of experiments showed that hydrogen could be consistently generated from a range of minerals. It is a microbially driven process; it can potentially have a major affect on subsurface microbial processes. Both the type of mineral and physical treatment of the mineral (grinding) influences processes and community structure. Our community structure resembled deep subsurface communities and could be a good analogue, for this habitat. It was decided based on these findings to increase the temperature range of experiments and do a full temperature profile, more detailed molecular work and chemical analysis to better understand these processes and the impact/significance of these findings.

Chapter 4

Temperature characteristics of basalt reactions in sediment slurries

4.1 Introduction

Hydrogen generation from basalts has been subject to much debate in recent years. The focus being on whether basalt/water, interactions can liberate hydrogen, which may be capable of supporting prokaryotic life independent of photosynthetic energy capture (Stevens and McKinley, 1995; Anderson et al., 1998; Stevens and McKinley, 2000) this combined with the fact that hydrogen based subsurface communities have been found in association with basalts (Chapelle et al., 2002), has fuelled speculation on the exact nature of hydrogen generation from basalts. Considering these issues, research in this project while concentrating on differing mineral types (varying Fe and Si composition), conducted extensive experiments using basalt (Table 3.2).

Basalt also has a composition that is generally reflective of the group of minerals we analysed, consisting of a mixture of Si and Fe, with concentrations close to the median in comparison to the other minerals used.

The experiments presented in this chapter are as follows 1) Temperature characterisation of slurries without basalt addition, conducted over a large temperature range on the thermal gradient incubation system, in order to establish a "baseline", to quantify the direct effect of basalt addition on sedimentary prokaryotic reactions. 2) Temperature characterisation of slurries with basalt addition, to examine the effect of basalt addition on prokaryotic sedimentary processes at a range of temperatures 3) Temperature characterisation of sterile slurries with basalt addition, to gauge the effect that prokaryotes have on these sedimentary reactions. Are prokaryotes driving H_2 generation reactions? 4) Temperature characterisation of sterile anoxic mineral salt solution alone and basalt, to quantify the effect of ground minerals and anoxic mineral salt solution, especially H_2 generating potential. Serpentinization type reactions,

involving the interaction of basalts and seawater can produce high levels of hydrogen, at hydrothermal field sites i.e. the lost city hydrothermal field (Kelley et al., 2005). Reactions of this type were also the bases of previous hypothesis on sources of hydrogen generation from basalts (Stevens and McKinley, 2000) . This experiment was in effect a control to see if freshly ground minerals and anoxic mineral salt solution produced any detectable hydrogen at biologically relevant temperatures and if it did, how do these concentrations compare to quantities found to be generated in the presence of sedimentary prokaryotes. 5) Molecular profiling of prokaryotic community structure to analyse the community present and see the effect of temperature on community structure 6) A basalt ramping experiment was conducted using pressurised incubation vessels (Chapter 2). This was conducted so as to simulate processes occurring over a defined temperature range, through sequential temperature increases mimicking rapid burial rather than a range of single temperatures as conducted in previous experiments. Using these pressure vessels we were able to extend the temperature range beyond the limits of the thermal gradient system (100/105°C) into a definite abiotic temperature zone (>120°C). This experiment was subject to rapid ramping 10°C every 10 days. This was due to time constraints on the experiment, and this was essentially a trial experiment to test the feasibility of running this pressure system up to 155°C and handling high temperature pressurised sub-sampling. Due to this rapid ramping, it was recognised that it would be a challenge for the prokaryotic community to respond. A sterile control was also run, this was to determine abiotic reactions at temperatures > 100°C and their potential to supply H_2 to the base of the biosphere and the effects if any, that microbial interaction with minerals at biotic temperature have on interactions occurring at higher abiotic temperatures.
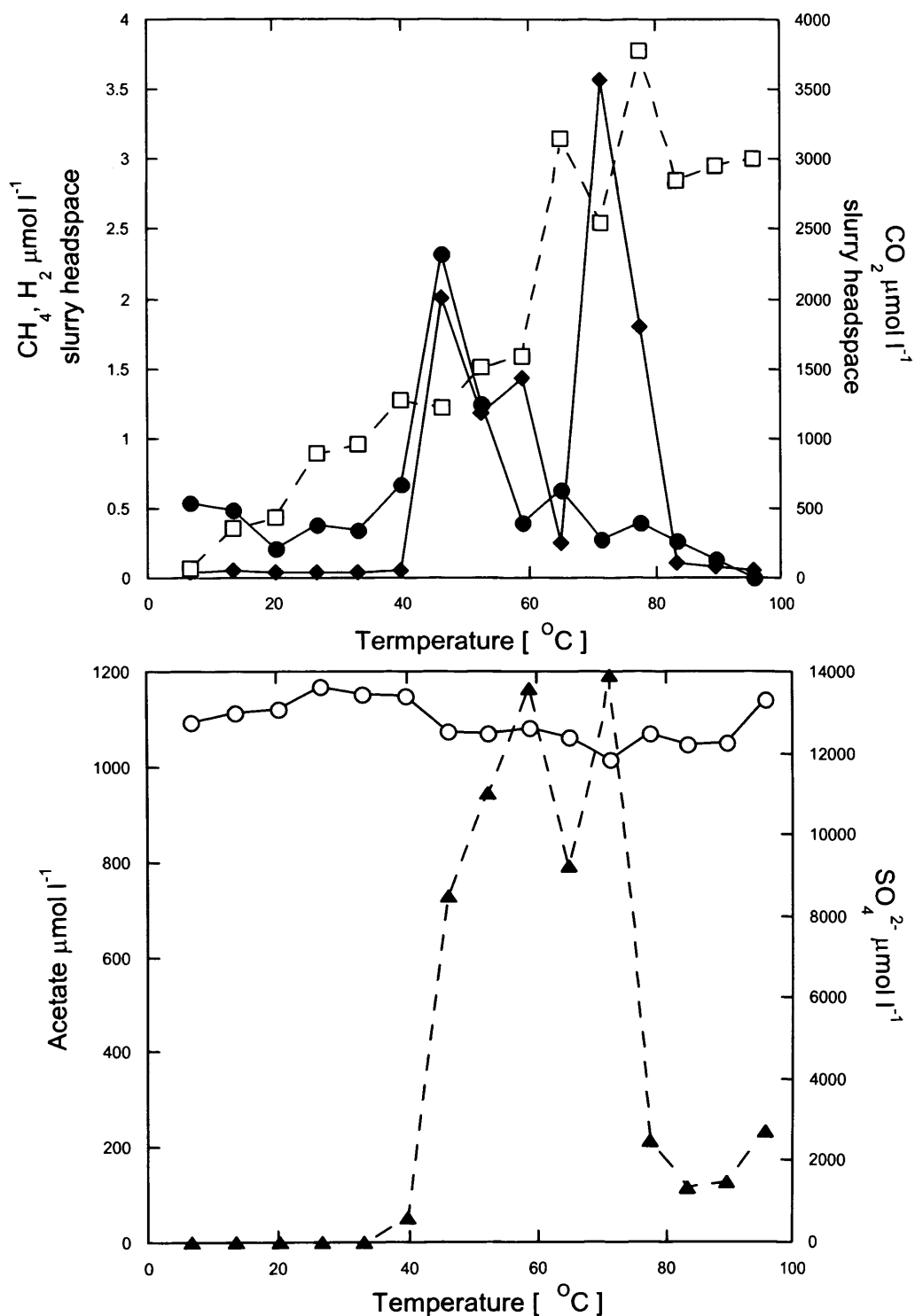
Fig 4.1 No mineral addition 3 days incubation.

Key CH_4 (●), CO_2 (□), H_2 (◆), acetate (▲) and SO_4^{2-} (○).
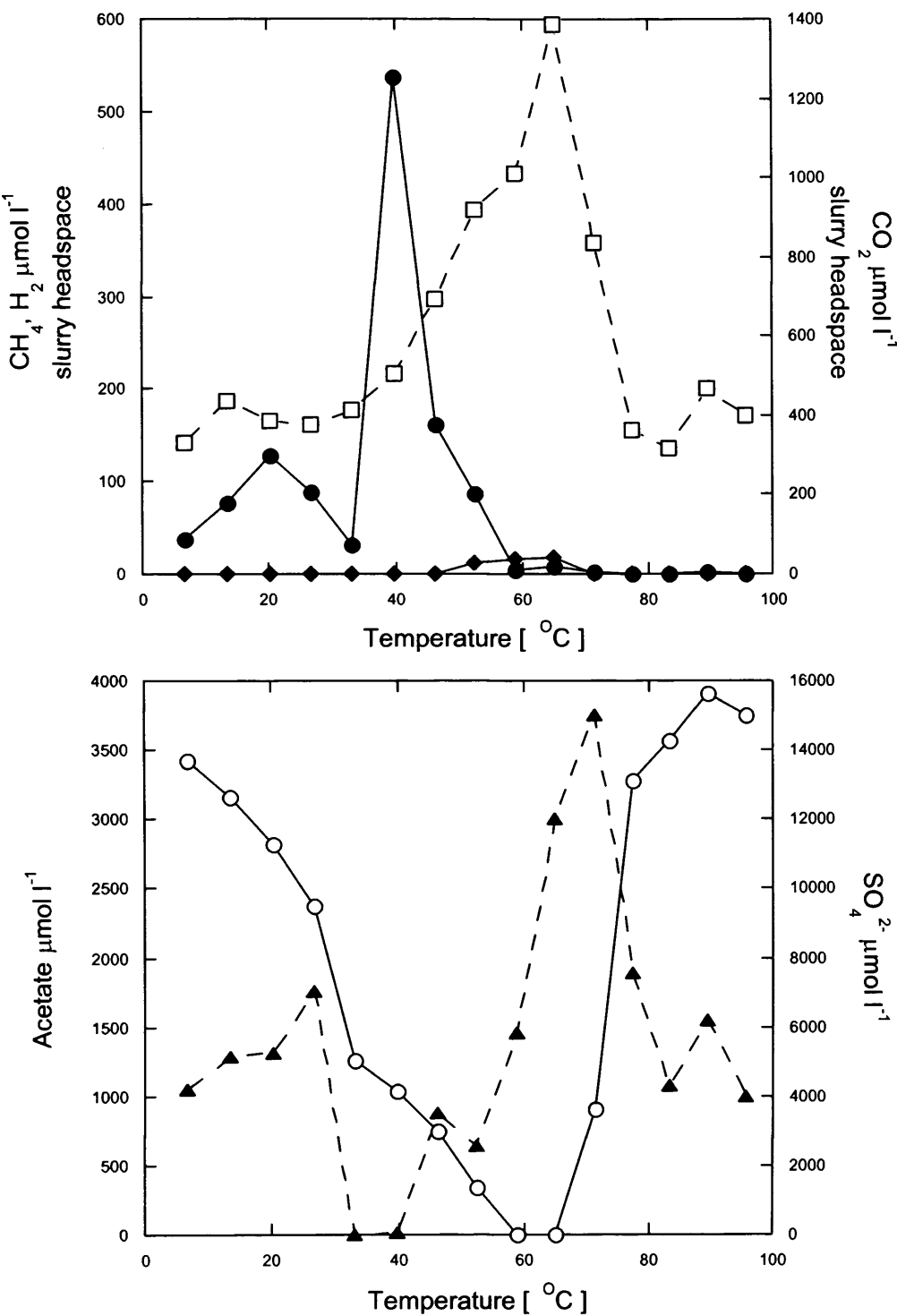
Fig 4.2 No mineral addition, 93 days incubation.

Key: CH_4 (●), CO_2 (□), H_2 (◆), acetate (▲) and SO_4^{2-} (○).

Cation concentrations in sediment only (no mineral addition) incubation after 93 days.
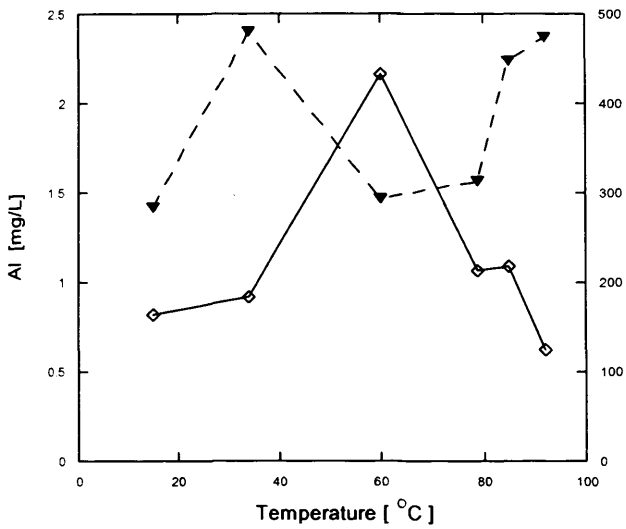
Fig 4.3 No mineral addition. Al and K cation concentrations after 93 days incubation, across selected key temperature points.

Al: inverted closed triangle. K: open Diamond
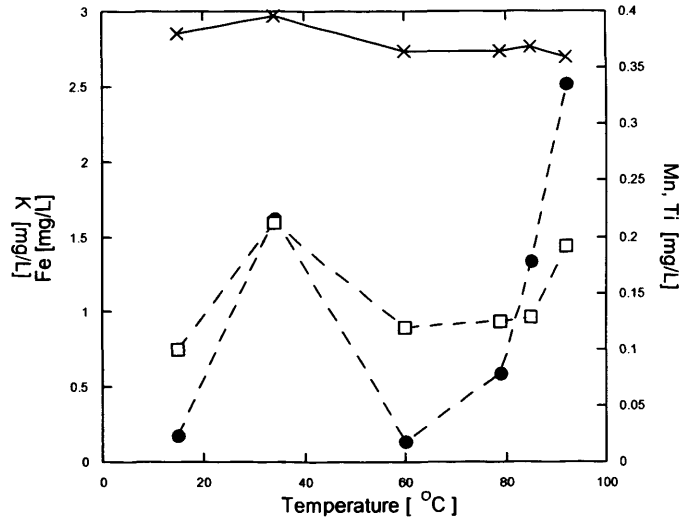
Fig 4.4 No mineral addition. Fe, Mn and Ti cation concentrations after 93 days incubation, across selected key temperature points.

Fe: closed circle. Mn: x. Ti: open box
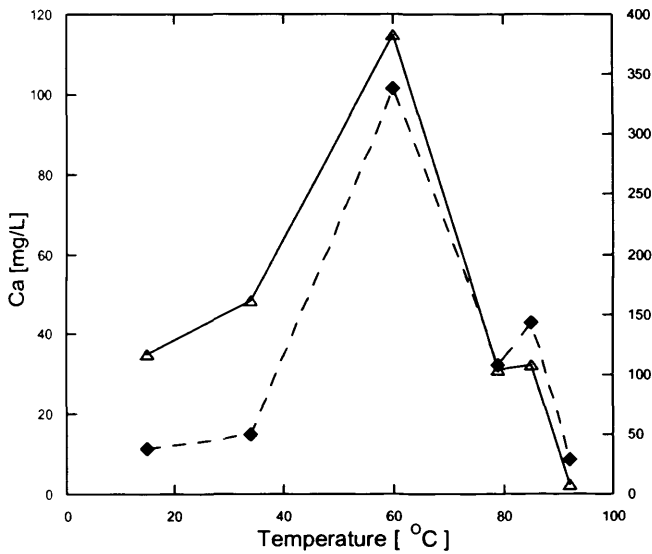
Fig 4.5 No mineral addition. Ca and Mg cation concentrations after 93 days incubation, across selected key temperature points.

Ca: closed Diamond. Mg: open triangle
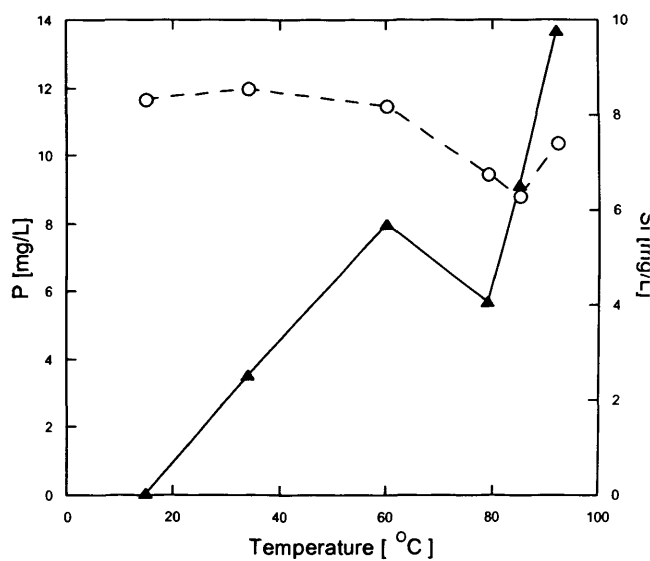
Fig 4.6 No mineral addition. P and Si cation concentrations after 93 days incubation, across selected key temperature points.

P: open circle. Si: closed triangle

103

4.2 Results, sediment only incubation (Figs 4.1-4.6)

This experiment was conducted to quantify the effect of heating of the sediment matrix used in the mineral addition experiments. In order to clearly define the effect that mineral addition was having on heating experiments (baseline establishment).

The affects of heating on the sediment matrix are clearly shown in this experiment (Fig 4.2). Experimental data shows VFA and gas data after 3 and 93 days plus cation data at 93 days only.

After 3 days incubation no significant amounts of methane were detected (max value of 2.3 μmol l^{-1}) . Hydrogen values were low with a maximum concentration of 3.5 μmol l^{-1} detected at 71°C but proceeds from 40°C. Acetate concentrations start to increase from 0 μmol l^{-1} at 33°C to 1190 μmol l^{-1} at 71°C. This increase is not uniform and a decrease is noted at 65°C where concentrations decrease by 374 μmol l^{-1} to 791 μmol l^{-1} before increasing again. Highest concentrations of acetate occurred at 71°C after 3 days. Acetate concentrations decrease after 71°C, reaching 212 μmol l^{-1} at 79°C. Some sulphate removal occurs over the first 3 days. Sulphate values decrease from approx 13.4 mmol l^{-1} at 33°C to a minimum of 11.8 mmol l^{-1} at 71°C (1.6 mmol l^{-1} reduction). No removal takes place at 95°C. The zone of sulphate removal was from 39 to 95°C. Carbon dioxide values gradually increase with temperature reaching 3776 μmol l^{-1} by 77°C before dropping and reaching 3000 μmol l^{-1} by 95°C.

After 93 days incubation distinct biogeochemical patterns have occurred associated with temperature. Methane values show two distinct temperature peaks. Firstly one peaking at 20°C reaching 120 μmol l^{-1} and the other at 40°C with a maximum of 535 μmol l^{-1}. Methane decreases after 40°C becoming undetectable past 71°C. Carbon dioxide levels seem to broadly mirror sulphate removal; maximum carbon dioxide concentrations of 1400 μmol l^{-1} occur near the zone of maximum sulphate removal at 71°C carbon dioxide decreases after this, which is mirrored by a decrease in sulphate reduction. Sulphate removal stops at 77°C with concentrations similar to start concentrations (13.1 mmol l^{-1}). However sulphate concentrations are seen to increase to

15 mmol l^{-1} at the final sampling point which is unusual. Perhaps this is due to anaerobic S^{2-} oxidation.

Hydrogen concentrations are undetectable for majority of temperatures. Low concentrations however, are detected between 55-70°C overlapping the zone of sulphate depletion. Acetate and methane levels seem to be linked as the second methane peak decreases acetate increases. Starting concentrations for acetate at 6°C was 1045 μmol l^{-1} increasing to 1756 μmol l^{-1} at 26°C before decreasing to zero at 33°C and 11 μmol l^{-} at 39°C. This decrease co-occurs with the start of the second peak in methane concentrations possibly indicating the occurrence of acetoclastic methanogenesis. Acetate values increases considerably as methane concentrations begin to decrease, with the most rapid increase noted when methane concentration drops to near zero at 60°C. Acetate increases from 1.4 mmol l^{-1} to 3 mmol l^{-1} by 65 °C and continues to a maximum concentration of 3.75 mmol l^{-1} at 71°C. Acetate decreases rapidly after this to 1.07 mmol l^{-1} at 83°C. a slight increase occurs toward the end similar to carbon dioxide concentrations increasing to 1.55 mmol l^{-1} at 89°C and decreasing to 1 mmol^{-1} at 95°C

Cation results indicate that various elements react differently during 93 days incubation at varying temperatures. K concentrations follow the inverse of sulphate reduction similar to carbon dioxide values. Calcium and magnesium concentrations also have a profile similar to CO$_2$ (Fig 4.5) (offset observed in this could be lack of sampling resolution) Silica values increased with temperature reaching a maximum of 9.4mg/l. Mn values showed a slight decrease at higher temperature from 0.38 to 0.36 mg/l.

Total iron values increased initially concurrent with the second methane peak at 40°C then decreases to minimum values when Ca Mg and K increased. Total Fe then consistently increased with temperature from 60°C to a maximum value of 2.45 mg/l at 95°C. Ti concentrations were at there highest when methane concentration were at there maximum.
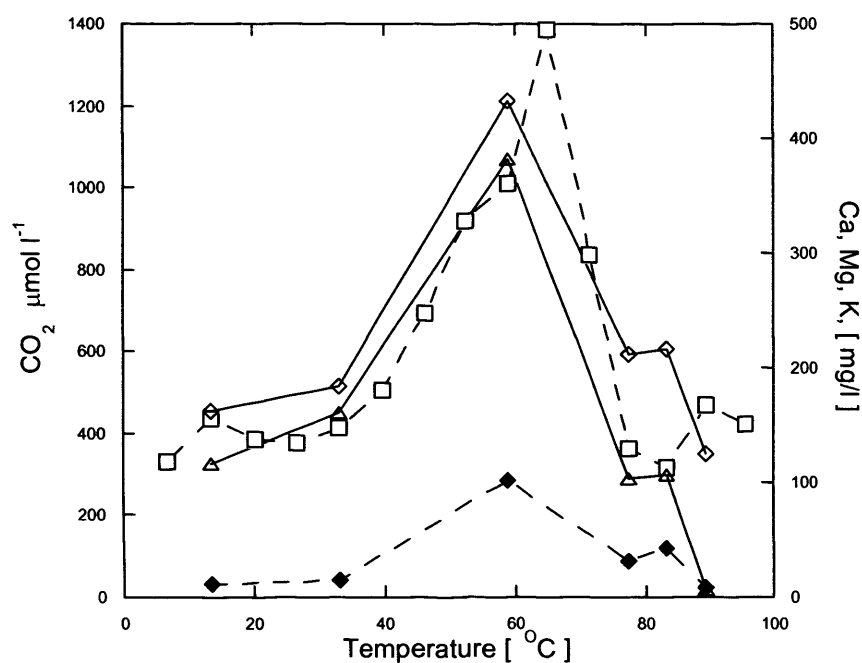
Fig 4.7 . Comparison of carbon dioxide concentrations over the incubation temperature generated after 93 days, with the Ca, Mg and K cations concentrations found in the incubation slurry after 93 days.

Key :CO_2 open box: Ca closed diamond: Mg open triangle: K open Diamond.
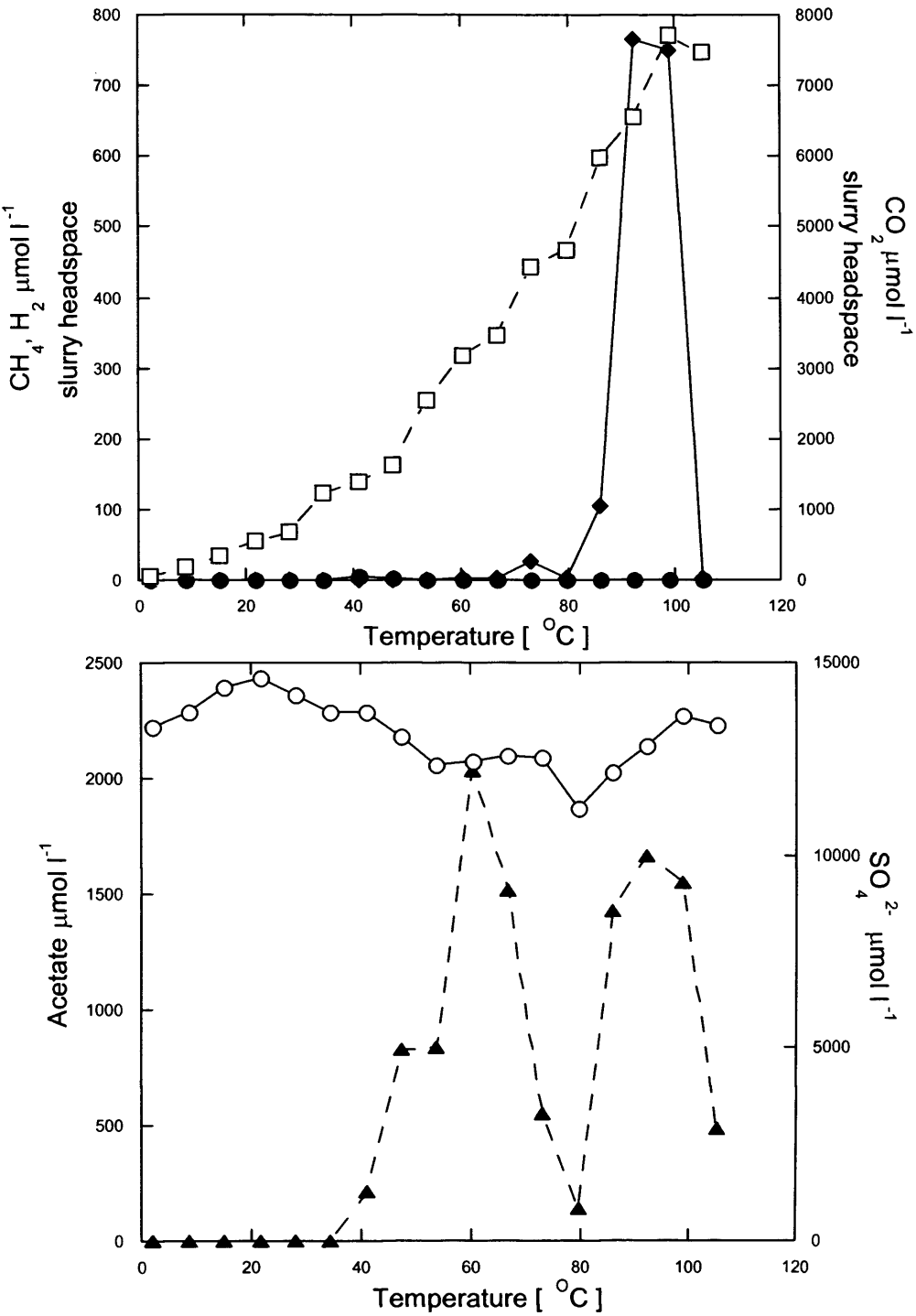
Fig 4.8. Basalt slurry 3 day incubation.

Key CH$_4$ (●) CO$_2$ (□) H$_2$ (♦) acetate (▲) and SO$_4^{2-}$ (○)
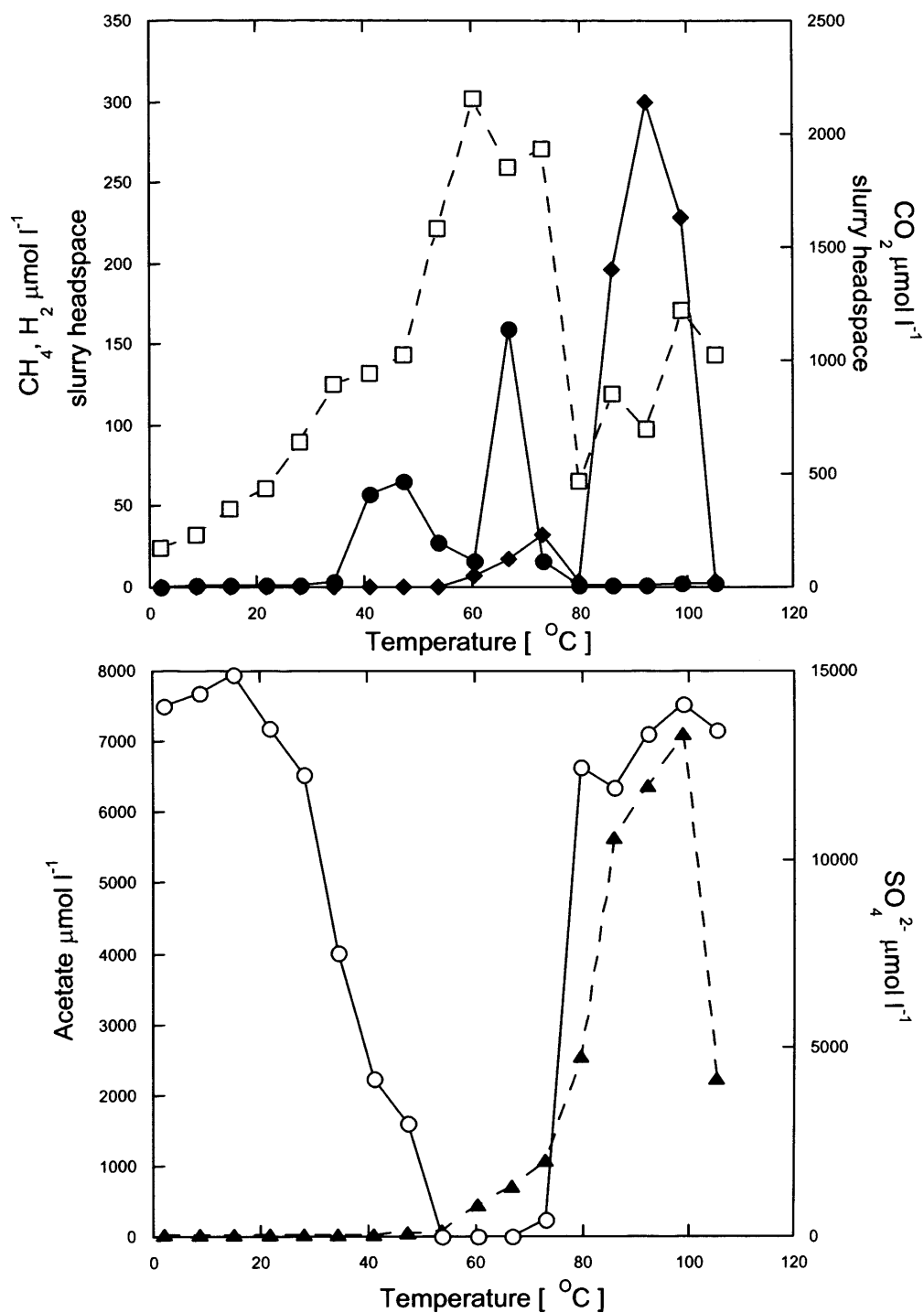
Fig 4.9 Basalt slurry 83 day incubation.

Key CH$_4$ (●), CO$_2$ (□), H$_2$ (◆), Acetate (▲) and SO$_4^{2-}$ (○)

Cation concentrations found in Basalt sediment slurry after 83 days incubation.
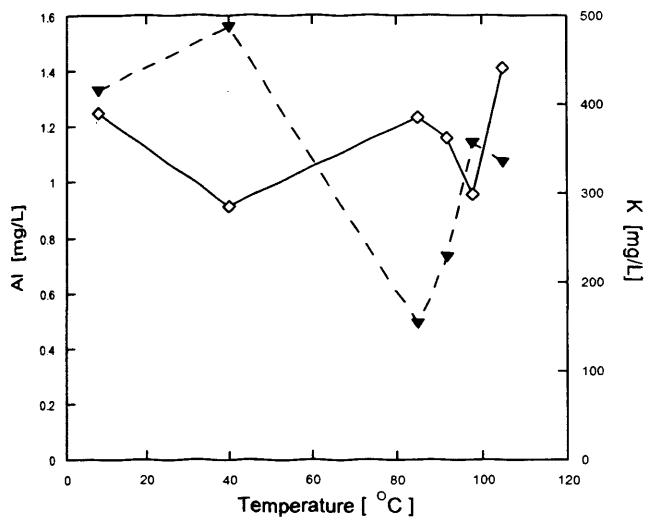
Fig 4.10 Basalt mineral addition. Al and K cation concentrations after 83 days, over selected key temperatures

Al: inverted triangle. K: open Diamond
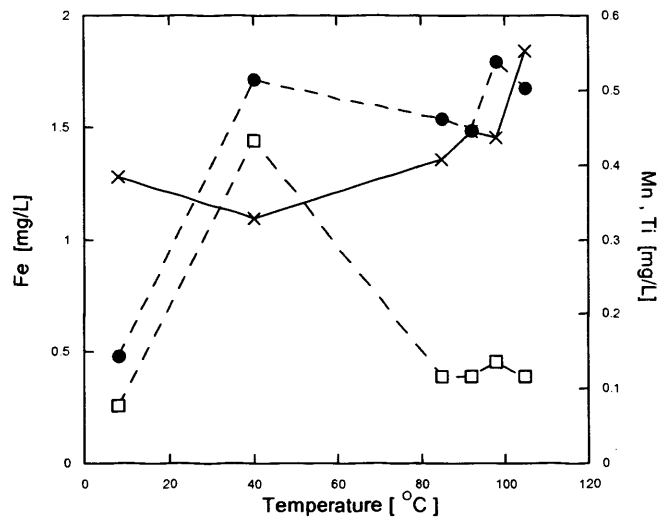
Fig 4.11 Basalt mineral addition, Fe, Mn and Ti cation concentrations after 83 days, over selected key temperatures

Fe: closed circle. Mn: x. Ti: open box
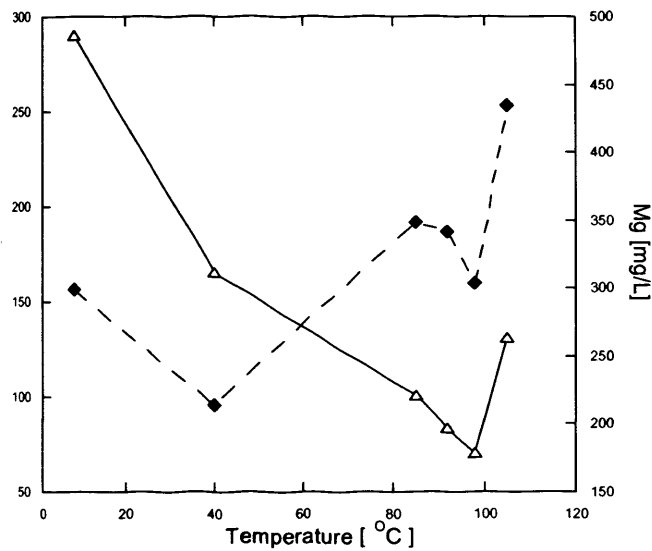
Fig 4.12 Basalt mineral addition, Ca and Mg cation concentrations after 83 days, over selected key temperatures.

Ca: Diamond. Mg: open triangle
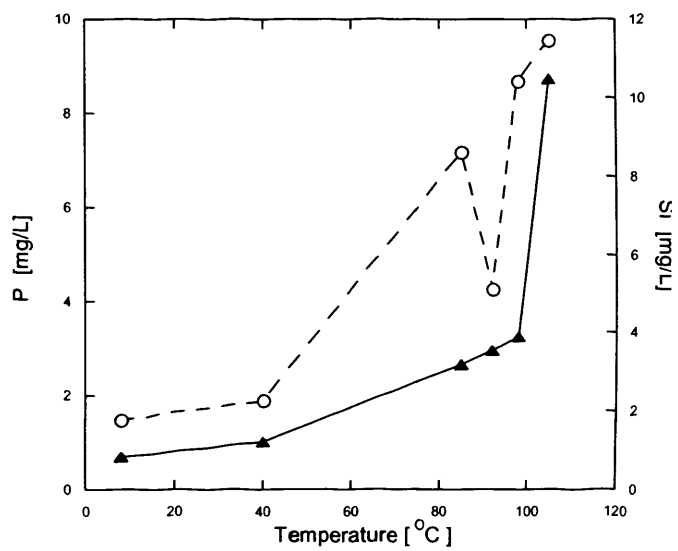
Fig 4.13 Basalt mineral addition, P and Si cation concentrations after 83 days, over selected key temperatures

P: open circle. Si: triangle

4.3. Results basalt sediment incubation (Figs 4.8-4.13)

No significant methane was detected after 3 days incubation, with a maximum concentration observed of 5 μmol l^{-1} at 40°C. However, methane concentrations were still higher than the sediment only incubation, by a factor of 2. Carbon dioxide concentrations increased with temperature, reaching a maximum of 7709 μmol l^{-1} at 98°C. This is also approximately a factor of two times greater than the sediment only incubation, max concentration (3776 μmol l^{-1}).

Hydrogen concentrations were substantially greater (x218) than the sediment only incubation. High levels of hydrogen were detected between 80-105°C. With maximum concentrations of 766 μmol l^{-1} detected at 92°C. However, no hydrogen was formed above 100°C. Initial concentrations of sulphate were approx 14.5 mmol l^{-1}. Sulphate removal occurred between 20-98°C, with a maximum removal of 3.3 mmol l^{-1} occurring at 79°C. Significant amounts of acetate were present by day 3. Acetate values increase from 0 μmol l^{-1} (34°C) to 2030 μmol l^{-1} (60°C), before decreasing to 143 μmol l^{-1} (79°C), acetate increases again similar hydrogen to 1664 μmol l^{-1} at 92°C before decreasing towards and after 100°C. The decrease in the amount of acetate at 79°C coincides with the point of maximum sulphate removal indicating perhaps acetoclastic sulphate reduction taking place. ($\sim$ 3000 μmol l^{-1} and $\sim$ 2000 μmol l^{-1} reduction in acetate)

After 83 days of incubation, carbon dioxide concentrations increase to a maximum of 2160 μmol l^{-1} at 60°C. Carbon dioxide increases were contiguous with sulphate removal with maximum concentrations of carbon dioxide, occurring in the zone of sulphate depletion. Rapid decrease in CO_2 occurs at 73°C (1932 μmol l^{-1}) to 465 μmol l^{-1} at 79°C. This decrease coincides with rapid increases in acetate. Acetate formation can consume carbon dioxide and hydrogen.

$$2CO_2 + 4H_2 \rightarrow CH_3COOH + 2H_2O \quad \Delta G^{o'} = -104.6 \text{ kj/reaction.} \textbf{ (Eq 4.1)}$$

110
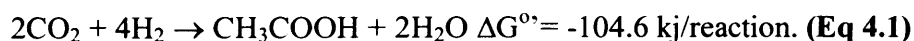
However H_2 is increasing this leads to the assumption that H_2 is being produced in excess.

Some methane formation occurs during sulphate removal, with two distinct peaks being distinguishable which were close to or in the SO_4^{2-} depletion zone. Maximum concentrations of 65 µmol l^{-1} at 47°C and 159 µmol l^{-1} at 66°C. Methane formation occurs at a higher temperature than no mineral slurry incubation, but surprisingly not to higher concentrations.

$\delta^{13}C$-CH_4 values were obtained for these samples and they show values consistent with biogenic methane formation from acetate (Whiticar, 1999) (Table 4.1)

\

Table 4.1 Methane isotope for basalt incubation

Temperature	$\delta^{13}C$-CH_4	SD	$\delta^{13}C$-CO_2	SD
66°C	-54.7‰	0.9	-21‰	0.4
47°C	-60.8‰	0.8	-20‰	0.2

SD= standard deviation.

Hydrogen occurs at high concentrations 300 µmol l^{-1} at 92°C. Lower levels are present in the zone of sulphate depletion 32 µmol l^{-1} at 73°C, which is also close to where the highest methane concentrations occurred . Acetate concentrations increase in the zone of sulphate depletion to 700 µmol l^{-1} at 66°C (indicating that acetate formation in this zone is greater than sulphate reduction), before rising rapidly when sulphate removal slows to reach a maximum concentrations of 7.1 mmol l^{-1} at 98°C similar to hydrogen a rapid decrease above 100°C occurs, to 2.2 mmol l^{-1} at 105°C. Sulphate concentrations start at approx 14.4 mmol l^{-1} removal begins at 15°C (decrease to 13.4 mmol l^{-1} at 21°C) sulphate values reach zero (depletion) between 53-66°C and removal decreases above this temperatures. Increases in acetate during decrease in sulphate removal rates indicate possible use of acetate in sulphate reduction.

$$\text{Acetate}^- + SO_4^{2-} + 3H^+ \rightarrow 2CO_2 + H_2S + 2H_2O \quad \Delta G^{O'} = -57 \text{ kj/reaction.} \textbf{(Eq 4.2)}$$
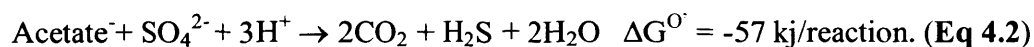
Cation analysis showed several cation profiles were different than the no mineral control, such as K, Ca, and Mg other elements are similar such as Al, Si, Mn and P. Al concentration commences at 1.38 mg/l decreasing to a lowest level of 0.49 mg/l at 85°C followed by an increase. This decrease occurs close to the time of rapid acetate generation and slow down of sulphate reduction. K concentrations show a decrease at 40°C and 98°C from 390 to 280 mg/l and 362 to 299 mg/l respectively. Fe and Mn concentrations broadly increase with temperature most rapid increase in Fe occurs from 8 to 40°C (0.4 to 1.72 mg/l) this co-occur with first large methane peak this is rather different than the no mineral incubation (Fig 4.4) where we see this rapid increase followed by an equally rapid drop in Fe close to the zone of sulphate depletion. Ti is broadly similar to no mineral addition increase over the first 40°C decreasing over the remainder of the temperatures. Ca and Mg are both very different to the no mineral incubation. Mg concentrations at 8°C of 486 mg/l decrease to 178 mg/l by 98°C before increasing at 98°C from 178 mg/l to 263 mg/l. Ca levels start at a higher concentration than the no basalt incubation (157 mg/l as opposed to 16 mg/l) decreasing at 40°C to 96 mg/l before increasing to 253mg/l at 105°C (a slight decrease occurs between 92 and 98°C). Ca and Mg concentrations are significantly higher in the basalt incubation than the no mineral control.

Si concentrations are broadly similar in both basalt and no basalt incubations increase with temperature (a small decrease is however, noted at ~ 80°C in the no mineral incubation). Si stepwise increases with temperature, 0.8 mg/l at 8°C to 10.4 mg/l 105°C. Phosphorus concentrations are quite different; basalt incubation starts at a lower level by a factor approx 6 at 1.48 mg/l increasing with temperature but with a decrease at 85°C coinciding with the start of hydrogen generation. Final concentration at 105°C, is 9.5 mg/l.
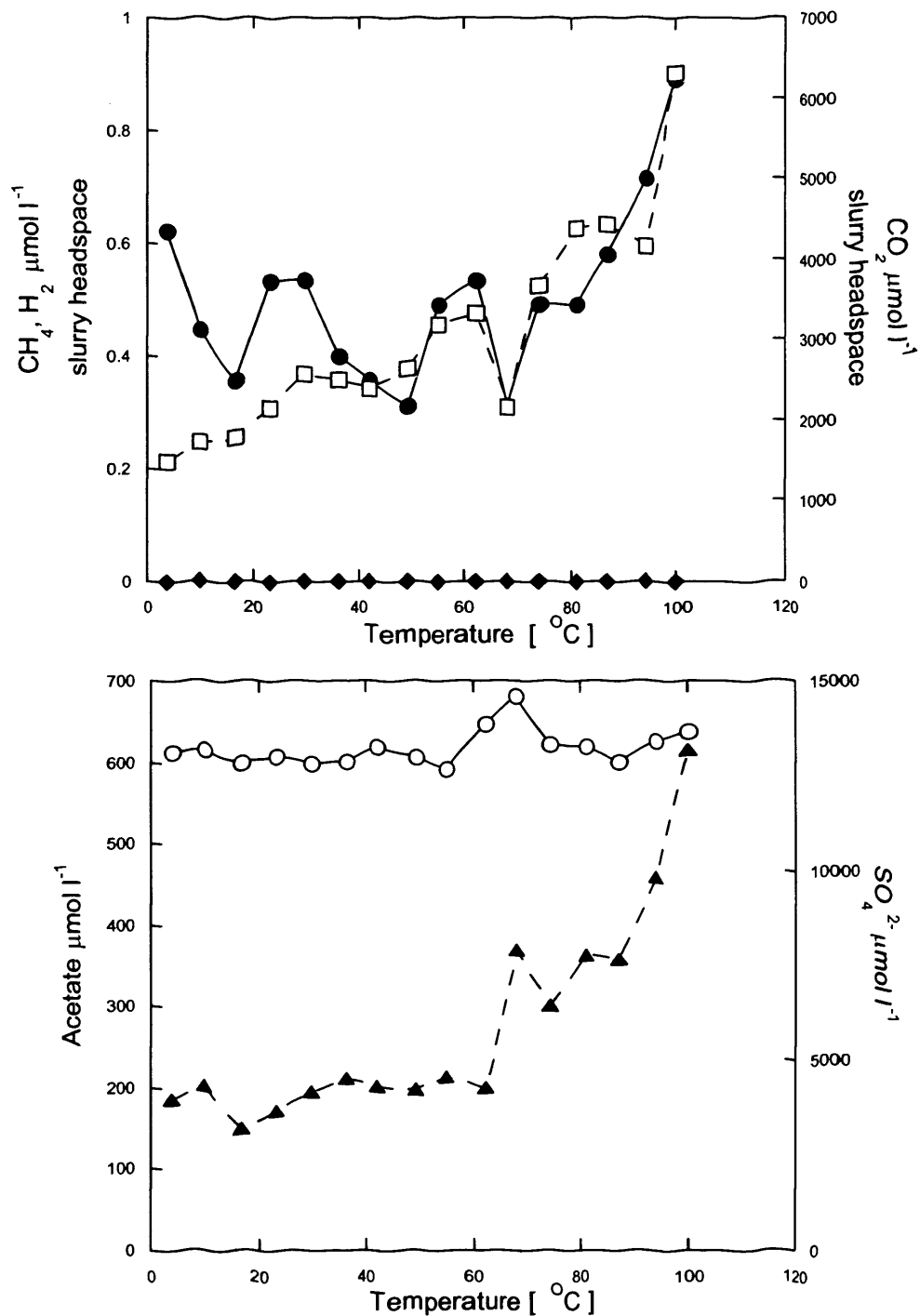
Fig 4.14 Basalt slurry sterile control 3 days.

Key CH$_4$ (●), CO$_2$ (□), H$_2$ (♦), acetate (▲) and SO$_4^{2-}$ (○).
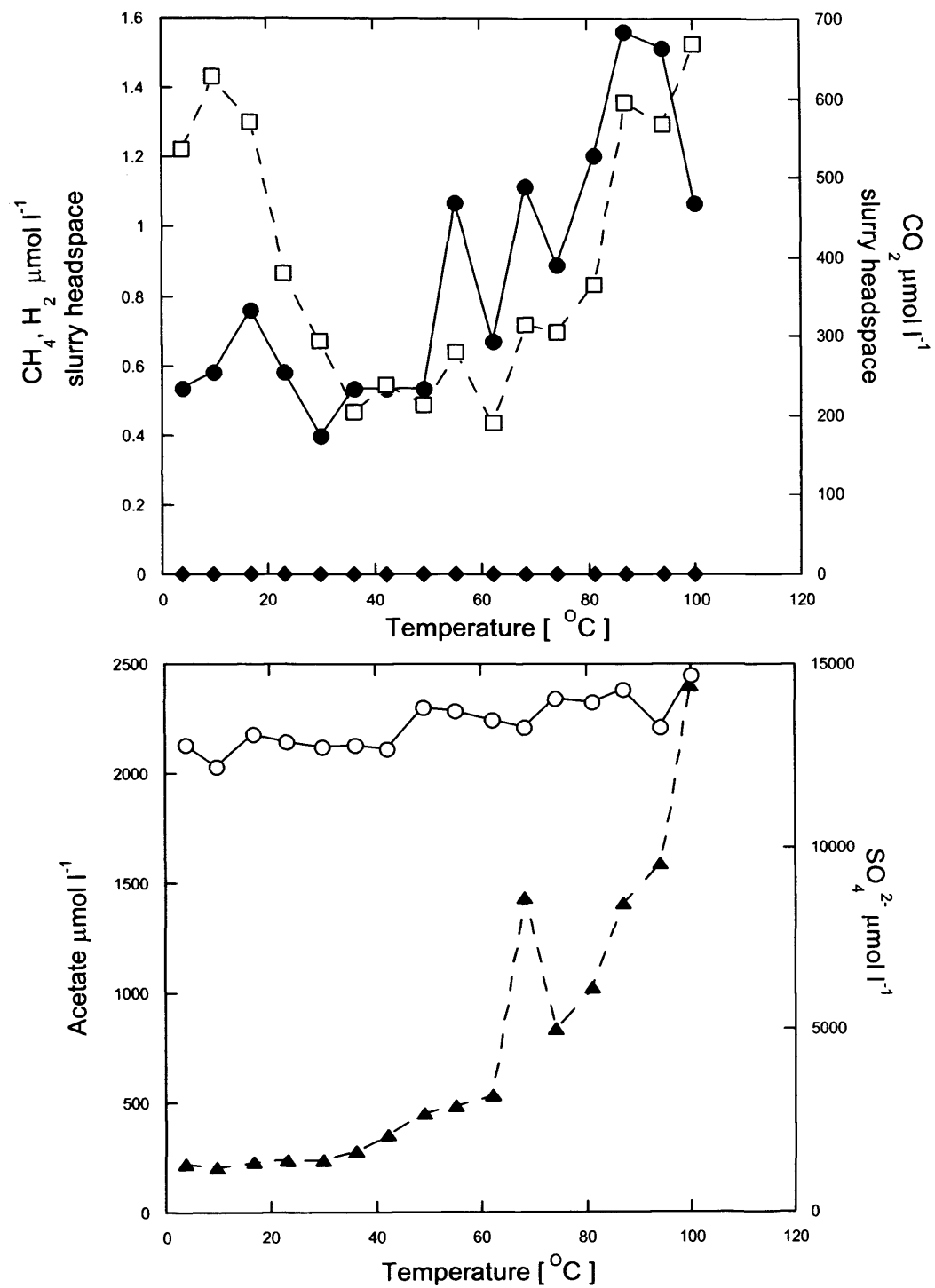
Fig 4.15 Basalt slurry sterile control. 130 days.

Key CH$_4$ (●), CO$_2$ (□), H$_2$ (◆), acetate (▲) and SO$_4{}^{2-}$ (○).

Basalt sterile control, cation concentrations, after 133 days of incubation.
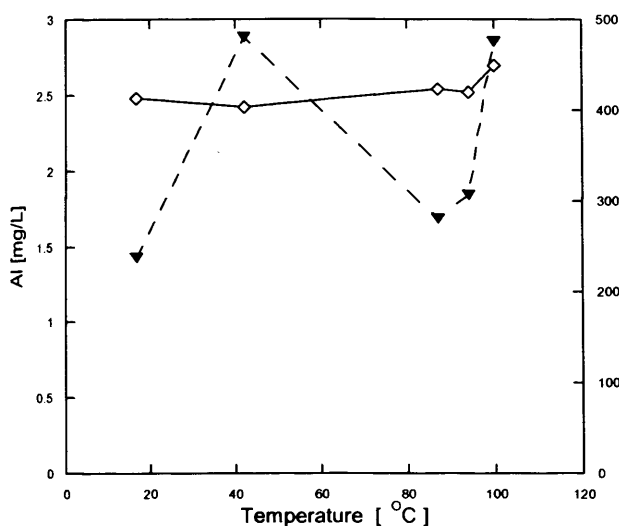
Fig 4.16 Basalt sterile control. Al and K cation concentrations after 133 days, over selected key temperatures

Al: inverted triangle. K: open Diamond
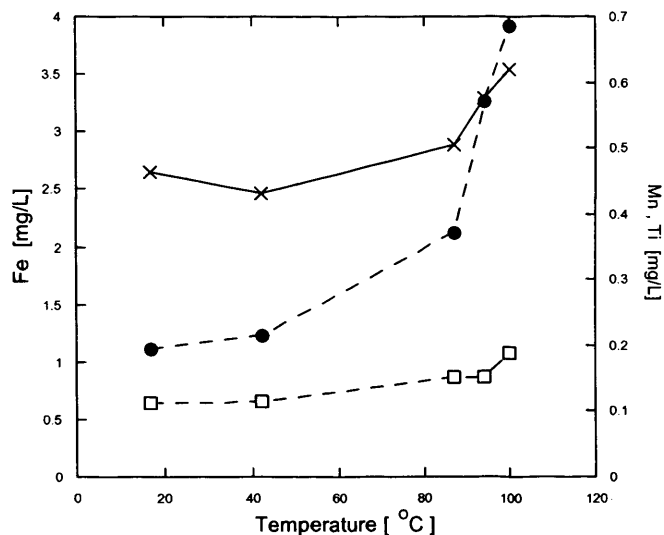
Fig 4.17 Basalt sterile control. Fe, Mn, and Ti cation concentrations after 133 days, over selected key temperatu

Fe: Solid circlet. Mn: x. Ti: open box
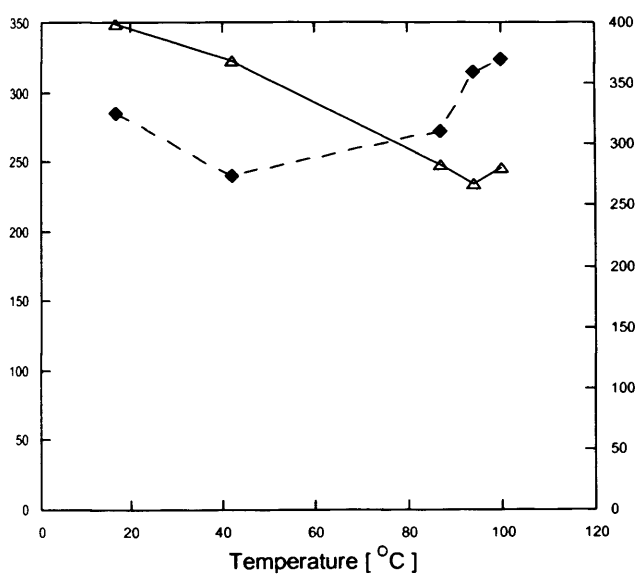
Fig 4.18 Basalt sterile control. Ca and Mg cation concentrations after 133 days, over selected key temperatures

Ca: Diamond. Mg: open triangle
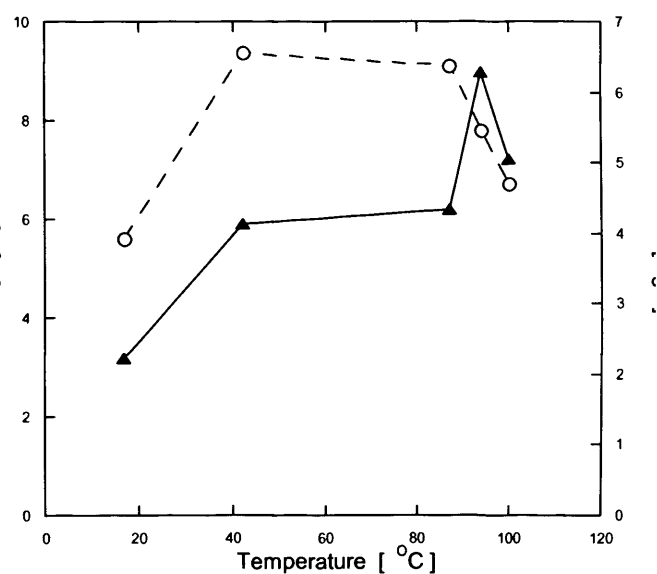
Fig 4.19 Basalt sterile control. P and Si cation concentrations after 133 days, over selected key temperatures

P: open circle. Si: triangle

4.4. Results sterile control incubation (Figs 4.14-4.19)

No hydrogen was detected over any temperature range in the absence of prokaryotes, after 3 days of incubation. Extremely low levels of methane were detected with the highest value of 0.89 μmol l^{-1} at 100°C. Carbon dioxide increased with temperature with a maximum concentration of 6303 μmol l^{-1} also at 100°C. Initial sulphate concentrations were 13.1 mmol l^{-1} no sulphate removal occurred, but there was a slight increase to 13.6 mmol l^{-1} at 100°C. The initial concentration of acetate was 185 μmol l^{-1} this remained constant until 62°C (199 mmol l^{-1}) before consistently increasing with temperature to a maximum value of 614 μmol l^{-1} at 100°C.

After 130 days incubation (this was longer to see if any slower abiotic reactions could be occurring over the course of the incubation which, may have an effect on biogeochemical processes) methane concentrations are still very low with a maximum value of 1.56 μmol l^{-1} present at 87°C. No hydrogen was detected at any temperature. Carbon dioxide levels are substantially lower than the 3 day incubation with a maximum of 667 μmol l^{-1} (5690 μmol l^{-1} lower). Carbon dioxide decreases from 4°C (535 μmol l^{-1}) to 190 μmol l^{-1} at 62°C (a small increase of ~100 μmol l^{-1} is noticed at 9°C) before increasing with temperature to a maximum of 667 μmol l^{-1} at 100°C. This is the inverse of both prokaryotic experiments. No sulphate removal takes place over the course of the experiment in fact a slight increase was noted over the temperature gradient. Concentrations were 12.8 mmol l^{-1} at 4°C whilst at 100°C concentrations of 14.7 mmol l^{-1} where noted. This increase could perhaps be due to FeS/FeS$_2$ oxidation.

Surprisingly high levels of acetate were produced and this increased with temperature above ~40°C, however, no acetate consumption was obvious. Acetate levels increase with temperature with a more exponential increase noted at higher temperatures, maximum concentration of acetate was, 2401 μmol l^{-1}.

Cation profiles after 130 days, show differences to incubations conducted in the presence of prokaryotes in both experiments with or without basalt. Potassium (K) concentration shows no variation across temperature ranges unlike biotic experiments. Al

is similar to other experiments increasing to a max at 42°C (2.88 mg/l) before decreasing to 1.6 mg/l at 87°C and increasing to a final value of 2.85 at 100°C. Fe and Mn concentrations differ than those in the presence of prokaryotes. Increase is not as rapid initially with Fe, but a clear increase with temperature is noted and the maximum value is higher in biotic basalt incubations 3.92 mg/l as opposed to 1.7 mg/l found in abiotic incubations. Mn also increases with temperature from 0.4 mg/l at 17°C to 0.6 mg/l at 100°C. Ti slightly increases, but values are very low from 0.11 mg/l at 17°C to 0.18 mg/l at 100°C. Mg profile is similar in the sterile control to biotic experiments however the concentration changes are not with the basalt incubation decreasing by 250 mg/l as opposed to 100 mg/l in the sterile control. Mg decrease with temperature from values of 399 mg/l at 17°C to 267 mg/l at 94°C before a slight rise to 280 mg/l at 100°C. Ca concentrations decrease slightly to 239 mg/l at 42°C before increasing to a maximum value of 323 mg/l at 100°C. Ca concentrations seem to increase more rapidly when acetate increases again this is similar to biotic experiments, but concentration changes are more extreme when prokaryotes are present. P concentrations increase rapidly to a maximum concentration of 9.37 mg/l at 42°C, plateauing until 87°C (9.13 mg/l) decreasing for remainder 100°C (6.7 mg/l). Si is similar to biotic experiments increase with temperature with a more rapid increase to 40°C. Concentrations are lower than biotic experiments with the highest concentration occurring at 94°C (6.2 mg/l) decreasing to 5.05 mg/l 100°C.
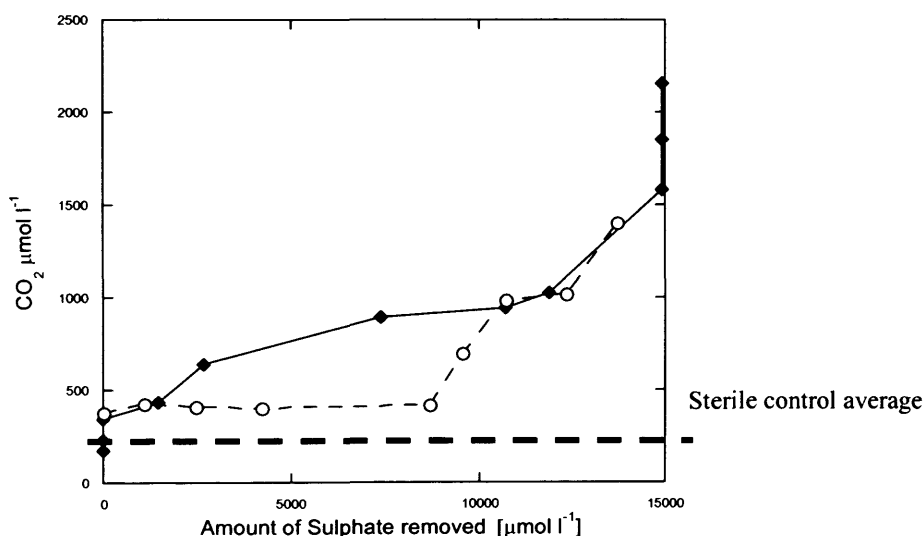
Fig 4.20. Sulphate removed against carbon dioxide generated
Key: Basalt incubation diamond. Sediment only, open circle.
Sterile control dotted line. Average was taken as no sulphate was
removed

117

4.5. Mineral and Anoxic mineral salts solution only incubation (Fig 4.21)

To analyse the effect of freshly ground mineral and anoxic mineral salts on hydrogen generation a limited temperature, thermal gradient experiment was set up. Only gas production was measured and incubation temperatures where chosen where hydrogen was generated in the thermal gradient experiment containing basalt and prokaryotes. The results were as follows.
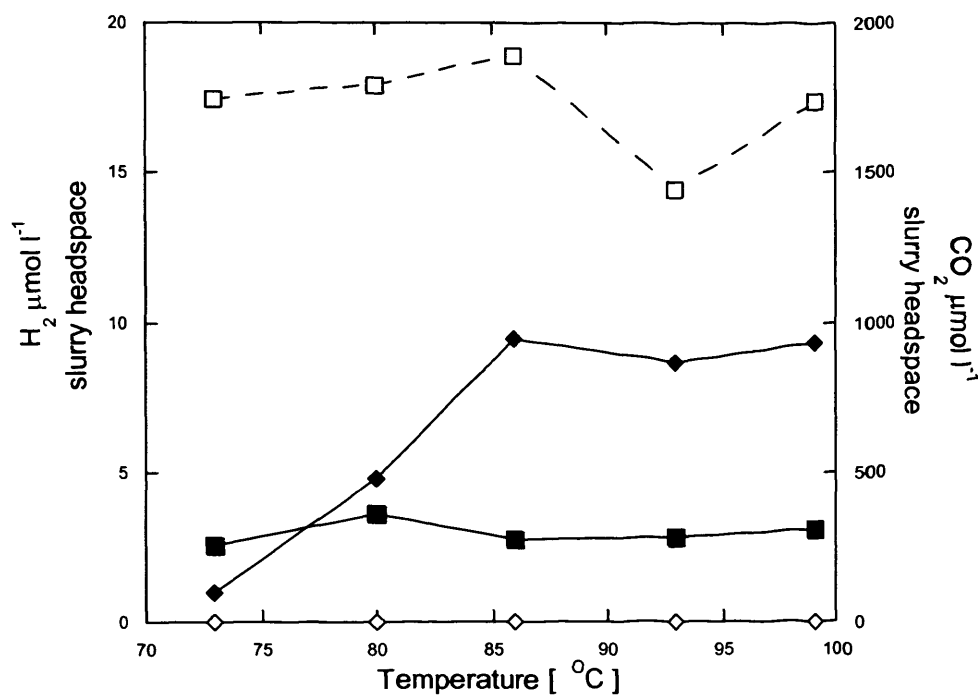
Fig 4.21 Ground Basalt and mineral salt solution.

Key : H_2 3 days($\Diamond$) 28 days ($\blacklozenge$): CO_2, 3 days ($\square$) 28 days ($\blacksquare$)

4.6 Results mineral and anoxic mineral salt solution (Fig 4.21)

Some low levels of hydrogen were generated in the presence of ground basalt and sterile anoxic mineral salt solution, this matches the amounts of hydrogen generated in similar abiotic experiments previously conducted (Stevens and McKinley, 2000). However a maximum of 9 μmol l^{-1} was produced as opposed to 600 to 700 μmol l^{-1} (Fig 4.8 and 4.9

after 3 days) in the presence of microbes is generated. Hydrogen generation increased with both time and temperature up to 85°C before plateauing for the remainder of the experiment. Carbon dioxide levels show little temperature effect (Fig 4.21). Sterile controls with sediment showed a clear temperature effect with a small decrease above 85°C at 3 days (Fig 4.14). This indicates that perhaps the added sediment was involved in the observed CO_2 removal. Carbon dioxide significantly decreased with time from a maximum concentration of 1891 μmol l^{-1} after 3 days, in the absence of prokaryotes, to 363 μmol l^{-1} after 28 days. These results shows that mineral only experiments can be misleading in terms of potential of minerals for hydrogen generation, and that the presence of a sedimentary matrix has a significant effect.

4.7 Bacterial molecular analysis of basalt thermal gradient experiment

M   15   34   47   60   66   92   98   M   +Ve
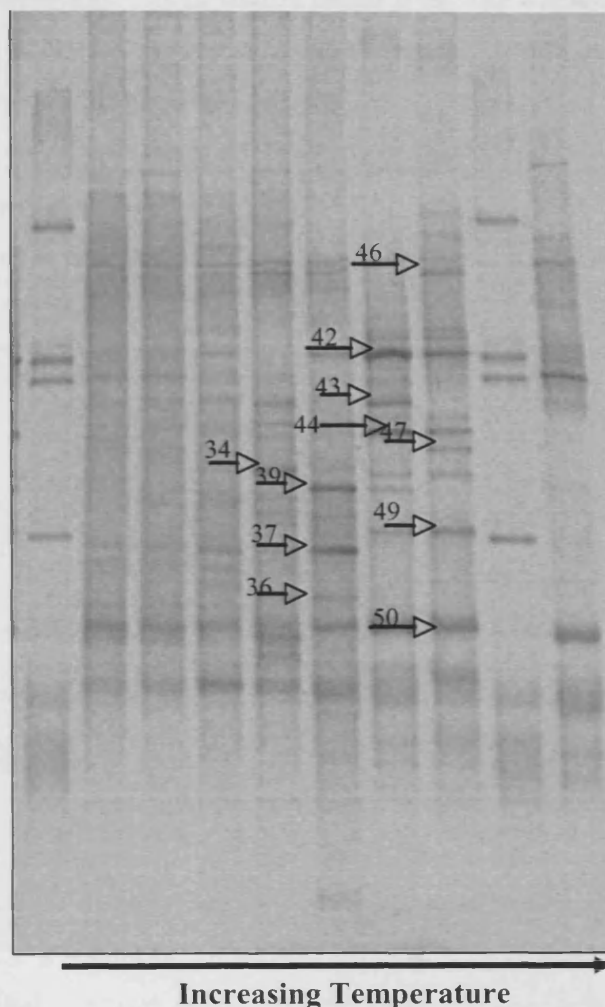
Increasing Temperature
Fig 4.22 Bacterial DGGE gel, of basalt thermal gradient
incubation after 83 days incubation.

Fig 4.22 is a Bacterial DGGE profile of Basalt and sediment thermal gradient experiment after 83 days incubation (Fig 4.9). Gel was a 30-60% denaturing gel using primers, 27F-1492R nested with 907F-357R bands were excised and certain bands were chosen for sequencing. Temperature of samples shown above the profile M= DGGE marker and +Ve is positive control. The following tables show the bacterial results. (Additional band shown on the gel are bands extracted and sequenced but deemed to be not of sufficient quality for inclusion)

Table 4.2. Blastn analysis of bands taken from the basalt DGGE gel using bacterial primers (Fig 4.22). Given are the nearest match, phylogenetic affiliation of that match and the isolation environment.

Number	Nearest match by Blastn search (Accession number)	Sequence Similarity (%)	Phylogenetic Affiliation	Isolation environment nearest match
34	UC clone MPCa_6DO8 (EF414087)	91%	*Firmicutes*	Marine estuary
37	Uncultured Clone M55_D15_L_B_A12 (EF586041)	96%	*Firmicutes, Clostridia*	Anaerobic solid waste digester
39	Thermotogales bacterium Ag55 (AB260049)	80%	*Firmicutes, Clostridia*	Laboratory
42	Delftia clone Zy_B13 (EU376041)	100%	*Betaproteobacteria, Burkholderia*	Soil sample
44	Clone: KW-6. (AB186284)	97%	*Gammaproteobacteria*	Oil storage Reservoir
49	Delftia clone ZY-B13 (EU376041)	96%	*Betaproteobacteria, Burkholderia*	Soil
50	Uncultured clone FLSED16 (EU552848)	96%	*Unknown (possible) Betaproteobacteria;*	Gas condensate Aquifer

4.8 Molecular analysis Basalt thermal gradient archaeal profile

M 15 34 47 60 66 92 98 M, +Ve
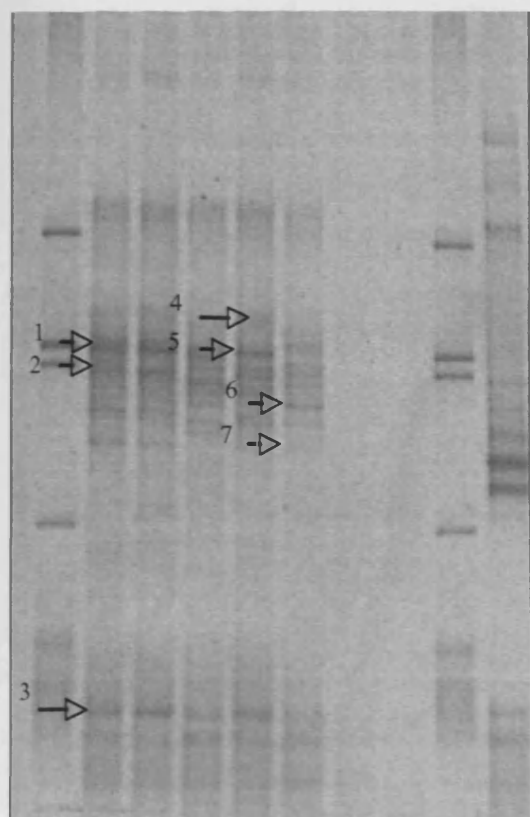
Fig 4.23 (a) :30-60% Archaeal Basalt

Increasing Temperature

M 15 34 47 60 66 92 98 M +Ve
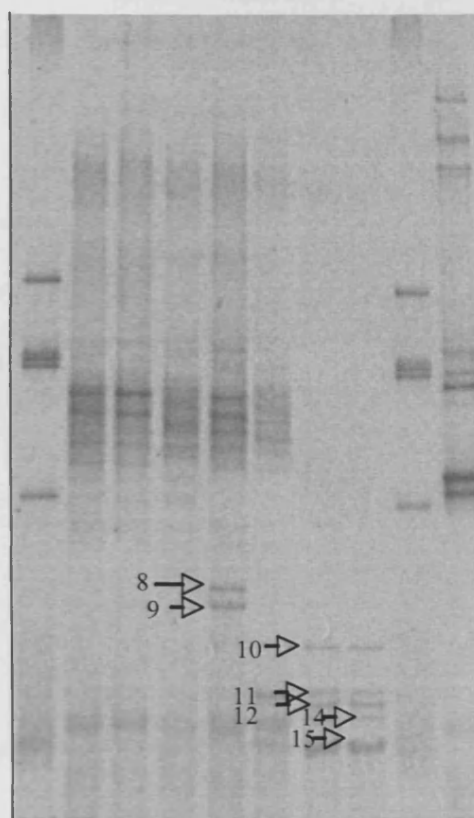
Fig 4.23 (b) 30%-80% Archaeal Basalt

Increasing Temperature

Figs 4.23a And 4.23b Show Archaeal run DGGE profile of prokaryotic basalt thermal gradient experiment. Samples were ran on 2 differing percentage gels. This is due to the high temperature nature of the samples. Note the appearance of extra bands at higher temperature in the 30-80 % gel, this is due to the high GC content of thermostable Archaea being "held" on the 80 % gel. Primers were 109F-958R nested with Parch519r-

Saf. Bands were excised and certain bands were sequenced. The following tables show the results

Table 4.3 Blastn analysis of the 30-60% Denaturant DGGE gel (Fig 4.23 a) Archaeal sequences

Number	Nearest match by Blastn search (Accession number)	Sequence Similarity (%)	Phylogenetic Affiliation	Isolation environment of nearest match
1	Clone 3A066 EF203557	96%	MBG-D	Tidal sediments
2	TfC20L37Ar (EU362355)	94%	MBG-D *Thermoplasmatalaes*	Tidal sediments
3	TfC20L37Ar (EU362355)	96	MBG *Thermoplasmatalaes*	Tidal sediments
4	TfC20L37Ar (EU362355)	92	MBG *Thermoplasmatalaes*	Tidal sediments
5	Gom GC185 601A (AY211715)	97	*Thermoplasmatalaes*	Marine Gas Hydrate
6	AJ5960-5 (AB426458)	96%	MBG-D	Deep Sea microbial mat
7	Kazan-3A-10 (AY592034)	97%	MBG-D	Marine sediment

Table 4.4. Showing Blastn analysis of the 30-80% Denaturant DGGE gel (Fig 4.23 (b)) Archaeal sequences.

Number	Nearest match by Blastn search (Accession number)	Sequence Similarity (%)	Phylogenetic Affiliation	Isolation environment of nearest match
8	TfC20L37Ar (EU362355)	96	MBG-D *Thermoplasmatalaes*	Tidal sediments
9	TfC20L37Ar (EU362355)	96	MBG-D *Thermoplasmatalaes*	Tidal sediments
11	*Methanothermus fervidus* (M32222)	80	*Methanobacteriales; Methanothermus*	Hydro thermal system
12	TfC20L37Ar (EU362355)	94	MBG-D *Thermoplasmatalaes*	Tidal sediments

Fig 4.24 is a bar chart showing tentative identification based on band position relative to sequenced bands from the basalt TG and bands from ilmenite and other gels relative to marker ran. Temperature is plotted against percentage community composition, showing changes in composition with temperature increase.
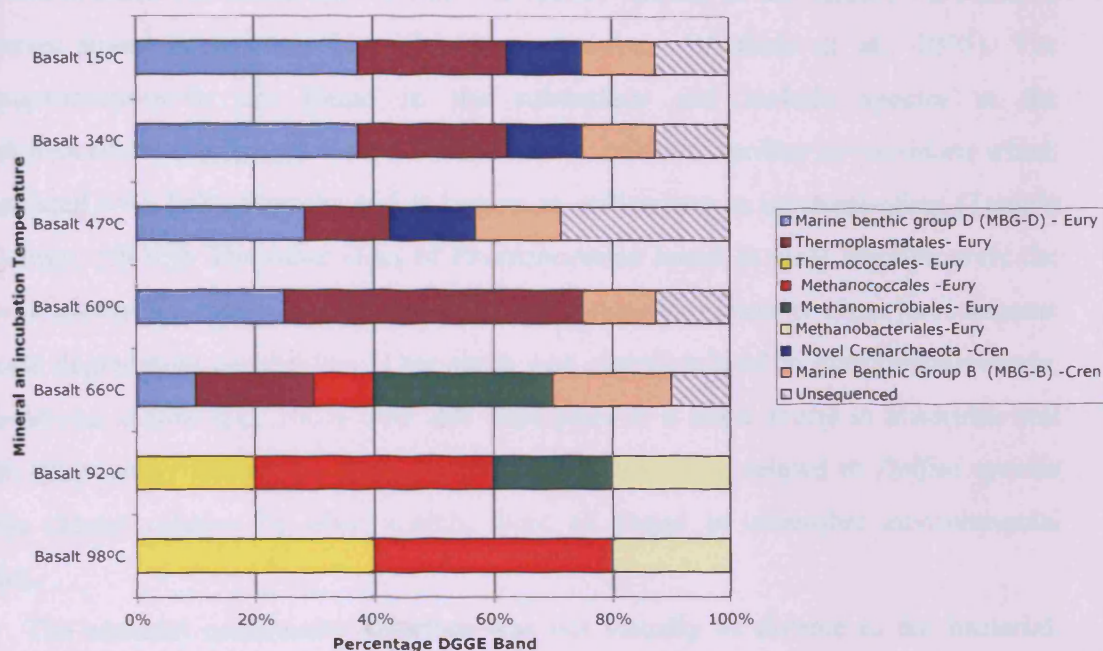
Fig 4.24. Bar graph showing archaeal changes with temperature

4.8.1 Molecular results

Many more bands were sequenced, but deemed not to be of suitable quality for inclusion, only those that had distinguishable base pair amounts of over 100bp, were included. The bacterial profile, by visual analysis appeared to be more complex at lower temperatures than the archaeal. Even at higher temperatures (98°C) more bacterial bands are noticeable in the 60% gradient gel. Bacterial samples were also run on an 80% gradient gel however, as no new bands appeared this was not included in the results. Those bands, which were sequenced in the bacterial profile, belonged to the following phylogenetic groups: *Firmicute's, Clostridia* and *Proteobacteria (Gamma* and *Beta). Clostridia* are often found in environmental samples, are exclusively anaerobic and are normally

associated with fermentation, with end products being acetate and lactate as well hydrogen in some cases (e.g. *C.thermocellum*). *Clostridia* species are used sometimes in bioreactors for hydrogen generation (Chin et al., 2003). It is possible that the high acetate amounts being produced during some incubation's could be the result of the activity of *Clostridia* present. The *Gammaproteobacteria* related species in this sample were related to species found in a anaerobic oil storage reservoir (Yoshida et al., 2005). The *Gammaproteobacteria* are found in the subsurface and include species in the *Acidithiobacillales* (Kelly and Wood, 2000) such as *Acidithiobacillus ferrooxidans* which is associated with FeS_2 deposits and is known to utilise iron in its metabolism (Temple and Colmer, (1951)). The other class of *Proteobacteria* found in these samples were the *Betaproteobacteria*. Many species found in the *Betaproteobacteria* class have organic molecule degradation capabilities. One clone was closely related to *Betaproteobacteria, Burkholderias delftia* spp ,100% over 200 base pairs to a clone found in anaerobic soil sample (physiology unknown). Both *Betaproteobacteria* were related to *Delftia* species and the closest relative by blast search, were all found in anaerobic environmental samples.

The archaeal community structure was not visually as diverse as the bacterial, diversity that is based on the number of bands on the DGGE gels. Only sequences of a certain quality were included. Two gels were run, firstly a 60% denaturant gel, which at higher temperatures yielded no archaeal bands. Secondly an 80% denaturant gel which did yield bands at higher temperatures. This is due to the fact that thermophilic and hyperthermophilic prokaryotes have a higher GC content (for greater thermostability). Separation of bands during DGGE is based on GC content so a higher gradient is needed to "catch" this thermostable DNA. Bands excised and sequenced from the 60% denaturant gel showed percentage similarities to both marine benthic group D and the *Thermoplasmatalaes*. Similarity is quite low in some cases 92% so nothing can be inferred about the physiological function of these archaea. The *Thermoplasma* are cell wall less archaea capable of growth at high temperature and at sometimes low pH, they are anaerobic and have been found in associations with deep subsurface and sub sea communities and it is often associated with coal and pyrite (Segerer et al., 1988), as

metabolism can be based on compounds leeched from coal, it is thought to respire sulphur.

Sequences excised from the 80% gel were also closely associated with the miscellaneous benthic group (MBG) and *Thermoplasmatales*. Also found were species who's most closely related match was an 80% match to *Methanothermus fervidus* (Stetter et al., 1981) species. Which is a thermophilic methanogen growing optimally at 83°C but can grow up to 96°C. Again this is quite phylogenetically distant and hence physiologically distinct from the detected sequence. Closely related archaeal representatives all come form relevant marine and subsurface(Mills et al., 2003; Heijs et al., 2007) and tidal flat (Kittelmann and Friedrich, 2008) environments.

The bar graph represents the change in archaeal community structure with temperature (Fig 4.24). Lower temperatures are dominated by MBG-D and thermoplasmatales associated sequences. Proportions of MBG-D gradually decreases with temperature until 66°C disappearing at 92°C. *Thermoplasmatale*s dominates at medium range temperatures 60°C while the upper temperature range 92 and 98°C is dominated by *Methanococcales* and *Thermococcales* with fewer *Methanobacteriales* methanogen sequences.

4.9 Ramping experiment

The ramping experiment was set up as follows: Start temperature was 65°C ramping 10°C every ten days to 155°C. Sampling regime was, gas sampling after 3 days and 10 days at each temperature before ramping to the next temperature and VFA sampling after 10 days at each temperature before ramping. The exception being the 65°C ramp where VFAs were also taken after 3 days.
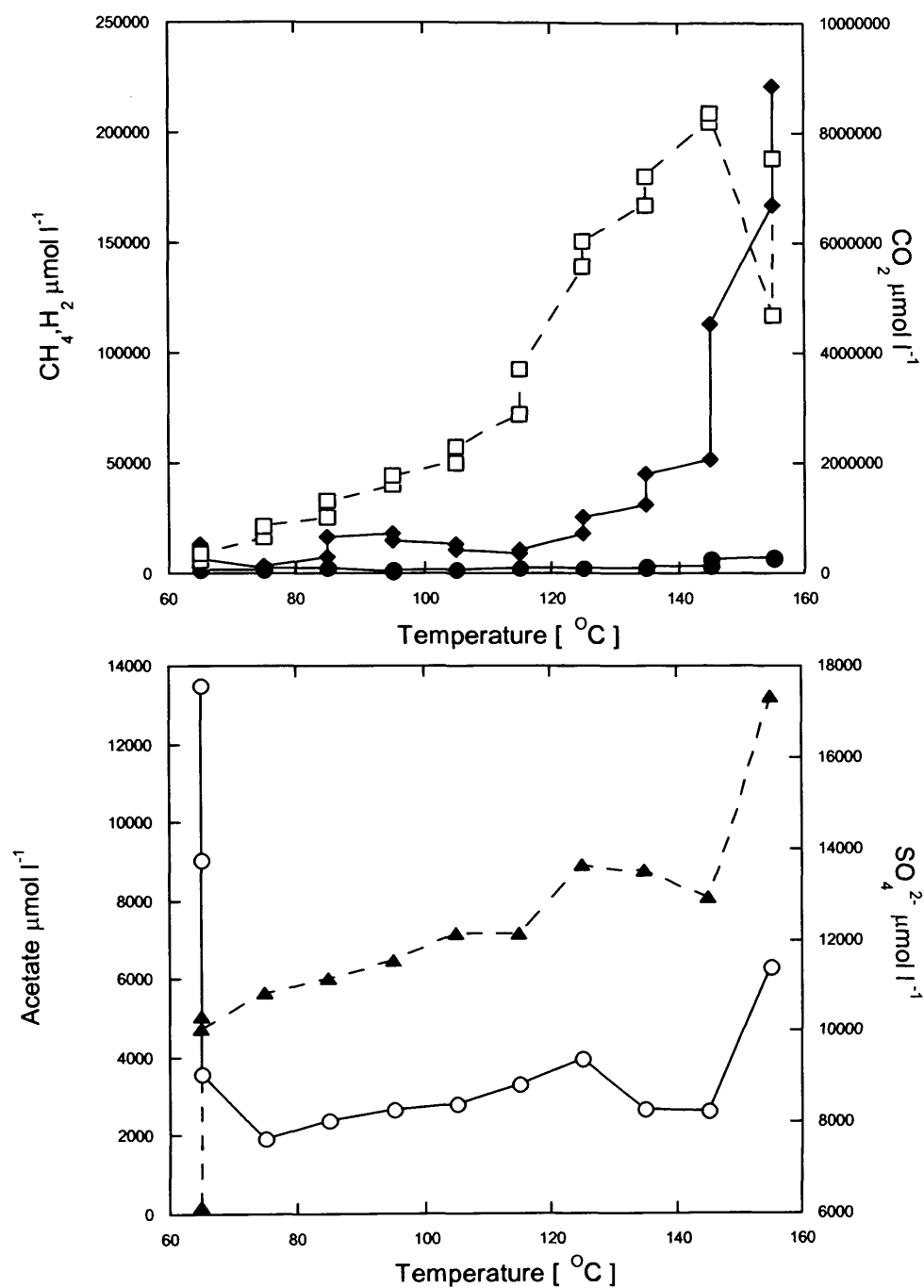
Fig 4.25 Basalt ramping experiment.

Key CH₄ (●), CO₂ (▭), H₂ (◆), acetate (▲) and SO₄²⁻ (○).
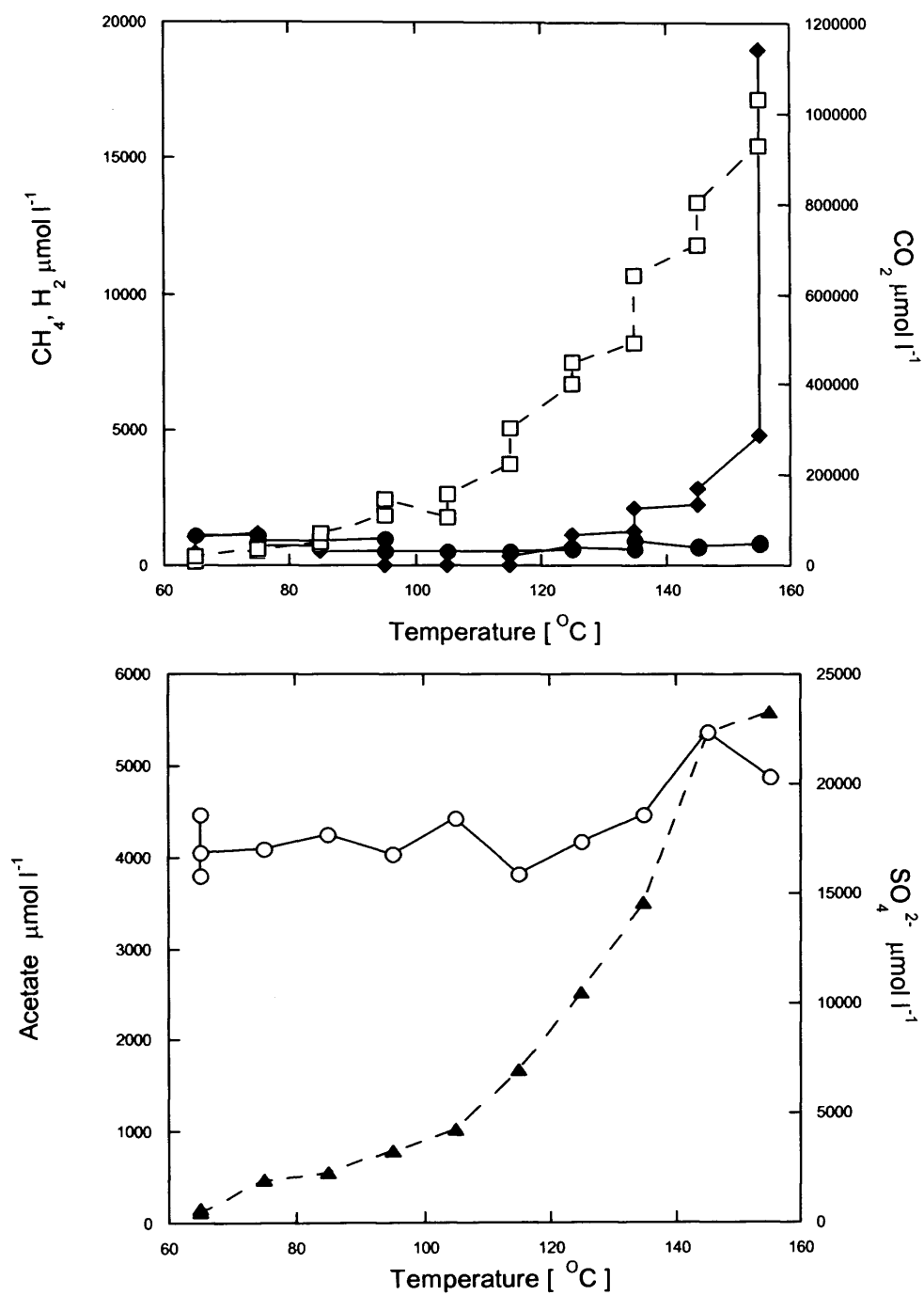
Fig 4.26 Basalt ramping sterile control.

Key CH_4 (●), CO_2 (□), H_2 (◆), acetate (▲) and SO_4^{2-} (○).
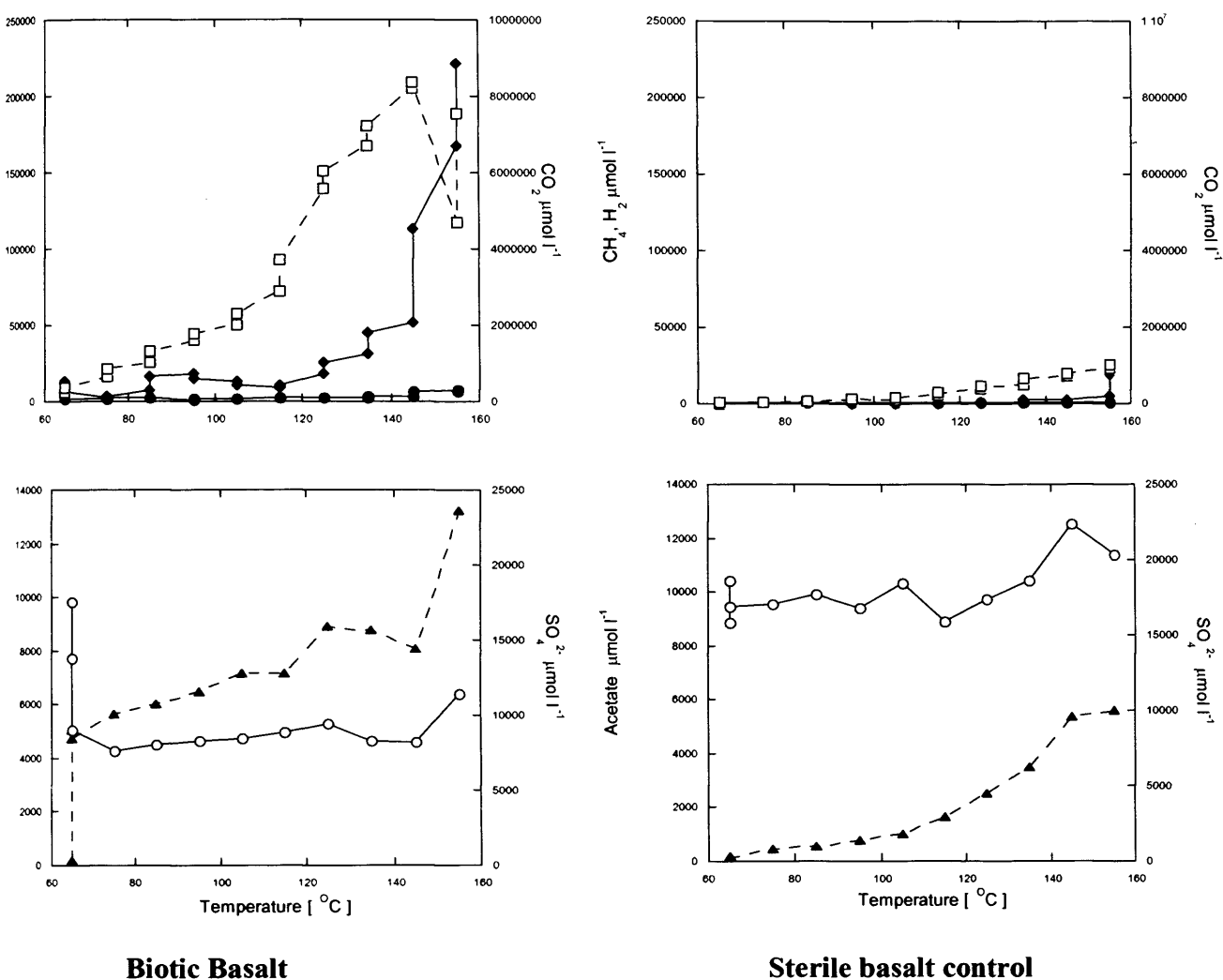
Biotic Basalt   **Sterile basalt control**

Fig 4.27 Basalt ramping comparison of biotic and sterile control. 130 .
Key CH₄ (●), CO₂ (□), H₂ (◆), acetate (▲) and SO₄²⁻ (○).

Comparison of cation concentrations between the Basalt ramping experiment and the
Basalt ramping Sterile control.
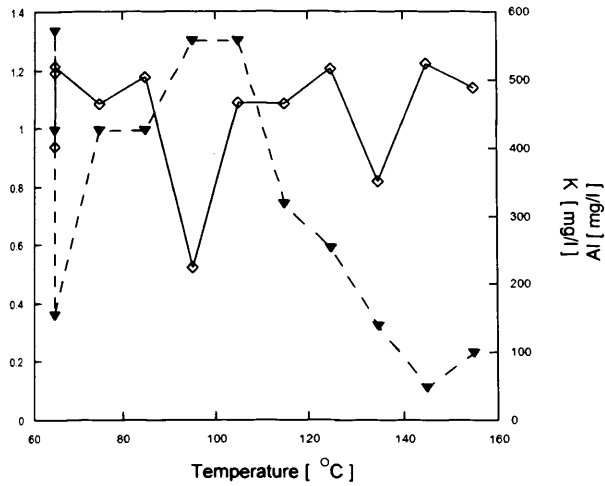
Fig 4.28 Basalt ramping incubation.

Al: inverted triangle. K: transparent Diamond
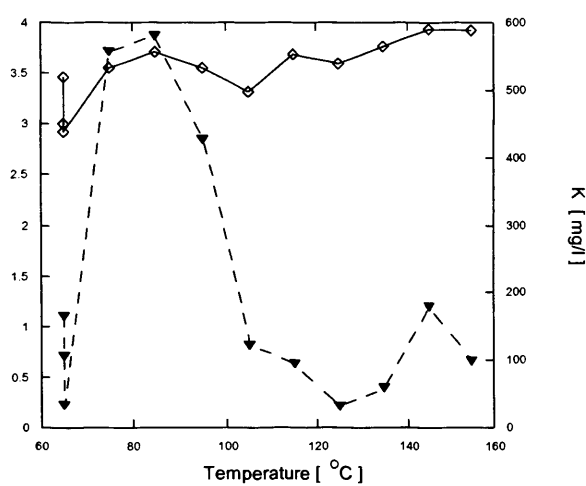
Fig 4.29 Basalt sterile control ramping incubation

Al: inverted triangle. K: transparent Diamond
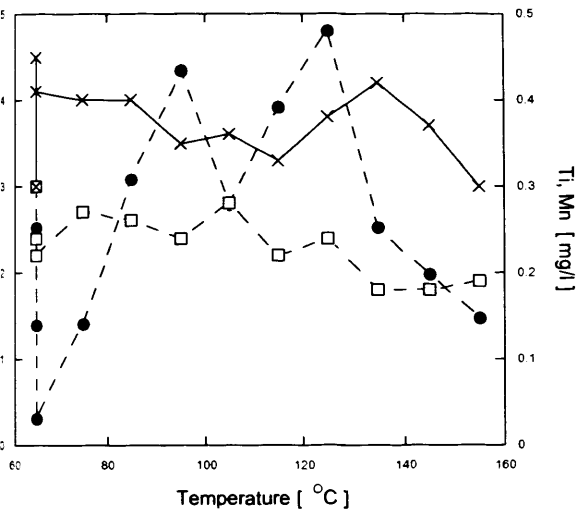
ig 4.30 Basalt ramping incubation.

e: closed circle. Mn: x. Ti: open box
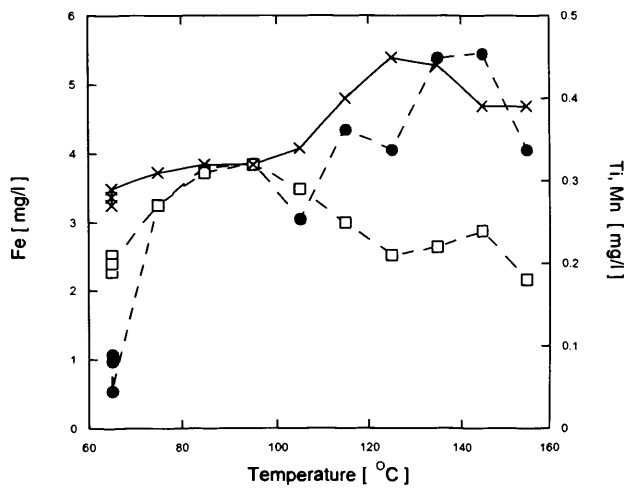
Fig 4.31 Basalt sterile control ramping incubation.

Fe: closed circle. Mn: x. Ti: open box

130
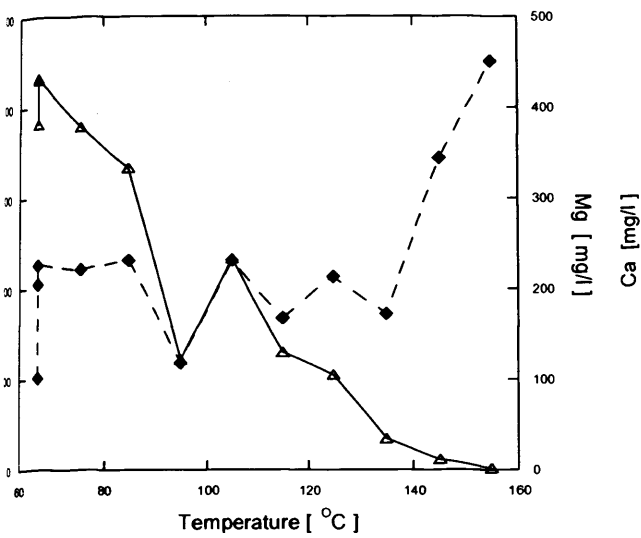
Fig 4.32 Basalt ramping incubation.

Ca: Diamond. Mg: transparent triangle
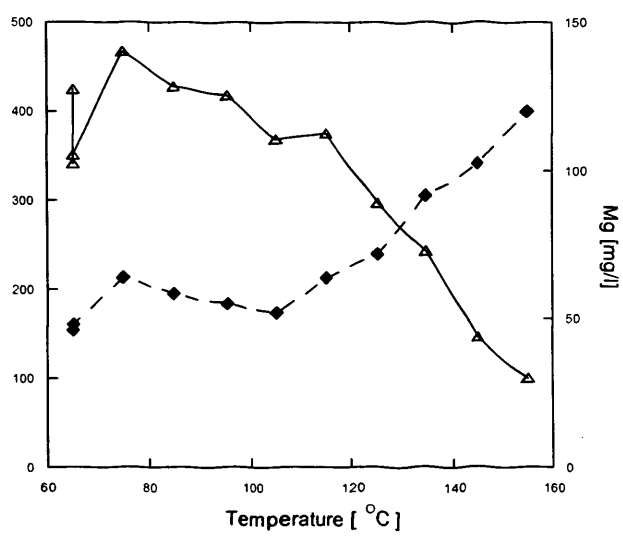
Fig 4.33 Basalt sterile control ramping incubation.

Ca: Diamond. Mg: transparent triangle
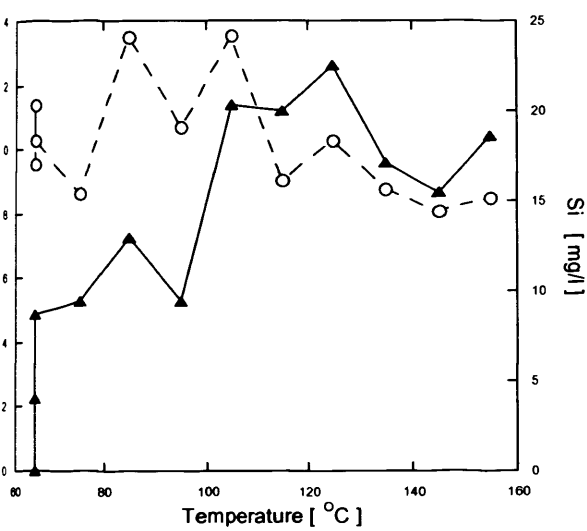
Fig 4.34 Basalt ramping incubation.

P: transparent circle. Si: triangle
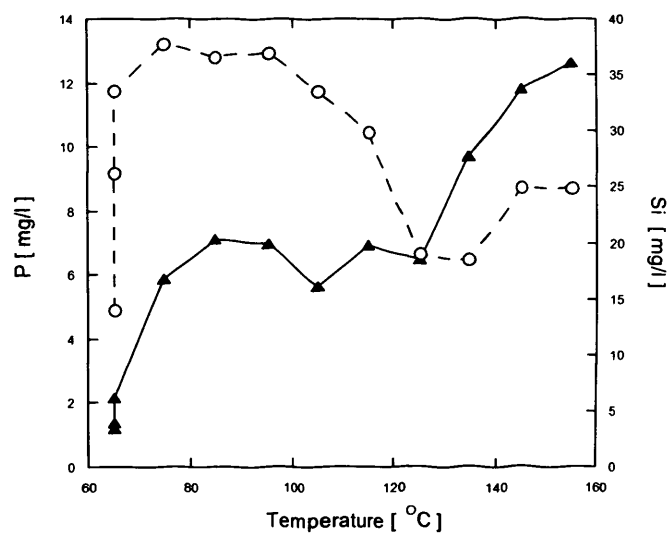
Fig 4.35 Basalt sterile control ramping incubation,

P: transparent circle. Si: triangle

131

4.10 Results ramping experiment

The basalt ramping experiment showed a clear difference between biotic and abiotic impact on simulated sediment burial. In the biotic experiment methane values remained low over the course of the experiment with highest concentrations of 7524 μmol l⁻¹ at 155°C, 3 days after temperature increase. Carbon dioxide levels increased with temperature from 234.95 mmol l⁻¹ at 65°C to 8363 mmol l⁻¹ at 145°C before decreasing to 4689 mmol l⁻¹ after 3 days at 155°C, increasing again to 7530 mmol l⁻¹ after 10 days. Hydrogen levels increase with temperature relatively slowly until 145°C 13 mmol l⁻¹ to 51 mmol l⁻¹ at 145°C after 3 days of incubation. From 145 to 155°C concentrations increase from further to 221 mmol l⁻¹ (after 10 days at 155°C). Acetate concentrations increase with temperature with a rapid increase occurring between 3 days and 10 days incubation at 65°C (203 μmol l⁻¹ to 5058 μmol l⁻¹). Increase is then gradual from 65 to 145°C, 5058 to 8094 μmol l⁻¹, increasing substantially from 145 to 155°C (13.2 mmol l⁻¹). Sulphate removal occurs during incubation at 65 and 75°C from 13 mmol l⁻¹ after 3 days at 65°C to 7.65 mmol l⁻¹ after 10 days at 75°C. Sulphate removal stops when temperature is ramped to 85°C after which sulphate slightly increases with a dip occurring between 125°C and 145°C. The most rapid increase in sulphate occurs between 145-155°C where sulphate increases from 8.2 to 11.2 mmol l⁻¹. This sulphate increase at higher temperatures may be due to the oxidation of previously formed FeS.

In the ramped sterile control experiment, low levels of methane were detected, maximum amount 1144 μmol l⁻¹ at 75°C, this is less than formed in the biotic experiment by a factor of 6.5. Carbon dioxide increased with temperature to a maximum of 1030 mmol l⁻¹ at 155°C as opposed to 8363 mmol l⁻¹ in the biotic experiment which is 8.1 times less. Hydrogen levels increase slowly with temperature from 65 to 145°C (435-2829 μmol l⁻¹) before a substantial increase to a maximum of 19 mmol l⁻¹ at 155°C. Compared to the maximum biotic experimental H_2 concentration of 221 mmol l⁻¹, this is 11.6 times lower. Acetate values increased exponentially with temperature from 166 to 5583 μmol l⁻¹ (65 to 155°C a smaller increase is noted between 145 and 155°C). Maximum values are less than biotic experiment by a factor of 2.3. No sulphate removal

takes place, in fact sulphate values increase towards the end from 16.5 mmol l⁻¹ at 115°C to a final concentration of 20.3 mmol l⁻¹ at 155°C this includes a slight decrease between 145-155°C. Concentrations of hydrogen methane and acetate were much higher in the biotic experiment as opposed to the sterile control (Fig 4.25). Hydrogen levels increased substantially in the biotic control when ramped to abiotic temperatures (120-155°C) compared to the abiotic control. It would appear that prior exposure of minerals to prokaryotic activity in biotic temperature zones (65-120°C) affects the formation of hydrogen and related products at higher abiotic temperatures.

Cation results are graphed to enable comparison of the biotic experiment and the sterile control. Al profiles are quite similar. However, the sterile control concentrations are higher than the biotic with a maximum concentration of 3.8 mg/l as opposed to 1.3 mg/l for the biotic control. Both show an initial increase before decreasing with temperature the biotic incubation decreases from 105°C and the sterile control decreases after 85°C. K concentrations for the biotic experiment starts at 509 mg/l 65°C and finishes at 488 mg/l (155°C) which is fairly constant, there is however, considerable variability in between. A large decrease occurs between 85 and 95°C (502 to 224 mg/l). Before increasing to 467 mg/l, at 105°C . K concentrations in sterile control slowly and consistently increase with temperature from 520 mg/l at 65°C to 588 mg/l at 155°C. Fe concentrations in the biotic incubation decreases initially from 2.5 mg/l to 0.3 mg/l whilst incubated at 65°C then begins to increase from 75°C before increasing to a maximum of 4.8 mg/l at 125°C, before decreasing to 1.4 mg/l at 155°C. In the sterile control, Fe concentrations more gradually increase with temperature and does not display such a large concentration decrease as the biotic incubation does, close to the high temperature zone of maximum hydrogen formation. Sterile Fe concentrations begin at 1.3 mg/l (65°C) increasing to 4.05 mg/l at 155°C, with a maximum of 5.45 occurring at 145°C. Ti concentrations in both incubations slightly increase between 65-115°C before decreasing above 115°C. The biotic experiment starts at a concentration of 0.30 mg/l and concludes at 155°C with a concentration of 0.19 mg/l. The sterile control starts at a concentrations of 0.19 mg/l and concludes at a concentration of 0.18 mg/l. Mn concentrations for the biotic incubation begins at 0.45mg/l decreasing slightly to 0.3mg/l at 155°C. A slight

increase occurs around 115°C from 0.33 to 0.42 mg/l. Mn concentrations slowly increase in sterile control from a start concentration of 0.28mg/l to 0.39 mg/l (155°C). Mg profiles looks broadly similar for both incubations. Generally decreasing over the course of the incubation, following a slight initial increase. In the biotic incubation Mg concentrations start higher than the sterile control 430 mg/l and 127 mg/l respectively. Both decrease through the temperature profile, with the biotic incubation decreasing to 1 mg/l which is a decrease of 429mg/l. The sterile control decreased to a final concentration of 30 mg/l, which is a decrease of 97 mg/l. Ca in contrast increases in both, from a start concentration 101 mg/l and 153 mg/l (biotic and sterile) to final concentrations for each at 155°C of 451 and 400 mg/l (biotic and sterile). In the sterile control the increase is more gradual increasing from ~105°C with the most rapid increase in the biotic experiment occurring from 135°C. Phosphorus (P) and silica (Si) profiles in each of the different incubations. Si increases with temperature broadly for both incubations with a more rapid increase and higher concentrations found in the sterile control. The sterile control increases till 75°C and remains constant till 120°C and rapidly increases to 36 mg/l at 155°C. The biotic incubation shows a slightly different profile increasing over the 65°C incubation remaining constant till 95°C and rapid increase occurs between 95 and 115°C before decreasing slightly towards the upper temperature, with a final concentration of 18 mg/l at 155°C

Both biotic and sterile P concentrations follow a similar pattern. Initial increase until approx 105-115°C followed by a decrease. Biotic concentrations are initially higher 9.5 mg/l as opposed to 4.3 mg/l both finish at a similar concentration at 155°C, biotic concentrations were 8.4 mg/l ,while sterile control concentrations were 8.7 mg/l. maximum values were biotic 13.5 mg/l at 105°C and sterile 13.2 mg/l at 75°C.

4.12 Discussion

The aim of this chapter was to quantify the effect that addition of basalt, has on set sediment slurry incubations conducted in the presence and absence of sedimentary prokaryotes over a defined temperature range (4-105°C). The specific aim was to examine hydrogen generation, its biogeochemical impact and to compare results obtained from previous sterile incubations conducted at 30 and 60°C (Stevens and McKinley, 2000). High temperature ramping experiments were also conducted, in order to examine the effects of sequential heating on mineral : prokaryote interaction and to simulate continuous temperature increases during deep burial. This included into the high temperature abiotic ranges 120-150°C investigating whether previous prokaryotic activity influences subsequent high temperature reactions.

Table 4.5 maximum concentrations for hydrogen methane and acetate (μmol l^{-1})

Experiment	Hydrogen	Acetate	Methane
Sediment only	3.5	3000	535
Sediment and mineral	766	7100	150
Sterile Sediment and mineral	0	2401	1.5
Mineral and sterile salts.	9	0	0

In Table 4.5 several aspects are distinguishable. In the absence of basalt no significant amounts of hydrogen were present up to 93 days incubation and to 100°C. Basalt mineral addition is the key source of hydrogen. Also no significant hydrogen is produced in the absence of prokaryotes. Hence basalt mineral interactions with sedimentary prokaryotes are responsible for significant hydrogen generation (Table 4.5). Hydrogen generation is temperature specific (thermophilic and hyperthermophilic prokaryotes are responsible). Hydrogen production from basalt minerals seems to be a process dependent on 2 things, the correct temperature and the presence of sedimentary prokaryotes. Rates of processes have also previously been shown to be increased by activation of fresh mineral surfaces

(Chapter 3) Whether microbes are directly responsible for hydrogen generation or catalyze another associated reaction necessary for production is unknown e.g. direct removal of electrons from the basalt surface plus proton reduction, or mineral weathering producing new reactive surfaces

It is also probable that hydrogen formation increases the rates of acetogenesis and methanogenesis and sulphate removal, indicated by higher concentrations of end products or reactant removed (Fig 4.4) H_2 formation is sufficient to overcome threshold limitation for competing terminal electron accepting processes. Such as sulphate reduction methane production acetate formation which often occur together. The produced acetate may also be an important substrate for sulphate reduction and methanogenesis. $\delta^{13}C$-CH_4 values for the basalt incubation are consistent with methane produced biotically via acetoclastic methanogenesis. (Whiticar, 1999).

The basalt ramping experiment even with very fast ramp rates $10°C/10d$ showed very significant prokaryotic impact on reactions (Fig 4.25) This includes mineral incubations previously subject to prokaryotic activity,that produce more products such as acetate, hydrogen and methane than sterile systems. In terms of burial of sediment and possible sources of deep hot microbial energy at depth this has clear implications.

The molecular data shown in this chapter indicates that the prokaryotic community structure changes with temperature and that at higher temperature (in the zones of hydrogen generation) the microbial community present is similar to those found at similar temperatures in environmentally relevant areas (oil reservoirs and hydrothermal vent areas). This chapter has demonstrated that high concentrations of hydrogen can be generated from basalt minerals over long time periods (98 days) and that this process is microbially controlled or driven and is biogeochemically relevant. Further analysis in Chapter 5 and 6 will investigate what effect mineral composition has on these processes for example is hydrogen generation dependent on Fe concentrations? Plus provide a more detailed analysis of microbial community through 16S rRNA gene clone libraries.

Chapter 5

Temperature characteristics of ilmenite, pyrite, hematite and magnetite reactions in sediment slurries

5.1 Introduction

This Chapter presents the results of temperature characterisation experiments conducted on mineral slurry incubations over a temperature range of 0 to 105°C

Minerals analysed were, ilmenite, pyrite, hematite and magnetite. Minerals were chosen based on iron concentration and presented in this chapter in that order. Starting with the lowest, concluding with the highest. Iron was measured in terms of wt% Fe_2O_3 (ICP-OES). Pyrite (theoretically 46.6%), Ilmenite 50.7 %, Hematite 54.2%, and Magnetite 99.4%. Pyrite concentrations are given theoretically due to previous mentioned (Chapter 3) limitations of analysis.

In Chapter 3 it was determined that mineral composition affected rates of processes such as methanogenesis, sulphate reduction and acetogenesis, at 60°C. In chapter 4 it was determined that basalt slurry incubations generated hydrogen at high temperatures between 85 to 100°C. This hydrogen generation was microbially driven and was the direct result of microbial basalt interactions. Hydrogen fuelled acetogenesis, methanogenesis and sulphate reduction either directly or indirectly e.g. acetoclastic sulphate reduction.

During the course of this study much thought has gone into the exact mechanism of hydrogen production from minerals. One of the aims of this chapter was to investigate the effect of Fe concentrations on hydrogen generation at a range of temperatures. The redox transition of iron between Fe(II) and Fe(III) valence states, has a fundamental role in environmental biogeochemistry. Fe(II) can function as an electron donor for iron-oxidizing prokaryotes and Fe(III) can function as a terminal electron acceptor for Fe reducing microbes. Microbial Fe reactions are known to occur at high temperature (Vargas et al., 1998), and hence, different mineral Fe concentrations might have an effect

on high temperature hydrogen generation. The importance of iron and reactions involving iron is discussed in Chapter 1. If high temperature H_2 generation is an iron-controlled reaction, then the magnetite incubation should produce the greatest amounts, or at least substantial amounts, considering its composition of 99% iron (Table 3.2). This chapter provides a comparison with chapter 6, which shows reactions involving highly felsic minerals, including 100% SiO_2.

In this Chapter detailed molecular analysis was carried out. Clone Libraries were constructed for the ilmenite and pyrite incubations at varying temperatures. Phylogenetic trees were constructed and analysed to gain a more detailed understanding of the microbial community composition.
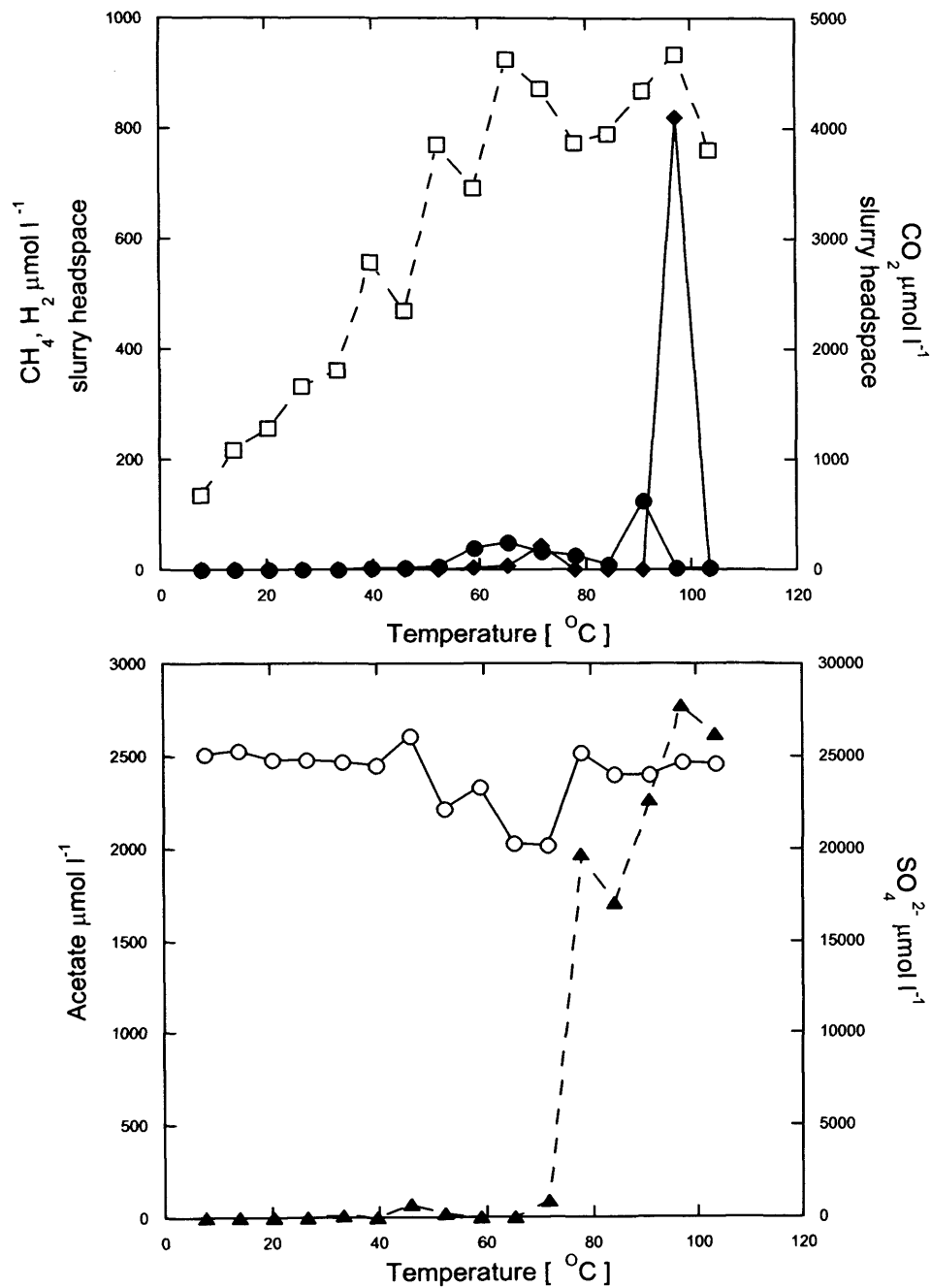
Fig 5.1. Pyrite results after 3 days incubation.

Key CH_4 (●), CO_2 (□), H_2 (♦), acetate (▲), and SO_4^{2-} (○).
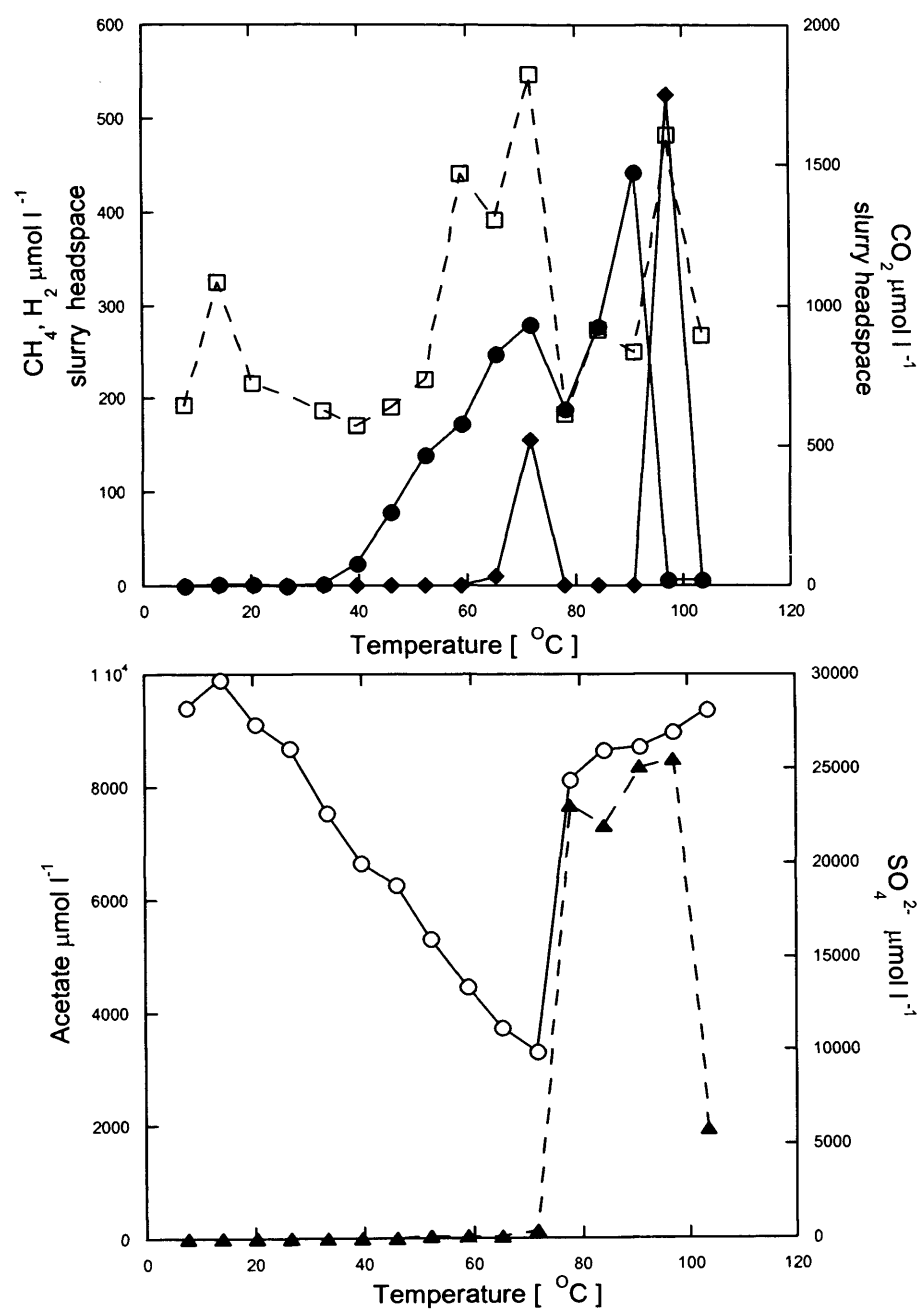
Fig 5.2. Pyrite results after, 110 days incubation.

Key: CH_4 (●), CO_2 (□), H_2 (◆), acetate (▲), and SO_4^{2-} (○)

Cation concentrations for the pyrite slurry incubation after 110 days
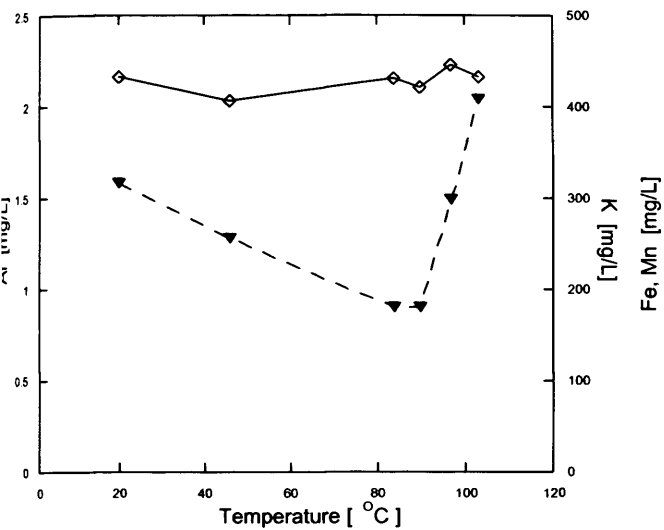
Fig 5.3 Pyrite incubtation. Al and K cation concentrations at selected temperatures after 110 days incubation.

Al: inverted closed triangle. K: open Diamond
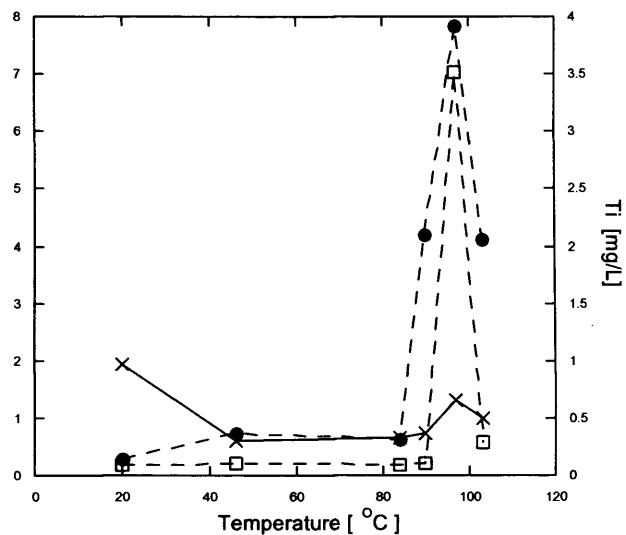
Fig 5.4 Pyrite incubation. Fe, Mn and Ti cation concentrations at selected temperatures after 110 days incubation.

Fe: closed circle. Mn: x. Ti: open box
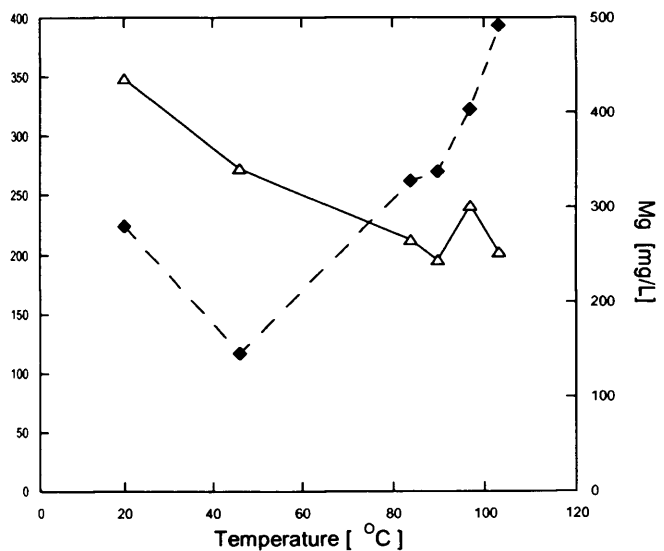
Fig 5.5 Pyrite incubation, Ca and Mg cation concentrations at selected temperatures after 110 days incubation.

Ca: closed Diamond. Mg: open triangle
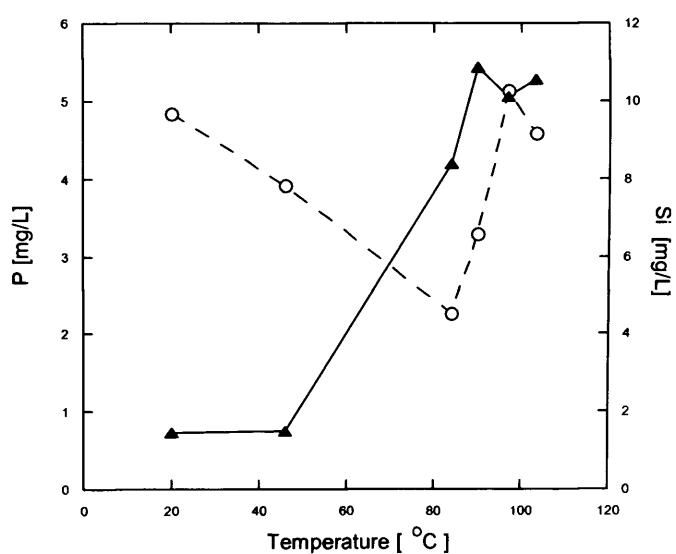
Fig 5.6 Pyrite incubation, P and Si cation concentrations at selected temperatures after 110 days incubation.

P: open circle. Si: closed triangle

141

5.2 Pyrite Results (Figs 5.1-5.6)

After 3 days incubation high amounts of hydrogen were detected at elevated temperatures, with a maximum concentration of 820 μmol l^{-1} detected at 97°C (188 μmol l^{-1} higher than similar ilmenite incubation). However, unlike the previous ilmenite incubation (Fig 5.1) methane concentrations produced are relatively high and occur at high temperature, 125 μmol l^{-1} at 90°C. Carbon dioxide increases with temperature from 679 μmol l^{-1} at 7°C to a maximum concentration of 4673 μmol l^{-1} at 97°C. A slight dip is noticeable between 65 and 90°C and a decrease is also noted after 97°C with concentrations of 3798 μmol l^{-1} at 103°C. Initial concentrations of sulphate were 25 mmol l^{-1} this was greater than in other thermal gradient incubations, due to the grinding effect on pyrite as discussed in Chapter 3. However, as the time between grinding and addition was low (less than 10 minutes). The initial sulphate concentrations are low in comparison to the 60°C pyrite experiment (Fig 3.7), in which SO_4^{2-} concentrations were in excess of 80 mmol l^{-1}. After 3 days sulphate removal had begun from 20°C with a maximum removal of approx 5 mmol l^{-1} at 71°C. No removal detected above 78°C. Acetate values below 78°C are low, 89 μmol l^{-1} at 71°C, however, a rapid increase occurs after 71°C with concentrations of 1972 μmol l^{-1} at 78°C. This rapid increase coincides with sulphate removal ceasing. Maximum acetate concentrations were detected at 97°C (2770 μmol l^{-1}), which is 1477 μmol l^{-1} (114%) higher than the ilmenite experiment. Maximum acetate concentrations are detected at the same temperature as maximum hydrogen concentrations.

After 110 days incubation peaks of elevated hydrogen occurred at two temperatures. Firstly, 154 μmol l^{-1} at 71°C, this was the most active area in terms of sulphate removal. This indicates that hydrogen is produced at lower temperatures than 97°C, however it may be undetectable due to its use in sulphate reduction and other metabolisms. Secondly, similar to the 3 day incubation, large amounts of hydrogen were detected at 97°C (525 μmol l^{-1}) 295 μmol l^{-1} less than after 3 days. Carbon dioxide concentrations increases in a complex manner with temperature, reaching a maximum

concentration of 1821 μmol l^{-1} at 71°C, this coincides with maximum sulphate removal. CO_2 decreases when sulphate removal slows decreasing to 611 μmol l^{-1} at 78°C. The carbon dioxide profile can be broken into 3 distinct increases and 3 decreases. Increase one from 7 to 14°C followed by decrease 1 from 14-52°C, increase 2 from 52-71°C decrease 2 from 71-87°C and increase 3 from 78-97°C followed by decrease 3 above 97°C . Methane concentrations occurred from 33°C (2.8 μmol l^{-1}) (CO_2 decrease 1) increasing with temperature to a maximum concentration of 443 μmol l^{-1} at 90°C (active alongside sulphate reduction) decreasing to near zero concentrations above this. δ^{13}C-CH_4 isotope analyses were performed (Table 5.1).

Table 5.1 δ^{13}C values for pyrite incubation

Temperature	δ^{13}C-CH_4	SD	δ^{13}C-CO_2	SD
90°C	-42.8‰	0.7	-19.2‰	0.2
84°C	-46.9‰	0.9	-19.9‰	0.1
78°C	-46.7‰	1.1	-18.6‰	0.2
71°C	-52‰	0.8	-24.1‰	0.1
65°C	-55.3‰	1.3	-22.4‰	0.3
58°C	-56.7‰	1.9	-21.1‰	0.5
52°C	-52.7‰	0.7	-20.9‰	0.1
46°C	-53.3‰	1	-20.3‰	0.4

SD= standard deviation. n=4

These indicate methane production probably from an acetoclastic pathway (Whiticar, 1999). However, several values fall outside of the Whiticar model for biological methane formation, noticeably high temperature values (e.g. -42‰ at 90°C). There is a clear temperature effect on values at elevated temperatures.
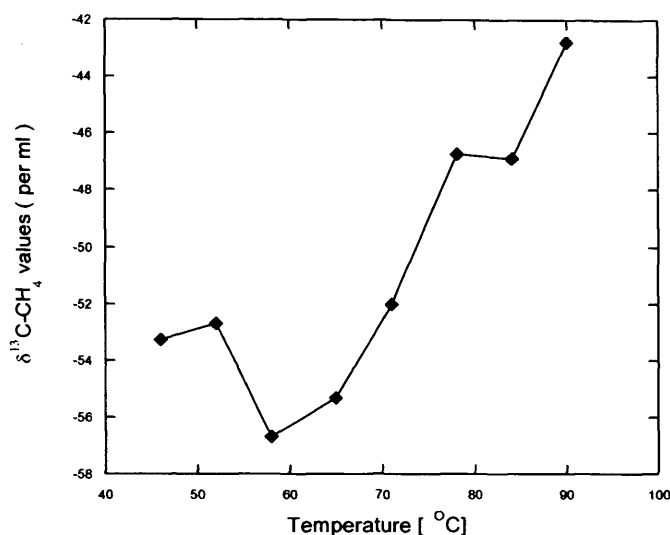
Fig 5.7 Pyrite methane isotope data. Temperature effects on δ^{13}C values

Maximum sulphate removal takes place at 71°C, with 18.3 mmol l^{-1} of sulphate removed, sulphate reduction starts at 20°C. Removal slows dramatically above 71°C with values of 24 mmol l^{-1} at 78°C. This coincides with a rapid increase in acetate from 122 μmol l^{-1} to 7681 μmol l^{-1}, a probable indication of acetate utilisation during sulphate reduction. Maximum concentrations of acetate were at 97°C (8503 μmol l^{-1}), decreasing at 100°C, similar to hydrogen concentrations (1916 μmol l^{-1} at 103°C).

Cation results showed that K concentrations remain relativity constant throughout the incubation, which is unlike the fluctuations seen during the ilmenite and basalt incubations (Chapter 4). Al decreases slightly from 1.5 mg/l at 20°C to 0.9 mg/l at 90°C increasing thereafter to a maximum concentration of 2.04 mg/l at 103°C. This increase occurs during high acetate concentrations. The most interesting pattern observed are the Fe and Ti profiles. Both increase substantially in the area of highest hydrogen detection before decreasing similar to hydrogen at temperatures above 100°C. Fe reaches a maximum of 7.8 mg/l at 97°C before decreasing to 4.1 mg/l at 103°C. Ti increases to 3.5

mg/l at 97°C before decreasing to 0.28 mg/l at 103°C. Hydrogen and Fe concentration are plotted below in Fig (5.8)
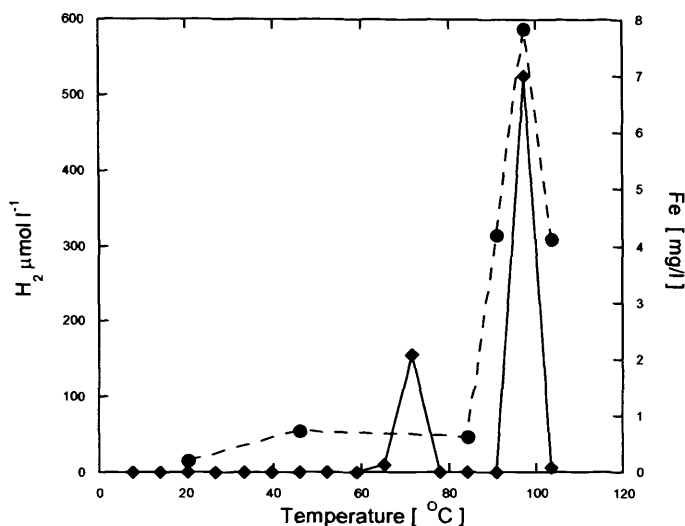
Fig 5.8 Pyrite incubation showing Fe and Hydrogen concentrations.

In contrast Mn concentrations remain low, decreasing from 2 mg/l at 20°C to 0.8 mg/l at 46°C with a slight increase noted similar to Fe and Ti occurring at 97°C, increasing to 1.2 mg/l before decreasing to 0.97 mg/l at 103°C.

Ca concentrations initially decrease from 223 mg/l at 20°C to 116 mg/l at 46°C increasing for the remainder of the incubation with temperature, with a maximum concentration of 393 mg/l at 103°C. Mg concentrations had a contrasting trend with decreases with temperature from a concentration of 436 mg/l at 20°C to 243 mg/l at 90°C, then a slight increase to 301 mg/l at 97°C during the period of peak acetate and hydrogen production, before decreasing again to 252 at 103°C. Si concentrations initially remain constant at 1.4 mg/l until 46°C then increases markedly with temperature after this to 10.9 mg/l at 90°C plateuing after 90°C to concentrations of 10.5 mg/l at 103°C. P concentrations decrease from 4.8 mg/l at 20°C to 2.3 mg/l at 83°C. Before increasing to

5.2 mg/l at 97°C. and decreasing to 4.5 mg/l at 103°C. This rapid increase is similar to the increase in acetate and peaks at maximum concentrations for acetate and hydrogen coupled with a decrease above 100°C.
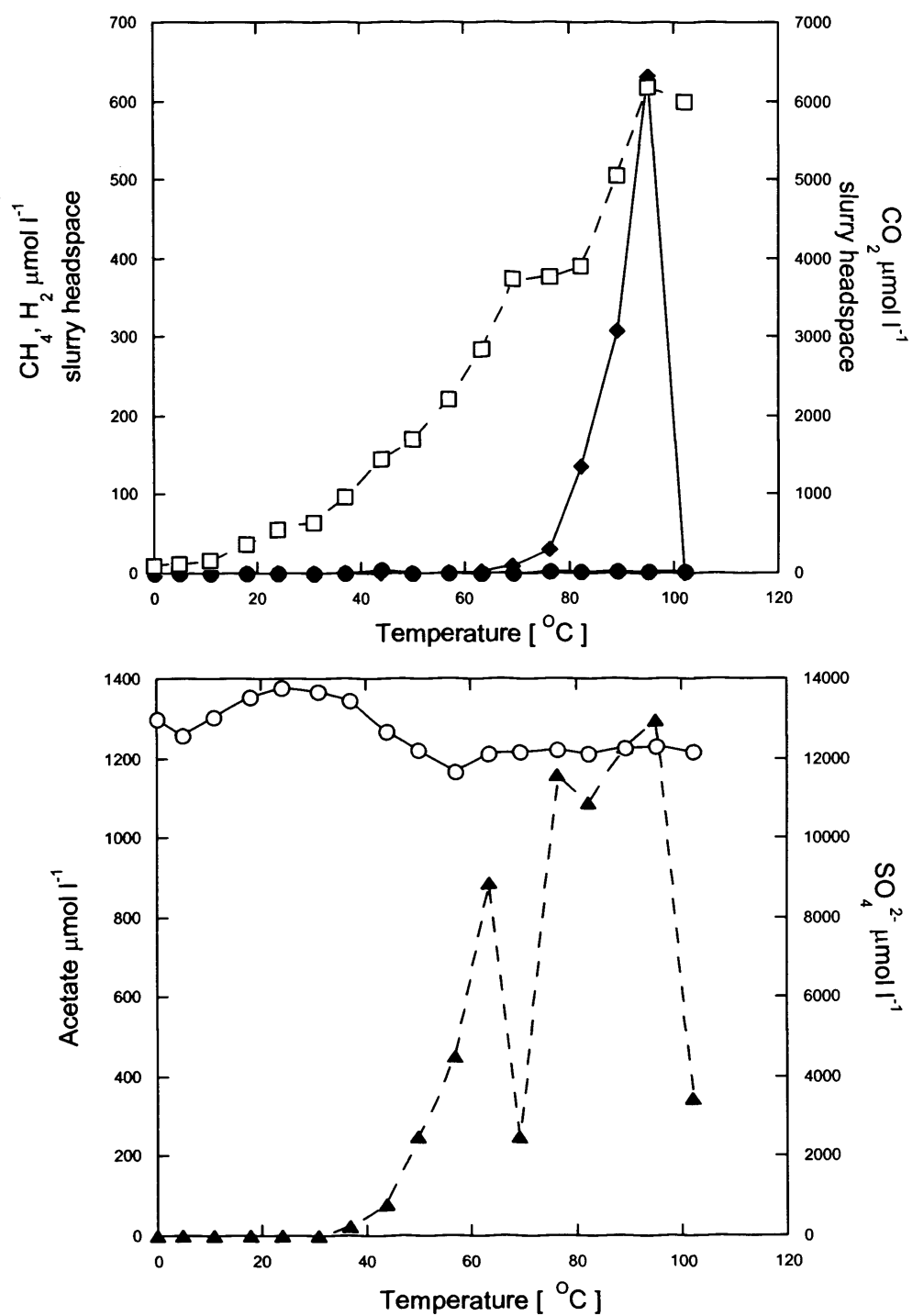
Fig 5.9 Ilmenite addition, 3 days incubation.

Key CH₄ (●), CO₂ (□), H₂ (♦), acetate (▲) and SO₄²⁻ (○)
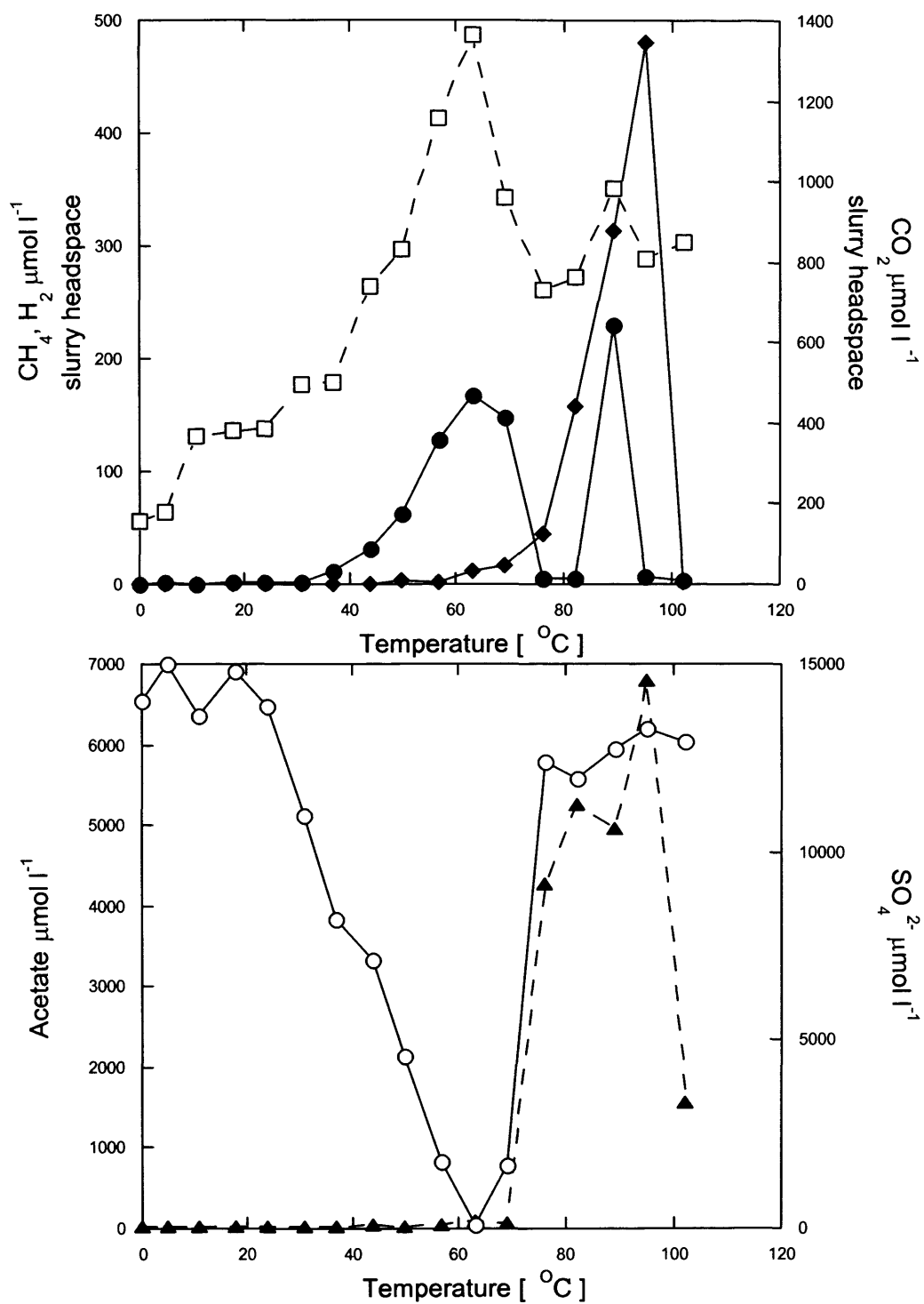
Fig 5.10 Ilmenite addition, 83 days incubation.

Key: CH_4 (●), CO_2 (□), H_2 (◆), acetate (▲) and SO_4^{2-} (○)

Cation concentrations for the ilmenite slurry after 83 days of incubation
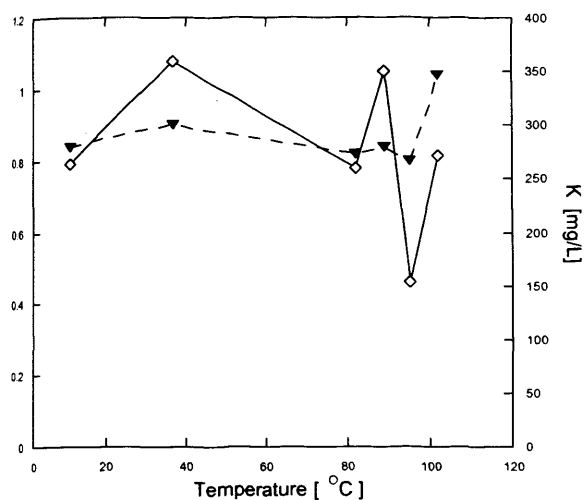
Fig 5.11 ilmenite incubation. Al and K cation concentrations at selected temperatures after 83 days incubation.

Al: inverted closed triangle. K: open Diamond
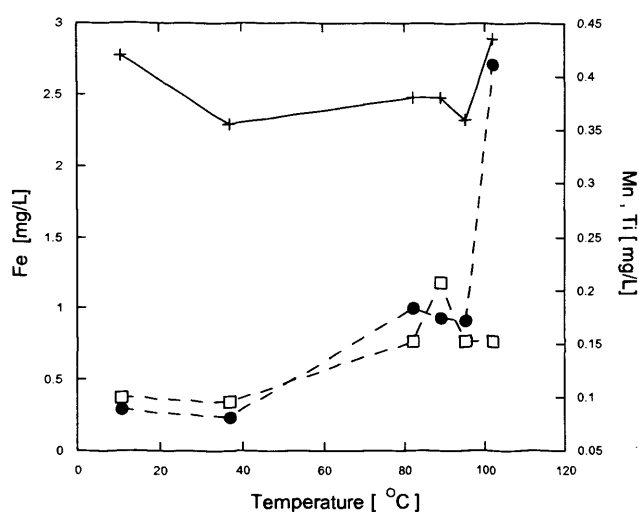
Fig 5.12 ilmenite incubation, Fe, Mn and Ti cation concentrations at selected temperatures after 83 days incubation.

Fe: closed circle. Mn: x. Ti: open box
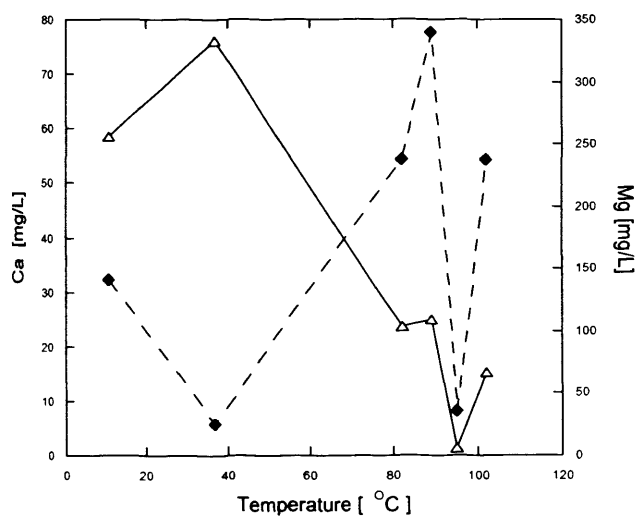
Fig 5.13 ilmenite incubation. Ca and Mg cation concentrations at selected temperatures after 83 days incubation.

Ca: closed Diamond. Mg: open triangle
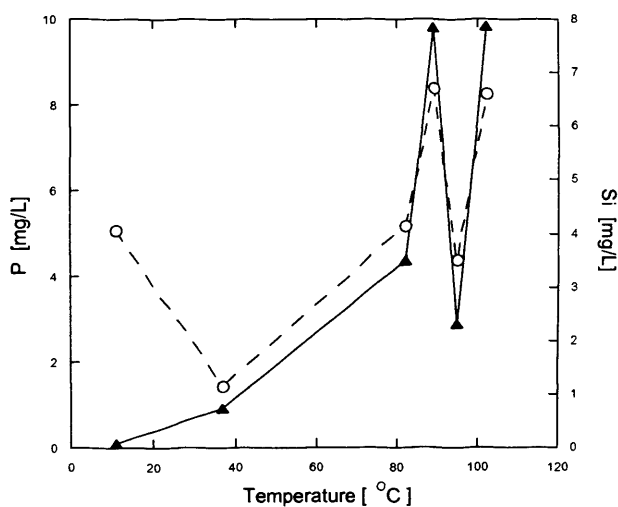
Fig 5.14 ilmenite incubation. P and Si cation concentrations at selected temperatures after 83 days incubation.

P: open circle. Si: closed triangle

149

5.3 Ilmenite results (Figs 5.9-5.14)

In the ilmenite incubation, similar to basalt high concentrations of hydrogen were produced within 3 days above 69°C, but not above 100°C. Hydrogen concentrations increased from 8.6 µmol l^{-1} at 69°C, to a maximum concentration of 632 µmol l^{-1} at 95°C, decreasing to 1.1 µmol l^{-1} by 102 °C. No significant amounts of methane were detected after 3 days incubation. Carbon dioxide concentrations overall increased with temperature, reaching a maximum of 6176 µmol l^{-1} at 95°C, with a slight decrease to 6002 µmol l^{-1} by 102°C (but with a plateau in concentrations between ~70-80°C). Acetate concentrations increase rapidly from 23 µmol l^{-1} at 37°C to 885 µmol l^{-1} at 63°C. Then dipped to 246 µmol l^{-1} at 69°C, before increasing again to 1159 µmol l^{-1} by 76°C and continuing to increase but more slowly reaching a maximum of 1293 µmol l^{-1} at 95°C. Again similar basalt incubations in (Chapter 4), a decrease occurs above 100°C, decreasing to 346 µmol l^{-1} at 102°C. Initial sulphate concentrations was 13 mmol l^{-1} which decrease slightly at 37°C, reaching a concentration of 12.1 mmol l^{-1} at 102°C.

After 83 days incubation high concentrations of hydrogen were detected at elevated temperatures. Maximum concentration of 480 µmol l^{-1} occurs at 95°C, which is 143 µmol l^{-1} less than the 3 day incubation. Methane concentrations are elevated in two zones firstly between 35 and 75°C, that has a maximum concentration of 147 µmol l^{-1} at 63°C. The second peak has a maximum concentration of 230 µmol l^{-1} at 89°C. The first methane peak occurs in the zone of sulphate depletion once methane concentrations begin to decrease a rapid rise in acetate occurs. This also coincides with a rapid decrease in sulphate removal rates. $\delta^{13}C$-CH$_4$ isotope data were obtained for the lower temperature peak (table 5.1) and values obtained are consistent with methane produced through the acetoclastic pathway (Whiticar, 1999). Unfortunately no values for the upper temperature methane peak were obtained. Carbon dioxide increases with temperature to maximum of 1385 µmol l^{-1}, contiguous with the maximum zone of sulphate removal occurring at 63°C. CO$_2$ concentrations then decrease sharply before slowly increasing with a peak

concurrent with that for methane, at 89°C reaching 989 µmol l^{-1}. This is a good indication of acetoclastic methanogenesis. The cleavage of acetate to CH_4 produces CO_2 (Eq 5.1)

$$CH_3COO^- + H_2O \rightarrow CH_4 + HCO_3^- \quad \Delta G^{O'} = -31kj/reaction \quad \textbf{(Eq 5.1)}$$
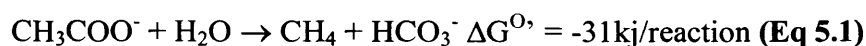
Table 5.2 $\delta^{13}C$ values for ilmenite incubation

Temperature	$\delta^{13}C$-CH_4	SD	$\delta^{13}C$-CO_2	SD
69°C	-53.2‰	0.7	-20.8‰	0.3
57°C	-55‰	1.1	-20.1‰	0.2

SD, Standard Deviation, n=4

Sulphate removal began at 24°C with maximum removal occurring at 63°C to a concentration of 90 µmol l^{-1} this is a total removal of 12.9 mmol l^{-1}. Complete removal does not occur. Methanogenesis occurs during sulphate removal. Acetate concentrations rapidly increase when sulphate removal slows. Indicating possible use of acetate not alone in methanogenesis, but also in sulphate reduction suggesting excess substrates, which enables these potentially competitive processes to co-occur. Acetate increases from 74 µmol l^{-1} at 69°C to a maximum concentration of 6792 µmol l^{-1} at 95°C. A rapid decease occurs above 100°C decreasing to 1569 µmol l^{-1} by 102°C therefore acetate production seems to be biogenic rather than thermogenic.

Cation concentrations after 83 days were as follows. Al values remain constant throughout the course of the experiment until 95°C. Starting concentrations were 0.84 mg/l at 11°C at 95°C concentrations were 0.8 mg/l after which a 24% increase occurs to 1.04 mg/l at 102°C. This coincides with a rapid decrease in hydrogen concentrations (Fig 5.10). K concentrations have an initial concentration of 263mg/l at 11°C fluctuated slightly with concentrations of 349 mg/l at 89°C, decreasing to 153 mg/l at 95°C before increases to 265mg/l at 102°C. The decrease at 95°C (56%) coincides with detection of highest concentrations of hydrogen and acetate. Mn concentrations at 11°C were 0.42 mg/l with a concentration at 102°C of 0.43 mg/l concentrations are similar at the upper

and lower temperature with a decrease to 0.36 mg/l noted between ~40-90°C. Fe concentrations show an initial increase with temperature from 0.3 mg/l at 11°C to 0.92 mg/l at 95°C. After 95°C a rapid increase to 2.7 mg/l at 102°C occurs, a 6% increase between 95 and 102°C. Ti concentrations increase with temperature from 0.1 at 11°C, to a maximum concentration at 89°C of 0.20 mg/l co-occurring with the 2nd CH_4 peak, and then decreasing slightly with concentrations of 0.15 found at 102°C. Ca concentrations at 11°C were 32.3 mg/l decreasing to 5 mg/l at 37°C before increasing with temperature to a maximum concentration of 77 mg/l at 89°C. A dip in concentrations occurs between 89 at 95°C (8.2 mg/l) a decrease of 68 mg/l this decrease co-insides with maximum concentrations of hydrogen (Fig 5.15). Once hydrogen concentrations decrease Ca increases to 54 mg/l at 102°C

Mg concentrations initially increase from 256 mg/l at 11°C to 332 mg/l at 37°C. Before decreasing to 6 mg/l at 95°C (concurrent with elevated hydrogen and acetate) then increasing to 66 mg/l at 102°C. Si concentrations generally increase exponentially with temperature but with a decrease noted, similar to phosphorus, at 95°C, Si increases from 0.08 mg/l at 11°C to 7.7 mg/l at 77°C. Decreasing to 2 mg/l at 95°C. Increasing again to 7.8 mg/l at 102°C. A similar pattern is noted for phosphorus, except there is a decrease from 5 mg/l , at 11°C, to 1.4 mg/l at 37 °C. Subsequently, there is increasing concentration with temperature, with a maximum concentration of 8.4 mg/l at 89°C. A dip in concentration of 48% occurs to 4.3 mg/l at 95°C, before an increase close to maximum values of 8.2 mg/l at 102°C. Both phosphorus and silica show a similar pattern of large decreases close to maximum concentrations of hydrogen and acetate.
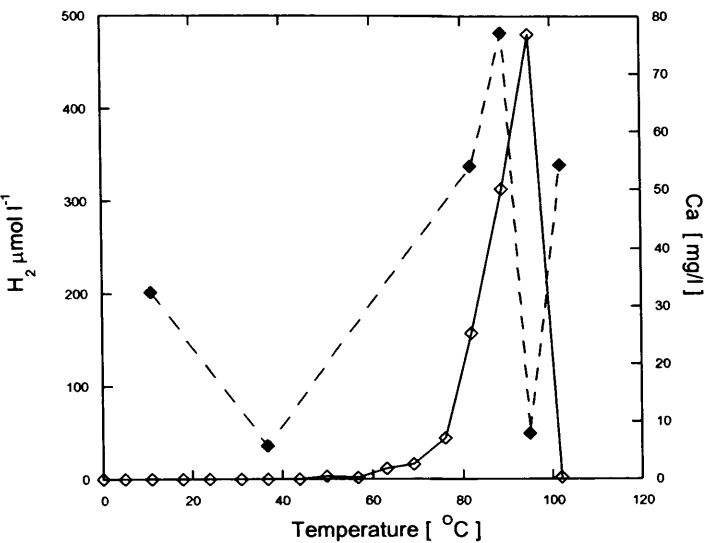
Fig 5.15 ilmenite incubation H₂ and Ca concentrations after 83 days incubation
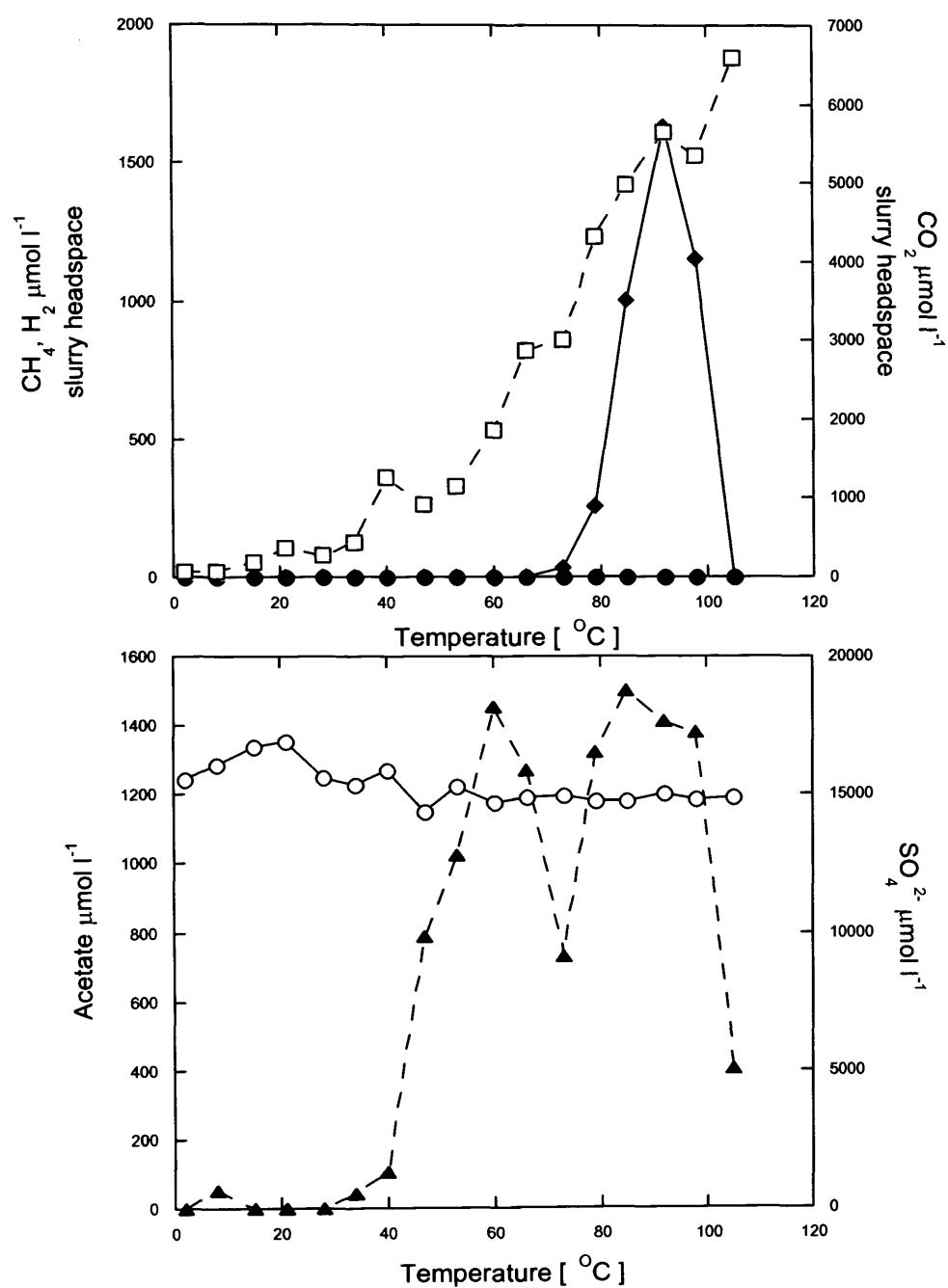
Fig 5.16. Hematite addition, 3 days incubation.

Key: CH₄ (●), CO₂ (□), H₂ (◆), acetate (▲), and SO₄²⁻ (○)
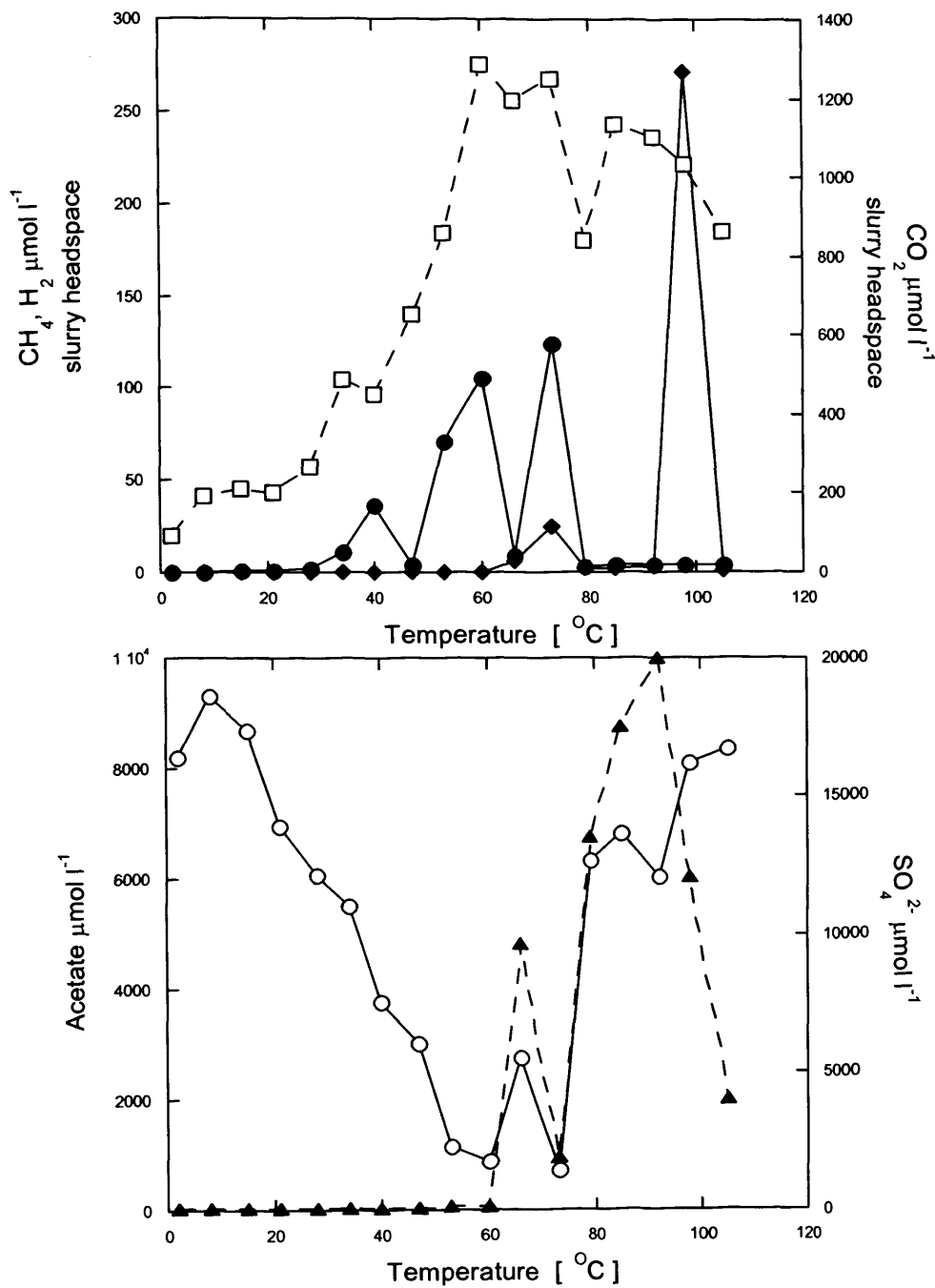
Fig 5.17 Hematite addition, 100 days incubation.

Key: CH_4 (●), CO_2 (□), H_2 (◆), acetate (▲), and SO_4^{2-} (○).

Hematite slurry incubation, cation concentrations after 100 days of incubation
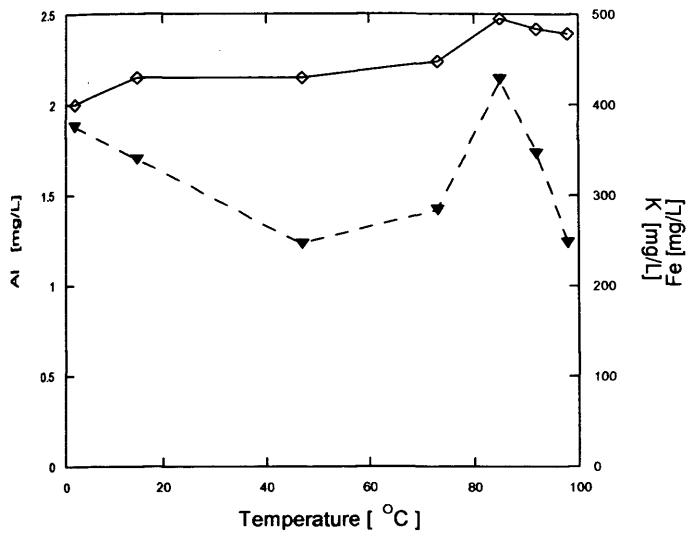
Fig 5.18 Hematite incubation. Al and K cation concentrations at selected temperatures after 100 days incubation.

Al: inverted closed triangle. K: open Diamond
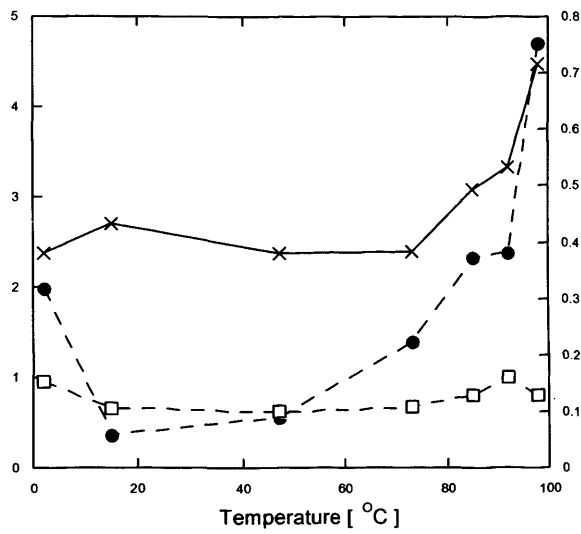
Fig 5.19 Hematite incubation. Fe, Mn and Ti cation concentrations at selected temperatures after 100 days incubation.

Fe: closed circle. Mn: x. Ti: open box
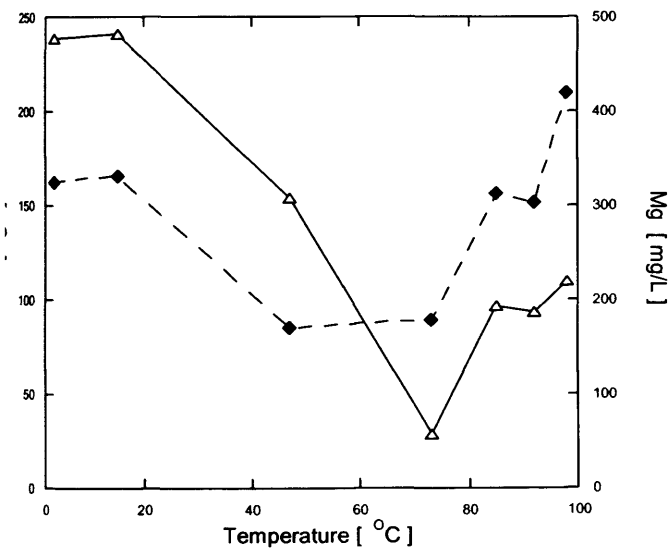
Fig 5.20 Hematite incubation, Ca and Mg cation concentrations at selected temperatures after 100 days incubation.

Ca: closed Diamond. Mg: open triangle
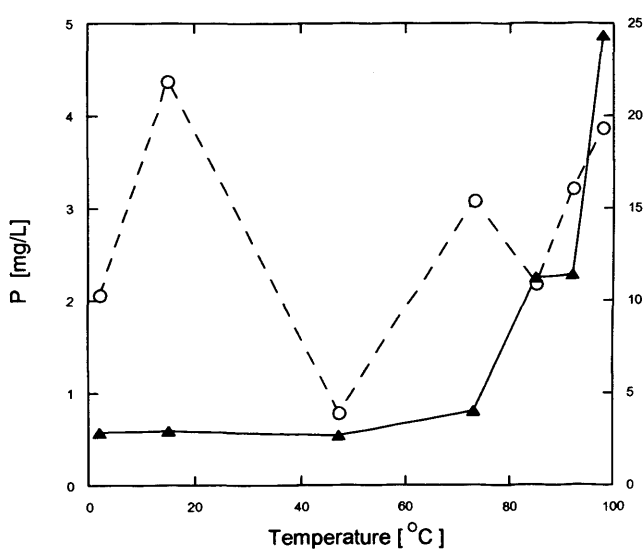
Fig 5.21 Hematite incubation. P and Si cation concentrations at selected temperatures after 100 days incubation.

P: open circle. Si: closed triangle

156

5.4 Hematite results (Figs 5.16-5.21)

After 3 days the hematite incubation produced no significant amounts of methane, a maximum of only 2 μmol l^{-1} occurring at 105°C this is in contrast to the pyrite incubation where 125 μmol l^{-1} was produced despite the higher SO_4^{2-} concentration (Fig 5.1). Significant amounts of hydrogen were also generated with a maximum concentration of 1155 μmol l^{-1} at 92°C. Which was 335 μmol l^{-1} more than during the pyrite incubation. No hydrogen is detected above 100°C. Carbon dioxide increases with temperature, with a maximum concentration of 6580 μmol l^{-1} occurring at 105°C. No significant sulphate removal took place over the first 3 days, although the small apparent increase in SO_4^{2-} up to ~ 20°C makes this difficult to judge. Acetate values rapidly increase at 40°C from 104 μmol l^{-1} to 1451 μmol l^{-1} (60°C). After this rapid increase, acetate decreases to 723 μmol l^{-1} at 73°C, before increasing to a maximum of 1501 μmol l^{-1} at 85°C. Acetate values then decrease up to 100°C to 406 μmol l^{-1} at 105°C, similar high temperature decreases have occurred in all incubations thus far. The amount of acetate generated is substantially less than generated in the pyrite incubation (2770 μmol l^{-1}, Fig 5.1) this combined with the lack of methane generation, could be a contributing factor to greater quantities of hydrogen accumulating in this incubation, as opposed to the pyrite incubation.

After 100 days of incubation elevated hydrogen concentrations were detected at two temperatures; 25 μmol l^{-1} at 73°C and 271 μmol l^{-1} occurring at 98°C. This is similar to the pyrite incubation. Carbon dioxide increases with temperature up to 60°C a maximum of 1286 μmol l^{-1} this occurs in the zone of most sulphate removal. Carbon dioxide plateaus after this, before a dip in concentration close the end of the 73°C CH_4 peak, decreasing further past 100°C (862 μmol l^{-1} at 105°C). Methane formation begins to be detectable at 34°C (10 μmol l^{-1}) increasing to a maximum of 123 μmol l^{-1} at 73°C. Two decreases in methane are noted at 47 and 66°C, the second decrease at 66°C co-

occurs with an increase in acetate concentrations and a decrease in the sulphate removal rate.

$\delta^{13}C$-CH_4 isotope values were obtained from these samples and they suggest methane production via acetoclastic pathway (Table 5.3)

Table 5.3 $\delta^{13}C$ values for hematite incubation.

Temperature	$\delta^{13}C$-CH_4	SD	$\delta^{13}C$-CO_2	SD
60°C	-54.6‰	0.9	-20.5‰	0.2
53°C	-57.2‰	0.9	-20.3‰	0
40°C	-55.4	1.8	-18.2‰	0

SD=standard deviation n=3

Sulphate removal proceeds most rapidly at 73°C with a concentration of 1470 μmol l^{-1} representing a total removal of 17.1 mmol l^{-1}. Interestingly removal of sulphate at 66°C is slower than neighbouring temperatures (5510 μmol l^{-1} remaining). This decrease in removal rate is coupled to an increase in acetate to 4835 μmol $^{-1}$. If you normalise sulphate removal rates to mirror the average removal rates of the adjoining samples e.g. 73°C has a concentration of 1470 μmol l^{-1} this leaves the sulphate concentration in the 66°C sample in excess by 4040 μmol l^{-1}. Acetate concentrations have risen from zero at 60°C, to 4835 μmol l^{-1} at 66°C. Considering sulphate reduction using acetate is at a ratio of 1:1 (Eq 5.2) this to gives SO_4^{2-} at 4040 μmol l^{-1} and acetate in excess by 4835 μmol l^{-1} thus giving possible evidence of growth of sulphate reducers using acetate.

$Acetate^{-1} + SO_4^{2-} + 3H^+ \rightarrow 2CO_2 + H_2S + 2H_2O$ $\Delta G^{O} = -57.5$ kj/reaction **(Eq 5.2)**
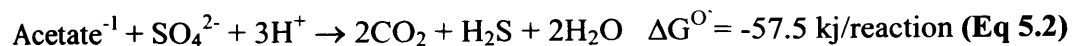
Sulphate removal ceases at 98°C. Acetate rapidly increases when sulphate removal slows at 73°C from 941 μmol l^{-1}, consistent with acetate being used as a substrate (Eq 5.2) and continues to increase to a maximum concentration of 10 mmol l^{-1} at 92°C decreasing rapidly thereafter to 2007 μmol l^{-1} at 105°C in common with other experiments.

Cation analysis showed a slight increase in K concentrations with increasing temperature from 400 mg/l at 2°C to 487 mg/l at 98°C. Al concentrations start at 1.8 mg/l at 2°C and show an initial decrease to 45°C before increasing to a maximum concentration of 2.15 mg/l at 84°C and decreasing at higher temperature to 1.2 mg/l at 98°C. Fe and Mn values remain level before increasing with temperature. Fe initial concentrations are 1.9 mg/l at 2°C decrease to 1.4 mg/l at 73°C before increasing substantially from 74°C to 4.7 mg/l at 98°C. Mn has an initial concentration of 0.38 mg/l (2°C) and remains stable until 73°C (0.38 mg/l at 73°C) before increasing with temperature reaching a maximum of 0.71 mg/l at 98°C. Similar to both pyrite and ilmenite incubations elevated amounts of Fe occur close to the zone of greatest acetate /hydrogen formation.

Ti remains relatively constant over the course of the experiment between 0.1 and 0.15mg/l. Initial calcium concentrations start at 162 mg/l, calcium concentrations decrease and plateau in the temperature zone between 47 and 73°C decreasing to 84 mg/l at 47°C and 89 mg/l at 73°C. After 73°C, Ca increases over the remaining temperatures to a maximum concentration of 209 mg/l at 98°C. Mg concentrations are constant to 18°C then decrease with temperature from 476 mg/l at 2°C to 57 mg/l at 73°C which is the lowest concentration reached. Increasing after this to 219 mg/l at 98°C. Si concentrations remain constant from 2°C until 47°C (2.8 mg/l at 2°C and 2.6 mg/l at 47°C). After 47°C Si concentrations exponentially increase with temperature reaching a maximum concentration of 24 mg/l at 98°C The most rapid increase occurring in the zone of hydrogen generation from 92 to 98°C (Fig 5.21). An approximate doubling, of Si concentrations in this temperature range. High temperature Si increases occurs with all 3 previous examined minerals. P concentrations fluctuate over the course of the incubation, increasing initially from 2 mg/l at 2°C to 4.3 mg/l at 15 °C decreasing to 0.7 mg/l at 47°C followed by an increase to 3.0 mg/l at 73°C and then a decrease to 2.1 mg// at 85°C. Gradually increasing with temperature after this point to 3.8 mg/l at 98°C.
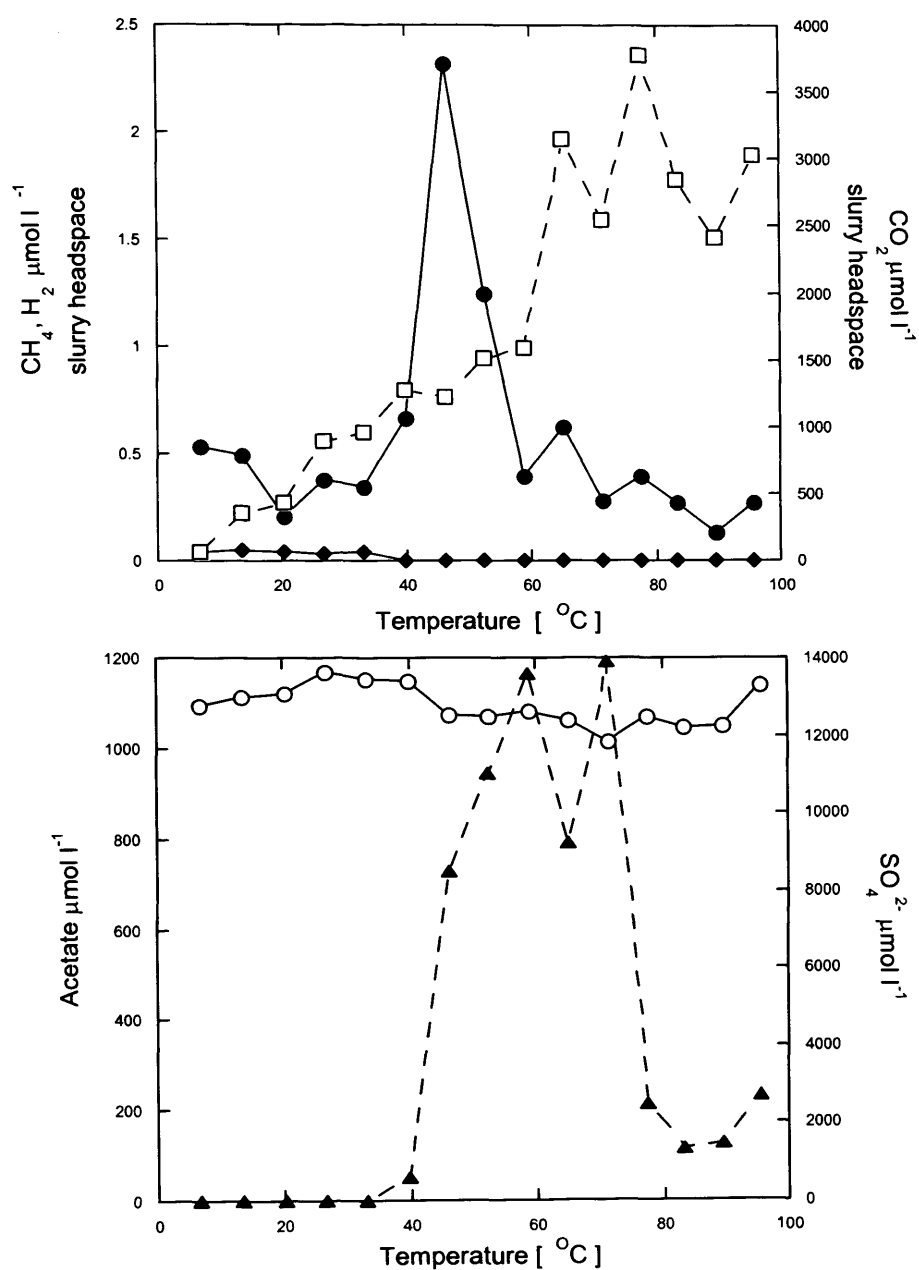
Fig 5.22. Magnetite addition, 3 days incubation.

Key: CH$_4$(●), CO$_2$ (□), H$_2$ (◆), acetate (▲), and SO$_4^{2-}$ (○).
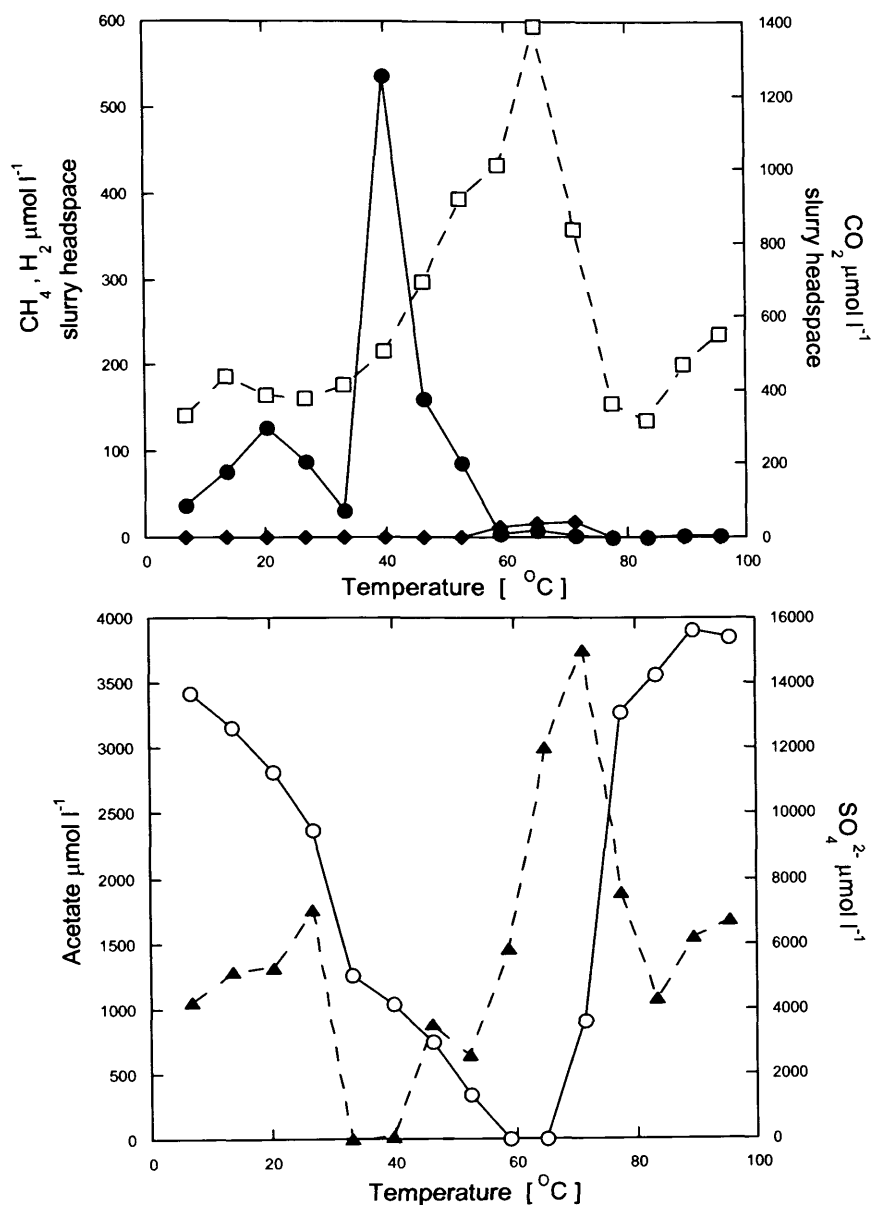
Fig 5.23. Magnetite, incubation after 92 days.

Key: CH_4 (●), CO_2 (□), H_2 (◆), acetate (▲) and SO_4^{2-} (○).

5.5 Magnetite results (Fig 5.22-5.23)

After 3 days incubation no significant hydrogen was detected at any temperature, with the maximum detectable hydrogen 0.05 μmol l^{-1} at 14°C. This is in stark contrast with the previous mineral incubations, which produced hydrogen at elevated temperatures (80°C plus). Carbon dioxide concentrations increase gradually with temperature up to 60°C, then more rapidly reaching a maximum of 3776 μmol l^{-1} at 77°C before decreasing slightly for the remaining temperatures (3058 μmol l^{-1} at 95°C). Detectable methane concentrations were very low with a maximum concentration of 2.3 μmol l^{-1} occurring at 46°C. Small quantities of sulphate have been removed from an initial concentration of 13 mmol l^{-1}. A maximum removal of 1.2 mmol l^{-1} occurs at 71°C (11.8 mmol l^{-1}). Rapid increase in acetate concentrations occurs from 39°C increasing from 51 μmol l^{-1} to 1165 μmol l^{-1}at 58°C. A dip in concentrations occurs at 65°C to 791 μmol l^{-1} before continuing to increase to a maximum concentrations are reached of 1190 μmol l^{-1} at 71°C. This is lower than achieved in any of the previous incubations. Acetate decreases rapidly above 71°C concentrations reaching 230 μmol l^{-1} at 95°C.

After 92 days incubation no hydrogen was detected at any temperature. Distinct peaks of methane however did developed with methane production and sulphate removal occurring together, however not in the sulphate depletion zone. The first peak at 20°C had a concentration of 128 μmol l^{-1}. Whilst the second peak accounts for the maximum concentration of methane detected 536 μmol l^{-1} at 39°C. The other incubations ilmenite (Fig.5.10) hematite (Fig 5.17) and pyrite (Fig 5.2) all produced methane at high temperatures (above 60°C) this was not the case with magnetite. Carbon dioxide increases with temperature from 33°C (413 μmol l^{-1}) to a maximum concentration of 1385 μmol l^{-1} at 65°C, this coincides with sulphate depletion and hence maximum SRB activity. After which carbon dioxide decreases rapidly to 317 μmol l^{-1} at 83°C before a slight increase to 550 μmol l^{-1} at 95°C. Sulphate removal occurs from 6°C onwards with maximum removal to 0 μmol l^{-1} (total removal of 13700 μmol l^{-1}) occurring between 58

and 65°C. with no removal occurring above 78°C. Initial sulphate concentrations were 13.7 mmol l^{-1}, however sulphate increases to 15 mmol l^{-1} at 95°C.

Acetate formation increases with temperature from 1045 μmol l^{-1} at 6°C to 1756 μmol l^{-1} at 26°C. After 26°C acetate concentration decreases to zero and 11 μmol l^{-1} between 33 and 39°C respectively. It is in this temperature range that the highest concentration of methane is detected (536 μmol l^{-1} at 39°C). This Possibly indicates that acetoclastic methanogenesis is occurring at this temperature. After this methanogenesis decrease Acetate increases to a maximum concentration of 3757 μmol l^{-1} at 71°C, this is followed by ` rapid decrease to 1078 μmol l^{-1} at 83°C before a slight increase to 1678 μmol l^{-1} at 95°C. This increase from 83 to 95°C is similar to the carbon dioxide profile. Unfortunately magnetite was one of the initial thermal gradients ran and no cation or $\delta^{13}C$ were obtained.

5.6 AODC counts

AODC counts were conducted on the hematite incubation in order to analysis the effect of temperature on prokaryote numbers..

Selected hematite samples were counted after 100 days incubation.
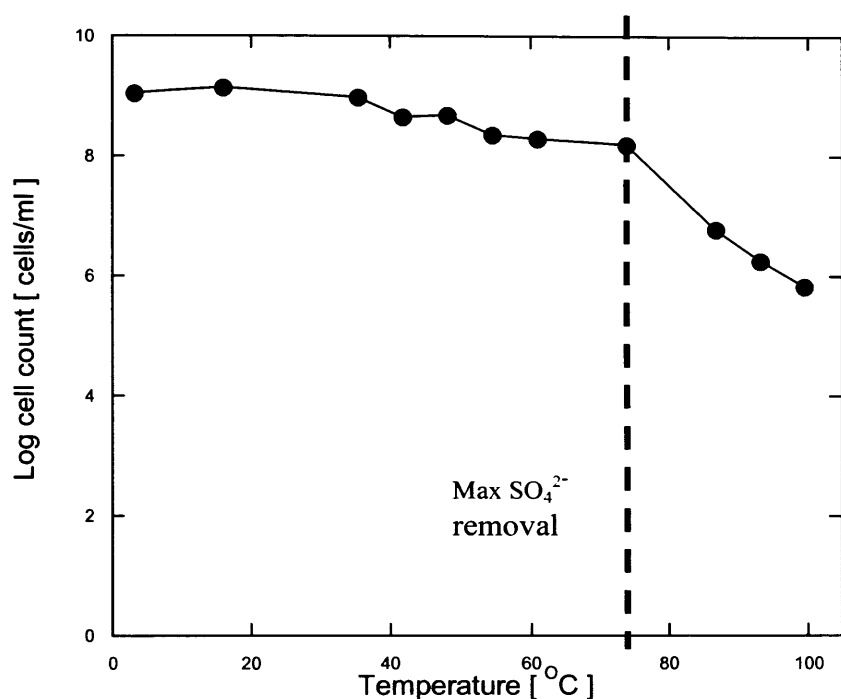
Fig 5.24 Hematite, incubation cell count across selected temperatures after 100 days incubation. Counts courtesy of Falko Mathes

AODC counts (all values are in log cell count/ml). Shows two rates of cell number decreases a slow decrease from 9.06 (1.14×10^9 cells/ml) at 3°C to 8.3 (1.99×10^8 cells/ml) at 73°C. Interestingly the rate of decrease becomes more rapid above 73°C, after sulphate reduction becomes inhibited. Perhaps sulphate reducing bacteria and other prokaryotes are generally being inhibited by the high temperatures. Numbers decrease from 8.3 (1.99×10^8 cells/ml) at 73°C to 5.85 (7.07×10^5 cells/ml) at 99°C.

5.7 DGGE results for ilmenite bacterial incubation after 83 days.

M 18 37 50 63 76 89 95 M
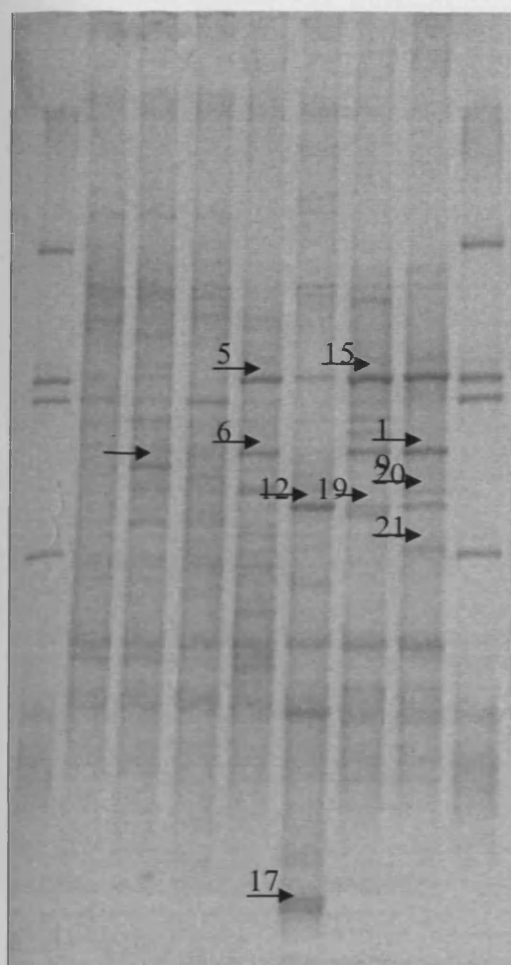
Fig 5.25 Bacterial DGGE Gel ilmenite 30-60%
Using primers 27F-1492R
Nested with 357F-907R
Increasing sample temperature left to right.
Temperature [^{O}C] indicated above gel

Increasing Temperature

Table 5.4 DGGE bacterial results for ilmenite

Number	Nearest match by Blastn search (Accession number)	Sequence Similarity (%)	Base Pair	Phylogenetic affiliation	Isolation environment of nearest match
1 (5)	*Delftia acidovorans* SPH-1, (CP000884)	100%	178/178	*Burkholderiales, Delftia acidovorans*	Subsurface marine
2 (12)	*Thermosipho* sp. TH70-3 (AB260053)	98%	176/178	*Thermotogales, Thermosipho*	Hydrothermal vent
3 (15)	Uncultured *Delftia* (EU376041)	100%	177/177	*Burkholderiales, Delftia acidovorans*	Terrestrial soil sample
4 (19)	Clone KW-7 (AB186285)	97%	177/182	*Gamma proteobacteria*	Oil reservoir
5 (20)	*Delftia* sp. clone M3_11 (EU560926)	97%	189/194	*Burkholderiales, Delftia acidovorans*	Subsurface sediment
6 (17)	*Thermotoga* sp. KOL6 (AJ872272),	98%	175/178	*Thermotogales; Thermotoga*	Marine sediment

165

5.8 DGGE for ilmenite Archaeal incubation after 83 days

Archaeal primers were used 109F-958R,

Nested with Saf-Parch519r.

M 18 37 50 63 76 89 95 M   M 18 37 50 63 76 89 95 M
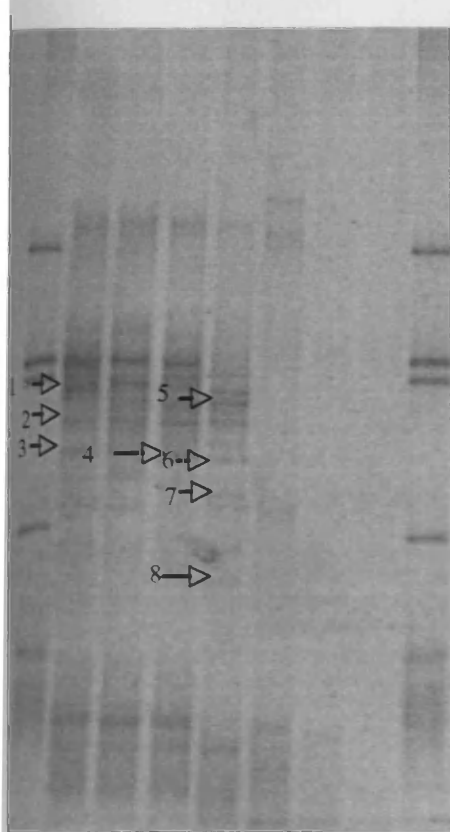
Increasing Temperature   Increasing Temperature

Fig 5.26a Archaeal DGGE profile   **Fig 5.26b** Archaeal DGGE
60% denaturant gel.   profile 30-80% ilmenite.
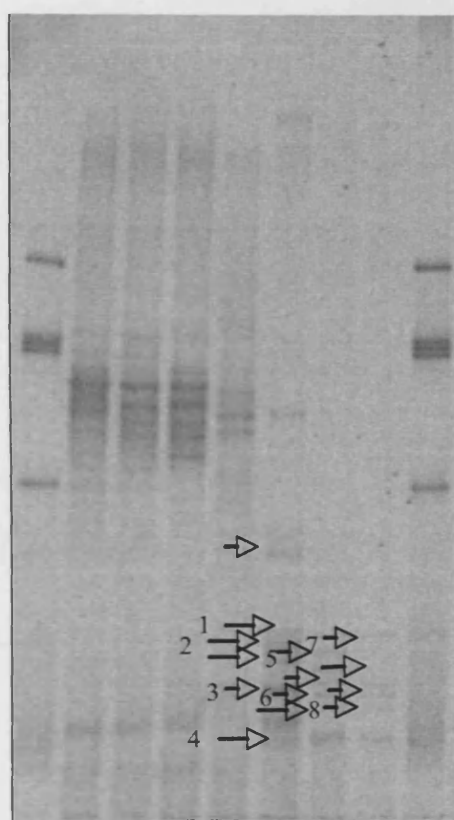
Table 5.5 DGGE *Archaea* Ilmenite 60% results (18-63°C)

Sample	Nearest match by blastn (accession number)	Percentage similarity %	Phylogenetic affiliation	Isolation environment of nearest match
1	Clone TFC20L37AR (EU362355)	97%	*Crenarchaeota MBG-C*	Tidal sediments
2	SBAK-mid-48 DQ640209	97%	*Crenarchaeota*	Marine sediments
3	SBAK-deep-18 (DQ522910)	98%	*Crenarchaeota*	Marine sediments
4	GNA10H07 (EU731608)	98%	*Euryarchaeota; Thermoplasmata*	Hypersaline Microbial mat
5	Kazan-2A-40 (AY592016)	97%	*Novel crenarchaeota*	Cold seep
6	Kazan-2A-40 (AY592016)	98%	*Novel crenarchaeota*	Cold seep
7	TfP20L15Ar (EU362377)	96%	*Crenarchaeota*	Tidal sediments
8	TfC20L36Ar (EU362354)	99%	*Crenarchaeota*	Tidal sediments

Table 5.6 DGGE Archaea Ilmenite 80% results (76-95°C)

Sample	Nearest match by blastn (accession number)	Percentage similarity %	Phylogenetic affiliation	Isolation environment of nearest match
1	PW15.7A (EU573156)	92%	Unknown	High temperature Oil reservoir
2	PW15.7A (EU573156)	95%	Unknown	High temperature Oil reservoir
3	PW15.7A (EU573156)	97%	Unknown	High temperature Oil reservoir
4	PW15.7A (EU573156)	97%	Unknown	High temperature Oil reservoir
5	Desulfurococcales archaeon clone YNP_BP_A32 (DQ243730)	93%	*Crenarchaeota; Thermoprotei; Desulfurococcales;*	Yellow stone Hot springs
6	Desulfurococcales clone: pYK04-8A-2 (AB235327	86%	*Crenarchaeota; Thermoprotei; Desulfurococcales*	Hydrothermal vent
7	Thermococcales (AB208561)	97%	*Euryarchaeota; Thermococci*	Hydrothermal vent
8	Thermococcales (AB208561)	95%	*Euryarchaeota; Thermococci*	Hyrothermal vent

5.11 Clone libraries

Clone libraries were set up and analysed for the ilmenite and pyrite incubation this was undertaken in order to achieve a more detailed analysis than can be achieved through DGGE band extraction. The product size for analysis was 500 bp. Temperature chosen for clone library construction were ilmenite incubation at 63°C and 89°C, pyrite incubation at 65°, and 90°C.

The following four trees show the archaeal clone libraries for theses samples Neighbour joining method was used with the tree based on 500 bases of aligned 16S rRNA gene sequences all trees are rooted using *Korarchaeota* species SR1-306 (AF255604).

No bacterial clone libraries were constructed. Test clones for all similar temperatures for bacterial libraries, indicated all poor quality samples with every clone similar in majority of samples.
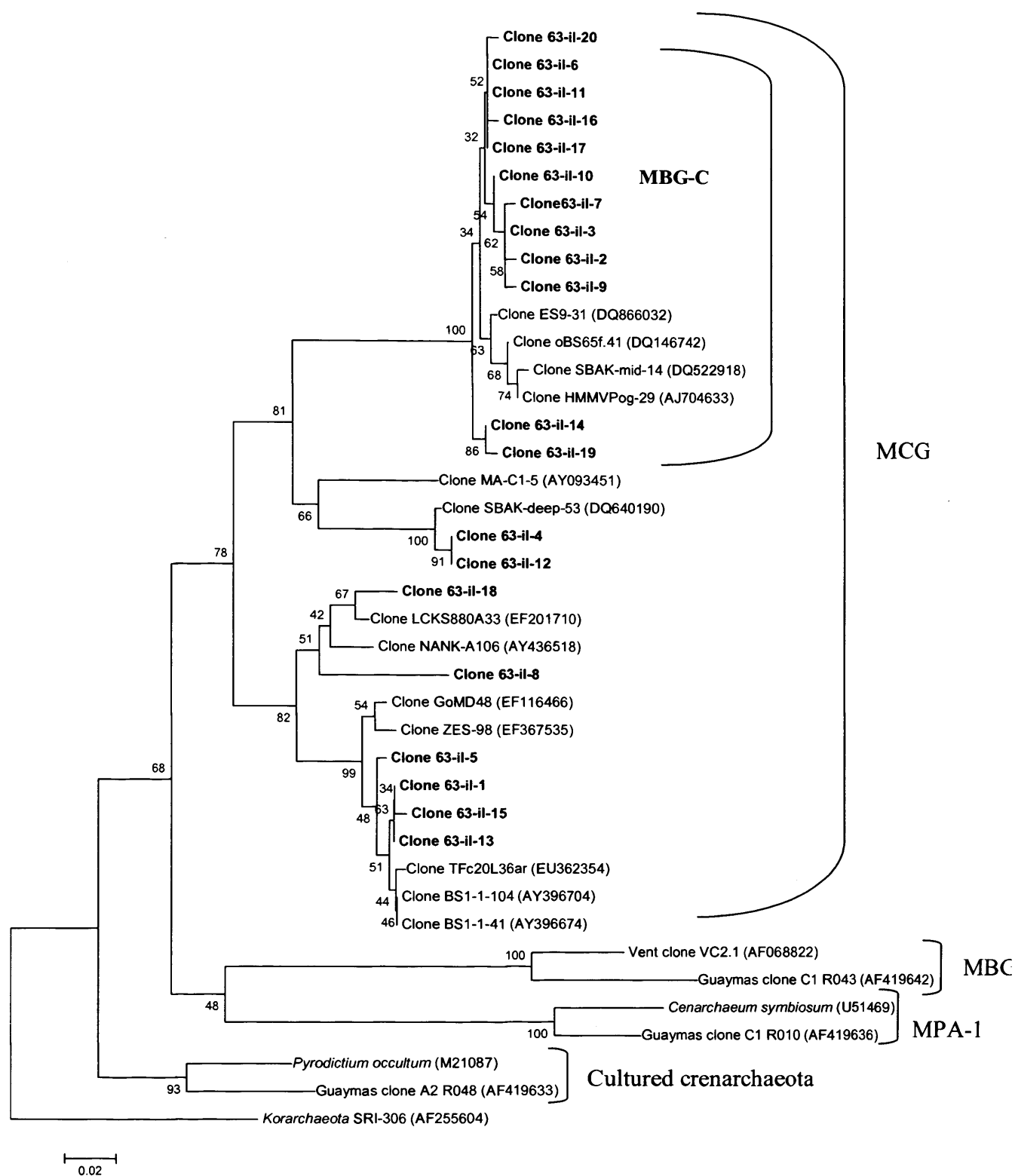
Fig 5.27. Ilmenite Phylogenetic tree for *Archaea* clone library, after 83 days incubations at 63°C

A
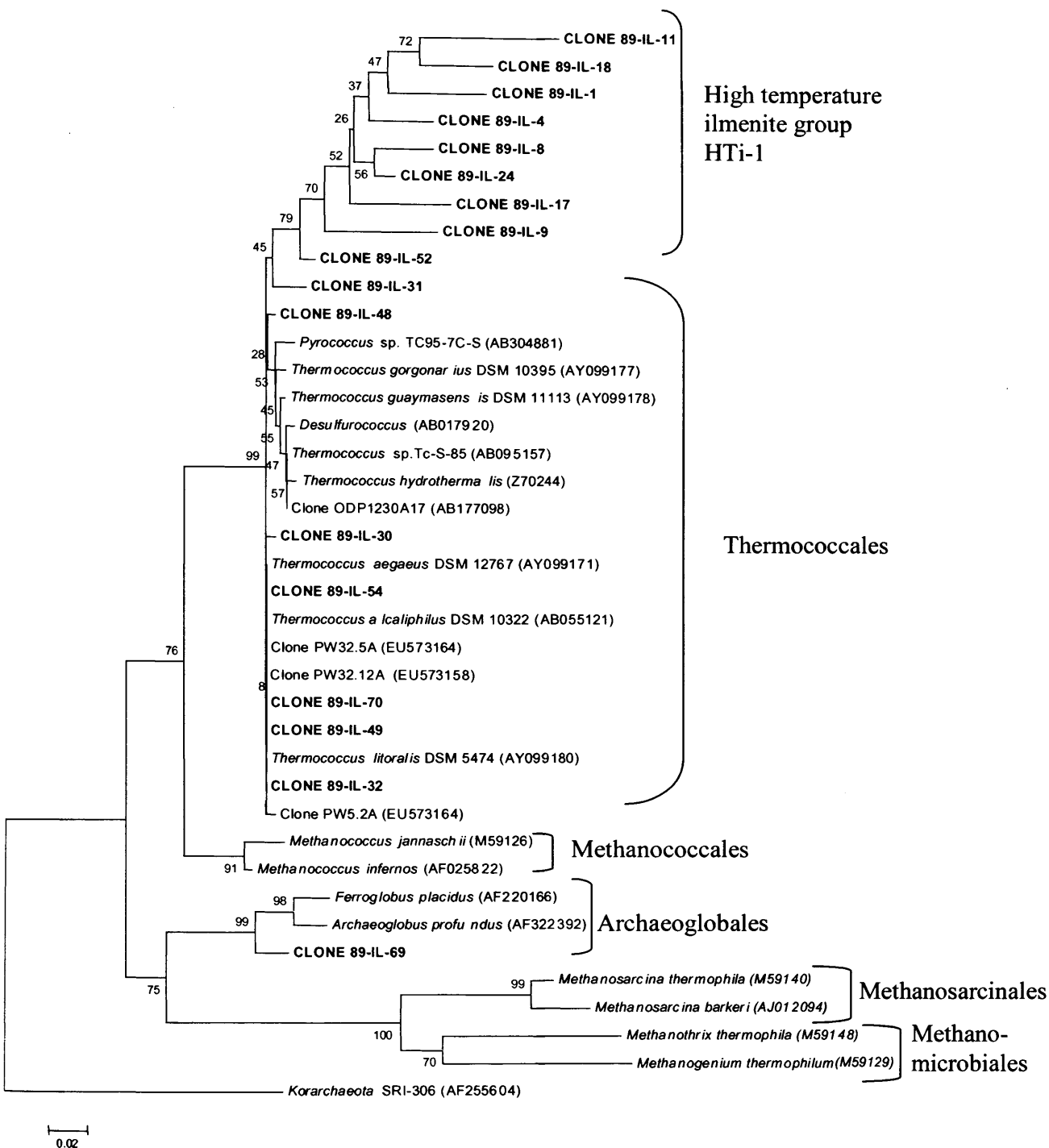
Fig 5.28 Ilmenite phylogenetic tree for _Archaea_ clone library after 83 days incubation at 89°C

B
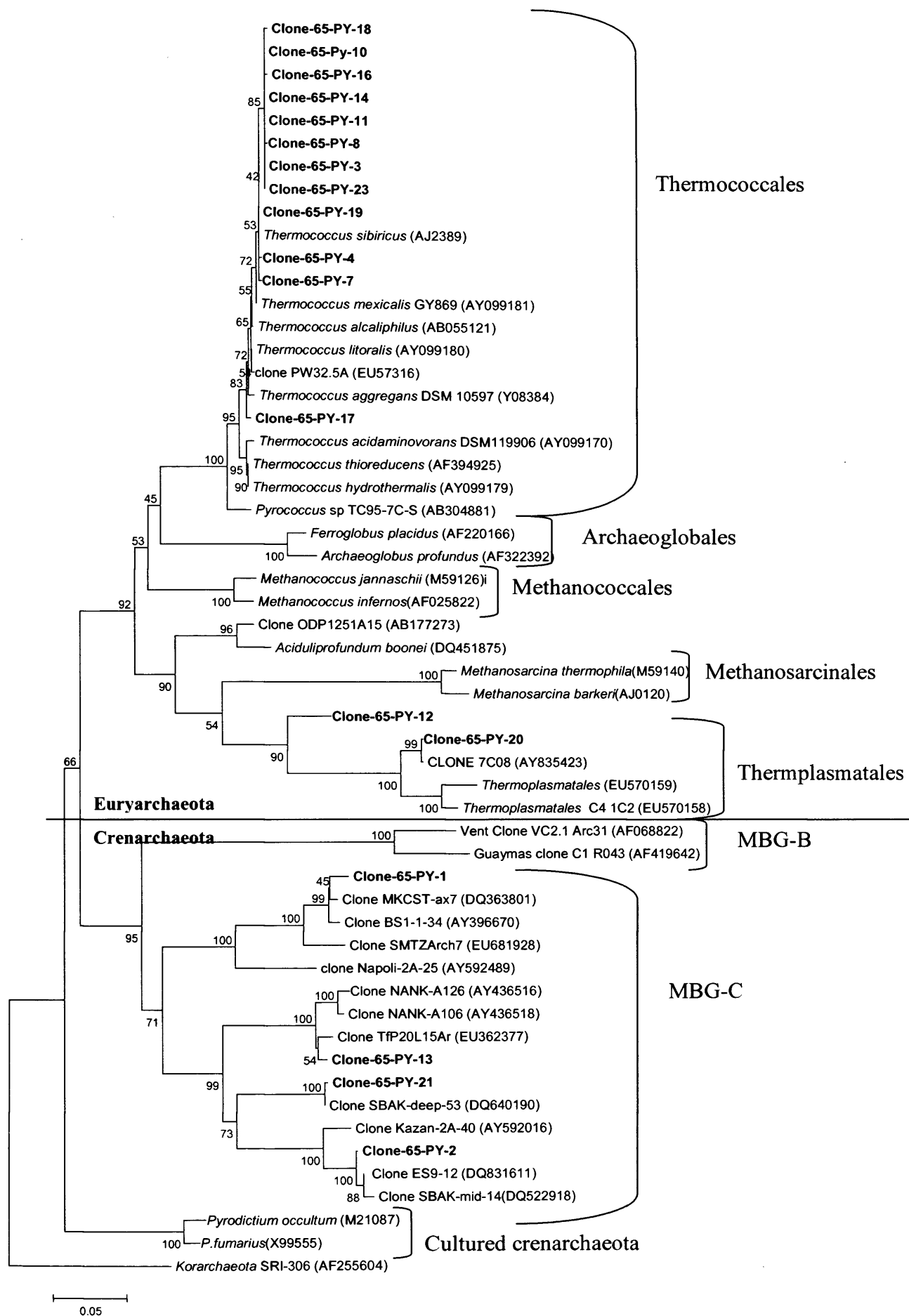
Fig 5.29 Pyrite phylogenetic tree for archaeal clone library after 110 days of incubation at 65°C

C

Clone-90-py-9
Clone-90-py-12
60 Clone-90-py-16
Clone-90-py-17
56 Clone-90-py-14
Clone-90-py-10
91 Clone-90-py-18

High temperature pyrite group-1 (HTP-1)

Clone-90–py-3
92 Clone-90-py-15
48 53 Clone-90-py-5
34 Clone-90-py-6

HTP-2

68 Clone pCIRA-L (AB095122)
Clone pCIRA-12 (AB095137)
24 95 Clone CH4 2 9N EPR (AY672469)
59 Clone CH8 35 (AY672490)
68 Clone CH1 16 (AY672482)

Vent Chimney
euryarchaeotal group

83 Methanococcus jannaschii (M59126)
99 Methanococcus infernos (AF025822)

Methanococcales

Thermococcus acidaminovorans DSM 11906 (AY099170)
Clone-90-py-7
66 Thermococcus guaymasensis DSM 11113 (AY099178)
17 Clone-90-py-4-
Clone-90-py-19
21 Clone PW25.2 (EU573154)
Thermococcus sp 83-5-2 (AB235309)
87 Clone-90-py-13
21 Thermococcus alcaliphilus (AB055121)
Clone-90-py-8
Thermococcales T17a-44 (AJ585957)
Thermococcus chitonophagus (AY099175)
Pyrococcus sp.MZ4 (AY017173)
66 Pyrococcus woesei (AY519654)
Pyrococcus furiosus (U20163)

Thermococcales

100 Methanosarcina thermophila (M59140)
Methanosarcina barkeri (AJ012094)

Methanosa-
rcinales

99 Methanogenium thermophilum
100 (M59129)

Euryarchaeota

Crenarchaeota Desulfurococcus fermentans (AY264344)
97 Clone B1-57 (EU559691)
52 Clone-90-py-11
19 Geogemma indica strain 296 (DQ492260)
50 Ignisphaera sp.Tok1 (DQ060320)
72 Desulfurococcales YNP_BP_A32 (DQ243730)

Cultured
Crenarchaeota

Korarchaeota SRI-306 (AF255604)

0.02

Fig 5.30 Pyrite phylogenetic tree for archaeal clone library after 110 days incubation at 90°C

D

5.12 Molecular results for ilmenite and pyrite thermal gradient incubations

Based on DGGE band sequences from the ilmenite incubation the bacterial composition is a mixture of 3 different Phylotypes, *Burkholderiales* (*Delftia acidovorans*) the *Thermotogales* and the *Gammaproteobacteria*. All species were related to species found in with high temperature subsurface environments. *Delftia* is a facultative anaerobe and has been found in anaerobic high temperature hydrothermal environments (Glamoclija et al., 2004).Substantial checks were carried out in order to determine, whether this occurrence of *Delftia* was contamination, running of blanks from extractions and checking of all reagents used, but all were negative. Visually the intensity strength of the *Delftia* band increased, from ~63°C, this could either be a response to temperature i.e. thermophilic, or conversely lack of other bacterial species at high temperature, making the activity of *Delftia* more noticeable. *Thermotoga* (Huber et al., 1986) are found in environments at high temperature, normal salinity and close to neutral pH.

The archaeal diversity from DGGE band sequencing shows interesting diversity. At lower temperature incubations < 63°C *Crenarchaeota* were dominant. At higher temperatures to 95°C the *Euryarchaeota*, particularly the *Thermococcales* dominated. All species were from relevant marine environments. Visual analysis of both DGGE gels shows a clear change in community structure with temperature.

Difference in Archaeal phylotypes can be observed depending on incubation temperature. Two samples, from each mineral incubation were chosen. First temperatures chosen were samples occurring in the sulphate reduction zone (63°C and 65°C) for ilmenite and pyrite. The second temperature was 89 and 90°C close to the maximum upper temperature for both in terms of H_2 generation and acetate formation (Fig 5.28,5.30).

The Phylogenetic trees showed differences between the mineral incubated and differences between the incubation temperatures. At low temperatures, Crenarchaeotic phylotypes are more prevalent than at the two higher temperature samples. The ilmenite incubation at 63°C (Fig 5.27). Is totally dominated by the crenarchaeota. The dominant phylotype belonged to the Miscellaneous Crenarchaeotic group (MCG), with 33% of clones within Marine Benthic Group-C. The remainder of clones were also MCG which

is a large group composed of uncultured phylotypes including sequences from the marine subsurface (Reed et al., 2002; Inagaki et al., 2003; Webster et al., 2006). Within the marine benthic group C cluster, clones with similarity to sequences obtained from deep subsurface Nank-A106(Newberry et al., 2004), clone 63-il-18 and clone 63-il-8 were found. Remainder of the clones were found to have similarities to clones found in tidal flat sediment, clone63-il-13, and 15 and 1.

The 65°C incubation with pyrite addition did not have such a complete bias to the *Crenarchaeota* with only 22% of clones falling within this group and all of these are within the Marine Benthic Group-C. These are similar to clones found in tidal flat sediments, (Kim et al., 2005) and in the deep marine environment (Newberry et al., 2004). Unlike the ilmenite incubation however, the majority of clones in the pyrite incubation fall into the *Euryarchaeota* (77%) with the majority of these (85%) falling inside the *Thermococcales* group. The majority of these *Thermococcales* sequences are related to species isolated from hydrothermal systems, *Thermococcus mexicalis* and *Thermococcus hydrothermalis* (Lepage et al., 2004). The only clones in the *Euryarchaeota* to fall outside of the *Thermococcales*, clustered within the *Thermoplasmatales,*(clone 65-py-12 and clone 65-py-20), also closely related to species isolated from hydrothermal systems, Guaymas clone 7C08 (Dhillon et al., 2005).

The high temperature incubation for ilmenite, 89°C, is in contrast to the lower 63°C temperature incubation, as all clones are within the *Euryarchaeota* (Fig 5.28). All clones except one are within the *Thermococcales* with 8 of these clones slightly further removed from the *Thermococcales*, provisionally labelled high temperature ilmenite group 1 (HTi-1) with a similarity matrix average of 96% similarity to closest isolated clone. The remaining 5 are closely related to previously isolated *Thermococcales* spp such as *thermococcus aegaeus* (Lepage et al., 2004). Only one clone fell outside of the *thermococcales* related species, which was clone 20-il-69 and fell within the *Archaeoglobales* and was most closely related to *Archaeoglobus profundus* (Burggraf et al., 1990) which is an hyperthermophilic sulphate reducing archaeon and hence consistent with the experimental temperature.

Unlike the high temperature ilmenite incubation, the pyrite clone library did not consist of *Euryarchaeota* alone (Fig 5.30). One clone (90-py-11) was within the

Crenarchaeota in the cultured crenarchaeota related to species of high temperature sulphate reducers such as *Desulfurococcus fermentans* (Perevalova et al., 2005)

Roughly one-third 29% of clones clustered closely in the *Thermococcales*, similar to the ilmenite incubation. The majority of clones however, (65%) clustered in two groups named here high temperature pyrite (HTP) group 1 and HTP group 2. These are most closely related to clones (pCIRA-L and pCIRA-12) taken from possible high temperature hydrogen driven subsurface communities (HyperSlime) (Takai et al., 2004). These clones were taken from the hydrothermal vent system in the Indian ridge, close to black smokers emitting superheated discharges of up to 365°C. They belong to the deep-sea hydrothermal Vent Euryarchaeotic group. Communities from this proposed ecosystem were similar to this study mostly dominated by the *Thermococcales*. To determine the similarity percentage between these clones and their most closely related isolates a similarity matrix was performed using RDP (ribosomal database project analysis RDP version 8.1). Percentage similarities were as follows between clone pCIRA-L and 90-py-15 was 90%, 90-py-6 was 92%. Between hydrothermal vent clone CH1 16 (Kormas et al., 2006) and 90-py-15 are 90% ,90-py-6 are 92%.

171

5.13 Discussion

The experiments in this chapter suggests that mineral composition affects hydrogen production which in turn impacts on processes which use hydrogen as a substrate, such as acetogenesis, sulphate reduction and methanogenesis. High levels of hydrogen (1633 μmol l^{-1} for hematite and 820 μmol l^{-1} for pyrite) were detected at elevated temperatures ~ 85-98°C, from all samples except magnetite. This seems to disprove initial hypothesis linking H_2 generation to Fe content. Table.5.7 shows maximum concentrations of hydrogen, acetate, carbon dioxide and methane over the first 3 days of incubation.

Table 5.7 Maximum concentrations recorded after 3 days,(μmol l^{-1})

Sample	Fe_2O_3 wt%	H_2	CH_4	CO_2	Acetate
Ilmenite	50.7	632	5,7	6176	1293
Pyrite	*46.6(% Fe)	820	125	4673	2770
Hematite	54.2	1633	2	6580	1501
Magnetite	99.4	0	2.3	3776	1190

*Theoretical value.

From Table 5.7 it can be seen that Fe concentrations do not play a defining role in hydrogen generation. This can be seen by the fact that the sample containing the most Fe (magnetite) produced the lowest concentrations of acetate and carbon dioxide with no detectable hydrogen. In addition, the amount of ferrous iron does not seem to control H_2 generation as proposed for basalt weathering/ serpentinization, as hematite contains theorectically, fully oxidised ferric (Fe_2O_3), yet this produced the largest initial H_2 concentrations. Of interest is the role of other mineral combinations most noticeably Si Al and Ti (Table 5.8)

Table 5.8 Mineral composition and maximum hydrogen generation.

Sample	SiO_2 wt%	AlO_3 wt%	TiO_2 wt%	H_2
Hematite	20.53	17.7	0.79	1633
Ilmenite	1.06	1.28	47.3	632
Magnetite	2.57	1.05	0.05	0

In terms of mineral composition Si content (SiO_2) might play a role in hydrogen generation, as hematite produces the most hydrogen and also has the highest concentration of SiO_2 (20.53%) it also has the highest amounts of AlO_3 (17.7%). Ilmenite produced 2.5 times less hydrogen than hematite despite, having similar concentrations of Fe. Ilmenite has low concentrations of SiO_2 and AlO_3. However unlike hematite and magnetite, ilmenite has high amounts of TiO_2 (47.3%). Magnetite produces no detectable hydrogen and has very low levels of Si/Al/Ti , but has high levels of iron. These results indicate that iron concentration does not play a role in high temperature hydrogen generation, in fact it may be a barrier to hydrogen production. It seems more likely that in these experiments hydrogen production is mediated by Si or a combination of factors involving Ti/Al and Si.

All samples producing H_2 have a maximum temperature of 100°C above which no hydrogen was produced. Noticeably between minerals producing hydrogen and magnetite is a temperature difference in zones of maximum activity in terms of acetogenesis and methanogenesis, sulphate reduction occurs at the same temperature with maximum depletion occurring between 60-70°C. However, methane production and acetate formation occur at higher temperatures in samples producing hydrogen (Fig 5.2). Magnetite shows no high temperature methane formation with CH_4 formation peaking at 40°C. Ilmenite, pyrite and hematite all show high temperature methane formation between 60-90°C but not always at the same temperatures. A similar profile is noted during acetate formation. Acetate formation begins to substantially increase for magnetite

at 40°C peaking at ~70°C with no substantial high temperature formation. Acetate generation in the hydrogen producing incubations substantially increases from 60°C with maximum concentrations coinciding with maximum hydrogen concentrations 90-100°C. (Fig 5.30)
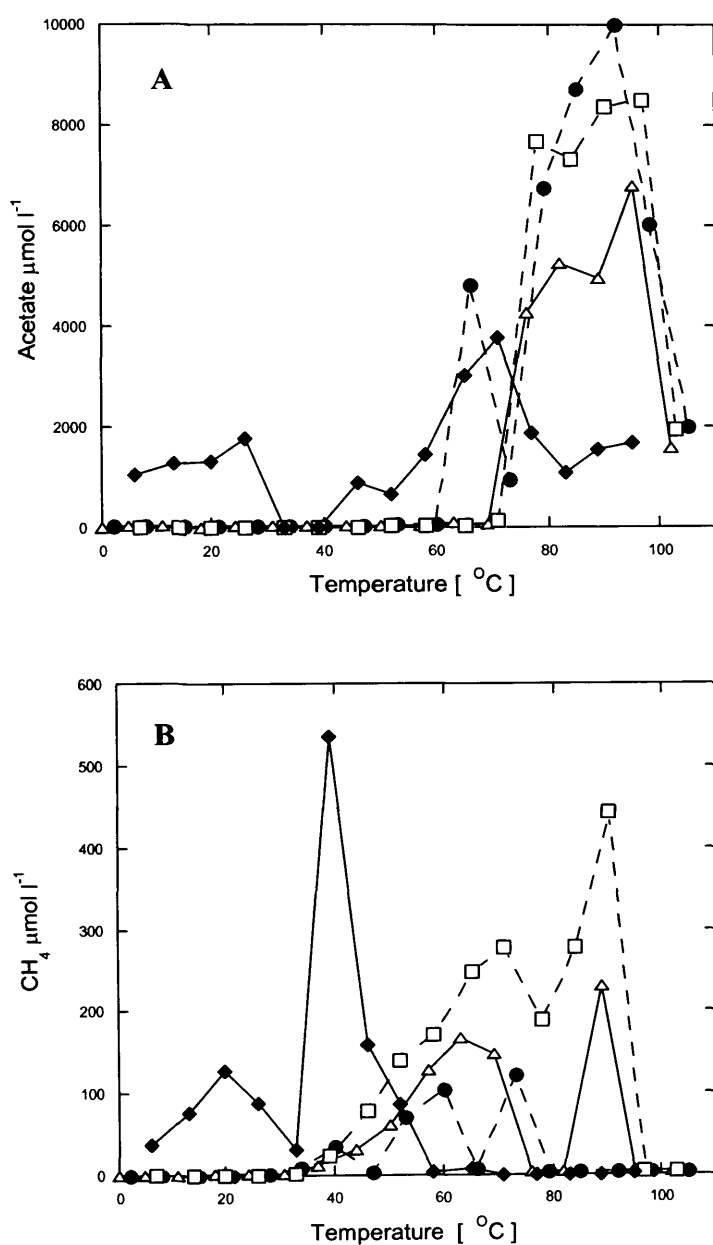
Fig 5.31 combined graphs of methane A and acetate B
Key: Ilmenite, open triangle. Hematite: closed circle. Pyrite: open square. Magnetite: closed Diamond
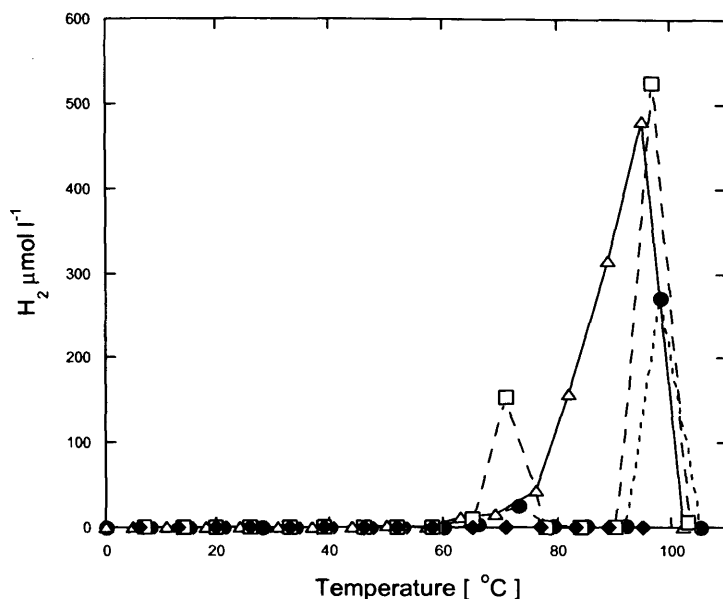
Fig 5.32. Combined graph showing hydrogen generation at last sampling point.
Key: Ilmenite, open triangle. Hematite: closed circle. Pyrite: open square. Magnetite: closed Diamond

δ^{13}C-CH$_4$ data is quite interesting with a range of values being found generally increasing with temperature, e.g -42‰ for pyrite at 90°C compared to -55‰ at 65°C. Methane produced at these high temperatures is clearly of biotic origin, however δ^{13}C values like these could be mistaken for methane produced through abiotic thermogeneic reactions and have been interpreted as such in the past, this includes in the Guaymas basin (Teske et al., 2002) sediments. Where the inoculum for these incubations was obtained

175

For the major cations. A general profile was observed. Fe concentrations increased with temperature with all incubations. Highest iron concentrations occur in the zone of hydrogen generation and highest acetate formation. Silica also increased with temperature with the maximum concentration for silica occurring at he highest temperature.

Molecular analysis by the use of clone library construction gave a more detailed view of the archaeal community structure with temperature for ilmenite and pyrite. The difference in terms of *Crenarchaeota* and *Euryarchaeota* composition is clear with less *Crenarchaeota* present at high temperature ~90°C than at lower ~65°C, the ilmenite incubation has all *Crenarchaeota* at the lower temperature incubation and all *Euryarchaeota* at higher temperature. The dominant species at high temperature are the *Thermococcales* for ilmenite, for pyrite however most clones' fall within two groups labelled PHT-1 and PHT-2. Most closely related species to these are the vent chimney *Euryarchaeotal* group, clones thought to be associated with HyperSlime communities (Takai K, 2004).

Chapter 6
Temperature characteristics of Olivine, Hornblende, Labradorite and Silica reactions in sediment slurries

6.1 Introduction

This chapter presents the results obtained from mineral addition incubations conducted over a temperature range of 0 to 105°C. Using olivine, hornblende, labradorite and silica (quartz). Results are presented in order of increasing silica content (Table 3.2) measured as SiO_2 using ICP-OES which is olivine 41.82 wt%, hornblende 49.95 wt%, labradorite 52.2 wt% and silica 100 wt%. This chapter is intended to be in contrast to chapter 5, which describes mineral addition experiments, ordered in terms of increasing iron content. Ordering minerals in terms of increasing silica also had the effect of arranging minerals in terms of decreasing iron content. (Fe_2O_3 wt%) olivine 7.94, hornblende 7.87, labradorite 0.62 and silica (quartz) 0.

This chapter should expand our knowledge of the mechanism responsible for hydrogen generation and show whether this process is predominantly associated with silica as previously considered in chapter 5. It has been proposed that freshly fractured silica, has been responsible for elevated hydrogen concentrations found at fault zones (Kita et al., 1982). Maybe a similar type of reaction is occurring in our thermal gradient experiments, with hydrogen production also being enhanced in the presence of sedimentary prokaryotes and elevated temperature.

If this is the case then incubation of pure silica (quartz) mineral (freshly ground) sediment slurries, should produce high concentrations of hydrogen comparable if not greater, than minerals containing mixed amounts of silica and other compounds such as iron and aluminium.
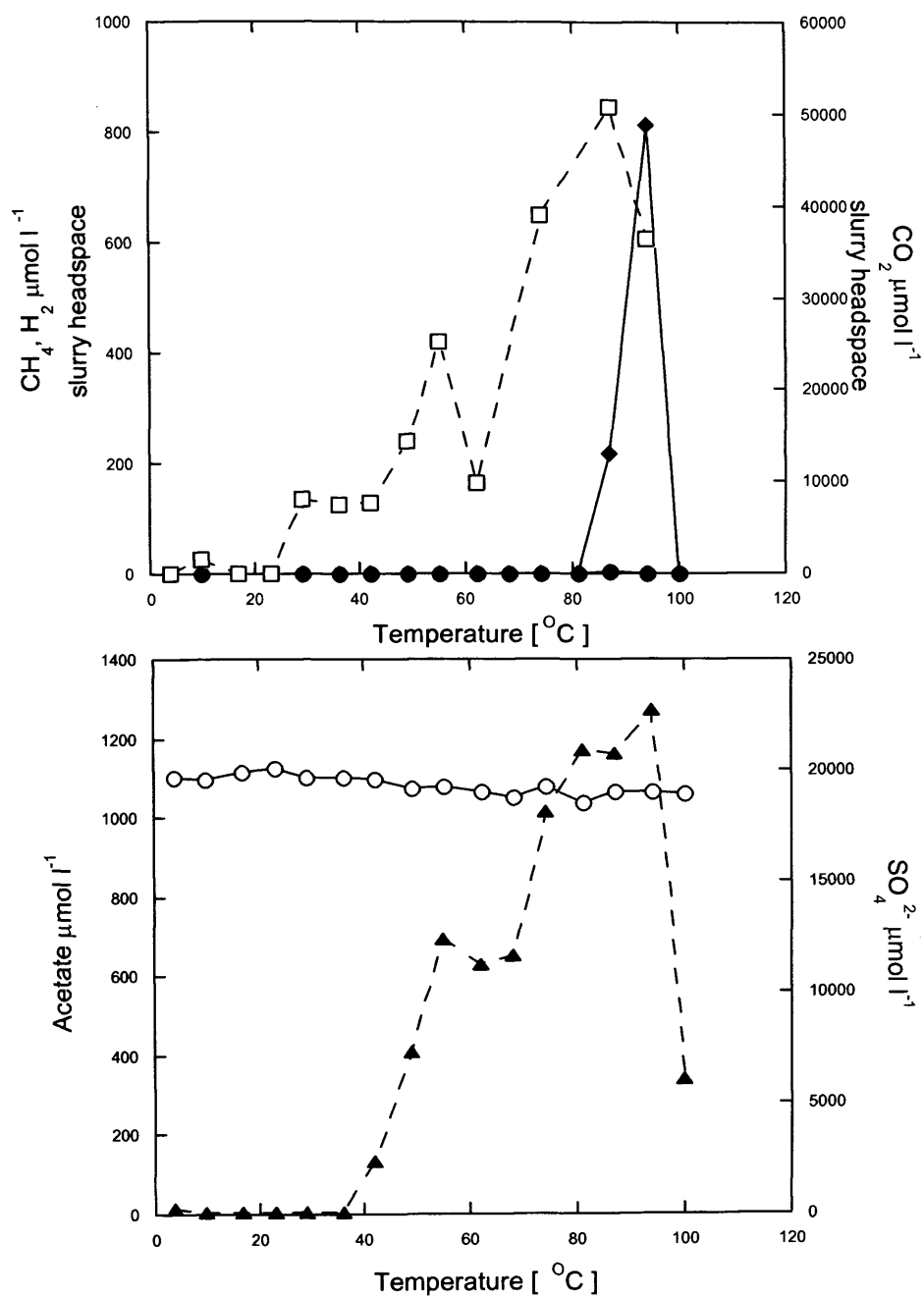
Fig 6.1 Olivine incubation after 3 days incubation.

Key CH_4 (●), CO_2 (□), H_2 (◆), Acetate (▲) and SO_4^{2-} (○).
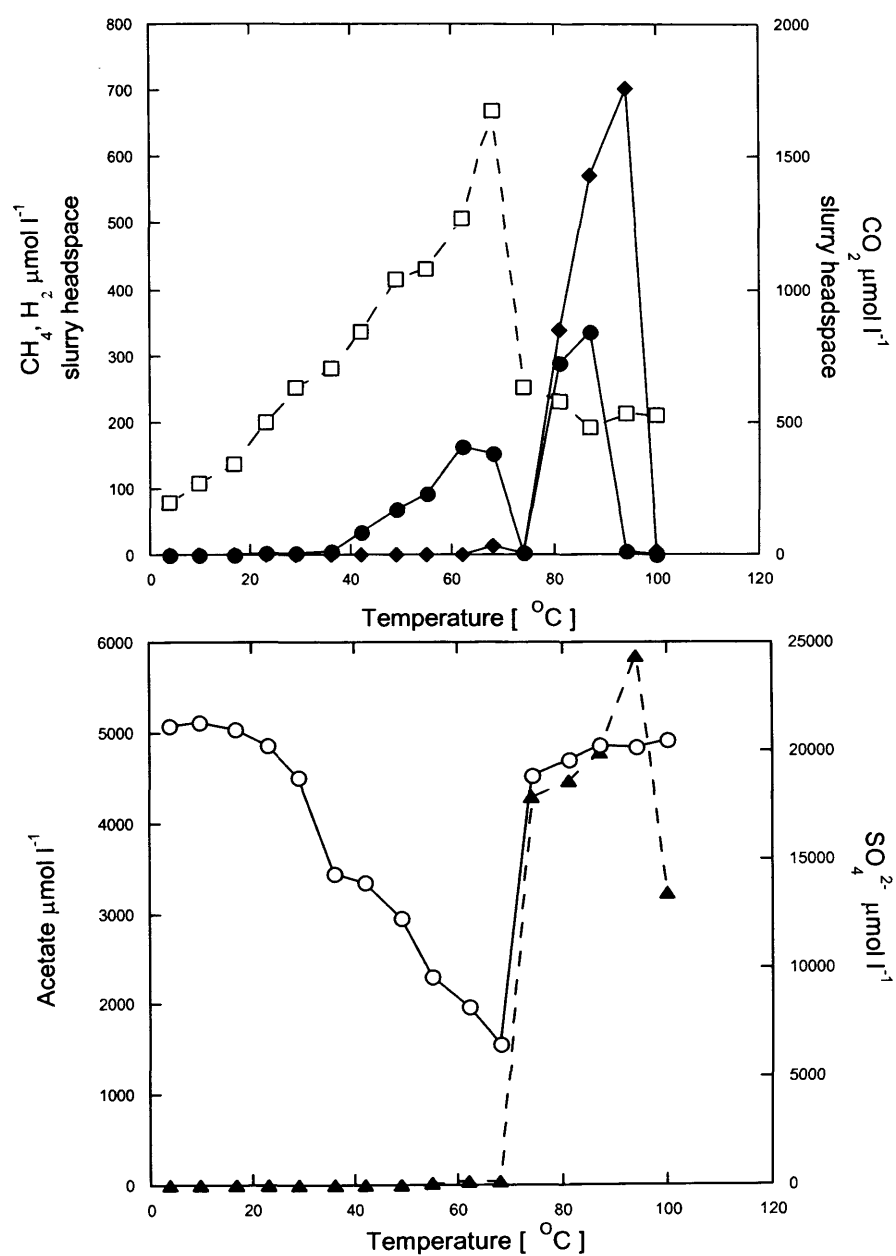
Fig 6.2 Olivine incubation after 61 days incubation.

Key CH_4 (●), CO_2 (□), H_2 (◆), Acetate (▲) and SO_4^{2-} (○).

6.2 Olivine Results (Figs 6.1 and 6.2)

After 3 days incubation no significant amounts of methane were detected, a maximum concentration of 1.9 µmol l^{-1} was recorded at 87°C (Fig 6.1). Similar to incubations presented in Chapters 4 and 5, high concentrations of hydrogen were detected at elevated temperatures (81-100°C), with a maximum concentration of 812 µmol l^{-1} at 94°C. No hydrogen was detected at 100°C or below 81°C. Carbon dioxide concentrations overall increased with temperature reaching a maximum of 50.7 mmol l^{-1} at 87°C, decreasing after this to 36.4 mmol l^{-1} at 94°C. A slight dip in concentrations is also noted at 62°C during the initial increase in carbon dioxide, this co-occurs with a slight decrease and plateau in acetate concentrations. No sulphate removal was found to take place; initial concentrations are approx 19.5 mmol l^{-1}. Interestingly high concentrations of CO_2 are not associated with sulphate reduction, which was the case in previous Chapter 5 experiments. Acetate concentrations remain low until 36°C (3.8 µmol l^{-1}) after which concentrations increase with temperature up to 94°C except for the 62°C plateau in concentrations. Acetate continues to increase to a maximum of 1275 µmol l^{-1} at 94°C. Highest concentrations of acetate and hydrogen occur at the same temperature.

This incubation and the hornblende incubation are conducted over a shorter time period 61d. This is because they were among the first experiments conducted and a failure in the thermal gradient system meant the last incubation point, scheduled for sampling at 90d could not be trusted as accurate. After 61 days incubation high amounts of hydrogen are detected at 94°C. Which is similar to those detected after 3 days but maximum concentrations were 13% less (704 µmol l^{-1}), and H_2 was produced over a broader temperature range ~75°C-100°C. Two distinct peaks of methane are observed. First with a maximum of 164 µmol l^{-1} at 62°C occurring in the zone of most active sulphate removal 49-74°C and the second peak at higher temperature 74-94°C, with a maximum of 335 µmol l^{-1} at 87°C, which is the highest amount of methane detected. δ^{13}C-CH$_4$ isotope data was obtained (Table 6.1) for methane at 62°C and suggests an acetoclastic pathway for methane production (Whiticar, 1999).

Table 5.1 δ^{13}C values for olivine incubation

Sample	δ^{13}C-CH$_4$	SD	δ^{13}C-CO$_2$	SD
Olivine 62°C	-54.4‰	0.7	Na	Na

SD, standard deviation, n=3

No δ^{13}C-CO$_2$ values were obtained as the storage of samples in acidified KCl, renders these values undetectable. Carbon dioxide increases with temperature to a maximum of 1674 μmol l^{-1} at 68°C (more rapid increase occurs from ~ 60°C. The carbon dioxide maximum is contiguous with the maximum temperature for most rapid sulphate removal and decreases when sulphate removal slows rapidly at elevated temperatures. The amount of carbon dioxide detected is far less than detected after 3 days (- 48.3 mmol l^{-1}) which is consistent with previous incubations such as ilmenite, pyrite, and hematite(Chapter 5). Carbon dioxide decreases rapidly after 68°C before plateauing, and reaching a final of concentration of 528 μmol l^{-1} at 100°C.

Sulphate removal is most active at 68°C with the removal of approx 14.4 mmol l^{-1}, leaving a concentration of 6500 μmol l^{-1} at 68°C. Sulphate removal rapidly decreases after 68°C. Between 68°C and 74°C there is a difference of 11.5 mmol l^{-1} in terms of sulphate removed. Interestingly sulphate concentrations even at 100°C, never reach original concentration (800 μmol l^{-1} less). This decrease in concentration maybe evidence of high temperature sulphate removal, or perhaps could be due to analytical error, due to the difficulty in measuring high temperature samples. High temperature samples produce a lot of organic compounds that are visible on and lower the sensitivity of IC columns, so high temperature samples are diluted 1 in 50 or 1 in 100 before analysis which adds some slight analytical error. Acetate values rapidly increase coinciding with decrease in sulphate removal, from 40 μmol l^{-1} at 68°C to 4281 μmol l^{-1} at 74°C. Acetate continues to increase with temperature with a peak of maximum concentration at 5841 μmol l^{-1} and 94°C before decreasing rapidly to 3223 μmol l^{-1} at 100°C. Some acetate was removed between 40 and 68°C as elevated concentrations were present in this zone at 3 days (> 600 μmol l^{-1}) Fig 6.1.
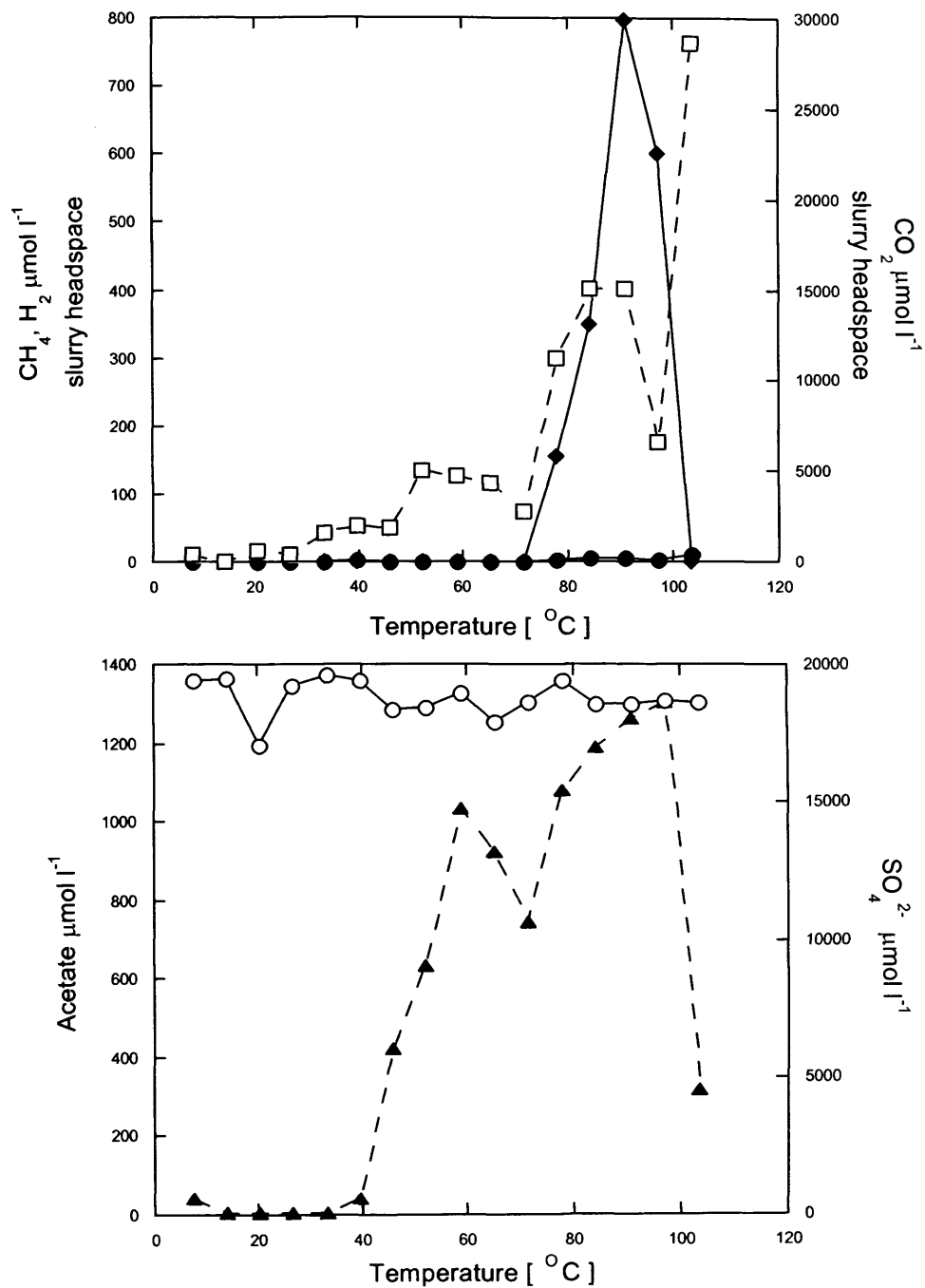
Fig 6.3. Hornblende incubation, after 3 days.

Key CH$_4$ (●), CO$_2$ (□), H$_2$ (◆), acetate (▲) and SO$_4{}^{2-}$ (○).
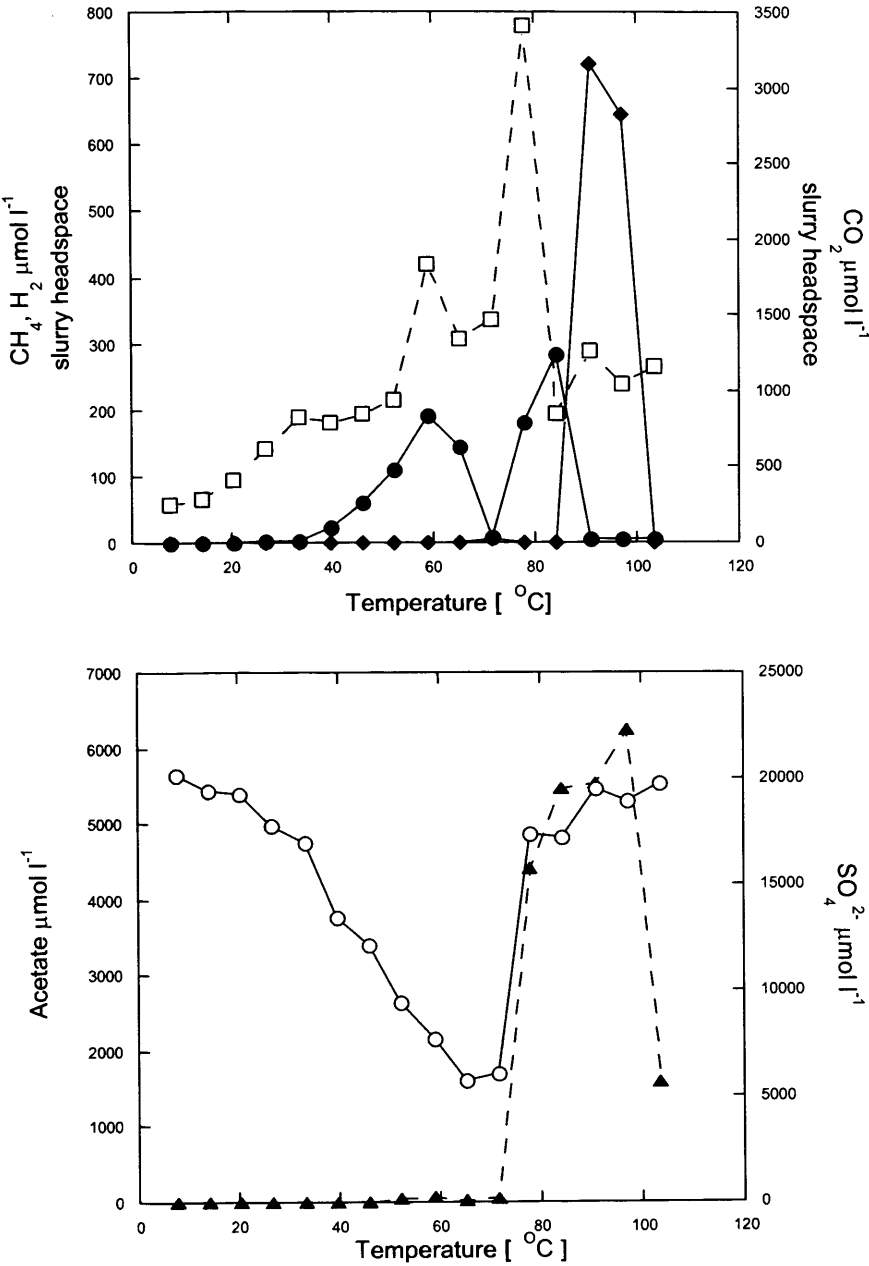
Fig 6.4 Hornblende incubation, 61 days.

Key: CH_4 (●), CO_2 (□), H_2 (♦), acetate (▲) and SO_4^{2-} (○).

6.3 Hornblende results (Figs 6.3-6.4)

After 3 days of incubation high levels of hydrogen were observed at elevated temperatures ~75-100°C, with a maximum concentration of 798 μmol l^{-1} occurring at 90°C (Fig 6.3). This is very similar to the concentration detected in the olivine incubation (812 μmol l^{-1}). This is not surprising as composition of both minerals is similar (Table 3.2). No significant methane formation was detected with a maximum concentration of 10 μmol l^{-1} at 103°C. Carbon dioxide increases with temperature in a stepwise manner, with a rapid increase occurring simultaneously to the initial hydrogen increase at 68°C. A dip to 8454 μmol l^{-1} occurs between 90-97°C, before carbon dioxide increases to its maximum of 28.5 mmol l^{-1} at 103°C. Concentrations of CO_2 are not high in comparison with olivine which had 22.2 mmol l^{-1} more carbon dioxide than hornblende. No noticeable sulphate removal took place over the first 3 days with an approximate starting concentration of 20 mmol l^{-1} and a final concentration of ~19 mmol l^{-1} most likely this variation is due to analytical error. Acetate concentrations increase rapidly from 39 μmol l^{-1} at 39°C to 1035 μmol l^{-1} at 58°C before decreasing slightly to 743 μmol l^{-1} at 71°C close to the initial increase in H_2. Subsequently acetate continues to increase to a maximum concentration of 1304 μmol l^{-1} at 97°C, before deceasing rapidly to 316 μmol l^{-1} at 103°C.

After 61 days of incubation high concentrations of hydrogen were detected between 85 and 100°C with a maximum concentration of 720 μmol l^{-1} at 90°C. This is only slightly lower (78 μmol l^{-1}) than detected after 3 days, however high H_2 occurs over a narrower temperature range indicating consumption. Carbon dioxide again increased stepwise with temperature reaching a maximum concentration of 3413 μmol l^{-1} at 78°C. A slight dip of approx 500 μmol l^{-1} occurs at 63°C this coincides with a dip in methane concentrations. Rapid build up of CO_2 occurs from 71°C to 78°C increasing from 1472 μmol l^{-1} to 3413 μmol l^{-1}. The maximum carbon dioxide concentrations do not coincide with the maximum temperature for sulphate removal as seen with previous incubations but coincides with slowing of SO_4^{2-} and rapid increase in acetate. Carbon dioxide

decreases rapidly above 78°C (853 μmol l^{-1} at 84°C) plateuing around this level with a concentration of 1163 μmol l^{-1} at 103°C. Methane production similar to olivine (Fig 6.2) shows two distinct peaks/zones of methanogenesis and similar concentrations. The first zone(46-71°C) has a maximum concentration of 192 μmol l^{-1} at 58°C while the second zone (71-90°C) has a maximum concentration of 282 μmol l^{-1}at 84°C. The first peaks in the zone of sulphate reduction and the second occurs during rapid acetate formation and CO_2 decrease. $\delta^{13}C$-CH_4 Isotope values are in Table 6.2.

Table 6.2 $\delta^{13}C$ values for hornblende incubation

	Sample	$\delta^{13}C$-CH_4	SD	$\delta^{13}C$-CO_2	SD
Zone 2	78°C	-46.9‰	0.3	Na	Na
Zone 1	58°C	-53.6‰	1.0	Na	Na
	46°C	-52.8‰	1.1	Na	Na

SD, standard deviation. n=4

No CO_2 sample data is available due to the long-term storage of methane in acidified KCl. The isotope data is interesting, and are similar to other incubations presented in chapter 5 (Pyrite). The value at 78°C achieved are not normally associated with biotic production of methane (acetoclastic methanogenesis $\delta^{13}C$ -65 to -50‰. but are more associated with methane produced via abiotic origins from much higher temperatures (Whiticar, 1999) although Whiticar does suggest a link between temperature increases and kinetic isotopic effect (KIE)* decreases which is consistent with previous values obtained. Sulphate removal begins at 16°C with maximum removal taking place at 65°C with an approx removal of 14.4 mmol l^{-1}, leaving a remaining concentration of 5780 μmol l^{-1}, complete removal does not occur, no significant removal occurs above 90°C. A rapid slow down in removal rates occur at 78°C. Acetate concentrations increase rapidly when sulphate removal slows from 58 μmol l^{-1} at 71°C increasing to 4398 μmol l^{-1} at 78°C. Acetate concentrations reach a maximum of 6238 μmol l^{-1} at 97°C before decreasing to 1780 μmol l^{-1} at 103°C.

*KIE is the change in reaction rates that occurs when a isotope is substituted for an atom , also called fractionation
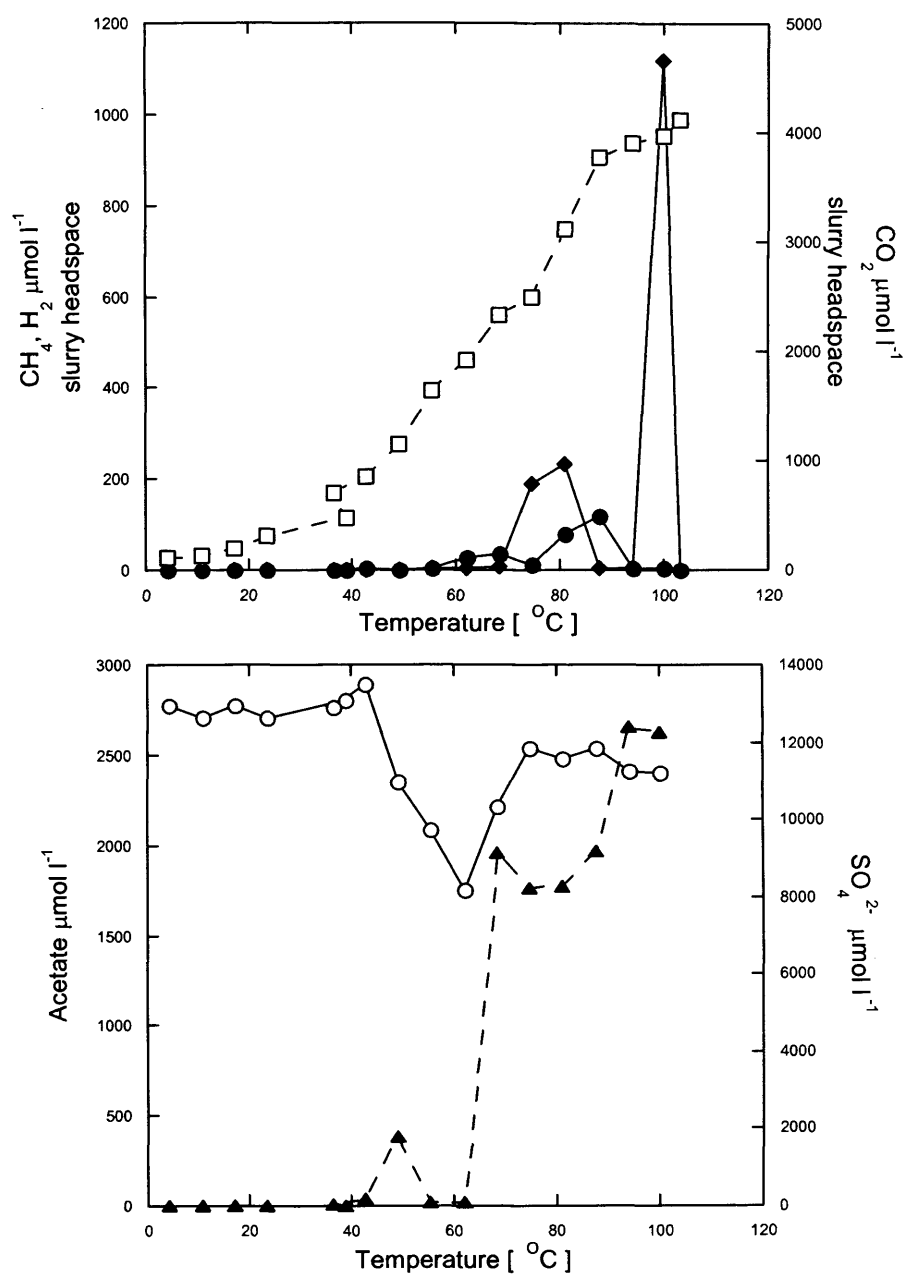
Fig 6.5 Labradorite incubation after 3 days.

Key: CH₄(●), CO₂(□), H₂(◆),Acetate (▲) and SO₄²⁻ (○).
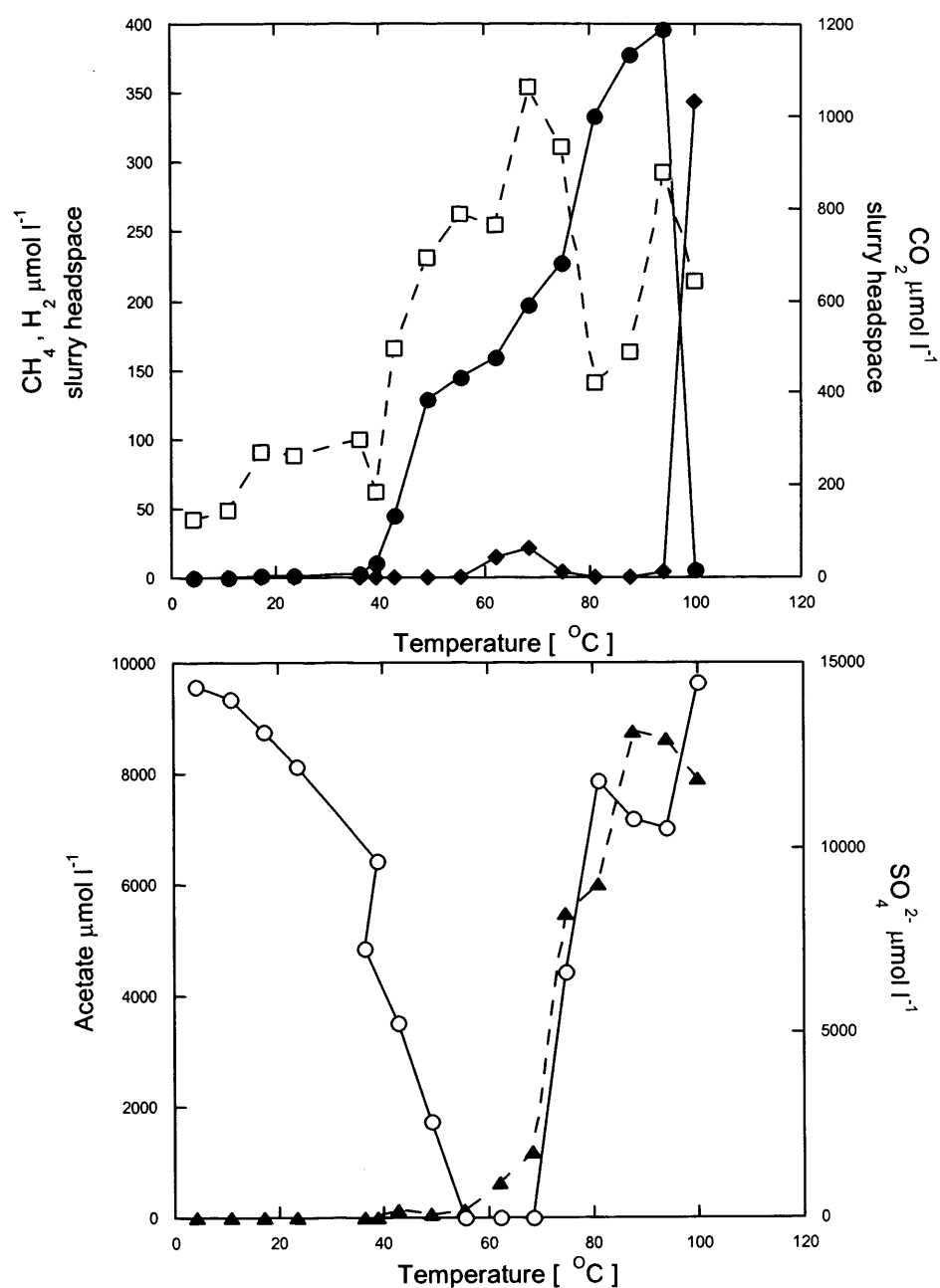
Fig 6.6 Labradorite incubation after 108 days.

Key: CH$_4$(●), CO$_2$(□), H$_2$(◆),Acetate (▲) and SO$_4^{2-}$ (○).

Labradorite slurry incubation, cation concentrations after 108 days incubation.
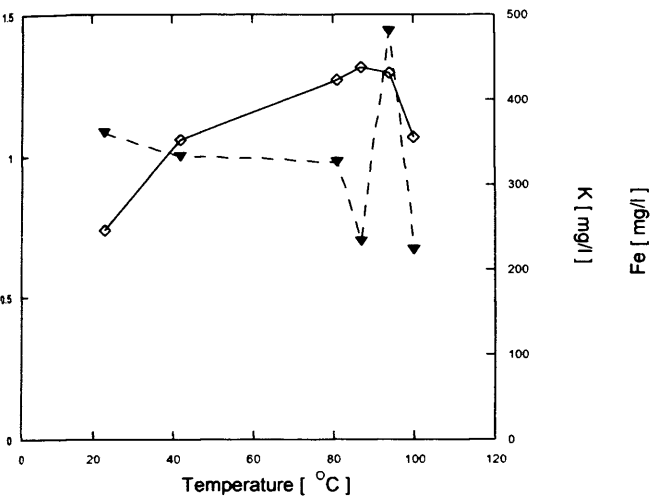
Fig 6.7 Labradorite incubation, Al and K cation
concentrations at selected temperatures after 108 days

Al: inverted closed triangle. K: open Diamond
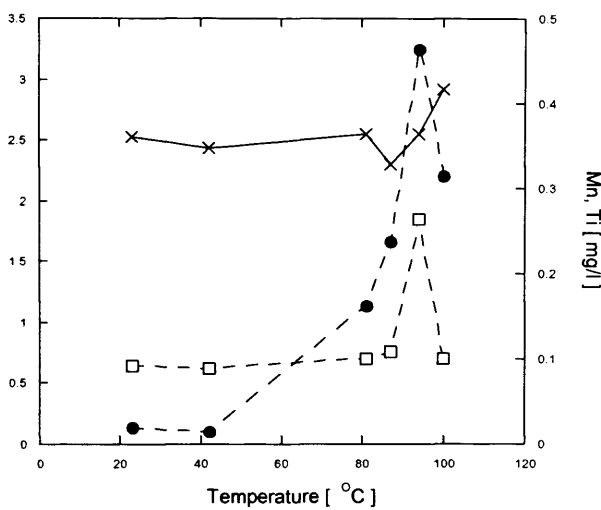
Fig 6.8 Labradorite incubation. Fe, Mn and Ti cation
concentrations at selected temperatures after 108 days

Fe: closed circle. Mn: x. Ti: open box
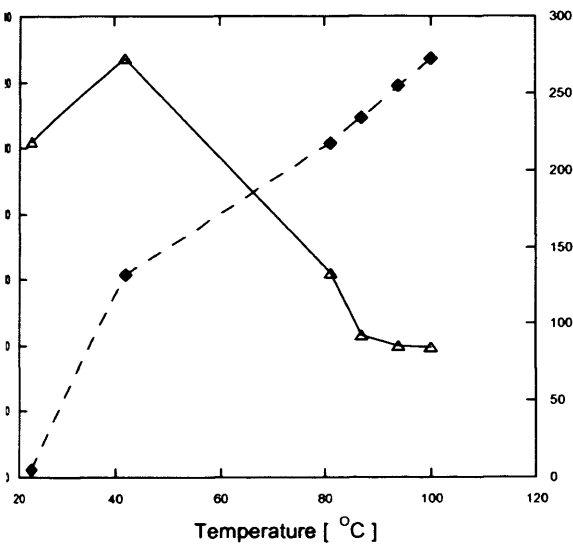
Fig 6.9 Labradorite incubation. Ca and Mg cation
concentrations at selected temperatures after 108 days

. Ca: closed Diamond. Mg: open triangle
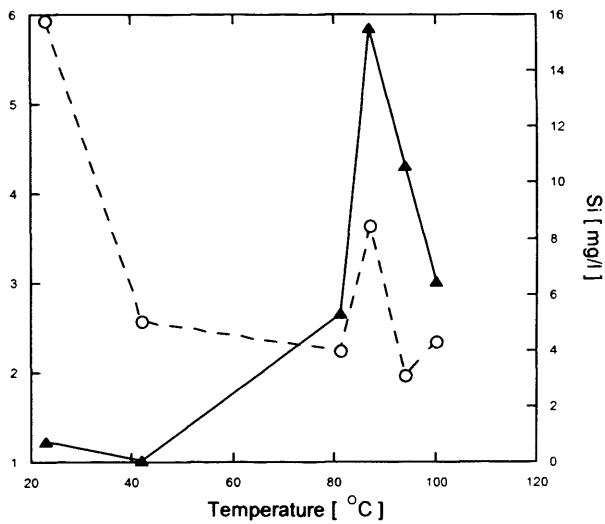
Fig 6.10 Labradorite incubation, P and Si cation
concentrations at selected temperatures after 108 days

P: open circle. Si: closed triangle

188

6.4 Labradorite results (Figs 6.5 to 6.10)

After 3 days, high concentrations of hydrogen were detected with a maximum concentration of 1118 μmol l^{-1} at 100°C. Two peaks are noticeable between 64-87°C and 94-100°C. Maximum H_2 concentrations occur in peak 2 while the maximum concentration in peak one is 231 μmol l^{-1} at 81°C. This maximum concentration is higher than the olivine (812 μmol l at 94°C) or hornblende (798 μmol l^{-1} at 90°C) incubations, and occurs at a higher temperature. No hydrogen is detected above 100°C. Methane concentrations were high in comparison to those detected after 3 days in other incubations (1.9 μmol l^{-1} at 87°C for olivine) with a maximum of 118 μmol l^{-1} detected at 87°C. This overlaps with a decrease in hydrogen concentrations from the first hydrogen peak. Carbon dioxide increases with temperature reaching a maximum concentration of 4110 μmol l^{-1} at 103°C. This increase occurs in 3 different phases 1 a slow increase from 4 to 42°C (111-850 μmol l^{-1}) the second a rapid increase from 42 to 87°C (850-3765 μmol l^{-1}) and phase 3 a slow increase between 87-103°C (3795-4110 μmol l^{-1}). Sulphate removal has begun by day 3 at temperatures above 42°C. Maximum sulphate removal occurs at 62°C where concentrations are 8190 μmol l^{-1} which is an approximate removal of 4.81 mmol l^{-1}. However unlike all previous minerals, sulphate removal occurs at all sampling temperatures from 42°C to 103°C (103°C has a concentration of 11.1 mmol l^{-1}, which is an approximate removal of 1.8 mmol l^{-1}). Amounts of acetate generated are low until 49°C where 382 μmol l^{-1} is detected, this decreases to 25 μmol l^{-1} at 55°C. A rapid increase in acetate occurs at 68°C, coinciding with a slowing in the sulphate reduction rate. Acetate increases from 21 μmol l^{-1} at 62°C to 1955 μmol l^{-1} at 68°C. A decrease in acetate is noted between 68 and 87°C this u shaped decrease is associated with the production of methane and the generation of the second peak of hydrogen. After 87°C acetate concentrations again increase reaching a maximum concentration of 2658 μmol l^{-1} at 94°C with little change to 103°C.

After 108 days max concentrations of hydrogen occur at 100°C (344 mmol l^{-1}). Unfortunately due to sample vessel failure after 100 days, no sample above 100°C was

available for analysis. A small hydrogen peak also occurred in the zone of sulphate depletion (21 μmol l^{-1} at 68°C). This may be an indication of hydrogen usage during sulphate reduction, as it coincides with the zone of complete SO_4^{2-} removal, hence substrates that were being used by sulphate reduction could build up transitionally. This is not seen in the other mineral incubations in this Chapter, as complete sulphate removal does not occur. Once sulphate reduction ceases hydrogen can be liberated for use in other processes (e.g. acetogenesis). Carbon dioxide increases stepwise with temperature until 68°C where a maximum concentration of 1062 μmol l^{-1} occurs. Which is in the zone of complete sulphate removal, hence maximum activity of sulphate reducers. Carbon dioxide decreases above this temperature, decreasing to 422 μmol l^{-1} at 81°C before increasing to 879 μmol l^{-1} at 94°C and decreasing again at 100°C. This decrease in carbon dioxide occurs during a rapid increase in acetate. One explanation of this is, that acetate production from H_2 consumes carbon dioxide; this may also explain the CO_2 dip at 60°C. Methane concentrations start to increase from 36°C (10 μmol l^{-1}) increasing continually to a maximum concentration of 396 μmol l^{-1} at 94°C. Methane concentrations drop to 4 μmol l^{-1} at 100°C. However two changes in temperature response a rapid increase from 36°C (10.4 μmol l^{-1}) to 49°C (128 μmol l^{-1}), and then a slower almost growth curve like response from 49°C to maximum concentrations at 94°C. This could be perhaps a response to a change in substrates and is similar to the 2 methane peaks seen in other incubations, with the exception that these values are overlapping. $\delta^{13}C$ isotope analysis were performed and the results are shown in table (6.3)

Table 6.3 $\delta^{13}C$ values for labradorite incubation

Sample	$\delta^{13}C$-CH_4	SD	$\delta^{13}C$-CO_2	SD
87°C	-42.8‰	0.6	-19.2‰	0.4
81°C	-46.1‰	0.9	-20.3‰	0.2
74°C	-46.1‰	0.7	-21.4‰	0.3

SD standard deviation. n = 4

Similar to previous incubations pyrite and hornblende (Tables 6.2 and 6.3) $\delta^{13}C$ isotope values for methane produced at higher temperature, gives values more recognisable as abiotic methane formation (Whiticar, 1999).

Sulphate depletion begins at 2°C with complete removal occurring between 55 and 68°C, which is a total removal of approx 14.7 mmol l^{-1}. Sulphate reduction then slows rapidly but continues to be removed until 94°C with no removal occurring at 100°C. Acetate values increase once complete sulphate removal is achieved, increasing from 48 µmol l^{-1} at 49°C to a maximum concentration of 8757 µmol l^{-1} at 87°C. Acetate decreases slightly to 7912 µmol l^{-1} at 100°C.

K increases with temperature from 246 mg/l at 23°C to 438 mg/l at 87°C (which correlates with the temperature for maximum acetate formation) before decreasing from 87°C to 355 mg/l at 100°C. Al concentrations remain relatively constant until 81°C 1 mg/l at 23°C and 0.98 mg/l at 81°C. A slight dip occurs to 0.7 mg/l at 87°C before peaking to 1.4 mg/l at 94°C. This peak coincides with maximum CH_4 concentrations. Al concentrations decrease to 0.6 mg/l at 100°C. Iron concentration increase simultaneously with those of acetate (Fig 6.11) increasing from 0.14 mg/l at 23°C to a maximum concentration of 3.2 mg/l at 94°C (CH_4 maximum Fig 6.6) decreasing to 2.2 mg/l at 100°C. Ti concentrations show a very slight increase with temperature with a peak of 0.26mg/l at 94°C before decreasing to 0.1 mg/l at 100°C, this peak is close to the maximum Fe peak. Mn concentrations remain constant to 80°C with a small dip at 85°C then increasing with temperature to 100°C (0.41 mg/l). Ca concentrations increases with temperature from an initial concentration of 2 mg/l at 23°C to 127 mg/l at 100°C. Mg concentrations show an initial increase in concentration from 218 mg/l at 23°C to 272 mg/l at 42°C above this mg concentrations decrease steadily until reaching it lowest concentration of 84 mg/l at 100°C. Si concentrations have a temperature profile similar to Fe and acetate concentration increases (Fig 6.11 b). Maximum concentration of Si detected was 15.5 mg/l at 87°C, before decreasing to 6.4 mg/l at 100°C. P concentrations show a decrease from 5.9 mg/l at 23°C with a rapid drop at 40°C , where CH_4 starts and

is then relatively stable until 100°C with a peak at 85°C to 3.55 mg/l . Final concentration at 100°C were 2.3 mg/l
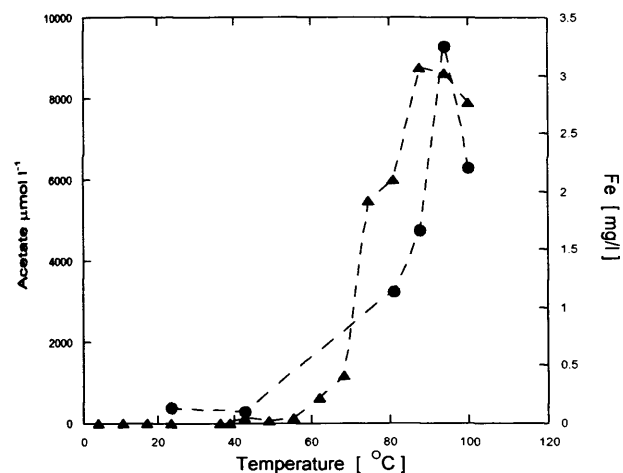
Fig 6.11a Labradorite Acetate and Fe

Acetate: closed triangle. Fe: closed circle.
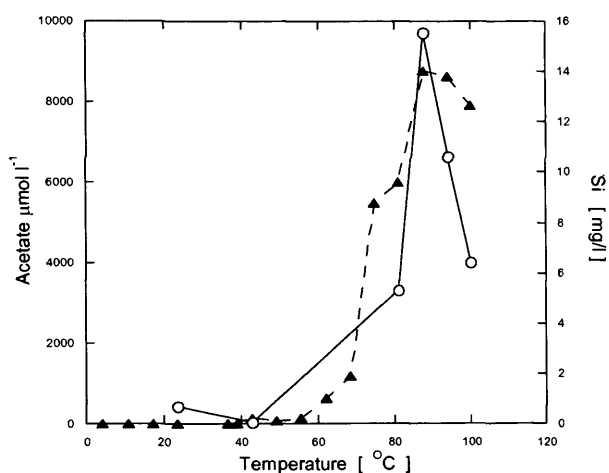
Fig 6.11b Acetate and Silica

Acetate: closed triangle Si: open circle
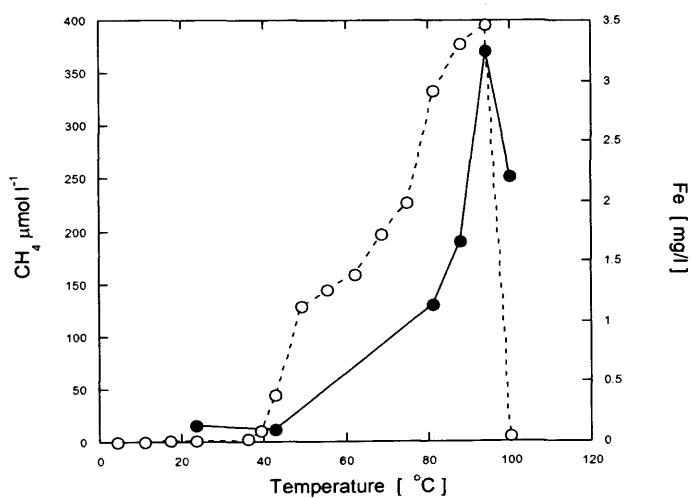
Fig 6.12 Labradorite: Methane and Fe concentrations after 108 days incubation.

Key; methane: open circle. Fe: closed circle
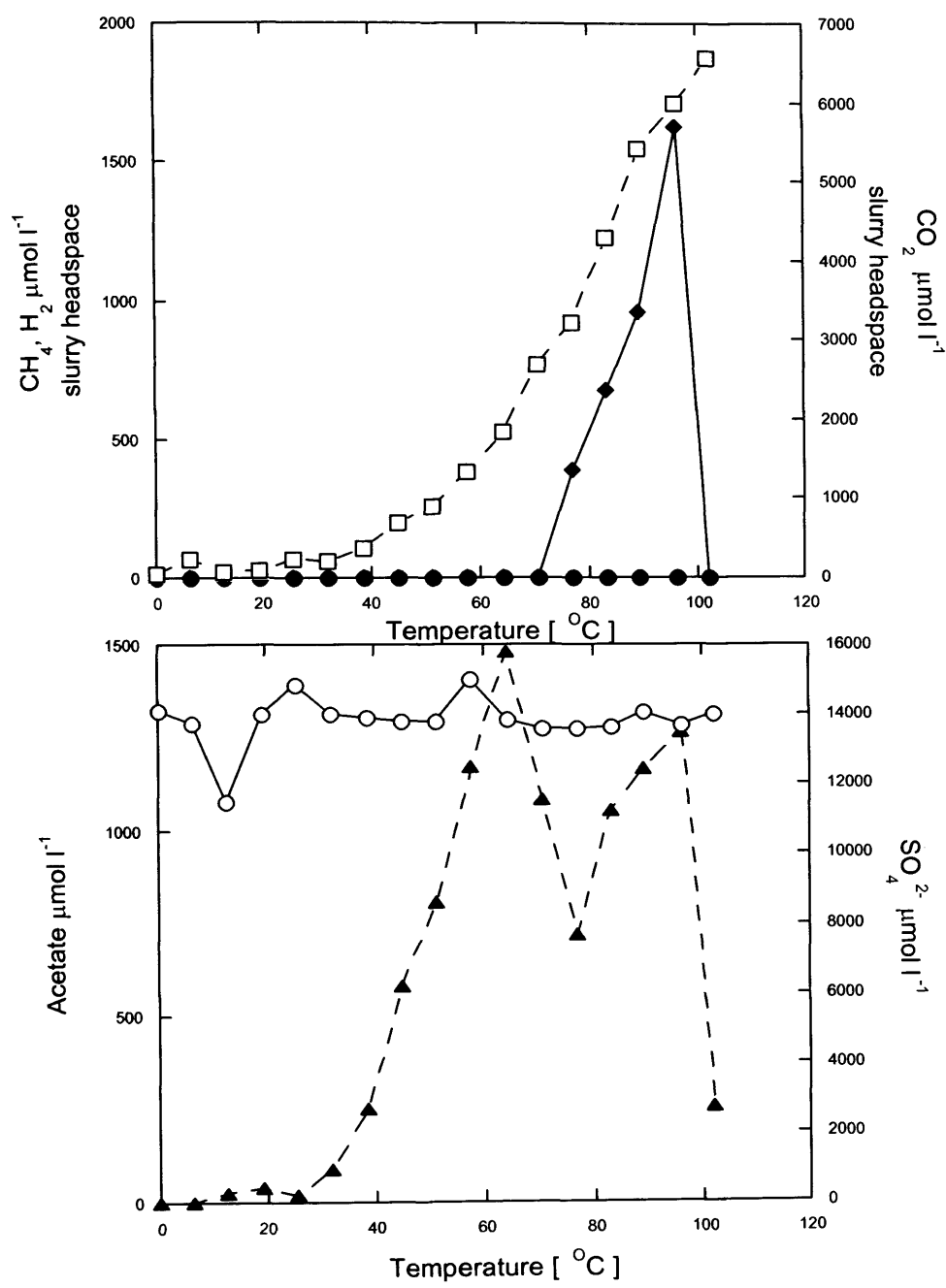
Fig 6.13 Silica addition, 3 days incubation

Key:CH_4 (●), CO_2 (□), H_2 (◆), acetate (▲) and SO_4^{2-} (○).
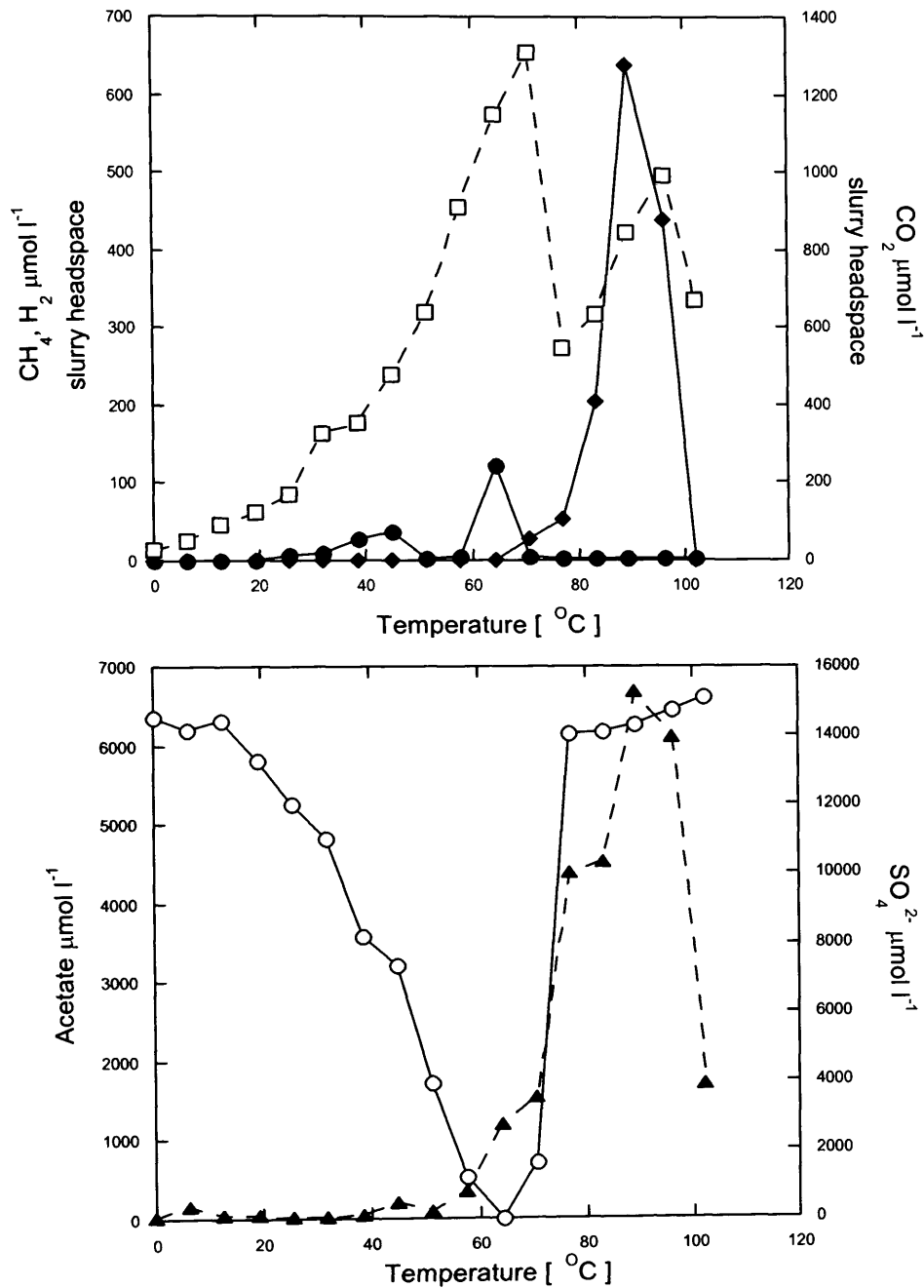
Fig 6.14 Silica addition, 97 days incubation

Key: CH$_4$ ($\bullet$), CO$_2$ ($\square$), H$_2$ ($\blacklozenge$), acetate ($\blacktriangle$) and SO$_4^{2-}$ ($\circ$).

Silica (quartz) slurry incubation, cation concentrations after 97 days incubation.
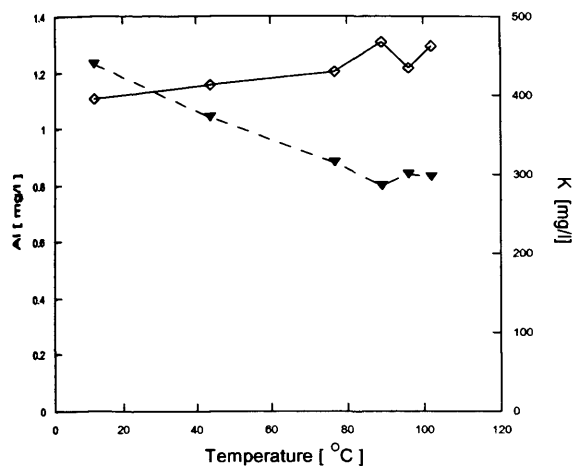
Fig 6.15 Silica incubation, Al and K cation concentrations at selected temperatures after 97 days incubation.

Al: inverted closed triangle. K: open Diamond
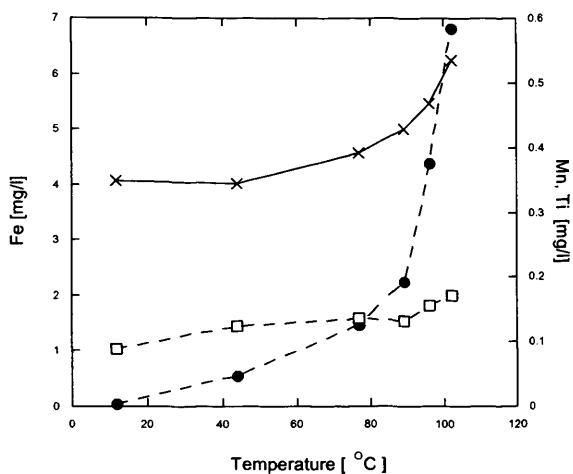
Fig 6.16 Silica incubation. Fe, Mn and Ti cation concentrations at selected temperatures after 97 days incubation.

Fe: closed circle. Mn: x. Ti: open box
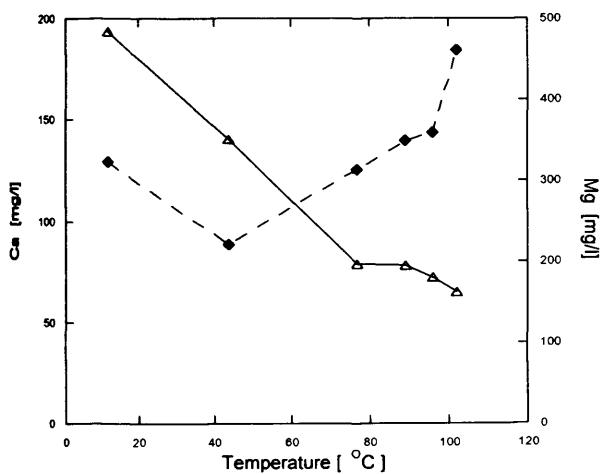
Fig 6.17 Silica incubation. Ca and Mg cation concentrations at selected temperatures after 97 days incubation.

Ca: closed Diamond. Mg: open triangle
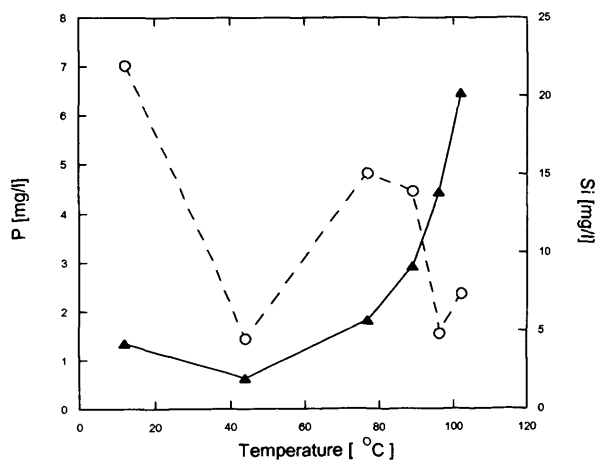
Fig 6.18 Silica incubation. P and Si cation concentrations at selected temperatures after 97 days incubation.

P: open circle. Si: closed triangle

195

6.5 Silica Results (Figs 6.13-6.18)

After 3 days of incubation high concentrations of hydrogen were detected between 70 and 102°C, with a maximum concentration of 1692 μmol l^{-1} at 96°C. This is the highest amount of hydrogen detected after 3 days of incubation, of any thermal gradient experiment presented in Chapters 4, 5 or 6. However, no significant concentrations of methane were detected, the maximum concentration being 0.75 μmol l^{-1} at 87°C as opposed to 118 μmol l^{-1} for labradorite. Carbon dioxide concentrations increase almost exponentially with temperature and reach a maximum concentration of 6564 μmol l^{-1} at 102°C. No significant sulphate removal occurred after 3 days. Acetate concentrations increase with temperature from 20 μmol l^{-1} at 25°C to a maximum concentration of 1478 μmol l^{-1} at 64°C. A sharp decrease occurs between 64 and 77°C with acetate decreasing to 718 μmol l^{-1}. Acetate increases rapidly after this dip rising to 1266 μmol l^{-1} at 96°C before, similar to hydrogen and acetate in all other samples decreasing over 100°C, reaching 258 μmol l^{-1} at 102°C.

After 97 days incubation high concentrations of hydrogen were still present at elevated temperatures between 64 and 102°C, with a maximum concentration of 638 μmol l^{-1} at 89°C. Which is 60% lower than after 3 days incubation and at 7°C lower demonstrating H$_2$ consumption. No hydrogen is detected above 100°C (0 μmol l^{-1} at 102°C). Carbon dioxide initially increases exponentially with temperature to a maximum concentration of 1310 μmol l^{-1} at 70°C, which is in the zone of maximum sulphate removal and when H$_2$ first starts to accumulate. After which, carbon dioxide decreases to 546 μmol l^{-1} at 77°C. This rapid decrease (58%) co-occurs with rapid slowing in the sulphate removal rate and a rapid increase in acetate concentrations. Both of which could be contributing factors. Methane was present in two zones, between 32 and 51°C and between 57 and 70°C. Maximum peak in zone one occurred at 44°C (36 mmol $^{-1}$) and the highest concentration occurred in zone 2 with a maximum of 120 μmol l^{-1} at 64°C. Methane in both zones occur during active sulphate removal. Methane concentrations are low in comparison to some of the other minerals, labradorite maximum of 396 μmol l^{-1}

and olivine of 335 μmol l^{-1}. Unfortunately methane never reached sufficient concentrations during incubation for δ^{13}C-CH_4 analyses to be performed.

Initial concentrations for sulphate are approximately 14.5 mmol l^{-1} with maximum sulphate removal occurring at 64°C, with no significant sulphate removal occurring at 77°C (14.08 mmol l^{-1}). Interestingly a slight increase in sulphate concentrations is noted at high temperature from 95°C with sulphate concentrations reaching 15 mmol l^{-1} at 102°C. Acetate values begin to increase close to the temperature range of maximum sulphate removal increasing from 87 mmol l^{-1} at 51°C, to 1542 mmol l^{-1} at 70°C. More rapid increase takes place when SO_4^{2-} removal slows, increasing to 4395 μmol l^{-1} at 77°C. Acetate continues to increase reaching a maximum concentration of 6679 μmol l^{-1} at 89°C before a slight decrease to 6100 μmol l^{-1} at 96°C. A major decrease in acetate subsequently occurs above 100°C (1710 μmol l^{-1} at 102°C) which coincides with the H_2 decrease.

Cation concentrations after 97 days. K concentrations show a slight increase with temperature, increasing from 395 mg/l at 12°C to 462 mg/l at 102°C. Al concentrations conversely, decrease with temperature from 1.2 mg/l at 12°C to 0.8 mg/l at 89°C, then stabilising up to 102°C.

Fe concentrations increase exponentially with temperature from 0.04 mg/l at 12°C to 6.8
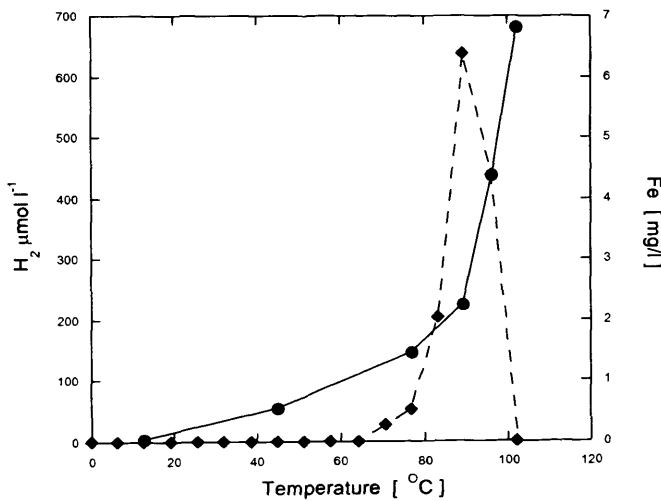
mg/l at 102°C (which is double the maximum labradorite concentration of 3.2 mg/l).

Fe is plotted against H_2 generation in Fig 6.19. This temperature profile is rather different to that for H_2.

Mn concentration also increases exponentially with temperature above 44°C, increasing from 0.34 mg/l at 44°C to 0.53 mg/l at 102°C. Ti concentrations only increase slightly with temperature from 0.08 mg/l at 12°C to 0.17 mg/l at 102°C.

Mg concentrations continuously decrease with increasing temperature, from 483 mg/l at 12°C to 197 mg/l at 77°C. After 77°C the rate of decrease slows (this coincide with slowing in rate of sulphate removal and rapid increase in acetate). Mg decreases to 162 mg/l at 102°C. Ca concentrations initially decrease from 129 mg/l at 12°C to 88 mg/l at 44°C. Subsequently increases with temperature to a maximum concentration of 184 mg/l at 102°C (the rate of increase rises after 98°C. The silica profile is a very similar profile to Fe (Fig 6.20). There is an initial decrease from 4.2 mg/l at 12°C to 2 mg/l at 44°C. Si then starts to increase exponentially with temperature to reach a maximum concentration of 20.1 mg/l at 102°C.
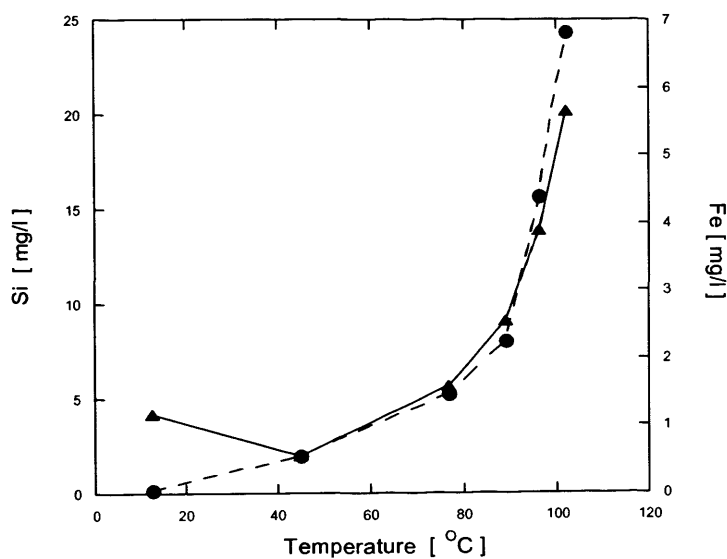
Fig 6.20 Silica and iron concentrations.
Silica: closed triangle. Fe: closed circle.

Similar to Fe, Si concentrations are elevated at zones of high hydrogen concentrations (Fig 6.20). But unlike H_2, silica concentrations continue to increase with elevated temperatures (Fig 6.21) as does Fe (Fig 6.19 & 6.20)
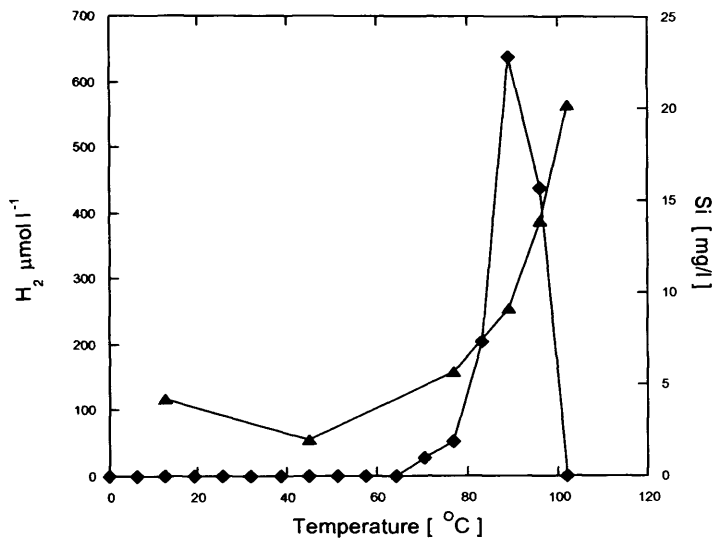
Fig 6.21 Hydrogen concentration against porewater silica concentration. Silica, solid triangle: hydrogen, solid diamond.

P concentrations, fluctuates considerably with incubation temperatures. Initially decreasing from 7 mg/l at 12°C to 1.01 mg/l at 44°C. Before increasing to 4.8 mg/l and 4.4 mg./l at 77 and 89°C respectively and decreasing to 1.5 mg/l at 96°C before reaching a final concentration of 2.3 mg/l at 102°C.

6.6 AODC counts on silica incubation
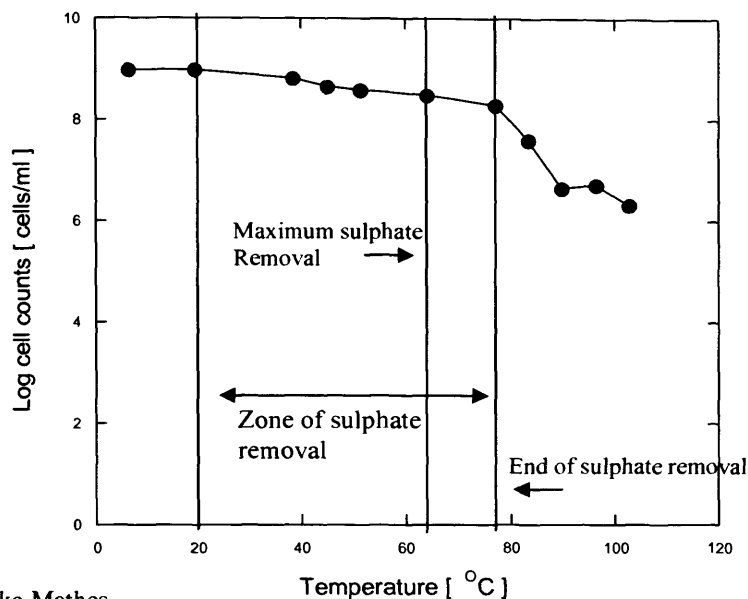
Courtesy of Falko Mathes

Fig 6.22 AODC counts on silica thermal gradient incubation

AODC counts (all values are in log cell counts/ml) were conducted on the silica incubation in order to analyze the effect of temperature on prokaryotic cell numbers. Selected silica samples were counted after 97 days incubation. There seems to be two rates of cell decrease. Initially reduction in cell numbers is slow from 8.97 (9.33 x 10^8 cells/ml) at 6°C to 8.28 (1.90 x 10^8 cells/ml) at 77°C. Above 77°C cell decrease becomes more rapid decreasing to 6.33 (2.13 x 10^6 cells/ml) at 102°C. Interestingly sulphate removal is inhibited above 77°C perhaps sulphate reducing bacteria and associated prokaryotes are generally being inhibited by high temperature. In zone two 77-102°C it is also noteworthy that temperature seems to be the dominant factor controlling cell numbers as numbers continue to decline irrespective of high amounts of acetate and hydrogen being produced in this temperature zone. This is also true for zone one below 77°C, this indicates that probably terminal oxidizing prokaryotes form only a small part

of the community. At 80°C and above, these constitute hyperthermophilic conditions, fewer prokaryotes can grow at these temperatures perhaps this is responsible for this decrease, which continues with increasing temperature.

6.7 Discussion

Results from incubations conducted in this Chapter clearly show that, iron content of the mineral added has no effect on the amounts of hydrogen generated. This in turn affects processes such as sulphate reduction, acetogenesis and methanogenesis, using hydrogen or hydrogen derived products e.g. acetate as a substrate. This is best shown, after 3 days incubation, pure silica mineral addition produced the highest quantity of hydrogen (Table 6.4).

Table 6.4 Maximum H$_2$, CH$_4$ and acetate concentrations after 3 days incubation (μmol l^{-1})

Sample	SiO$_2$ wt%	Hydrogen	Methane	Acetate
Olivine	41.82	812	1.9	1273
Hornblende	49.95	798	10.5	1304
Labradorite	52.5	1118	118	2658
Silica	100	1626	0.7	1266

Although silica addition produced the highest quantities of hydrogen after 3 days, labradorite far exceeds all other incubations in the production of acetate (x2 over hornblende the next highest) and methane (x11.2 over hornblende the next highest in terms of methane also).

Table 6.5 Maximum concentrations at final sampling point (μmol l^{-1})

Sample	SiO$_2$ wt%	Days incubation	Hydrogen	Methane	Acetate
Olivine	41.82	61	704	335	5841
Hornblende	49.95	61	720	282	6238
Labradorite	52.5	108	344	396	8757
Silica	100	97	638	120	6679

All incubations produced methane, however, silica produced less than all other incubations and hence δ^{13}C-CH$_4$ isotope analysis was not possible. Isotope analysis of the remaining samples (Tables 6.1, 6.2 and 6.3) showed values distinct for acetoclastic methanogenesis. Higher temperature incubations however, produced more depleted values, which normally would be interpreted as being due to abiotic methane formation (δ^{13}C-CH$_4$ >-50‰). However it is noted (Whiticar, 1999) that temperature does influence the δ^{13}C-CH$_4$ values, even for biogenic CH$_4$, with KIE (Kinetic isotope effect) decreasing with increasing temperature which is consistent with the findings presented here (Fig 6.23)
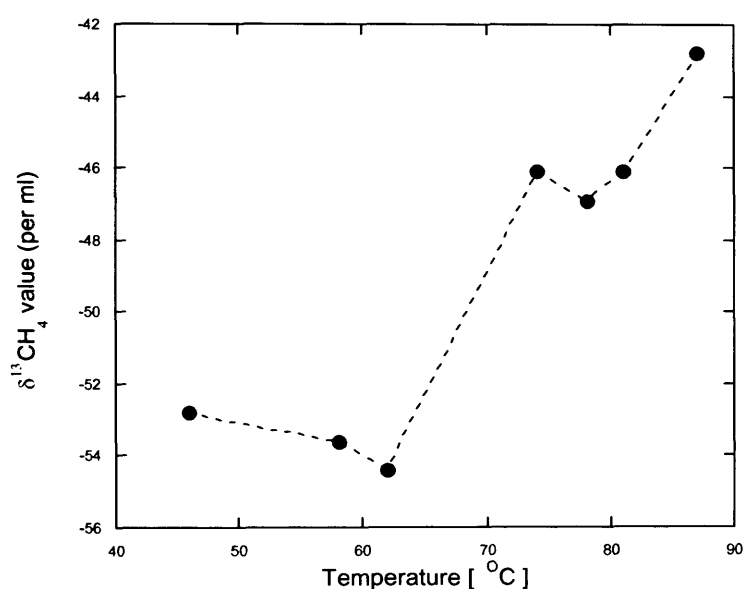
Fig 6.23. δ^{13}C-CH$_4$ data for all data in chapter 6 plotted against temperature

Differences in the methane concentration temperature profile at final concentrations are also noticeable with the highest amounts of methane produced in the labradorite incubation (Fig 6.5), labradorite also shows continuous CH$_4$ production from ~40 to 95°C after 108 d , through the most intense Sulphate reduction zone, where H$_2$ concentrations

increase slightly, both indicating excess H_2 formation. This is in contrast to the olivine and hornblende incubations, which have two distinct zones of methanogenesis olivine 36-74°C and 74 to 94°C with little to no methane in the transition zone 74°C and hornblende 33-71°C and 71-90°C a similar scenario of little methane in the 71°C transition zone this transition zone occurs close to zone of maximum sulphate removal. This does not occur in the labradorite incubation however, complete sulphate removal is achieved in this and not achieved in olivine or hornblende

All final incubations presented show a similar profile of rapid acetate increases coupled to the slowing down of sulphate removal rates. This could either mean that sulphate reduction is being performed using acetate as a substrate (acetoclastic sulphate reduction) or hydrogen is being utilised for sulphate reduction and once sulphate reduction slows hydrogen is liberated for use by acetogens. Highest concentrations of acetate always occur in the zone of highest hydrogen formation. Maximum Sulphate reduction in all samples occurs in the same temperature zone 60-70°C. However, again labradorite seems slightly different, in that sulphate removal also occurs at higher temperatures than the other incubations up to 94°C (inclusive) silica SO_4^{2-} reduction stops at ~80°C olivine and hornblende ~88°C. This could however, also be the result of the slightly longer incubation time associated with the labradorite incubation 108 days as opposed to 61 days for olivine and hornblende.

Pore water cation values were only available for labradorite and silica and show some broadly similar trends. Iron concentrations exponentially increase with temperature (Figs 6.8 & 6.16) but surprisingly the silica mineral addition produced double the amount of final total iron concentration than labradorite. Si generally increased with temperature (Figs 6.10 & 6.18) although for labradorite a dip occurs past approximately 85°C. Not surprisingly the silica addition contained the most silica in pore water but not substantially (Si 20.1 mg/l, labradorite 15 mg/l). Also overall Ca increased with temperature in both and Mg decreased, whilst there were slight increases in Al with temperature, decreasing slightly in labradorite at high temperature.

In conclusion this chapter suggests that hydrogen generation is not reliant on Fe concentrations and in fact could be a reaction-involving silica radials. Possibilities for this type of mechanism are discussed in detail in chapter 7.

Chapter 7
Discussion

7.1 Introduction

The main aim of this research project was, a) to determine if H_2 could be generated from the addition of minerals to sediment slurry incubations, b) whether prokaryotes are directly involved in this H_2 generation, c) the effect of temperature on this process and biogenic & abiogenic interactions, d) the effect of mineral composition. The minerals used in this study (Table 3.1) were all natural rock minerals from outcrop sites, no synthesised or purified minerals were used, hence composition (Table 3.2) may be different to standard, this was in order to try and accurately represent *in situ* mineral composition. Hydrogen is one of the most energetically favourable substrates for deep subsurface prokaryotes (Morita, 1999; Amend and Shock, 2001). If additional mechanisms of hydrogen generation could be found, and if this was enhanced by prokaryotic activity, this would change the current understanding of potential energy sources in the subsurface. Substantial numbers of prokaryotes are present at depth (Parkes et al., 1994; Schippers et al., 2005; Lipp et al., 2008; Roussel et al., 2008) due to nutrient limitation and the recalcitrance of sedimentary organic matter this is surprising, and suggests that, our knowledge of energy sources sustaining these communities is incomplete. Processes that provide energy and reducing power for subsurface, anaerobic, chemoautotrophic microbial communities such as H_2, have thus far been thought of as being derived solely from abiotic activity. These include; the oxidation of Fe^{2+} containing minerals (Stevens and McKinley, 1995), serpentinization type reactions (Sleep et al., 2004), the decomposition of alkanes, which are catalysed by compounds within certain iron minerals (Seewald, 2001), radiolytic decomposition of water (Lin et al., 2002) and the formation of pyrite from H_2S and FeS (Drobner et al., 1990). All have been hypothesised to produce enough H_2 to support microbial metabolisms, and not to have any direct prokaryotic involvement. The aromatization of organic matter (Parkes et al., 2007) ,however, is one exception, as it was argued that prokaryotes are involved in this H_2 producing reaction at elevated temperature. This could be an indication that prokaryotes may be involved in other/similar H_2 producing reactions. The majority of abiotic H_2

formation processes occur at extremely high temperatures, e.g. serpentinization and decomposition of alkanes / carboxylic acids (> 300°C), which is substantially above the upper temperature for prokaryotic life (~113-121°C, (Kashefi and Lovley, 2003). In these circumstances H_2 is then thought to migrate to cooler zones, where it can be utilised for microbial activity.

7.2. Concentrations of hydrogen generated, temperature effects and abiogenic/biogenic reactions.

During the course of this study, it was shown (Chapter 3) that specific minerals incubated at 60°C, produced a peak of hydrogen over the course of the first 3 days of incubation (e.g. hornblende Fig 3.1, ilmenite Fig.3.2 and olivine Fig 3.3). H_2 utilising prokaryotic processes such as, acetogenesis, methanogenesis and sulphate reduction all then proceeded rapidly, with hydrogen concentrations becoming undetectable after 3 days. Since H_2 is a know substrate for all 3 processes it is reasonable to assume that microbial activity is responsible for the H_2 removal. Other processes that could be responsible for removal of H_2 include Fe(III) oxidation and some weathering processes. In the olivine and olivine bombs incubation (Fig 3.3 and 3.4) H_2 concentrations increased again after ~85 days incubation this coincides with the total removal of sulphate, this indicates that H_2 is probably being used as a substrate for sulphate reduction, once sulphate reduction stops this enables H_2 to accumulate. It also shows that hydrogen generation is sustained throughout the incubation and is not confined to the early stages, just on initial mineral addition, unlike previous abiological experiments (Stevens and McKinley, 2000). Not all minerals however, produced H_2 to the same extent. While others produced no detectable hydrogen, this does not mean H_2 wasn't produced, as H_2 can be rapidly consumed for various metabolic processes as mentioned above (hematite Fig 3.6, pyrite Fig 3.7, pyrrhotite Fig 3.8, basalt Fig 3.9). Sterile controls produced no H_2 but also had no detectable sulphate reduction, methanogenesis or acetogenesis (Fig 3.10 a+b). Table 7.1 shows the highest detected amounts of hydrogen during the 60°C incubations conducted in Chapter 3. Olivine and olivine bombs produced the highest amounts (9137 and 8898 $\mu mol\ l^{-1}$).

The detection of varying amounts of H_2 indicates that H_2 could be produced from mineral addition, but also that mineral type and composition were important. Hydrogen generation appears to be a rapid process, with high concentrations generated during the first 24 hours of incubation. This is far more rapid than some other suggested processes such as radiolytic H_2 generation, where in the Witwatersrand Basin in south Africa rates of generation are estimated at ~1nM/year (Lippmann et al., 2003). But it is similar to abiotic experiments conducted with varying basalt minerals (labradorite, forsterite) where H_2 also increased rapidly over the first 3 days however, concentrations were much lower (~10-20 nM/g sample) and the pH was acidic (pH 6) (Stevens and McKinley, 2000). The lack of H_2 generation in our study during the initial basalt incubation at pH of 7.6, over the first 3 days (Table 7.1) correlates with other experiments conducted on basalts at pH 8 (Anderson et al., 1998) which is approximately the pH *in situ* in the Columbia river basin. Lack of hydrogen generation at environmentally relevant pH for basaltic aquifers was one of the major criticisms of previous studies with production only occurring under acidic conditions (pH 5-6). Our study is conducted at pH 7.6, for *in situ* conditions in marine sediments which rarely are outside pH 7.0 to 8.2 (Ben-Yaakov, 1973) which makes it more biologically relevant to environmental conditions.

Table 7.1 Maximum hydrogen concentrations, during 60°C incubations from Chapter 3

Sample	$H_2 \; \mu mol \; l^{-1}$	Time
Olivine	9137	24 hours
Olivine bombs	8898	24 hours
Hornblende	8451	24 hours
Labradorite	2560	24 hours
Ilmenite	1097	24 hours
Pyrite	0	NA
Pyrrhotite	0	NA
Hematite	0	NA
Basalt	0	NA

NA= not applicable since no H_2 was detectable

In Chapters 4,5 and 6 the temperature range of incubations were expanded. In these thermal gradient incubations, high concentrations of H_2 were generated at elevated temperatures (>85°C). Again maximum H_2 concentrations varied with mineral type (Table 7.2).

Table 7.2 Maximum concentration of hydrogen generated after 3 days using the thermal gradient incubation system (0-105°C)

Sample	H_2 μmol l^{-1}	Temperature [°C]
Hematite	1633	92
Silica	1626	96
Labradorite	1118	100
Pyrite	820	97
Olivine	812	94
Hornblende	798	90
Basalt	766	92
Ilmenite	632	95
No mineral	3	33
Magnetite	0	Na
Basalt Sterile	0	Na

NA= not applicable since no H_2 was detectable

For the thermal gradient incubation in Table 7.2. the results of H_2 generations are shown after 3 days, this is for 2 reasons firstly, H_2 concentrations were at a maximum after 3 days and subsequent values are a balance between formation and utilisation. Secondly although all experiments were analysed after 3 days, the final sampling points were not conducted after exactly the same length of incubation. Hence the initial 3 day sampling point gives a more comparable reflection of potential for H_2 generation. Final concentrations for H_2 are given in Table 7.4 for comparison. H_2 generation (Table 7.2) was highest in the hematite incubation with similar concentrations found in the silica incubation. Only comparatively insignificant amounts of H_2 were detected in the incubation without mineral addition (max of 3 μmol l^{-1}), and no H_2 was detected in the sterile control or in the magnetite incubation.

Crushing of minerals before addition creating "fresh" reactive surfaces was found to speed up reaction rates e.g. with hornblende, fresh grinding increased methanogenesis (x10) and CO_2 generation (x7) (Fig 3.13). H_2 production in Table 7.2 occurs at elevated temperatures 90-100°C only trace amounts of H_2 were produced below this (no mineral, 3 μmol l^{-1}), this indicates that elevated temperature stimulates H_2 production and may increase formation for some minerals e.g. Hematite and Pyrite, as suggested by (Stevens and McKinley, 2000).

Nowhere during the course of this study was the impact of prokaryotes on hydrogen generation shown more clearly than in the basalt ramping experiment (Figs 4.25, 4.26). Throughout the incubation the biotic experiment consistently produced far more H_2 through all biotic temperatures (85-115°C), for example at 95°C the biotic experiment has a H_2 concentration of 14968 μmol l^{-1}, where as the sterile control has no detectable hydrogen. This was after 40 days of incubation and was similar to the 60°C experiment mentioned above (olivine and olivine bombs) that long term H_2 generation in the presence of prokaryotes is independent of initial grinding and production of fresh surfaces, perhaps a form of microbial weathering is maintaining reactive surfaces.

Most interesting of all is the difference in H_2 concentrations occurring in the abiotic zone (> 121°C). The biotic incubation previously experiencing prokaryotic activity produced H_2 concentrations (x34) greater than the sterile control (Figs 4.25 and 4.26) after 3 days at 155°C. Thus it seems that not only does prokaryotic mineral interaction provide substrates during sequential heating at biotic temperatures, but also that previous exposure to prokaryotic activity has a major effects on subsequent reactions at abiotic temperatures. It has already been calculated that high temperature abiotically driven reactions could provide substrates for microbial activity in sediments at depth, which then migrate upward, fuelling the base of the microbial biosphere (Horsfield et al., 2006). The fact that previous exposure to prokaryotes has such a major effect has clear implications for these kinds of calculations and implications for sediment diagenesis with increasing temperature/depth of sediment. This result also has significance for all hydrous pyrolysis type experiments used to estimate high temperature thermogenic transformations (Lewan and Fisher, 1994).

Hydrous pyrolysis experiments use temperature as a substitute for time/depth, in order to provide laboratory simulation of the catagenesis of organic matter in

sediments and to provide an understanding of the processes involved in petroleum generation/organic acid generation. These experiments involve sediment heating to high temperatures ~200-500°C and then measuring the amounts of products liberated e.g. low molecular weight organic acids (Barth and Bjorlykke, 1993; Dias et al., 2002). For example in (Barth and Bjorlykke, 1993) samples were incubated between 200-350°C for 72 hours after which samples were analysed for acetate, formate, propionate and isotopic $\delta^{13}C$ analysis was performed. In (Kharaka et al., 1993) samples were incubated between 200-300°C for between 98-238d hours and again samples were analysed for acetate formate propionate, etc.

Results presented here indicate that concentrations of acetate and CO_2, the primary compounds analysed in the majority of studies, are significantly greater (Figs 4.25, 4.26) in sediments previously exposed to prokaryotic activity. Thus it may be that experiments incubated only at temperatures above the biotic temperature zone may not accurately reflect important geochemical changes with sediment depth or the amounts of substrates that could be generated as a potential energy sources in the deep subsurface.

Experiments reported here show clearly that mineral H_2 generation, a) involves prokaryotic mediated or catalysed reactions, and hence is dependent on the presence of sedimentary prokaryotes, b) it is influenced by the composition of the mineral c) enhanced by elevated temperatures, d) is initially substantially increased by the creation of freshly ground surfaces, e) is maintained in the presence of prokaryotic activity, possibly through processes similar to microbial weathering.

7.3 Mineral composition and relationship to H₂ generation

Minerals containing a range of iron and silica were used in this project, from 99 wt% Fe (magnetite) to 100% Si quartz sand. The rationale behind the use of such a range of minerals (Table 3.2) was two fold, 1) to compare our biotic experiments with previously published abiotic experiments which used a range of iron minerals (Anderson et al., 1998; Stevens and McKinley, 2000), 2) previously hypothesised mechanisms for H_2 generation from minerals involved the oxidation of ferrous in the mineral composition (Stevens and McKinley, 1995). A range of minerals with different Fe concentrations and oxidation states, including zero iron content, were used in order to test the validity of this assertion.

Table 7.3 Maximum hydrogen concentrations and relationship with Fe and Si, after 3 days incubation in the thermal gradient system (0-100°C) (see table 7.2 for temperature).

Sample	H_2 μmol^{-1}	Fe_2O_3 wt%	SiO_2 wt%
Hematite	1633	54.12	20.53
Silica	1626	0	100
Labradorite	1118	0.62	52.5
Pyrite	820	46.6*	0
Olivine	812	7.9	41.82
Hornblende	798	7.87	49.9
Basalt	766	12.6	47.5
Ilmenite	632	50.75	1.06
Magnetite	0	99.49	2.57
No mineral	0	0	0
Basalt Sterile control	0	12.6	47.5

*Theoretical value for pyrite,

The maximum H_2 concentration detected after 3 days incubation is shown in Table 7.3, also shown is the Fe and Si content for each mineral. It is clear that Fe content of the mineral was not positively related to initial hydrogen generation. As the mineral containing the most Fe (magnetite) produced no detectable hydrogen this agrees with previous findings (Stevens and McKinley, 2000). However, this is in contrast to (Parkes et al., 2007) where magnetite incubation at 60°C was found to produce low amounts of H_2 (~350 nM after 55 days). Perhaps in the experiments reported here some low amounts of H_2 are being produced but the active microbial community present consumes it before it reaches detectable concentrations. If a comparison is made by addition of the concentration of various potential products/uses of H_2, such as CH_4, acetate formation and sulphate reduction. The difference between no mineral addition and hematite is 23% and basalt 16% both producing more overall product than the mineral only addition. Even more interesting

is the fact that the addition of pure silica (containing no Fe, Table 3.2) produced almost the maximum hydrogen concentrations detected.

Freshly ground basalt to which was added anoxic mineral salt solution incubated in the temperature zone of maximum H_2 generation (~70-100°C) produced far less hydrogen than in the presence of sedimentary prokaryotes (Fig 4.21) (maximum of ~10 μmol l^{-1}). At 73°C H_2 concentrations (1 μmol l^{-1}) are similar to incubations conducted abiotically at 60°C (0.6 μmol l^{-1}) in previously published experiments which were trying to model hydrogen in groundwater in the basaltic system of the Columbia river basin (Stevens and McKinley, 2000). These experiments also involved "fresh" grinding of minerals. In comparison to the experiments with prokaryotes and sediment slurries presented in this study, these hydrogen concentrations are insignificant. According to (Stevens and McKinley, 2000) however, even these low concentrations would be enough to support a microbial community. Although this was highly disputed (Anderson et al., 1998) due to the composition of the *in situ* Columbia river aquifer, prokaryotic community being heterotrophic not autotrophic and a great reduction of hydrogen generation over an extended incubation after 12.5 days.
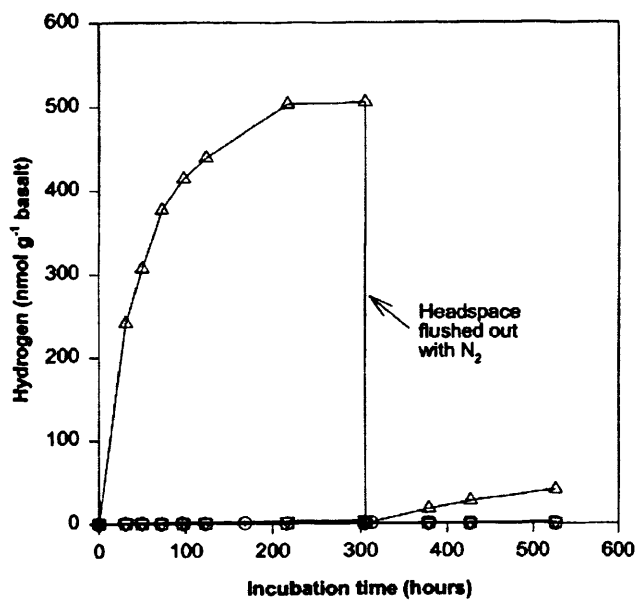
Fig 7.1 Production of H_2 over time by Snake River Plain basalt when incubated with ground water collected from the Snake River aquifer or phosphate buffers (oplus , ground water with basalt; +, ground water alone; triangle , pH 6 phosphate buffer with basalt; downtriangle , pH 8 phosphate buffer with basalt; square , basalt alone; circle , buffer alone) from (Anderson et al., 1998).

While there is no relationship between iron composition and hydrogen generation, there seems to be a relationship between silica concentrations in porewater and hydrogen generation. A comparison of the initial 3 day hydrogen concentrations and final maximum Si concentrations reveals a correlation (Fig 7.2). The rationale for using the initial 3-day hydrogen concentrations as opposed to the final concentration is as follows. Initial H_2 generation is quite rapid and gives a good indication of mineral potential for hydrogen generation. The final concentration of H_2 is affected by various processes which use H_2 (acetogenesis, methanogenesis, sulphate reduction) this and the varying incubation times used, effects the measured hydrogen concentration, and hence does not necessarily give a good indication of the total amount of H_2 produced by a mineral over time. H_2 generation is a continuing processes throughout the course of the incubation (e.g. as seen in the ramping experiment mentioned above Fig 4.25, therefore, if interactions with Si was responsible for H_2, production the longer the incubation is left the more likely a build up of a substrate such as Si
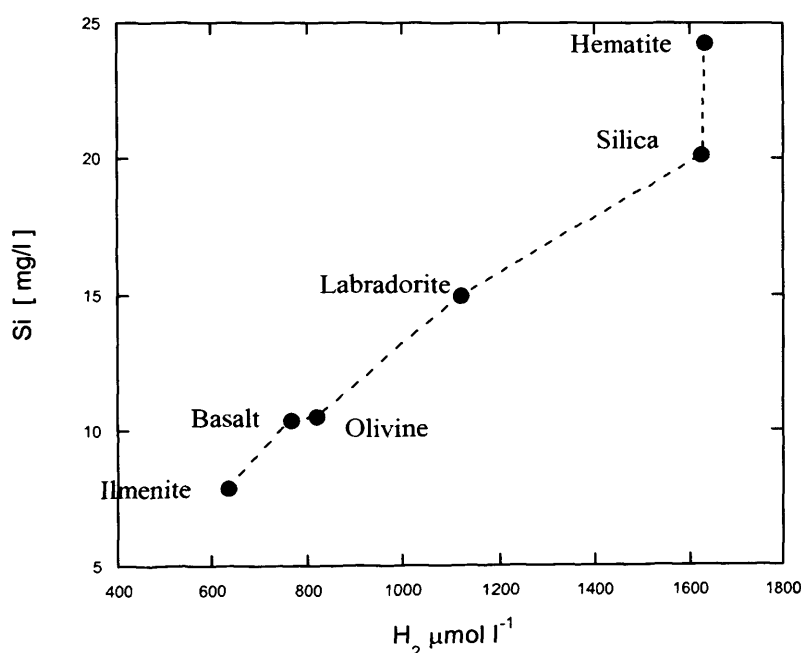
Fig 7.2 Maximum hydrogen concentrations after 3 days incubation, plotted against final Si concentrations (Pore water) in the thermal gradient experiments.

A correlation coefficient of 0.97 suggests there is a strong relationship (significant at the 0.01 probability level) between initial H_2 formation and final concentrations of Si in porewater. Microbes have previously been found to influence weathering of minerals, particularly silicates (Hiebert and Bennett, 1992). Prokaryotes can alter silicate solubility by directly attaching to the mineral, this affects the mineral-water equilibria/ reaction dynamics at the point of contact (Liermann et al., 2000; Bennett et al., 2001). A microenvironment can form around the mineral that can be distinct from the bulk solution. These can be highly reactive in respect to mineral surfaces (Fisk et al., 1998) and dissolution of Si can be speeded up in by the production of excess protons, addition of organic ligands, hydroxyls and extracellular polysaccharides (Malinovskaya et al., 1990; Welch et al., 1999). Perhaps there is a link between the reactivity of mineral surfaces, hydrogen production and silica dissolution.

While it is clear that the Fe concentration in the mineral is not directly related to H_2 generation, this does not mean that Fe does not play a more subtle or indirect role in hydrogen generation as both maximum H_2 and soluble Fe concentrations detected in porewater, often co-occurred at elevated temperatures (>60°C, e.g. Fig 6.19). In addition, the silica mineral incubation had maximum concentrations of Fe in pore water that was higher (6.8 mg/l, Fig 6.16), than several of the Fe containing minerals, e.g. hematite (4.7 mg/l, Fig 5.19) and ilmenite (2.7 mg/l, Fig 5.12) this Fe is presumably coming from the sediment itself. Fe may play perhaps an indirect role in this process e.g. electron shuttling.

Another possible explanation for increasing concentrations of Fe is, hyperthermophilic micro-organisms closely related to the species found at high temperature in our incubations, such as *Thermococcus* and *Archaeolglobus*, which can use Fe^{3+} as an electron acceptor, with H_2 or organic substrates, producing soluble ferrous. In addition, some prokaryotes can transfer electrons to humic substances and other extracellular quinines, given the presence of H_2 as an electron donor (Lovley et al., 2000). The ability to use Fe^{3+} is highly conserved in hyperthermophiles and has been used as a means of isolation and characterisation of previously unculturable species (Kashefi and Lovley, 2000; Kashefi et al., 2002a; Kashefi et al., 2002b). Thus reduction of Fe(III) can proceed without direct contact between the Fe(III) oxide and prokaryote. Coupled to this preliminary data (not shown) showed that the majority of the Fe in pore water in the basalt and ilmenite incubation (>95%) at high temperature

was Fe(II) (ferrozine determination Chapter 2). It is possible that such reactions may be occurring with some Fe coming from the sediment. Most of the mineral additions with the exception of silica have Fe, and there is a difference in pore water concentrations, the maximum Fe in the no mineral addition is 2.5 mg/l (Fig 4.4) while pyrite is 8 mg/l (Fig 5.4) and hematite is 4.3 mg/l (Fig 5.19). This seems to indicated that there is Fe being added to the pore water from the mineral addition. Acetate oxidation coupled to Fe^{3+} reduction at high temperatures could also be occurring, considering the relatively high acetate concentrations in all the thermal gradient incubations at elevated temperatures ~ 6 mmol l^{-1}. Acetate concentrations in the pyrite and hematite incubation were high 9999 and 8503 μmol l^{-1}.

Acetate oxidation coupled to Fe(III) reduction (Tor et al., 2001) produces Fe(II) and HCO_3^- according to the following equation

$$\text{Acetate}^- + 8Fe(III) + 4H_2O \rightarrow 2HCO_3^- + 8Fe(II) + 9H^+ \textbf{ Eq 7.1}$$
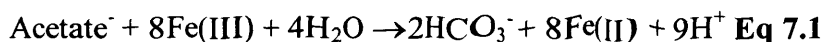
prokaryotes such as *Ferroglobus placidus* are known to catalyse this reaction, and this is closely related to clone 89-il-69 (Fig 5.27) present in the ilmenite slurry at 89°C.

7.4 Comparison to H_2 concentrations found in other experiments and environments

Concentrations of H_2 found in ground water from previous studies range from nM levels (Lovley and Goodwin, 1988) to higher concentrations found at the Lidy hotsprings (0.011-0.015 μM, (Chapelle et al., 2002) and Yellowstone hot springs and (0.002-0.325 μM, (Spear et al., 2005) and higher still in the Columbia river basin (Stevens and McKinley, 1995). In slurry incubations previously conducted with magnetite mineral addition, which had a similar experimental set up to this study, concentrations of H_2 in headspace with magnetite were a maximum of ~ 350 nM, without mineral addition maximum concentrations were ~ 15 nM (Parkes et al., 2007). The amounts of hydrogen generated in our incubations are higher than those found in these previous incubations (632-1633 μmol l^{-1}, Table 7.2). However, the previous results mentioned with the exception of (Parkes et al., 2007), H_2 concentrations are values for H_2 dissolved in ground waters, concentrations in this study are for headspace above the sediment/mineral slurry. H_2 is poorly soluble in water, (~ 13 mg

gas per 1Kg of water at 50°C (6500 μM) with solubility decreasing with temperature, this however is still significant in terms of prokaryotic metabolism, partitioning of H_2 to the headspace would effectively remove product from the reaction system. Previous experiments found that the difference in incubations with and without headspace was, approximately twice the amount of dissolved H_2 was found in samples when incubated with headspace as without (Stevens and McKinley, 2000). Build up of product appeared to inhibit the H_2 generating reaction, and removal to the headspace allowed the reaction to proceed, more efficiently, thus giving a greater yield of H_2. In the environment the largest concentrations of H_2 are detected at oceanic hydrothermal vent sites such as the Rainbow Field (12-16 mM, (Charlou et al., 2002) and the Lost City (1-15 mM / kg, (Kelley et al., 2005) Where serpentinization type reactions (Eq 7.1) are thought to dominate (Sleep et al., 2004)

$$3Fe_2SiO_4 + 2H_2O \rightarrow 3SiO_2 + 2Fe_3O_4 + 2H_2 \quad \textbf{(Eq 7.2)}$$
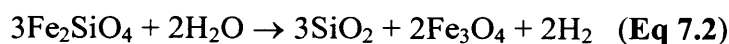
At the Kairei hydrothermal field (Central Indian ridge), H_2 concentrations emitting from hydrothermal fluids were ~2.5 mM, this is the site of a proposed HyperSlime community (Takai et al., 2004). Here H_2 is again considered to be from serpentinization reactions. High concentrations of H_2 (~2-8 mM) were formed in the absence of mafic and ultramafic minerals, at the Whitwatersrand site in South Africa (Lollar et al., 2007), an alternative mechanism of radiolytic decomposition of water producing H_2 (Lin et al., 2002) was suggested as the source. This occurs, when the decay of radioactive elements (e.g Th and U) dissociates water into H•, OH•, H_2, H_2O_2 and H^+ (Lin et al., 2005). H_2 concentrations in deep hot subsurface sediments have also been found to be elevated, recovered during oceanic drilling in (Parkes et al., 2007) IODP leg 190 site 1173 (nanki trough) , at ~630 mbsf, H_2 was ~8200 ppm (~100°C). Anaerobic respiration in the subsurface also plays a role in maintaining low hydrogen concentrations. H_2 is an excellent electron donor and used in many microbial metabolisms. Varying bacterial species can utilise H_2 at differing partial pressures (Lupton and Zeikus, 1984) leading to the ability to predict the predominant terminal electron accepting reactions in sediments by the H_2 concentration (Lovley and Goodwin, 1988). Fe(III) reducers utilise H_2 at a lower partial pressure than sulphate reducers which in turn can utilise H_2 at a lower level than methanogens,

leading to different H_2 concentrations depending on the process dominating (Lovley et al., 1994). Hence sulphate reduction and methanogenesis tend not to occur simultaneously, sulphate reducers out compete methanogens (Kristjansson et al., 1982) until H_2 concentrations are sufficiently high enough, (through the depletion of a substrate such as SO_4^{2-}) to allow utilisation by methanogens the approximate K_s values were ~1 μM for sulphate reducers and 6.6 μM for methanogens (Kristjansson et al., 1982). Various microbial processes limit the availability of H_2 thus the detectable H_2 may not be the amount generated in the subsurface but rather the excess between production and consumption, at high H_2 concentrations certain syntrophic reactions are no longer thermodynamically viable.

7.5 H_2 generation and effect on acetogenesis

It is shown in Table 7.4 that overall minerals generating the highest initial amount of H_2 produce the highest final concentration of acetate. In Table 7.4 minerals are ordered from production of highest initial acetate concentrations. The H_2 concentrations shown the Table 7.4 is the final H_2 concentration, which is the balance between consumption and production. Through the use of specific inhibition experiments acetate was found to be have a substantial contribution to both methanogenesis (Fig 5.15, 37.1%) and sulphate reduction (Fig 5.14, 25.4%). This also indicated that H_2 production is not just a process occurring at the initial stages of incubation, but continues throughout the whole incubation period up to and exceeding 100 days in the case of Hematite, Labradorite and Pyrite in addition, long term H_2 formation is dependent on the presence of minerals as with minerals H_2 is undetectable (Table 7.4). Fig 7.3 shows a negative relationship between acetate and hydrogen for samples in the thermal gradient when acetate concentrations are above 6000 $\mu mol\ l^{-1}$. There is a general trend indicated by the line of decreasing H_2 with increasing acetate this perhaps indicates consumption, through H_2/CO_2 acetogenesis. The exception being magnetite where no H_2, is detected perhaps H_2 production is too low and is consumed immediately by other prokaryotic activity preferentially, such as methanogenesis, which may limit acetate production and also make H_2 undetectable. This is true also for no mineral and sterile control.

Table 7.4 maximum acetate and hydrogen concentrations with temperature detected at the final sampling point of thermal gradient experiment.

Sample	H_2 μmol l^{-1}	Acetate μmol l^{-1}	Temperature [°C]	Days
Hematite	271	9999	92	100
Labradorite	344	8757	87	108
Pyrite	525	8503	97	110
Basalt	300	7117	98	83
Ilmenite	480	6793	95	83
Silica	638	6679	89	97
Hornblende	720	6238	97	61
Olivine	704	5841	94	61
Magnetite	0	3757	71	92
No mineral	0	3750	71	93
Sterile*	0	2401	100	0

* Basalt used in sterile control
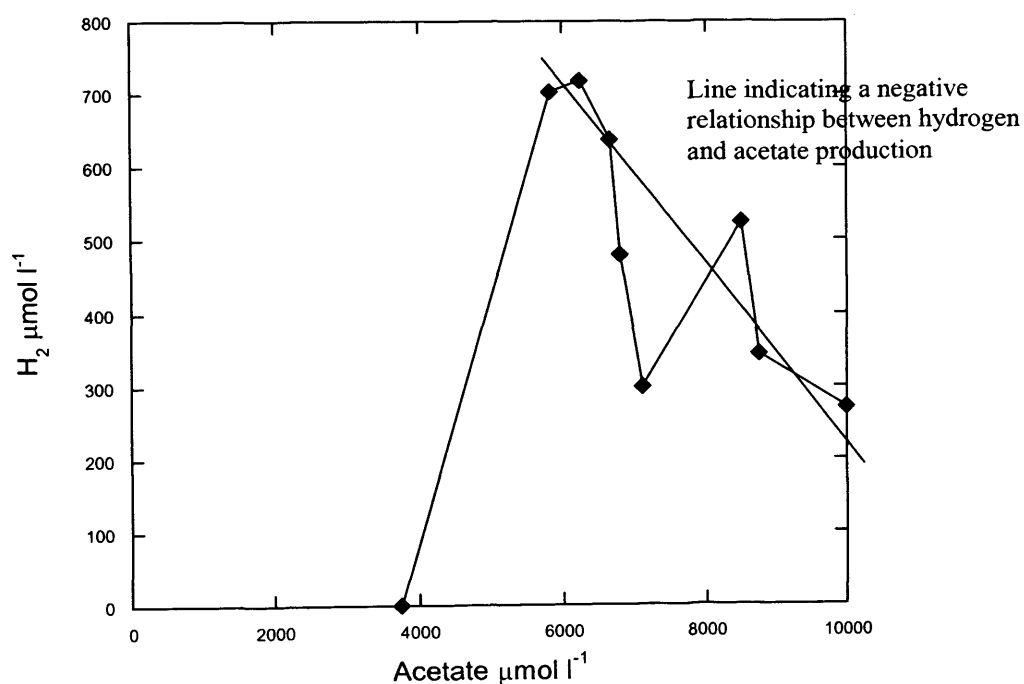
Fig 7.3 Final hydrogen concentration plotted against final acetate concentration using data from table 7.4 thermal gradient incubations

High acetate formation occurs at elevated temperatures >89°C similar to H_2 concentrations (e.g. Figs 5.15, 5.17). Hematite produced the highest initial concentration of H_2 (Table 7.2), while the incubation without mineral addition and the magnetite incubation had the lowest. This is consistent with maximum acetate concentrations (Table 7.4), which is not surprising as acetate can be formed by homoacetogens from H_2 (Eq 7.2). The sterile control produces approximate 24% as much acetate as the maximum concentration found in the hematite incubation but did not produce initial H_2. This may be due to the sterilisation technique which was triple autoclaving the sediment at 121°C, as heating sediment slurries can produce acetate even without prokaryotes (Cooles et al., 1987; Parkes et al., 2007). However in the absence of additional active acetogenesis in the sterile control acetate concentrations are lower than all other TG experiments, despite the absence of methanogenesis and sulphate reduction, removing acetate as in biotic experiments. Above 100°C acetate concentrations drop in all incubations (e.g Fig 5.16 hematite Fig 6.14 silica). This is linked to the decrease in H_2 concentrations above 100°C and hence reduction in autotrophic acetogenesis. Acetogens may also start to become directly inhibited by the high temperatures. The acetogen *Moorella thermoacetica* can grow up to 65°C (Drake and Daniel, 2004). Certain *Archaeoglobus* species e.g. *Archaeoglobus fulgidus* can also produce acetate through fermentation (~85°C).

$$4H_2 + 2HCO_3^- + H^+ \rightarrow Acetate^- + 4H_2O \quad \Delta G^{O\prime} \; -104 \; kj/reaction \quad \textbf{(Eq 7.3)}$$
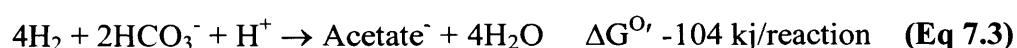
Also quite interesting is the initial acetate concentration, which builds up rapidly in the 60°C slurry incubations (Chapter 3) as acetate can be used as a substrate for both methanogenesis and sulphate reduction. For example after 2 days incubation ilmenite slurries (Fig 3.2) reach 3411 μmol l^{-1} and labradorite 2655 μmol l^{-1} (Fig 3.5). All Chapter 3 incubations with the exception of pyrite and pyrrohotite (Figs 3.7 and 3.8 ~2 to 5 μmol l^{-1}) have initial concentrations > 500 μmol l^{-1}. Previous experiments heating coastal near-surface sediment slurries, but without the addition of minerals (Wellsbury et al., 1997) also found high rates of acetate build up, with concentrations of ~3.5 mmol l^{-1} over 7 days at 60°C. Thermal gradient experiments also have elevated acetate concentrations at 60°C over the first 3 days (e.g. Figs 5.16, 5.22). After which acetate is probably utilised for sulphate reduction and methane formation,

as concentrations decrease and sulphate reduction and methane formation begins, inhibtion experiments (Fig 3.14, 3.15) indicated that acetate is a substrate in both. Acetate has been found to be key substrate in many anaerobic sedimentary environments due to it use in sulphate reduction which is the dominant terminal oxidising process (Jorgensen, 1982; Parkes et al., 1989). Greater than 60% of sulphate reduction in marine sediments is thought to involve acetate oxidation (Winfrey and Ward, 1983). All thermal gradient experiments tend to have low concentrations of acetate in the zone of maximum sulphate reduction $\sim$ 60-70°C, for example. pyrite (Fig 5.7/5.8), does not have high acetate at 60°C, concentrations of acetate only occur from 78°C when sulphate removal reduces. This is most likely due to the rapid use of acetate for SO_4^{2-} reduction, Eq 7.3

$$\text{Acetate}^- + SO_4^{2-} \rightarrow 2HCO_3^- + HS^- \quad \Delta G^{\circ\prime} = -47.6 \text{ kj/reaction} \qquad \textbf{Eq 7.4}$$
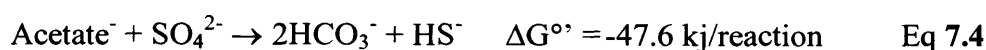
When SO_4^{2-} is in excess SRBs, which can utilise acetate at a lower concentration making it undetectable (Schonheit et al., 1982). Pyrite has a higher initial start concentration of sulphate. Although complete sulphate removal did not occur unlike other slurry incubations, the concentration of SO_4^{2-} removed was greater than any other sample (Table 7.6). Acetate appears also be key metabolite in our system with specific inhibition experiments for methane (Fig 3.15) and sulphate reduction (Fig 3.14) (25.4%), demonstrating acetate to be a major substrate for both. Methane isotope values also indicate the predominant methanogen pathway to be acetoclastic (Fig 7.3). Incubations that do not produce detectable H_2, which are magnetite and sediment only incubation (Table 7.4) have acetate maximums $\sim$ 20°C lower than all other incubations this shows that possibly the mechanism for H_2 generation may involve the production of acetate which can be used as a substrate for methane production, as H_2 can itself. This does not seem to effect sulphate reduction rates (Table 7.6) however the temperature range for methanogenesis seems to be effected as high temperature CH_4 is not detectable (Table 7.5), in the both samples with no H_2 production. This is most likely a result of substrate limitation at higher temperatures.

7.6 H_2 generation effect on methanogenesis

Concentrations of methane and the temperature ranges of methane production varied depending on the mineral used during incubation. Maximum methane concentrations occur at a higher temperature, in samples that produced detectable amounts hydrogen at elevated temperatures (Table 7.5)

Table 7.5 Maximum methane concentrations with temperature detected at during final incubation point in thermal gradient experiments.

Sample	CH_4 μmol l^{-1} max final	Temp [°C]	Zones
Hematite	123	73	2 (47-66)
			(66-89)
Silica	120	64	2 (32-51)
			(57-70)
Labradorite	396	94	1 (42-94)
Pyrite	443	90	1 (39-97)
Olivine	335	87	2 (42-74)
			(74-94)
Hornblende	282	84	2 (33-71)
			(71-90)
Basalt	159	66	2 (35-60)
			(60-80)
Ilmenite	230	89	2 (37-69)
			(82-95)
Magnetite	536	39	2 (13-33)
			(33-58)
No mineral	531	41	2 (6-35)
			(35-60)
Sterile*	0	0	0

* Basalt mineral used

The methane results in Table 7.5 are arranged in order of decreasing concentration of H_2 detected during the first sampling point after 3 days (Table 7.2), which has previously been used as an index for H_2 generating potential. Maximum

CH_4 does not directly correspond with 3 day H_2 maximum. Maximum methane concentrations for magnetite and no mineral incubation, which have no detectable 3 day H_2, occurred at 39°C and 41°C respectively. While those producing hydrogen after 3 days had maximum methane concentrations produced from 66 to 94°C. Unfortunately no $\delta^{13}C$ values were obtainable for either incubation as they were some of the first incubations done and storage of gas samples for subsequent analysis was not successfully.

Temperature range for methanogenesis occurred with 2 zones in most samples (Table 7.5). Certain samples such as Pyrite (Fig 5.2) had continuous methane produced from ~35 to 95°C (Fig 5.8). Which seems to be a joining together of the 2 methanogenic zones that occur in some of the other mineral slurries as there is a dip in CH_4 concentration between ~75-85°C. One of the reasons for this dip could be a stimulation of anaerobic methane oxidation (AOM), which occurs through a syntrophic relationship between ANME archaea and sulphate reducers. This dip occurs when sulphate reduction starts to slow and H_2 levels are still low, if CH_4 is high and SO_4^{2-} is dropping at the start of this dip in CH_4, then these are conditions mimicking the SO_4^{2-}/CH_4 transition zone where AOM is maximal. Or conversely the CH_4 profile may reflect 2 clear populations of methanogens (e.g. thermophilic/hyperthermophilic) Isotopic $\delta^{13}C$-CH_4 values are clearly influenced by temperature (Fig 7.4).

Pyrite 90°C and Labradorite 87°C.

Basalt
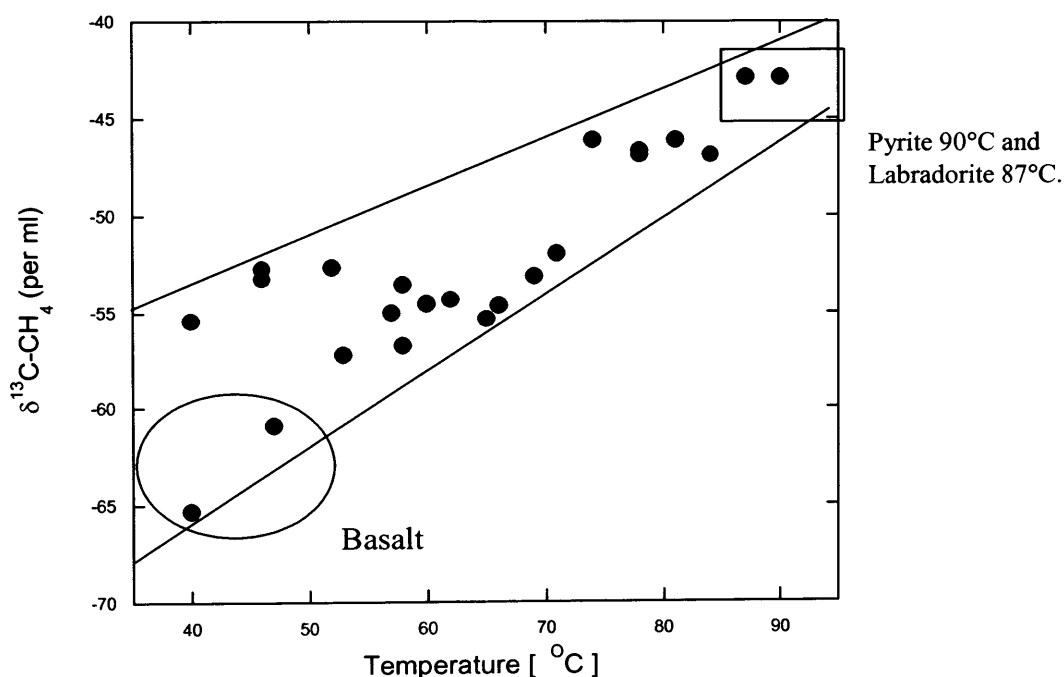
Fig 7.4. $\delta^{13}C$-CH_4 values for all thermal gradient experiments plotted against temperature.

The correlation coefficient is 0.89 between temperature and $\delta^{13}C$-CH_4 values and is highly significant with a 0.01 probability level. This raises the possibility of a relationship between the two. Several of these samples (e.g. 90°C pyrite CH_4 at -42.8‰ and 87°C labradorite CH_4 at -42.8‰ Table 5.2 and 6.3) occur outside of the values normally considered for biotic methane production (Whiticar, 1999) and could in another context be misidentified as being abiotic CH_4. This may call into question the determination of methane as abiotic based on $\delta^{13}C$-CH_4 values, of samples previously analysed, such as, from the Guaymas basin (Teske et al., 2002) and various mining sites from the Canadian and Fennoscandenavian shields (Lollar et al., 1993). The majority of the samples however, are indicative of acetoclastic methanogenesis (Whiticar, 1999). Spread of data is getting larger with temperature which may be a indication of mixed substrates, the 2 most depleted values have the lowest temperature and are from the basalt incubation (marked). Inhibition of methanogenesis by the use of BES in 60°C basalt incubations also indicated that acetate and not H_2 was the primary methanogeneic substrate (Fig 3.15). For the majority of $\delta^{13}C$-CH_4 values the Whiticar model holds, which states that prokaryotic methane production occurs in the range, -100 to -50‰, the cut of between acetoclastic methanogenesis and H_2/CO_2 is considered to be -60‰ more depleted to be H_2/CO_2 and less deplected to be acetoclastic. Values less depleted than -50‰ considered thermogenic. δD values plus C1/C1 +CM hydreaction values are often used as additional information to supplement δC-CH_4 values and effectively determine origin. However, increasing temperature does have an effect on fractionation although this is not fully understood. In the original Whiticar paper (Whiticar et al., 1986) a trend towards lower fractionations with increasing temperature was noted. Most relevant to this study is the paper of (Botz et al., 1996), who conducted culture experiments using *Methanococcales* and noted the temperature dependence of isotope fractionation during methanogenesis. Their values for incubations from 35-85°C gave a ε_c value of 76 to 47. It has also been suggested that isotope fractionation may also be depend on the amount of substrate available (reservoir effect) and rate of methanogenesis (Zyakun, 1992; Whiticar, 1999). Above all it is clear that mineral addition and H_2 generation has an affect on the amount and temperature of methanogenesis through the use of H_2 by homoacetogens producing acetate the main substrate to

methanogenesis in this study, and that this temperature affects the isotope fractionation. This can be seen with the slight dip in acetate concentrations occurring during high temperature methane formation for example in the pyrite and hematite incubation (Figs 5.12, 5.17). This isotopic signature is quite unique, methane produced at higher temperature may have different isotopic signatures than previously understood, which opens the question whether methane produced in environment such as hydrothermal systems, hot oil reservoirs (Jones D et al., 2007) or deep mines normally considered abiotic, may be the result of biotic interactions and thus further increases the role prokaryotes play in the subsurface

7.7 Hydrogen influences on sulphate reduction and carbon dioxide generation

Sulphate removal shows that sulphate reduction occurs in all incubations, with the exception of the sterile controls (Fig 4.15). Which shows sulphate removal is a biotic process.

Table 7.6 Mineral incubations comparison of sulphate removal rates and maximum temperature of activity in the thermal gradient experiments.

Sample	Start concentration mmol l^{-1}	Complete removal	Amount removed mmol l^{-1}	Rate of removal per day mmol l^{-1}	Temperature of maximum removal [°C]	Days incubation
Hematite	16.7	No	13.2	0.13	73	100
Silica	14.5	Yes	14.5	0.14. min	64	97
Labradorite	14.3	Yes	14.3	0.13 min	55 to 68	108
Pyrite	28.2	No	19.1	0.17	65 to 71	110
Olivine	21.1	No	14.7	0.24	68	61
Hornblende	20.1	No	14.4	0.22	65	61
Basalt	14	Yes	14.0	0.16 min	53 to 66	83
Ilmenite	14.9	No	14.0	0.16	63	83
No mineral	13.7	Yes	13.7	0.14 min	58 to 65	93
Magnetite	13.7	Yes	13.7	0.14 min	58 to 65	92

"min" When all sulphate was removed this rate was taken as the minimum rate

Given in Table 7.6 are the approximate concentration of sulphate removed, the rate of removal/day, the length of incubation and the temperatures of maximum sulphate

removal. Minerals are ordered in terms of maximum concentrations of H_2 detected after 3 days incubation (Table 7.3). The amount of H_2 generated does not seem to affect either the amount of sulphate removed which has a mean of ~ 14.56 mmol l^{-1} or the temperature of maximum removal which is between 53 and 73. In the pyrite incubation complete SO_4^{2-} removal is not achieved, even though 19.1 mmol l^{-1} is removed, which is more than any other incubation. Starting concentrations of SO_4^{2-} are higher in pyrite due to sulphide oxidation of the mineral and perhaps some oxidation post grinding before addition, as discussed previously in Chapter 3. If given a longer incubation period complete removal would most likely be achieved, the rate of sulphate removal (0.17 mM/ per day) is higher than many of the other incubations and amount removed is greater, it is unlikely that after 110 days of continuous sulphate reduction that this would stop before complete SO_4^{2-} removal. Inhibition experiments with molybdate, conducted on a 60°C basalt incubation indicated acetate as one of the primary substrates for sulphate reduction (25.4%) (Fig 3.14) this does seem quite low, and maybe the result of the inhibition of sulphate reducing bacteria could also inhibit other species including acetogens. It has previously been hypothesized that acetate may account for greater than 60% of sulphate reduction in marine sediments (Winfrey and Ward, 1983) as mentioned previously in section 7.5. Which is not the case in this study, other substrates, which can be used; include H_2, propionate, butyrate, lactate, methanol or carbon monoxide.

In the majority of incubations (e.g. ilmenite Fig 5.10, pyrite Fig 5.2 and labradorite Fig 6.6), once sulphate reduction slows with increasing temperature, concentrations of acetate increase rapidly. Also in the majority of incubations sulphate reduction slows rapidly above 80°C. (e.g. ilmenite Fig 5.10 basalt Fig 4.9) with the exception of labradorite (Fig 6.6 and hematite Fig 5.17) where a limited amount of sulphate reduction occurs at ~ 90°C. This leads to the conclusion that the highest temperature SRBs present in our samples are thermophilic. AODC counts of the hematite incubation (Fig 5.24) indicate that prokaryotic numbers decrease substantially once sulphate reduction slows. Similar incubations with cores taken from the Guaymas basin (source of the temperature inoculation for these experiments) also found that certain cores showed no sulphate reduction above ~ 75°C (Jorgensen et al., 1990). This is a paradox found in our incubations and also in geological settings such as deep, hot oil reservoirs. Some hyperthermophilic sulphate reducing

prokaryotes can function at extremely high temperatures up to 110°C (Jorgensen et al., 1992; Stetter et al., 1993). But generally in oil reservoirs and similar geological settings, sulphate reduction ceases above ~80°C, (Machel and Foght, 2000; Wilhelms et al., 2001) this is despite the apparent presence of all the components required for sulphate reduction. Sulphate reduction in geological settings does not necessarily always have to be biological, a process of thermochemical sulphate reduction may also occur. The minimum temperature for thermochemical sulphate reduction is inferred to be between 100-140°C (Machel, 1998). It is thought that a number of factors such as the concentration of organic acids, presence of metal complexes and possibly the action of Fe^{2+}, Ca^{2+} or similar, may enhance this process (Machel, 2001). However this does not appear to be happening in our incubations as the sterile controls actually show a slight increase in SO_4^{2-} rather than a reduction at higher temperatures from ~ >50°C (Fig 4.15)

A slight increase is also noted in the biotic ramping experiments with an increase of 3.5 mmol l^{-1} from the lowest sulphate concentration at 75°C to the final sampling point at 155°C (Fig 4.25). This increases in sulphate at high temperatures maybe the result of anaerobic iron sulphide oxidation, for example has previously been known that anaerobic oxidation of pyrite iron oxide minerals as an oxidant (Bottrell et al., 2000)

Carbon dioxide is a product of sulphate reduction Eq 7.3 and occurs in high concentrations throughout all samples the following section deals with CO_2 concentrations in slurry incubations Table 7.7

Table 7.7 Comparison of CO_2 concentrations with temperature and initial and final maximum concentration, plus correlation with SO_4^{2-} reduction in the thermal gradient experiment.

Sample	3 day max μmol l^{-1}	Temp [°C]	Final concentration	Temp[°C]	Days	Correlation with max SO_4^{2-} removal
Hematite	6580	105	1286/1249	60/73	100	Yes
Silica	6564	102	1310	70	97	No
Labradorite	4110	103	1002	68	108	Yes
Pyrite	4673	97	1821	71	110	Yes
Olivine	50788	87	1674	68	61	Yes
Hornblende	28596	103	3413	78	61	No
Basalt	7709	98	2160	60	83	Yes
Ilmenite	6176	95	1362	63	83	Yes
No mineral	3700	78	1400	65	93	Yes
Magnetite	3776	77	1385	68	92	Yes
Sterile control	6303	100	667	100	130	Na

The comparison of CO_2 value maximums from the thermal gradient experiment (Table 7.7) reveals some interesting trends. CO_2 concentrations after 3 days are consistently higher than concentrations at the final sampling point generally a factor of 3 to 6 times less; however, olivine is less by a factor of 30, which is the greatest. It also appears that initially at least the release of CO_2 is linked to temperature a possible product of CO_2 degassing and alteration of the CO_2 /HCO_3^- equilibrium from the bicarbonate buffer in the mineral salt solution (Table 2.1).

The chemical cycle of CO_2 in seawater is governed by a series of equilibria, which are written as follows

$$CO_2 \text{ (gas)} \Leftrightarrow CO_2 \qquad \text{Eq 7.4 (dissolved)}$$

$$CO_2 + H_2O \Leftrightarrow H_2CO_3 \qquad \text{Eq 7.5 (dissolved } CO_2 \text{ becomes hydrated)}$$
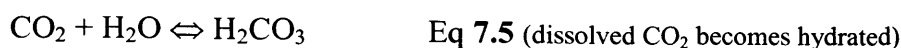
Rapid dissociation of carbonic acid

$$H_2CO_3 \Leftrightarrow H^+ + HCO_3^- \qquad \text{Eq 7.6 (bicarbonate ion)}$$

$$HCO_3^- \Leftrightarrow H^+ + CO_3^{2-} \qquad \text{Eq 7.7 (carbonate ion)}$$

The highest concentrations are always found near the maximum temperature after the first 3 days. The no mineral incubation (3700 μmol l^{-1}) and the magnetite incubation (3776 mmol $^{-1}$) produced only ~ 50% of the CO_2 that incubation with the other minerals produced. The sterile control which contained basalt and the biotic basalt incubation are similar (Table 7.7). This provides a link between the specific mineral added and CO_2 at elevated temperatures. Magnetite was the only mineral to produce no detectable H_2 during thermal gradient incubation. The sterile control, which contained basalt, produced CO_2 concentrations similar to the biotic incubations initially. The fact that the 2 biotic incubations (magnetite and no mineral) producing the lowest amount of CO_2 also produced no hydrogen at elevated temperature could be a coincidence, or it could be that a mixture of abiotic process enhanced by microbes (possibly microbial mineral weathering, as previously mentioned) is responsible for elevated H_2, and this is linked to high initial concentrations of CO_2.

Concentrations of CO_2 at the final sampling point are consistently lower for all incubations. And in nearly all cases the maximum concentration of CO_2 coincides with the maximum temperature for sulphate removal. This indicates another process of CO_2 formation, which is prokaryotic through heterotrophic sulphate reduction. Sulphate inhibition experiments indicated that in basalt incubations acetoclastic sulphate reduction was one of the dominant process (25.4% according to inhibition experiment) (Eq 7.8).

$$\text{Acetate}^- + SO_4^{2-} \rightarrow 2CO_2 + HS^- \qquad \Delta G^{O'} \text{ -47.7 kj/reaction Eq 7.8}$$

The rapid increase in acetate concentration at elevated temperature may be a contributing factor to the lowering of CO_2 concentrations. There are two possibilities for this either this could to due to acetate no longer being used for sulphate reduction,

or due to the fact that H_2 is no longer required for sulphate reduction and is available for acetogenesis. Inhibition experiments provided evidence approximately 25.4% of sulphate reduction was as a result of acetate usage. This gives the possibility that multiple substrates are being used for sulphate reduction, which may include H_2. It is possible that both processes are involved. CO_2 is used in acetate formation Eq 7.4 e.g. ilmenite incubation (Fig 5.10) CO_2 reaches it maximum concentration at 63°C which is also the maximum for sulphate reduction, sulphate reduction starts to slow after this and a sharp increase in acetate at 69°C is coupled with an equally sharp drop in CO_2.

$$4H_2 + 2HCO_3^- + H^+ \rightarrow \text{Acetate}^- + 4H_2O \quad \Delta G^{O'} -104 \text{ kj/reaction Eq } \textbf{7.9}.$$
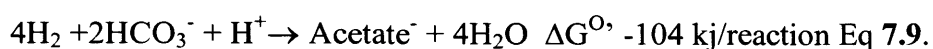
Initial CO_2 concentrations may be a indicator of potential for H_2 generation, provided the proper mix of sedimentary prokaryotes are present. Fig 7.5 shows initial H_2 and CO_2 concentrations plotted against each other (note olivine and hornblende are absent , due to the enormity of CO_2 produced which seems to be irregular in comparison to all the remaining minerals). There seems to be a slight visual correlation between H_2 and CO_2, however this is not statistically relevant.
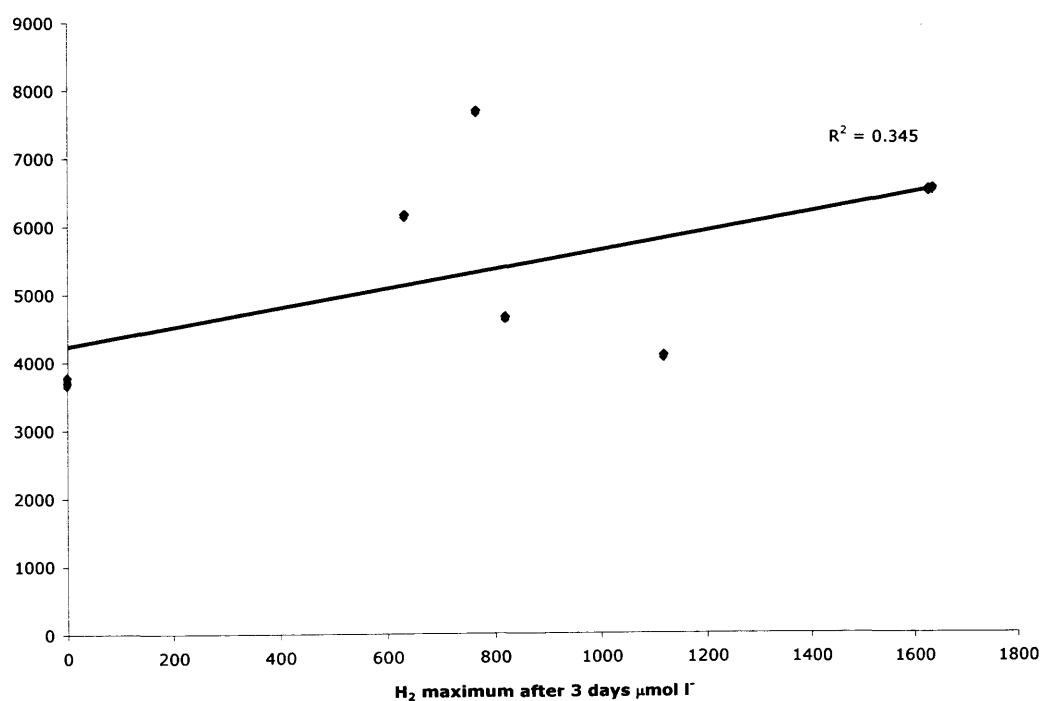
Fig 7.5 Initial CO_2 and H_2 concentrations after 3 days from the thermal gradient incubations

7.8 Characterisation of microbial community.

Microbial communities associated with individual mineral incubations were assessed using two methods. Firstly by DGGE profiling coupled to extraction of bands and sequencing. Secondly, by the construction of clone libraries and phylogenetic trees. Visual DGGE band analysis indicated that community structure at 60°C (Figs 3.11) varied significantly with mineral type, with the appearance and disappearance of bands of different prokaryotes and increases in band intensity indicating dominance of different prokaryotes with mineral type. Obvious changes are the appearance of bands related to anaerobic, fermentative and S^o respiring *Thermotogales* (92%) in the hornblende incubation which are a group of thermophilic/hyperthermophilic Bacteria (60-90°C) which grow at neutral pH and have been found in thermophilic subsurface environments (Huber et al., 1991) and have also been isolated from high temperature oil reservoirs (Stetter et al., 1993). Other bacterial species found in the 60°C incubation (Table 3.4) include *Clostridia (Firmicutes)* which are involved in fermentation of organic matter (sugars etc) often producing acetate and H_2. Other species belonged to candidate division OP9 (98%) which has unknown metabolism but has been detected in hydrothermal vent systems. *Gammaproteobacteria* related species have been found which are the most abundant division in subseafloor sediment libraries and have been found to be in the majority in some deep sediment volcanic ash layers (Inagaki et al., 2003). The divisions *Chloroflexi* and member of the candidate division JS1(Webster et al., 2004), together with the *Gammaproteobacteria* make up 63% of clones found in subsurface clone libraries to date (Fry et al., 2008). Only the *Gammaproteobacteria* were present in DGGE profile of the mineral sediment slurry samples. DGGE band extracted and sequenced from the labradorite incubation at 60°C (Table 3.4) was found to be 97% related to an uncultured clone belonging to the *Gammaproteobacteria, Methylococcales* this is a methane oxidising bacterium, which is aerobic. This is surprising since all incubations were anaerobic, however, the percentage relationship is only 97% related to an uncultured clone which perhaps from a *Gammaproteobacteria* with a different metabolism including the capacity for anaerobic metabolism. It has previously been found through the isolation of facultative anaerobic genera both aerobically (Biddle et al., 2005) and anaerobically (D'Hondt et al., 2004; Batzke et al., 2007) that many

heterotrophic bacteria in the deep-subsurface may be facultative anaerobes (Cragg et al., 1990) (*Delftia acidovorians* (*Beta proteobacteria*) sequences were also found). Expanding into the higher temperature DGGE profiles similar sequences were obtained from extracted bands in the ilmenite and basalt incubation (table 5.5 and Table 4.2) All sequences found were related to bacterial species found previously in subsurface environments such as hydrothermal vents, oil reservoirs and marine sediments and hot springs and some that have been isolated from anaerobic biomass digesters. A more detailed analysis of individual sequences found is dealt with in the relevant results Chapters. One Interesting point to note is that although sulphate reduction occurred in all samples, very few of the extracted bands belonged to the *Deltaproteobacteria* species which are the main genera containing sulphate reducers (1 band sequenced out of 23, 4 %). This may suggest a bias on the part of general PCR primers against sulphate reducing bacteria. It has previously been suggested (Parkes et al., 2005) that absence of SRBs from clones libraries may be in part due to their relative low abundance despite high activity, results in them being below the detection limit for PCR using general primers, and are therefore, absent from gene libraries.

Archaeal communities were assessed much more robustly with more incubations being analysed, both by the sequencing of extracted bands from DGGE profiles and the construction of clone libraries. No bacterial clone libraries were constructed; this was due to initial cloning indicating a possible contamination. A major problem in dealing with subsurface bacterial communities is the low bacterial numbers leads to problems with contamination either from the laboratory surroundings or from the reagents used in PCR or initial DNA extraction. The initial clone libraries (only 8 clones for each of the 4 samples chosen for analysis) were dominated by one phylotype which was related to the *Betaproteobacteria*, with 3 or 4 amplified bacterial bands in the negative although the positioning did not coincide with the bacterial profile, but they were *Betaproteobacteria,* as the results were unreliable it was decided not to proceed with the bacterial clones, and instead focus on the archaeal which were definitely free from contamination as all negative controls had no amplified archaeal DNA.

So far the majority of the molecular results published for hydrogen driven communities, only have archaeal results as these dominate at high temperature (Chapelle et al., 2002; Takai et al., 2004). DGGE profiles are dominated by

Thermoplasmatales related species and the Marine Benthic Group D. The ilmenite DGGE profile bears a resemblance to the ilmenite clone library with the lower temperature samples (18-63°C) (Table 5.5) being dominated by the *Crenarchaeota* (87%). All extracted bands belonging to *Crenarchaeota* were related to species from various marine environments, tidal sediments deep marine sediments and cold seeps (Heijs et al., 2007; Kendall et al., 2007; Kittelmann and Friedrich, 2008). One extracted band was related to a *Euryarchaeota, Thermoplasmata* (98%) clone which was isolated from a microbial mat, which is S^0 respiring, found in hot coal deposits. The higher temperature ilmenite incubation (76-95°C), is dominated equally by *Euryarchaeota* (25%) and *Crenarchaeota* 25% with the remainder being related to samples of unknown phylogenetic affiliation (Table 5.6).

Studies on the deep marine biosphere from the Pacific and the Atlantic have shown in the composition of gene libraries so far that the *Crenarchaeota* dominate the archaea (73.4%) while the Euryarchaeota accounted for (24.5%). Within the *Crenarchaeota* the Miscellaneous Crenarchaeotic Group (MCG) and Marine benthic group-B were the most dominant in marine subsurface sediments (Fry et al., 2008). This is similar to found in this study for samples below ~ 65°C, and shows that or community composition is similar to that of marine sediments.

The clone library phylogenetic tree constructed (Fig 5.27) from the ilmenite incubation at 63°C is dominated by the *Miscellaneous crenarchaeota group* 100% (20 clones) with clones related to species found in sub seafloor sediments such as the Nanki trough which has an elevated thermal gradient (Newberry et al., 2004) and certain mud volcano sites (Losekann et al., 2007). However, the pyrite clone library at 65°C is not dominated by the *Crenarchaeota* but rather has a mixture of *Crenarchaeota* (22%) and *Euryarchaeota* (78%) with the majority of the *Euryarchaeota* (85.7%) falling within the *Thermococcales* the remainder of the *Euryarchaeota* fell within the *Thermoplasmatales*. This difference may be due to the slight temperature difference (2°C) although this is unlikely; more likely is the fact that different minerals seem to actively play a role in selection of associated prokaryotic community. This difference between clone libraries shows that the major factor in determining community composition is temperature, but that also the mineral addition, and substrates generated as a result is also a major factor.

Even more interesting is the clone libraries constructed from the higher temperature samples, within the zone of high H_2/acetate generation. The 89°C ilmenite (Fig 5.28) clone library in stark contrast to the 63°C library (Fig 5.27), is dominated by the *Euryarcheota* (100%) with no *Crenarchaeota* detected. The majority of the clones fall with the *Thermococcales* or Novel *Thermococcales* related group (HTi-1). With one clone falling within the *Archaeoglobales* (89-il-69). This is most closely related (98%) to *Ferroglobus placidus* which as mentioned in the acetate discussion, can oxidise acetate by using Fe(III) as the sole electron acceptor, producing Fe(II). *Thermococcales* were also found to be one of the major microbial components in a proposed H_2 driven (HyperSlime) community (Takai et al., 2004), the other being *Methanococcales*. *Thermococcales* are also found to be a major component in other Hydrothermal vent environments (Lepage et al., 2004) in addition analysis of the deepest recorded prokaryotes found to date in the sub-sea-floor biosphere (1626 mbsf) found that in archaeal clone libraries *Thermococcales* (*Pyrococcus* and *Thermococcus*) were dominate at depths with temperatures *in situ* between 60-100°C (Roussel et al., 2008).

The pyrite clone library at 90°C is only slightly more diverse than ilmenite. One clone fell within the *Crenarchaeota* most closely related 99% to a clone isolated from a sulphide chimney in the Juan de Fuca deep marine trench (B1-57, EU559691) and other *Crenarchaeota*. The remaining clones were split between the *Thermococcales* and the HTP-1/ HTP-2 groups. Both the HTP groups appear to be novel with the closest related species again being clones pCIRA-L and pCIRA-12, which are also associated with high temperature H_2 driven ecosystems (Takai et al., 2004) samples from vent fluids emitting from a hydrothermal chimney. Unfortunately no physiological function can be inferred about these clones, except there high temperature capacity. The diversity of clone libraries presented here is not as great as one would expect, in general archaeal clone libraries are less diverse than bacterial generally only containing two of the main 14 archaeal taxa in many subsurface clone libraries, often in deep biosphere archaeal diversity appears low e.g. Peru margin only 5 main groups (Webster et al., 2006) this may be an artefact due to preferential PCR amplification of specific groups of genes, or may be a reflection of real variation (Webster et al., 2003; Fry et al., 2008). A recent paper has found evidence that the

amount of Archaea may be underestimated in the subsurface and that in fact archaea could be dominant (Lipp et al., 2008).

The microbiological results provide strong evidence that our incubations are a reasonable model for prokaryotic communities and hence processes in environments where high concentrations of H_2 are presents. (Takai et al., 2004) proposes a subsurface community thriving on H_2 sources derived from magmatic/serpentinization (Eq 7.2) reactions at high temperature >250°C which is used by microbes when the H_2 enriched fluids Migrate to cooler temperatures. Sampled (250-350°C) *Methanococcales* and *Thermococcales* dominate, and the clones obtained in this study are the most similar to the clones found in Takai's study. In deep gold mine studies groundwater, containing high levels of hydrogen were examined and found to contain only a single phylotype of thermophilic sulphate reducer belonging to the *Firmicutes* (Lin et al., 2006) this was because radiolysis of metal sulphides ensured a constant supply of SO_4^{2-} at elevated temperature in addition to H_2 from H_2O radiolysis. Previous studies have found methanogens belong to the *Methanococcales* to be dominate in a H_2 driven system in a subterranean hot spring (Chapelle et al., 2002) no clones found in this study were related to known methanogenic prokaryotes, however many of the clones were related to prokaryotes with unknown physiological function, and the production of methane demonstrates the presence of methanogens. The amount of studies conducted on hydrogen driven systems is small and those studies, which also incorporate a significant microbiological component are, even fewer. However, results presented here are similar to these studies as experiments contain several sequences that have been found previously in hydrogen driven communities and in the deep hot sub-surface. AODC counts of prokaryotic numbers match those from environmentally related sites. For example the deepest recorded depth of prokaryotes so far have been found (1626 mbsf) are at temperatures between 60-100°C (Roussel et al., 2008) and these fluctuate around 1.5×10^6 cells ml^{-1}. Incubations in this study at high temperature (e.g. hematite Fig 5.17) had similar cell numbers 86°C, 6.28×10^6 cells ml^{-1}, 93°C 1.81×10^6 cells ml^{-1}, 99°C 6.67×10^5 cells ml^{-1} which fits into the predicted cell/depth regression line for deep sub-surface sediments (Parkes et al., 1994). The combination of correct prokaryotic numbers, and similar molecular sequences from related

subsurface, hot environments lends robustness to the approach applied in this study, and suggests that the experiments are pertinent to the deep sub-seafloor biosphere.

7.9 Possible mechanism of hydrogen generation

Possible theories for generation of hydrogen in the environment mentioned previously have involved the low temperature (20-30°C) oxidation of Fe^{2+} containing minerals directly supplying prokaryotes (Stevens and McKinley, 1995) or involve very high temperatures reactions ~300°C such as serpentinization (Sleep et al., 2004) that indirectly supplies H_2 to prokaryotic communities via diffusion or advection. Temperatures involved in these reactions are far in excess of those used experimentally in this study (Seewald, 2001; Chapelle et al., 2002; Takai et al., 2004; Kelley et al., 2005) and are far higher than the known upper temperature for prokaryotes (120°C, (Kashefi and Lovley, 2003). Both of the above are unlikely to be the hydrogen generating process in this study. However, one explanation of hydrogen generation which has not been addressed is the mineral fracture induced reduction of water (Kita et al., 1982) a process termed mechanochemistry. This process can occur with a broad range of minerals and temperatures (25-270°C), it is not dependent on ferrous iron content. A brief summary follows which has been adapted from (Kita et al., 1982). Quartz contains Si-O bonds and when crushed radicals such as Si• and Si-O• are created from the breaking of these. When crushing occurs in the presence of H_2O, SiOH can be formed as follows.

$$Si• + H_2O \rightarrow SiOH + H• \qquad Eq\ 7.10$$

$$Si\text{-}O• + H• \rightarrow SiOH \qquad Eq\ 7.11$$

$$Si\text{-}O\text{-}Si + H_2O \rightarrow 2SiOH \qquad Eq\ 7.12$$
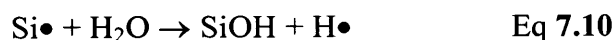
In the process of SiOH formation H• radials that are generated simultaneously cannot react with Si-O•, which is relatively stable, and hence two H• may combine forming H_2.

Eq 7.13 shows the mechanism involved in these reactions in the absence of O_2.

$$Si• + Si\text{-}O• + H_2O \rightarrow SiOH + \tfrac{1}{2} H_2 + (Si\text{-}O•)\ Eq\ 7.8$$

These radials are stable up to 120°C, which is within the temperature range of most experiments conducted in this study. This type of reaction would account for the high concentrations of H_2 observed with the silica addition and be consistent with no relationship between potential H_2 formation and iron content of minerals (Table 7.3) but a relationship with porewater Si (Fig 7.1) and also why no H_2 was evolved from magnetite, which according to ICP-OES (Table 3.2) analysis has a composition of 99% Fe_2O_3 but low levels of SiO_2. However an anomaly is ilmenite, in which H_2 is formed but the concentration of SiO_2 is low (1.06%). Unlike magnetite however concentrations of TiO_2 is high (47.31%). Also hematite produces the highest initial H_2 concentrations, but has not got the highest SiO_2 (20.5%), but does also have a relatively large Al_2O_3 (17.7%) content. It is clear that this hydrogen is a complex process reliant on a number of factors, and may be enhanced by the presence of other compounds in the mineral. Mechanochemical H_2 generation is a process that can occur with a range of minerals including those containing TiO_2. Ti and Al cannot be regarded as inert in this process and the reaction of Al• radicals with water is also thought to produce H_2 this has been proven by reactions of Al_2O_3 with H_2O generating as much H_2 as quartz (Si radial) reactions at both 25 and 200°C (Kita et al., 1982). Therefore reactions with Si, Al and Ti oxides plus a range of other minerals, maybe capable of H_2 generation from H_2O and these are common constituents of rocks, with H_2 generation increasing with increasing temperature..

Mechanochemical radial reactions, also explains why the addition of freshly ground minerals is important for rapid initial H_2 formation, however H_2 is also produced after long term incubations up to 97 days (silica addition Fig 6.14) 100 days (hematite Fig 5.15) and pyrite 110 days (Fig 5.2). Hence fresh surfaces appear to be only one aspect of the reactions observed in the experiments reported here. However the exact role of prokaryotes in this H_2 generation is unknown, but almost zero H_2 generation in sterile basalt controls (Fig 4.14), clearly demonstrate that they do have a considerable impact. It may be that the initial abiotic mechanochemical reaction is sustained and enhanced by the presence of prokaryotic mineral weathering activity, creating reactive surface and thus prolonging H_2 production. With some minerals iron compounds may also be involved, as hematite (54% Fe_2O_3) produced the largest initial 3 day H_2 concentrations and porewater Fe often increased at high temperature

alongside H_2 (Figs 5.19,5,17). However oxidation of ferrous directly seems an unlikely main mechanism as iron in hematite is theoretically completely oxidised. Although it needs to be noted that natural rock minerals were used for all our samples and some heterogeneity in composition might be present. However, the quartz sand was almost 99% silica SiO_2 (Table 3.2) Hence previous sterile water mineral experiment, conducted to gauge the potential of minerals for H_2 production may be misleading (Stevens and McKinley, 1995; Anderson et al., 1998; Stevens and McKinley, 2000; Anderson et al., 2001).

Production of freshly ground surfaces in the subsurface would enhance mineral H_2 production in areas where exposure of fresh surfaces can be achieved, such as around faults zones, with in excess of 20,000 measured significant earthquakes /year, with many more minor earthquakes (undetected), this may be reasonably common. The exact amount of H_2 formed would also depend on rock composition and temperature as demonstrated here. Elevated H_2 concentrations have been found previously associated with fault zones and were thought to be purely the result of abiotic processes (Wakita et al., 1980) which may not be the case. The production of CH_4 has also been previously linked to earthquake activity (Brauer et al., 2005) and may be a result of methanogenic activity utilising H_2 produced by mechanochemical process. H_2 from more common minor faulting may be consumed by subsurface prokaryotes and hence none may be detected at the surface, but this may be an important subsurface energy source

7.10 Conclusions

This study has provided evidence of the following

- Hydrogen can be generated from a number of minerals previously thought unreactive. This process is dependent on a number of factors
1) The presence of sedimentary prokaryotes
2) Elevated temperatures.
3) The composition of the mineral added
4) This reaction is enhanced through initial crushing and exposure of fresh reactive surfaces
- This reaction is independent of Fe content in the mineral, unlike in previously published studies

- It is possibly a reaction involving silica and other radicals

- This reaction is possibly facilitated over time by the presence of sedimentary prokaryotes, keeping the mineral surface active through a process similar to microbial weathering

- Hydrogen generated from this reaction can fuel subsurface prokaryotic metabolisms, including "deep" sulphate reduction, acetogenesis and methanogenesis.

- Hydrogen production can be sustained over prolonged periods >100 days

- Molecular analysis of the prokaryotes in these experiments shows similarities to those in HyperSLiMe communities proposed to be fuelled by deep sourced H_2

- Sequential temperature ramping experiments to 155°C showed that prokaryotic activity in the biotic zone (up to 120°C) has an effect on the products produced during subsequent higher temperature (up to 155°C) and thermal alteration in the abiotic zone, substantially increasing the amount of organic acids and gases such as hydrogen produced

- The results of the experiments presented have significant implications for sources of energy supply in the deep hot, biosphere/geosphere, suggesting increased energy sources and a greater biosphere than previously considered

7.11 Future work

This study has provided some new and exciting developments in the search for sources of energy and examining what effects this has on prokaryotes in the deep biosphere. However there is a lot more work to be done to examine fully the processes occurring. More research needs to be done on the exact mechanism of hydrogen production and how specifically prokaryotes interact with the mineral. Also more mineral specific analysis. Extending and prolonging the temperature ramping experiment (longer incubations at each temperature and starting at a lower temperature) could provide more detailed information regarding the transition between the biotic and abiotic processes and into the oil window. Addition of specific kerogens as well as differing minerals would be interesting. A more in depth molecular analysis of the hyperthermophilic community would be interesting, with substantially more cloning, and gene specific work *mcr*A / *dsrA*\B. Culturing although

probably quite difficult considering the high temperature involved, would be interesting. Pure culture and mixed culture mineral experiments would enable the role of prokaryotes and community interaction to be resolved. Stable isotope probing to follow the carbon flow, more inhibition and radiotracer work to confirm metabolic processes at a range of temperatures.

References

Aeckersberg, F., Bak, F., and F., W. (1991) Anaerobic oxidation of saturated hydrocarbons to CO2 by a new type of sulfate-reducing bacterium. *Arch. Microbiol.* **156**: 5-14.

Aeckersberg, F., Rainey, F.A., and Widdel, F. (1998) Growth, natural relationships, cellular fatty acids and metabolic adaptation of sulfate-reducing bacteria that utilize long-chain alkanes under anoxic conditions. *Archives of Microbiology* **170**: 361-369.

Allen, D.E., and Seyfried, W.E. (2003) compositional controls on vent fluids from ultramafic-hosted hydrothermal systems at mid oceanic ridges: an experimental study at 400°C, 500 bar. *Geochemica et Cosmochimica Acta* **67**: 1531-1542.

Aller, R.C. (1990) Bioturbation and manganese cycling in hemipelagic sediments. *Phil. Trans. Roy.Soc.Lon* **A331**: 51-68.

Alt, J.C., and Shanks, W.C. (1998) Sulfur in serpentinized oceanic peridotites: Serpentinization processes and microbial sulfate reduction. *Journal of Geophysical Research-Solid Earth* **103**: 9917-9929.

Amend, J., P., and Teske, A. (2005) Expanding frontiers in deep subsurface microbiology. *Palaeogeography, Palaeoclimatology, Palaeoecology* **219**: 131-155.

Amend, J.P., and Shock, E.L. (2001) Energetics of overall metabolic rections of thermophilic and hyperthermophilic Archaea and Bacteria. *FEMS Microbiology Reviews* **25**: 175-243.

Anderson, R.T., Chapelle, F.H., and Lovley, D.R. (1998) Evidence against hydrogen-based microbial ecosystems in basalt aquifers. *Science* **281**: 976-977.

Anderson, R.T., Chapelle, F.H., and Lovley, D.R. (2001) Comment on "Abiotic controls on H-2 production from basalt- water reactions and implications for aquifer biogeochemistry". *Environmental Science & Technology* **35**: 1556-1557.

Bach, W., and Edwards, K.J. (2003) Iron and sulfide oxidation within the basaltic ocean crust: Implications for chemolithoautotrophic microbial biomass production. *Geochimica Et Cosmochimica Acta* **67**: 3871-3887.

Bach, W., Garrido, C.J., Harvey, J., Paulick, H., and Rosner, M. (2004) Variable seawater-peridotite interactions-first insights from ODP Leg 209, MAR 15N. *Geochemistry, Geophysics, Geosystems* **5**: Q09F26, doi:10.1029/2004GC000744.

Baena, S., Fardeau, M.L., Labat, M., Ollivier, B., Garcia, J.L., and Patel, B.K.C. (1998) *Desulfovibrio aminophilus* sp.nov., a novel amino acid degrading and sulphate reducing

bacterium from an anaerobic diary wasterwater lagoon. *J. Syst, Appl. Microbiol* **21**: 498-504.

Bak, F., and Cypionka, H. (1987) A novel type of energy metabolism involving fermentation of inorganic sulfur compounds. *Nature* **326**: 891-892.

Bak, F., and Pfennig, N. (1987) Chemolithotrophic growth of *Desulfovibrio sulfodismutans* sp.nov., by disproportionation of inorganic compounds. *Archives of Microbiology* **147**: 184-189.

Barnes, R.O., and Goldberg, E.D. (1976) Methane production and consumption in anoxic marine sediments. *Geology* **4**: 297-300.

Barth, T., and Bjorlykke, K. (1993) Organic acids from source rock maturation:generation potentials, transport mechanisms and relevance for mineral diagenesis. *Applied Geochemistry* **8**: 325-337.

Batzke, A., Engelen, B., Sass, H., and Cypionka, H. (2007) Phylogenetic and physiological diversity of cultured deep-biosphere bacteria from equatorial Pacific Ocean and Peru margin sediments. *Geomicrobiology Journal* **24**: 261-273.

Ben-Yaakov, S. (1973) pH buffering of pore water of recent anoxic marine sediments. *Limnol. Oceanogr.* **18**: 86-93.

Bennett, P.C., Rogers, J.R., and Choi, W.J. (2001) Silicates, silicate weathering, and microbial ecology. *Geomicrobiology Journal* **18**: 3-19.

Biddle, J.F., House, C.H., and Brenchley, J.E. (2005) Microbial stratification in deeply buried marine sediments reflets changes in sulfate/methane profiles. *Geobiology* **3**: 287-295.

Bidle, K.A., Kastner, M., and Bartlett, D.H. (1999) A phylogenetic analysis of microbial communities associated with methane hydrate containing marine fluids and sediments in the Cascadia margin (ODP site 892B). *Fems microbial letters*: 101 - 108.

Blair, C., D'Hondt, S., Spivack, A., and Kingsley, R.H. (2007) Radiolytic Hydrogen and Microbial Respiration in Subsurface Sediments. *Astrobiology* **7**: 951-966.

Boetius, A., Ravenschlag, K., Schubert, C.J., Rickert, D., Widdel, F., Gieseke, A. et al. (2000) A marine microbial consortium apparently mediating anaerobic oxidation of methane. *Nature* **407**: 623-626.

Boone, D.R., Whitman, W.B., and Rouviere, P. (1993) *Methanogenesis*. New York & London: Chapman, Hall.

References

Bottcher, M.E., Thamdrup, B., M., G., and A., T. (2005) S^{34}/S^{32} and O^{18}/O^{16} fractination during sulphur disproportionation by *Desulfobulbus propionicus*. *Geomicrobiology Journal* **22**: 219-226.

Bottrell, S.H., Parkes, R.J., Cragg, B.A., and Raiswell, R. (2000) Isotopic evidence for anoxic pyrite oxidation and stimulation of bacterial sulphate reduction in marine sediments. *Journal of the Geological Society* **157**: 711-714.

Botz, R., Pokojski, H.D., Schmitt, M., and Thomm, M. (1996) Carbon isotope fractionation during bacterial methanogenesis by CO2 reduction. *Organic Geochemistry* **25**: 255-262.

Brauer, K., Kampf, H., Faber, E., Koch, U., Nitzsche, H., and Strauch, G. (2005) Seismically triggered microbial methane production relating to the Vogtland NW Bohemia earthquake swarm period 2000, Central Europe. *Geochemical Journal* **39**: 441-450.

Broda, E. (1977) Two kinds of lithotrophs missing in nature. *Z. Allg. Mikrobiol* **17**: 491-493.

Brosius, J., Dull, T.J., Sleeter, D.D., and Noller, H.F. (1981) Gene organization and primary structure of a ribosomal RNA operon from Escherichia coli. *Journal of Molecular Biology* **148**: 107-127.

Burggraf, S., Jannasch, H.W., Nicolaus, B., and Stetter, K.O. (1990a) Archaeoglobus-Profundus Sp-Nov, Represents a New Species within the Sulfate-Reducing Archaebacteria. *Systematic and Applied Microbiology* **13**: 24-28.

Burggraf, S., Fricke, H., Neuner, A., Kristjansson, J., Rouvier, P., Mandelco, L. et al. (1990b) Methanococcus-Igneus Sp-Nov, a Novel Hyperthermophilic Methanogen from a Shallow Submarine Hydrothermal System. *Systematic and Applied Microbiology* **13**: 263-269.

Canfield, D.E., and Teske, A. (1996) Late Proterozoic rise in atmospheric oxygen concentration inferred from phylogenetic and sulphur-isotope studies. *Nature* **382**: 127-132.

Canfield, D.E., Thamdrup, B., and Hansen, J.W. (1993) The Anaerobic Degradation of Organic-Matter in Danish Coastal Sediments - Iron Reduction, Manganese Reduction, and Sulfate Reduction. *Geochimica Et Cosmochimica Acta* **57**: 3867-3883.

Canfield, D.E., Jorgensen, B.B., Fossing, H., Glud, R., Gundersen, J., Ramsing, N.B. et al. (1993 a) Pathways of Organic-Carbon Oxidation in 3 Continental-Margin Sediments. *Marine Geology* **113**: 27-40.

Chapelle, F.H., and Bradley, P.M. (1996) Microbial acetogenesis as a source of organic acids in ancient Atlantic Coastal Plain sediments. *Geology* **24**: 925-928.

Chapelle, F.H., O'Neill, K., Bradley, P.M., Methe, B.A., Ciufo, S.A., Knobel, L.L., and Lovley, D.R. (2002) A hydrogen-based subsurface microbial community dominated by methanogens. *Nature* **415**: 312-315.

Charlou, J.L., Donval, J.P., Fouquet, Y., Jean-Baptiste, P., and Holm, N. (2002) Geochemistry of high H-2 and CH4 vent fluids issuing from ultramafic rocks at the Rainbow hydrothermal field (36 degrees 14 ' N, MAR). *Chemical Geology* **191**: 345-359.

Childers, S.E., Ciufo, S., and Lovley, D.R. (2002) Geobacter metallireducens accesses insoluble Fe(III) oxide by chemotaxis. *Nature* **416**: 767-769.

Chin, H., Chen, Z., and Chou, C. (2003) Fedbatch operation using Clostridium acetobutylicum suspension culture as biocatalyst for enhancing hydrogen production. *Biotechnol Prog.* **19**: 383-388.

Codispoti, L.A., Brandes, J.A., Christensen, J.P., Devol, A.H., Naqvi, S.W.A., Paerl, H.W., and Yoshinary, T. (2001) The Oceanic fixed nitrogen and nitrous oxide budgets: moving targets as we enter the anthropocene. *Sci. Mar.* **65**: 85-105.

Cooles, G.P., Mackenzie, A.S., and Parkes, R.J. (1987) Non-hydrocarbons of significance in petroleum-exploration - volatile fatty-acids and non-hydrocarbon gases. *Mineralogical Magazine* **51**: 483-493.

Cragg, B.A., Parkes, R.J., Fry, J.C., Herbert, R.A., Wimpenny, J.W.T., and Getliff, J.M. (1990) Bacterial biomass and activity profiles within deep sediment layers. *Proc. Ocean Drilling Program Scientific Results* **112**: 607-619.

D'Hondt, S., Rutherford, S., and Spivack, A.J. (2002a) Metabolic activity of subsurface life in deep-sea sediments. *Science* **295**: 2067-2070.

D'Hondt, S., Jorgensen, B.B., Blake, R., Dickens, G., Hindrichs, K., Holm, N. et al. (2002b) Microbial activity in deeply buried marine Sediments. *Geochimica Et Cosmochimica Acta* **66**: A163-A163.

D'Hondt, S., Jorgensen, B.B., Miller, D.J., Batzke, A., Blake, R., Cragg, B.A. et al. (2004) Distributions of microbial activities in deep subseafloor sediments. *Science* **306**: 2216-2221.

Dalsgaard, T., and Thamdrup, B. (2002) Factors controlling anaerobic ammonium oxidation with nitrite in marine sediments. *Applied and Environmental Microbiology* **68**: 3802-3808.

References

DeLong, E.F. (1992) Archaea in coastal marine environments. *Proceedings Of The National Academy Of Sciences Of The United States Of America* **89**: 5685-5689.

Dhillon, A., Lever, M., Lloyd, K.G., Albert, D.B., Sogin, M.L., and Teske, A. (2005) Methanogen diversity evidenced by molecular characterization of methyl coenzyme M reductase A (mcrA) genes in hydrothermal sediments of the Guaymas Basin. *Applied And Environmental Microbiology* **71**: 4592-4601.

Dias, R.F., Freeman, K.H., Lewan, M.D., and Franks, S.G. (2002) δ ^{13}C of low-molecular-weight organic acids generated by the hydrous pyrolysis of oil-prone source rocks. *Geochemica et Cosmochimica Acta* **66**

Dick, H.J.B., Lin, J., and Schouten, H. (2003) An ultraslow spreading class of ocean ridge. *Nature* **426**: 405-412.

Draganic, I.G., and Draganic, Z.D. (1971) *The radiation chemistry of water*. New York: Academic Press.

Drake, H.L. (1994) Acetogenesis, acetogeneic bacteria and the acetyl-CoA "Wood/Ljungdahl" pathway: past present and future prespectives. In *Acetogenesis*. Drake, H.L. (ed). New york: Chapman &Hall, pp. 3-60.

Drake, H.L., and Daniel, S.L. (2004) Physiology of thermophilic acetogen *Moorella thermoacetica. Research in Microbiology* **155**: 422-436.

Drake, H.L., Gobner, A.S., and Daniel, S.L. (2008) Old Acetogens, New Light. *Ann. NY. Acad. Sci.* **1125**: 100-128.

Drobner, E., Huber, H., Wachtershauser, G., Rose, D., and Stetter, K.O. (1990) Pyrite formation linked with hydrogen evolution under anaerobic conditions. *Nature* **346**: 742-744.

Edwards, K.J., Rogers, D.R., Wirsen, C.O., and McCollom, T.M. (2003) Isolation and characterization of novel psychrophilic, neutrophilic, Fe-oxidizing, chemolithoautotrophic alpha- and, gamma-Proteobacteria from the deep sea. *Applied and Environmental Microbiology* **69**: 2906-2913.

Ferry, J.G., and Kastead, K.A. (2007) Archaea molecular and cellular biology. *(ed. Cavicchioli, R.) ASM Washington DC*: 288-314.

Fisher, A.T., and Becker, K. (1991) Heat-Flow, Hydrothermal Circulation and Basalt Intrusions in the Guaymas Basin, Gulf of California. *Earth and Planetary Science Letters* **103**: 84-99.

Fisk, M.R., Giovannoni, S.J., and Furnes, H. (1998) Alteration of oceanic volcanic glass: textural evidence of microbial activity. *Science* **281**: 978-980.

Fredrickson, J.K., Zachara, J.M., Kennedy, D.W., Dong, H.L., Onstott, T.C., Hinman, N.W., and Li, S.M. (1998) Biogenic iron mineralization accompanying the dissimilatory reduction of hydrous ferric oxide by a groundwater bacterium. *Geochimica Et Cosmochimica Acta* **62**: 3239-3257.

Frimmer, U.F., and Widdel, F. (1989) Oxidation of ethanol by methanogenic bacteria. *Archives of Microbiology* **152**: 479-483.

Fry, J.C. (1988) Determination of biomass. In *Methods in Aquatic Bacteriology*. Austin.B (ed). Chichester: John Wiley, pp. 27-72.

Fry, J.C., Parkes, R.J., Cragg, B.A., Weightman, A.J., and Webster, G. (2008) Prokaryotic biodiversity and activity in the deep subsurface biosphere. *Fems Microbiology ecology*: In Press.

Fry, N.K., Fredrickson, J.K., Fishbain, S., Wagner, M., and Stahl, D.A. (1997) Population structure of microbial communities associated with two deep, anaerobic, alkaline aquifers. *Applied and Environmental Microbiology* **63**: 1498-1504.

Garcia, J.L., Patel, B.K.C., and Ollivier, B. (2000) Taxonomic phylogenetic and ecological diversity of methanogenic Archaea. *Anaerobe* **6**: 205-226.

Glamoclija, M., Garrel, L., Berthon, J., and Lopez-Garcia, P. (2004) Biosignatures and bacterial diversity in hydrothermal deposits of Solfatara Crater, Italy. *Geomicrobiology Journal* **21**: 529-541.

Glasauer, S., Weidler, P.G., Langley, S., and Beveridge, T.J. (2003) Controls on Fe reduction and mineral formation by a subsurface bacterium. *Geochemica et Cosmochimica Acta* **67**: 1277-1288.

Gold, T. (1992) The deep, hot biosphere. *Proc. Natl. Acad. Sci USA* **89**: 6045-6049. Gorby, Y.A., Yanina, S., McLean, J.S., Rosso, K.M., Moyles, D., Dohnalkova, A. et al. (2006) Electrically conductive bacterial nanowires produced by Shewanella oneidensis strain MR-1 and other microorganisms. *Proceedings Of The National Academy Of Sciences Of The United States Of America* **103**: 11358-11363.

Goulder, R. (1977) Attached and Free Bacteria in an Estuary with Abundant Suspended Solids. *Journal of Applied Bacteriology* **43**: 399-405.

Grossi, V., Cravo-Laureau, C., Méou, A., Raphel, D., Garzino, F., and Hirschler-Réa, A. (2007) Anaerobic 1-Alkene Metabolism by the Alkane- and Alkene-Degrading Sulfate Reducer Desulfatibacillum aliphaticivorans Strain CV2803T. *Applied and Environmental Microbiology* **73**: 7882-7890.

Grosskopf, R., Janssen, P.H., and Liesack, W. (1998) Diversity and structure of the methanogenic community in anoxic rice paddy soil microcosms as examined by

cultivation and direct 16S rRNA gene sequence retrieval. *Applied and Environmental Microbiology* **64**: 960-969.

Gruber, N., and Sarmiento, J.L. (1997) Global patterens of marine nitrogen fixation and denitrification. *Global Biogeochemical Cycles* **11**: 235-266.

Hafenbradl, D., Keller, M., Dirmeier, R., Rachel, R., Rossnagel, P., Burggraf, S. et al. (1996) Ferroglobus placidus gen nov, sp nov, a novel hyperthermophilic archaeum that oxidizes Fe2+ at neutral pH under anoxic conditions. *Archives of Microbiology* **166**: 308-314.

Hall, T. (1999) BioEdit: a user-friendly biological sequence alignment editor and analysis program for Windows 95/98/NT. *Nucleic Acids Symp* **41**: 95-98.

Harris, R.E., and Pimblott, S.M. (2002) ON ^{3}H B-Particle and ^{60}Co y irradiation of aqueous systems. *Radiation research* **158**: 493-504.

Hearn, P.P., Steinkampf, W.C., White, L.D., and Evans, J.R. (1986) Proc, U.S. Geol. Surv. Workshop on Environmental Geochemistry. *W. Wood and W.H. Low, Geol.Soc.Am. Bull* **97**: 1456.

Hedges, J.I., and Keil, R.G. (1995) Marine Chemistry Discussion Paper. Sedimentary organic matter preservation: an assessment and speculative synthesis. *Marine Chemistry* **4**: 81-115.

Heijs, S.K., Haese, R.R., van der Wielen, P.W., Forney, L.J., and van Elsas, J.D. (2007) Use of 16S rRNA Gene Based Clone Libraries to Assess Microbial Communities Potentially Involved in Anaerobic Methane Oxidation in a Mediterranean Cold Seep. *Fems Microbiology Ecology* **53**: 384-398.

Henstra, A.M., Dijkema, C., and Stams, A., J,M. (2007) *Archaeoglobus fulgidus* couples CO oxidation to sulphate reduction and acetogenesis with transient formate accumulation. *Environmental Microbiology* **9**: 1836-1841.

Hiebert, F.Z., and Bennett, P.C. (1992) Microbial control of Silicate weathering in organic-rich ground water. *Science* **258**: 278-281.

Hinrichs, K.-U., and Boetius, A. (2002) The anaerobic oxidation of methane: new insights in microbial ecology and biogeochemistry. In *Ocean margin systems*. G. Wefer, D. Billett, D. Hebbeln, B. B. Jørgensen, M. Schlüter, and Weering, T.V. (eds). Berlin: Springer-verlag, pp. 457-477.

Hinrichs, K.U., Hayes, J.M., Sylva, S.P., Brewer, P.G., and DeLong, E.F. (1999) Methane-consuming archaebacteria in marine sediments. *Nature* **398**: 802-805.

Hinrichs, K.U., Summons, R.E., Orphan, V., Sylva, S.P., and Hayes, J.M. (2000) Molecular and isotopic analysis of anaerobic methane-oxidizing communities in marine sediments. *Organic Geochemistry* **31**: 1685-1701.

Hirt, R.P., Logsdon, J.M., Healy, B., Dorey, M.W., Doolittle, W.F., and Embley, T.M. (1999) Microsporidia are related to Fungi: Evidence from the largest subunit of RNA polymerase II and other proteins. *Proceedings of the National Academy of Sciences of the United States of America* **96**: 580-585.

Hoehler, T.M., Alperin, M.J., Albert, D.B., and Martens, C.S. (1994) Field and Laboratory Studies of Methane Oxidation in an Anoxic Marine Sediment - Evidence for a Methanogen-Sulfate Reducer Consortium. *Global Biogeochemical Cycles* **8**: 451-463.

Horsfield, B., Schenk, H.J., Zink, K., Ondrak, R., Dieckmann, V., Kallmeyer, J. et al. (2006) Living microbial ecosytems within the active zone of catagenesis: implications for feeding the deep biosphere. *Earth and Planetary Science Letters* **246**: 55-69.

Huber, G., Huber, R., Jones, B.E., Lauerer, G., Neuner,A, Segerer, Stetter, K.O., and Degens, E.T. (1991) Hyperthermophilic Archaea and bacteria occurring within Indonesian hydrothermal areas. *System. Appl. Microbiol.* **14**: 397-404.

Huber, R., and Stetter, K. (1992 (a)) The order *Thermotogales*. In *The Prokaryotes*. Balows, A., Truper, H., G., Dworkin, M., Harder, W., and Schleifer, K.-H. (eds). Berlin: Springer-Verlag, pp. 3809-3815.

Huber, R., and Stetter, K. (1992 (b)) The *Thermotogales*. In *Hyperthermophilic and extremely thermophilic bacteria*. Kristjansson, J.K. (ed). Boca Raton FL: CRC press, pp. 185-194.

Huber, R., Kurr, M., Jannasch, H.W., and Stetter, K.O. (1989) A novel group of abyssal methanogenic archaebacteria (Methanopyrus) growing at 110oC. *Nature* **424**: 833-834.

Huber, R., Langworthy, T.A., Konig, H., Thomm, M., Woese, C.R., Sleytr, U.B., and Stetter, K.O. (1986) *Thermotoga-Maritima* sp-Nov represents a new genus of unique extremely thermophilic eubacteria growing up to 90-degrees-C. *Archives of microbiology* **144**: 324-333.

Inagaki, F., Suzuki, M., Takai, K., Oida, H., Sakamoto, T., Aoki, K. et al. (2003) Microbial communities associated with geological horizons in coastal subseafloor sediments from the Sea of Okhotsk. *Applied and Environmental Microbiology* **69**: 7224-7235.

Isaksen, M.F., Bak, F., and Jorgensen, B.B. (1994) Thermophilic sulfate-reducing bacteria in cold marine sediment. *FEMS Microbiol. Ecol.* **14**: 1-8.

Itoh, T., Suzuki, K.-I., and Nakase, T. (1998) *Thermocladium modestius* gen.nov.,sp. nov. a new genus of rod shaped, extremely thermophilic crenarchaeote. *Int. J. Syst. Bacteriol* **48**: 879-887.

Itoh, T., Suzuki, K.-I., Sanches, P.C., and Nakase, T. (1999) *Caldivirga maquilingensis* gen.nov.,sp.nov. a new genus of rod shaped crenarchaeote isolated from a hot spring in the philippines. *Int. J. Syst. Bacteriol* **49**: 1157-1163.

Jackson, B.E., and McInerney, M.J. (2002) Anaerobic microbial metabolism can proceed close to thermodynamic limits. *Nature* **415**: 454-456.

Jaffe, D.A. (2000) The nitrogen cycle. In *Earth System Science*. Jacobson, M.C., Charlson, R.J., Rohde, H., and Orians, G.H. (eds). San Diego, CA. USA: Academic press, pp. 322-342.

Janecky, D.R., and Seyfried, W.E. (1986) Hydrothermal serpentinization of peridotite within the oceanic crust: experimental investigations of mineralogy and major element chemistry. *Geochemica et Cosmochimica Acta* **50**: 1357-1378.

Jeter, R.M., and Ingraham, J.L. (1996) *The Denitrifying Prokaryotes*: Springer-verlag. Jetten, M.S.M., Cirpus, B., Kartal, B., Van Niftrik, L., van de Pas-Schoonen, K.T., Sliekers, A.O., and Haaijer, W. (2005) 10 years of research on anaerobic oxidation of ammonium. *Biochem. Soc. Trans.* **33**: 119-123.

Jones, D., M., Head, I., M., Gray, N.D., Adams, J.J., Rowan, A.K., Aitken, C.M. et al. (2007) Crude-oil biodegradation via methanogenesis in subsurface petroleum reservoirs. *Nature* **451**: 176-180.

Jones, W.J., Leigh, J.A., Mayer, F., Woese, C.R., and Wolfe, R.S. (1983) Methanococcus-Jannaschii Sp-Nov, an Extremely Thermophilic Methanogen from a Submarine Hydrothermal Vent. *Archives of Microbiology* **136**: 254-261.

Jonkers, H.M., Van der Maarel, M.J., Van Gemerden, H., and Hansen, T.A. (1996) Dimethylsulfoxide reduction by marine sulphate reducing bacteria. *Fems Microbiol Letters* **136**: 283-287.

Jorgensen, B.B. (1982) Mineralization of organic matter in the seabed - the role of sulphate reduction. *Nature* **296**: 643-645.

Jorgensen, B.B. (1983) *Processes at the Sediment-Water Interface*: The Major Biogiochemical Cycles and Their Interactions Ed B.Bolin & R.B. Cook, John Wiley, Chichester.

Jorgensen, B.B., Zawacki, L.X., and Jannasch, H.W. (1990) Thermophilic bacterial sulfate reduction in deep-sea sediments at the Guayamas Basin hydrothermal vent site (Gulf of California). *Deep-Sea Research* **37**: 695-710.

Jorgensen, B.B., Isaksen, M.F., and Jannasch, H.W. (1992) Bacterial sulphate reduction above 100°C in deep-sea hydrothermal vent sediments. *Science* **258**: 1756-1757.

Kartal, B., Kuypers, M.M.M., Lavik, G., Schalk, J., Op den Camp, H.J.M., Jetten, M.S.M., and Strous, M. (2007) Anammox bacteria disguised as denitrifers: nitrate reduction to dinitrogen gas via nitrite and ammonium. *Environmental Microbiology* **9**: 635-642.

Kashefi, K., and Lovley, D.R. (2000) Reduction of Fe(III), Mn(IV), and toxic metals at 100 degrees C by Pyrobaculum islandicum. *Applied and Environmental Microbiology* **66**: 1050-1056.

Kashefi, K., and Lovley, D.R. (2003) Extending the upper temperature limit for life. *Science* **301**: 934-934.

Kashefi, K., Holmes, D.E., Reysenbach, A.L., and Lovley, D.R. (2002a) Use of Fe(III) as an electron acceptor to recover previously uncultured hyperthermophiles: Isolation and characterization of *Geothermobacterium ferrireducens* gen. nov., sp nov. *Applied and Environmental Microbiology* **68**: 1735-1742.

Kashefi, K., Tor, J.M., Holmes, D.E., Van Praagh, C.V.G., Reysenbach, A.L., and Lovley, D.R. (2002b) *Geoglobus ahangari* gen. nov., sp nov., a novel hyperthermophilic archaeon capable of oxidizing organic acids and growing autotrophically on hydrogen with Fe(III) serving as the sole electron acceptor. *International Journal of Systematic and Evolutionary Microbiology* **52**: 719-728.

Kelley, D.S., Baross, J.A., and Delaney, J.R. (2002) Volcanoes fluids and life at mid-ocean ridge spreading centres. *Annu.Rev.Earth planet.Sci* **30**: 385-491.

Kelley, D.S., Karson, J.A., Fruh-Green, G.L., Yoerger, D.R., Shank, T.M., Butterfield, D.A. et al. (2005) A serpentinite-hosted ecosystem: The lost city hydrothermal field. *Science* **307**: 1428-1434.

Kelly, D.P., and Wood, A.P. (2000) Reclassification of some species of *Thiobacillus* to the newly designated genera *Acidithiobacillus* gen. nov., *Halothiobacillus* gen. nov. and *Thermithiobacillus* gen. nov."". *Int. J. Syst. Evol. Microbiol.* **50**: 489–500.

Kendall, M.M., Wardlaw, G.D., Tang, C.F., Bonin, A.S., Liu, Y., and Valentine, D.L. (2007) Diversity of Archaea in marine sediments from Skan Bay, Alaska,including cultivated methanogens, and description of Methanogenium boonei sp. nov. *Applied and Environmental Microbiology* **73**: 407-414.

Kharaka, Y.K., Lundegard, P.D., Ambats, G., Evans, W.C., and Bischoff, J.L. (1993) Generation of aliphatic acid anions and carbon dioxide by hydrous pyrolysis of crude oils. *Applied Geochemistry* **8**: 317-324.

Kim, B.S., Oh, H.M., Kang, H., and Chun, J. (2005) Archaeal diversity in tidal flat sediment as revealed by 16S rDNA analysis. *Journal Of Microbiology* **43**: 144-151.

Kirchman, D., Sigda, J., Kapuscinski, R., and Mitchell, R. (1982) Statistical-Analysis of the Direct Count Method for Enumerating Bacteria. *Applied and Environmental Microbiology* **44**: 376-382.

Kita, I., Matsuo, S., and Wakita, H. (1982) H_2 Generation By Reaction Between H_2O And Crushed Rock - An Experimental-Study On H_2 Degassing From The Active Fault Zone. *Journal Of Geophysical Research* **87**: 789-795.

Kittelmann, S., and Friedrich, M.W. (2008) Novel uncultured Chloroflexi dechlorinate perchloroethene to trans- dichloroethene in tidal flat sediments. *Environmental Microbiology* **10**: 1557-1570.

Kormas, K.A., Tivey, M.K., Von Damm, K., and Teske, A. (2006) Bacterial and archaeal phylotypes associated with distinct mineralogical layers of a white smoker spire from a deep-sea hydrothermal vent site (9 degrees N, East Pacific Rise). *Environmental Microbiology* **8**: 909-920.

Kostka, J.E., Stucki, J.W., Nealson, K.H., and Wu, J. (1996) Reduction of structural Fe(III) in Smectite by a pure culture of *Shewanella putrefaciens* strain MR-1. *Clays Clay Miner* **44**: 522-529.

Kostka, J.E., Dalton, D.D., Skelton, H., Dollhopf, S., and Stucki, J.W. (2002) Growth of Fe(III) reducing bacteria on clay minerals as the sole electron acceptor and comparison of growth yields on a variety of oxidized iron forms. *Applied and Environmental Microbiology* **68**: 6256-6262.

Kristjansson, J.K., Schonheit, P., and Thauer, R.K. (1982) Different Ks-Values for Hydrogen of Methanogenic Bacteria and Sulfate Reducing Bacteria - an Explanation for the Apparent Inhibition of Methanogenesis by Sulfate. *Archives of Microbiology* **131**: 278-282.

Kuenen, G.J. (2008) Anammox bacteria: from discovery to application. *Nature Reviews Microbiology* **6**: 320-325.

Kumar, S., Tamura, K., Jakobsen, I.B., and Nei, M. (2001) MEGA2: molecular evolutionary genetics analysis software. *Bioinformatics* **17**: 1244-1245.

Kuypers, M.M.M., Sliekers, A.O., Lavik, G., Schmid, M., Jorgensen, B.B., and Keunen, J.G. (2003) Anaerobic ammonium oxidation by anammox bacteria in the Black Sea. *Nature* **422**: 608-611.

Lake, J.A. (1994) Reconstructing Evolutionary Trees from DNA and Protein Sequences - Paralinear Distances. *Proceedings of the National Academy of Sciences of the United States of America* **91**: 1455-1459.

Lane, D.J. (1991) In *6S/23S rRNA sequencing. Nucleic Acid Techniques in Bacterial Systematics*. Stackebrandt, E., and Goodfellow, M. (eds). New York: John Wiley and Sons, pp. 115-175.

Lepage, E., Marguet, E., Geslin, C., Matte-Tailliez, O., Zillig, W., Forterre, P., and Tailliez, P. (2004) Molecular diversity of new Thermococcales isolates from a single area of hydrothermal deep-sea vents as revealed by randomly amplified polymorphic DNA fingerprinting and 16S rRNA gene sequence analysis. *Applied And Environmental Microbiology* **70**: 1277-1286.

Lewan, M.D., and Fisher, J.B. (1994) Organic acids from petroleum source rocks. *In Pittman, E.D. and Lewan, M.D., eds Organic Acids in Geological Processes: New York, Springer-Verlag*: 70-114.

Liermann, L.J., Barnes, A.S., Kalinowski, B.E., Zhou, X.Y., and Susan, L. (2000) Microenvironments of pH in biofilms grown on dissolving silicate surfaces. *Chemical Geology* **171**: 1-16.

Lin, L.H., Slater, G.F., Lollar, B., Sherwood., Lacrampe-Couloume, G., and Onstott, T.C. (2005) The yield and isotopic composition of radiolytic H_2, a potential energy source for the deep subsurface biosphere. *Geochimica et Cosmochimica Acta* **69**: 893-903.

Lin, L.H., Onstott, T.C., Lippmann, J., Ward, J., Hall, J., and Lollar, B.S. (2002) Radiolytic H-2 in continental crust: A potential energy source for microbial metabolism in deep biosphere. *Geochimica Et Cosmochimica Acta* **66**: A457-A457.

Lin, L.H., Wang, P.L., Rumble, D., Lippmann-Pipke, J., Boice, E., Pratt, L.M. et al. (2006) Long-term sustainability of a high-energy, low-diversity crustal biome. *Science* **314**: 479-482.

Lipp, J.S., Morono, Y., Inagaki, F., and Hinrichs, K.-U. (2008) Significant contribution of Archaea to extant biomass in marine subsurface sediments. *Nature* **454**: 991-994.

Lippmann, J., Stute, M., Torgersen, T., Moser, D.P., Hall, J.A., Lin, L. et al. (2003) Dating ultra-deep mine waters with noble gases and Cl-36, Witwatersrand Basin, South Africa. *Geochimica Et Cosmochimica Acta* **67**: 4597-4619.

Ljungdahl, L.G. (1994) The acetyl-CoA pathway and the chemiosmotic generation of ATP during acetogenesis. *In: Acetogenesis, H.L Drake, ED: New York: Chapman & Hall*: 63-87.

Lockhart, P.J., Larkum, A.W.D., Steel, M.A., Waddell, P.J., and Penny, D. (1996) Evolution of chlorophyll and bacteriochlorophyll: The problem of invariant sites in sequence analysis. *Proceedings of the National Academy of Sciences of the United States of America* **93**: 1930-1934.

Lollar, B., Sherwood., Frape, S.K., Weise, S.M., Fritz, P., Macko, S.A., and Welhan, J.A. (1993) Abiogenic methanogenesis in crystalline rocks. *Geochimica et Cosmochimica Acta* **57**: 5087-5097.

Lollar, B., Sherwood., Voglesonger, K., Lin, L.-K., Lacrampe-couloume, L., Telling, J., Abrajano, T.A. et al. (2007) Hydrogeologic Controls on the Episodic H_2 realease from Precambrian fractured rocks-Energy for the Deep Subsurface Life on Earth and Mars. *Astrobiology* **7**: 971-986.

Losekann, T., Knittel, K., Nadalig, T., Fuchs, B., Niemann, H., Boetius, A., and Amann, R. (2007) Diversity and abundance of aerobic and anaerobic methane oxidizers at the haakon mosby mud volcano, barents sea. *Applied and Environmental Microbiology* **73**: 3348-3362.

Lovley, D.R. (1993) Dissimilatory metal reduction. *Annual reviews microbiology* **47**: 263-290.

Lovley, D.R. (2000) Fe(III) and Mn(IV) reduction. *IN: The Prokaryotes; edited by Dworkin M, Falkow S, Rosenburg E, Schleifer K-H, Stackebrandt E. New York; Springer-Verlag, INC.*

Lovley, D.R. (2004) Dissimilatory Fe(III) and Mn(IV) reduction. *Advances in microbial physiology* **49**: 219-286.

Lovley, D.R., and Philips, E.J.P. (1987) Competitive mechanisms for inhibition of sulfate reduction and methane production in the zone of ferric iron reduction in sediments. *Applied and Environmental Microbiology* **53**: 2636-2641.

Lovley, D.R., and Goodwin, S. (1988) Hydrogen concentrations as an indicator of the predominant terminal electron-accepting reaction in aquatic sediments. *Geochimica et Cosmochimica Acta* **52**: 2993-3003.

Lovley, D.R., and Phillips, E.J.P. (1994) Novel Processes for anaerobic sulfate production from elemental sulfur by sulfate-reducing bacteria. *Applied and Environmental Microbiology* **60**: 2394-2399.

References

Lovley, D.R., and Philips, E.J.P. (1994) Reduction of chromate by *Desulfovibrio vulgaris* and its C3 cytochrome. *Applied and Environmental Microbiology* **60**: 726-728.

Lovley, D.R., and Chapelle, F.H. (1995) Deep subsurface microbial processes. *Reviews of Geophysics* **33**: 365-381.

Lovley, D.R., Chapelle, F.H., and Woodward, J.C. (1994) Use of dissolved H_2 concentrations to determine the distribution of microbially catalyzed redox reactions in anoxic ground water. *Environ. Sci. Technol.* **28**: 1205-1212.

Lovley, D.R., Roden, E.E., Phillips, E.J.P., and Woodward, J.C. (1993a) Enzymatic iron and uranium reduction by sulfate-reducing bacteria. *Marine Geology* **113**: 41-53.

Lovley, D.R., Coated, J.D., Blunt-Harris, E.L., Phillips, E.L., and Woodward, J.C. (1996) Humic substances as electron acceptors for microbial respiration. *Nature* **382**: 445-448.

Lovley, D.R., Kashefi, K., Vargas, M., Tor, J.M., and Blunt-Harris, E.L. (2000) Reduction of humic substances and Fe(III) by hyperthermophilic microorganisms. *Chemical Geology* **169**: 289-298.

Lovley, D.R., Giovannoai, S.J., White, D.C., Champine, J.E., Philips, E.J.P., Gorby, Y.A., and Goodwin, S. (1993b) *Geobacter metallireducens* gen.nov.sp.nv., a microorganism capable of coupling the complete oxidation of organic compunds to the redcution of iron and other metals. *Archives of Microbiology* **159**: 336-344.

Lupton, F.S., and Zeikus, J.G. (1984) Physiological basis for sulfate-dependent hydrogen competition between sulfidogens and methanogens. *Current Microbiology* **11**: 7-12.

Machel, H.G. (1998) Gas souring by thermochemical sulfate reduction at 140 C. *Am. Assoc. Pet. Geol. Bull.* **82**: 1870-1873.

Machel, H.G. (2001) Bacterial and thermochemical sulfate reduction in diagenetic settings-old and new insights. *Sedimentary Geology* **140**: 143-175.

Machel, H.G., and Foght, J. (2000) Products and depth limits of microbial activity in petroliferous subsurface settings. In *Microbial Sediments*. Awramik, R. (ed). Berlin: Springer, pp. 105-120.

Macy, J.M., Santini, J.M., Pauling, B.V., O'Neill, A.H., and Sly, L.I. (2000) Two new arsenate/sulphate-reducing bacteria: Mechanisms of arsenate reduction. *Archives of Microbiology* **173**: 49-57.

Malinovskaya, I.M., Kosenko, L.V., Votselko, S.K., and Podgorsjkii, V.S. (1990) Role of Bacillus mucilaginosus polysaccharide in degradation of silicate minerals. *Mikrobiologiya* **59**: 49-55.

References

Marchesi, J.R., Weightman, A.J., Cragg, B.A., Parkes, R.J., and Fry, J.C. (2001) Methanogen and bacterial diversity and distribution in deep gas hydrate sediments from the Cascadia Margin as revealed by 16S rRNA molecular analysis. *FEMS Microbiology Ecology* **34**: 221-228.

McCollom, T.M., and Shock, E.L. (1997) Geochemical constraints on chemolithoautotrophic metabolism by microorganisms in seafloor hydrothermal systems. *Geochimica et Cosmochimica Acta.* **61**: 4375 - 4391.

McCollom, T.M., and Seewald, J.S. (2001) A reassessment of the potential for the reduction of the dissolved CO_2 to hydrocarbons during serpentinization of olivine. *Geochemica et Cosmochimica Acta* **65**: 3769-3778.

McCollom, T.M., and Seewald, J.S. (2007) Abiotic sythesis of organic compounds in deep sea hydrothermal environments. *Chemical reviews* **107**: 382-401.

Miller, A.E.J. (1999) Seasonal investigations of dissolved organic carbon dynamics in the Tamar Estuary, UK. *Estuarine Coastal and Shelf Science* **49**: 891-908.

Mills, H.J., Hodges, C., Wilson, K., MacDonald, I.R., and Sobecky, P.A. (2003) Microbial diversity in sediments associated with surface- breaching gas hydrate mounds in the Gulf of Mexico. *Fems Microbiology Ecology* **46**: 39-52.

Morita, R.Y. (1999) Is H-2 the universal energy source for long-term survival? *Microbial Ecology* **38**: 307-320.

Mulder, A., Vandegraff, A.A., Robertson, L.A., and Kuenen, J.G. (1995) Ananerobic ammonium oxidation discovered in a denitrifying fluidized-bed reactor. *Fems Microbiology ecology* **16**: 177-183.

Muyzer, G., and Stams, A., J,M. (2008) The ecology and biotechnology of sulphate-reducing bacteria. *Nature Reviews Microbiology* **6**: 441-454.

Muyzer, G., Dewaal, E.C., and Uitterlinden, A.G. (1993) Profiling of Complex Microbial-Populations by Denaturing Gradient Gel-Electrophoresis Analysis of Polymerase Chain Reaction-Amplified Genes-Coding for 16s Ribosomal-Rna. *Applied and Environmental Microbiology* **59**: 695-700.

Muyzer, G., Brinkhoff, T., Nubel, U., Santegoeds, C., Schafer, H., and Wawer, C. (1998) Denaturing gradient gel electrophoresis (DGGE) in microbial ecology. In *Molecular microbial ecology Manual.* Akkermans, A., Van Elsas, J.D., and De Bruijin, F., J (eds): Kluwer Academic Publishers, pp. 1-27.

Nanninga, H.L., and Gottschal, J.C. (1987) Properties of *Desulfovibrio carbinolicus* sp.nov and other sulfate reducing bacteria isolated from an anaerobic purification planet. *Applied and Environmental Microbiology* **53**: 802-809.

Nazina, T.N., Ivanova, A.E., kanchaveli, L.P., and Rozanova, E.P. (1987) A new spore forming thermophilic methylotrophic sulphate reducing bacterium *Desulfotomaculum kuznetsovii* sp.nov. *Mikrobiologiia* **57**: 823-827.

Neubauer, H., and Gotz, F. (1996) Physiology and interaction of nitrate and nitrite reduction in Staphylococcus carnosus. *Journal of Bacteriology* **178**: 2005-2009.

Newberry, C.J., Webster, G., Cragg, B.A., Parkes, R.J., Weightman, A.J., and Fry, J.C. (2004) Diversity of prokaryotes and methanogenesis in deep subsurface sediments from the Nankai Trough, Ocean Drilling Program Leg 190. *Environmental Microbiology* **6**: 274-287.

Newman, D.K., and Kolter, R.A. (2000) A role for excreted quinones in extracellular electron transfer. *Nature* **405**: 94-97.

Nichols, D.S. (2003) Prokaryotes and the input of polyunsaturated fatty acids to the marine food web. *Fems Microbiology Letters* **219**: 1-7.

Nicol, G.W., Glover, L.A., and Prosser, J.L. (2003) The impact of grassland management on archaeal community structure in upland pasture rhizosphere soil. *Environmental Microbiology* **5**: 152-162.

Niewohner, C., Hensen, C., Kasten, S., Zabel, M., and Schulz, H.D. (1998) Deep sulfate reduction completely mediated by anaerobic methane oxidation in sediments of the upwelling area off Namibia. *Geochimica Et Cosmochimica Acta* **62**: 455-464.

O'Sullivan, L.A., Webster, G., Fry, J.C., Parkes, R.J., and Weightman, A.J. (2008) Modified linker- PCR primers facilitate complete sequencing of DGGE DNA fragments. *Journal of Microbiological Methods*: In press doi:10.1016/j.mimet.2008.1008.1006.

Oremland, R.S., and Polcin, S. (1982) Methanogenesis and Sulfate Reduction - Competitive and Noncompetitive Substrates in Estuarine Sediments. *Applied and Environmental Microbiology* **44**: 1270-1276.

Oremland, R.S., and Capone, D.G. (1988) Use of Specific Inhibitors in Biogeochemistry and Microbial Ecology. *Advances in Microbial Ecology* **10**: 285-383.

Orphan, V.J., House, C.H., Hinrichs, K.U., McKeegan, K.D., and DeLong, E.F. (2001a) Methane-consuming archaea revealed by directly coupled isotopic and phylogenetic analysis. *Science* **293**: 484-487.

Orphan, V.J., Hinrichs, K.U., Ussler, W., Paull, C.K., Taylor, L.T., Sylva, S.P. et al. (2001b) Comparative analysis of methane-oxidizing archaea and sulfate- reducing bacteria in anoxic marine sediments. *Applied and Environmental Microbiology* **67**: 1922-1934.

Pancost, R.D., Damste, J.S.S., de Lint, S., van der Maarel, M., and Gottschal, J.C. (2000) Biomarker evidence for widespread anaerobic methane oxidation in Mediterranean sediments by a consortium of methanogenic archaea and bacteria. *Applied and Environmental Microbiology* **66**: 1126-1132.

Parkes, R.J., Gibson, G.R., Mueller-Harvey, I., Buckingham, W.J., and Herbert, R.A. (1989) Determination of the Substrates for Sulfate-Reducing Bacteria within Marine and Estuarine Sediments with Different Rates of Sulfate Reduction. *Journal of General Microbiology* **135**: 175-187.

Parkes, R.J., Dowling, N.J.E., White, D.C., Herbert, R.A., and Gibson, G.R. (1993) Characterization of Sulfate-Reducing Bacterial-Populations within Marine and Estuarine Sediments with Different Rates of Sulfate Reduction. *Fems Microbiology Ecology* **102**: 235-250.

Parkes, R.J., Wellsbury, P., Mather, I.D., Cobb, S.J., Cragg, B.A., Hornibrook, E.R.C., and Horsfield, B. (2007) Temperature activation of organic matter and minerals during burial has the potential to sustain the deep biosphere over geological timescales. *Organic Geochemistry* **38**: 845-852.

Parkes, R.J., Cragg, B.A., Bale, S.J., Getliff, J.M., Goodman, K., Rochelle, P.A. et al. (1994) Deep Bacterial Biosphere in Pacific-Ocean Sediments. *Nature* **371**: 410-413.

Parkes, R.J., Cragg, B.A., Webster, G., Weightman, A.J., Newberry, C.J., Ferdelman, T. et al. (2005) Deep sub-seafloor prokaryotes stimulated at interfaces over geological time. *Nature* **436**: 390-394.

Pedersen, K. (1997) Microbial life in deep granitic rock. *Episodes* **20**: 7-9.

Perevalova, A.A., Svetlichny, V.A., Kublanov, I.V., Chernyh, N.A., Kostrikina, N.A., Tourova, T.P. et al. (2005) Desulfurococcus fermentans sp. nov., a novel hyperthermophilic archaeon from a Kamchatka hot spring, and emended description of the genus Desulfurococcus. *Int. J. Syst. Evol. Microbiol.* **55**: 995-999.

Raghoebarsing, A.A., Pol, A., van de Pas-Schoonen, K.T., Smolders, A.J.P., Ettwig, K.F., Rijpstra, W.I.C. et al. (2006) A microbial consortium couples anaerobic methane oxidation to denitrification. *Nature* **440**: 918-921.

Ragsdale, S.W. (1997) The eastern and western branches of the wood/Ljungdahl pathway: How the east and west was won. *Biofactors* **6**: 3-11.

Reeburgh, W.S. (1976) Methane consumption in Cariaco trench waters and sediments. *Earth and Planetary Science Letters* **28**: 337-344.

Reeburgh, W.S. (1980) Anaerobic methane oxidation: rate depth distribution in Skan Bay sediments. *Earth and Planetary Science Letters* **47**: 345-352.

Reed, D.W., Fujita, Y., Delwiche, M.E., Blackwelder, D.B., Sheridan, P.P., Uchida, T., and Colwell, F.S. (2002) Microbial communities from methane hydrate-bearing deep marine sediments in a forearc basin. *Applied and Environmental Microbiology* **68**: 3759-3770.

Reguera, G., McCarthy, K.D., Mehta, T., Nicoll, J.S., Tuominen, M.T., and Lovley, D.R. (2005) Extracellular electron transfer via microbial nanowires. *Nature* **435**: 1098-1101.

Reysenbach, A.L., Liu, Y.T., Banta, A.B., Beveridge, T.J., Kirshtein, J.D., Schouten, S. et al. (2006) A ubiquitous thermoacidophilic archaeon from deep-sea hydrothermal vents. *Nature* **442**: 444-447.

Roden, E.E., and Zachara, J.M. (1996) Microbial reduction of crystalline iron (III) oxides: influence of oxide surface area and potential for cell growth. *Environmental Science and Technology* **30**: 1618-1628.

Roh, Y., Liu, S.V., Li, G.S., Huang, H.S., Phelps, T.J., and Zhou, J.Z. (2002) Isolation and characterization of metal-reducing Thermoanaerobacter strains from deep subsurface environments of the Piceance Basin, Colorado. *Applied and Environmental Microbiology* **68**: 6013-6020.

Rother, M., and Metcalf, W.W. (2004) Anaerobic growth of Methanosarcina acetivorans C2A on carbon monoxide: An unusual way of life for a methanogeneic archaeon. *Proceedings of the National Academy of Sciences of the United States of America* **101**: 16929-16934.

Roussel, E.G., Cambon, B.M.A., Querellou, J., Cragg, B.A., Webster, G., Prieur, D., and Parkes, R.J. (2008) Extending the Sub-Sea-Floor Biosphere. *Science* **320**: 1046.

Sass, A., Rutters, H., Cypionka, H., and Sass, H. (2002) Desulfobulbus mediterraneus sp nov., a sulfate-reducing bacterium growing on mono- and disaccharides. *Archives of Microbiology* **177**: 468-474.

Sass, H., Wieringa, E., Cypionka, H., Babenzien, H.D., and J., O. (1998) High genetic and physiological diversity of sulfate-reducing bacteria isolated from an oligotrophic lake sediment. *Archives of Microbiology* **170**: 243 - 251.

Schink, B. (1997) Energetics of syntrophic cooperation in methanogenic degradation. *Microbial. Mol. Biol.Rev* **61**: 262-280.

Schippers, A., Neretin, L., N., Kallmeyer, J., Ferdelman, T.G., Cragg, B.A., Parkes, R.J., and Jørgensen, B.B. (2005) Prokaryotic cells of the deep sub-seafloor biosphere identified as living bacteria. *Nature* **433**: 861-864.

Schmid, M., Mass, B., Dapena, K., van de Pas-Schoonen, K.T., van de Vossenberg, B., Kartal, B. et al. (2005) Biomarkers for insitu detection of anaerobic ammonium-oxidizing (anammox) bacteria. *Applied and Environmental Microbiology* **71**: 1677-1684.

Schoell, M. (1988) Origins of methane in the Earth. *Chemical Geology* **71**.
Schonheit, P., Kristjensson, J.K., and Thauer, R.K. (1982) Kinetic mechanism for the ability of sulfate-reducers to out-compete methanogenes for acetate. *Arcives for Microbiology* **132**: 285 - 288.

Seewald, J.S. (2001) Aqueous geochemistry of low molecular weight hydrocarbons at elevated temperatures and pressures: constraints from mineral buffered laboratory experiments. *Geochimica et Cosmochimica Acta* **65**: 1641-1664.

Segerer, A., Langworthy, T.A., and Stetter, K.O. (1988) *Thermoplasma acidophilum* and *Thermoplasma volcanium* sp. nov. from solfataric fields. *Syst Appl Microbiol* **10**: 161-171.

Sleep, N.H., Meibom, A., Fridriksson, T., Coleman, R.G., and Bird, D.K. (2004) H_2-rich fluids from serpentinization: Geochemical and biotic implications. *Proceedings of the National Academy of Sciences of the United States of America* **101**: 12818-12823.

Slobodkin, A., Reysenbach, A.L., Mayer, F., and Wiegel, J. (1997) Isolation and characterization of the homoacetogenic thermophilic bacterium Moorella glycerini sp. nov. *International Journal Of Systematic Bacteriology* **47**: 969-974.

Smith, K.L. (1978) Benthic Community Respiration in the N.W, Atlantic Ocean *in situ* Measurements from 40-5,200 m. *Marine Biology* **47**: 337-347.

Sorensen, K.B., Finster, K., and Ramsing, N.B. (2001) Thermodynamic and Kinetic requirements in anaerobic methane oxidizing consorta exclude hydrogen, acetate and methanol as possible electron shuttles. *Microbial Ecology* **42**: 1-10.

Spear, J.R., Walker, J.L., McCollom, T.M., and Pace, N.R. (2005) Hydrogen and bioenergetics in the yellowstone geothermal ecosytem. *Proceedings of the National Academy of Sciences of the United States of America* **102**: 2555-2560.

Spinks, J.W.T., and Woods, R.J. (1990) An introduction to Radiation Chemistry. *John Wiley & Sons, New York.*

Stephens, J.A., Uncles, R.J., Barton, M.L., and F., F. (1992) Bulk properties of intertidal sediments in a muddy, macrotidal estuary. *Marine Geology* **103**: 445-460.

References

Stetter, K.O., Huber, R., Blochl, E., Kurr, M., Eden, R.D., Fielder, M. et al. (1993) Hyperthermophilic Archaea Are Thriving in Deep North-Sea and Alaskan Oil-Reservoirs. *Nature* **365**: 743-745.

Stetter, K.O., Thomm, M., Winter, J., Wildgruber, G., Huber, H., Zillig, W. et al. (1981) Methanothermus-Fervidus, Sp-Nov, A Novel Extremely Thermophilic Methanogen Isolated From An Icelandic Hot-Spring. *Zentralblatt Fur Bakteriologie Mikrobiologie Und Hygiene I Abteilung Originale C-Allgemeine Angewandte Und Okologische Mikrobiologie* **2**: 166-178.

Stevens, T.O., and McKinley, J.P. (1995) Lithoautotrophic Microbial Ecosystems in Deep Basalt Aquifers. *Science* **270**: 450-454.

Stevens, T.O., and McKinley, J.P. (2000) Abiotic controls on H-2 production from basalt-water reactions and implications for aquifer biogeochemistry. *Environmental Science & Technology* **34**: 826-831.

Stookey, L.L. (1970) Ferrozine - a new spectrophotometric reagent for iron. *Analytical Chemistry* **42**: 779-781.

Straub, K.L., Benz, M., Schink, B., and Widdel, F. (1996) Anaerobic, nitrate-dependent microbial oxidation of ferrous iron. *Applied and Environmental Microbiology* **62**: 1458-1460.

Strous, M., Kuenen, J.G., and Jetten, M.S.M. (1999a) Key physiology of anaerobic ammonium oxidation. *Applied and Environmental Microbiology* **65**: 3248-3250.

Strous, M., Fuerst, J.A., Kramer, E.H.M., Logemann, S., Muyzer, G., van de Pas-Schoonen, K.T. et al. (1999b) Missing lithotroph identified as new planctomycete. *Nature* **400**: 446-449.

Stumm, W., and Morgan, J.J. (1996) Aquatic chemistry; chemical equilibra and rates in natural waters. *John Wiley & Sons, New York*: 1022 pp.

.\
Takai, K., Gamo, T., Tsunogai, U., Nakayama, N., Hirayama, H., Nealson, K., and Horikoshi, K. (2004) Geochemical and microbiological evidence for a hydrogen-based, hyperthermophilic subsurface lithoautotrophic microbial ecosystem (HyperSLiME) beneath an active deep-sea hydrothermal field. *Extremophiles* **8**: 269-282.

Tanimoto, Y., and Bak, F. (1994) Anaerobic degradation of methylmercaptan and dimethyl sulfide by newly isolated thermophilic sulfate-reducing bacteria. *Applied and Environmental Microbiology* **60**: 2450-2455.

Taylor, B.F., and Oremland, R.S. (1979) Depletion Of Adenosine-Triphosphate In Desulfovibrio By Oxyanions Of Group-Vi Elements. *Current Microbiology* **3**: 101-103.

Taylor, S.R., and McLennan, S.M. (1985) *The continental crust; its composition and evolution.* Oxford: Blackwell.

Telling, J., Hornibrook, E., R,C., and Parkes, R.J. (2004) Microbial reactions in marine sediments. In *Hydrogeology of the oceanic lithosphere.* Davis, E., and Elderfield, H. (eds). Cambridge: University Press., pp. 579-605.

Temple, K.L., and Colmer, A.R. (1951) The autotrophic oxidation of iron by a new bacterium, *Thiobacillus ferrooxidans. J Bacteriol 62* **62**: 605-611.

Teske, A. (2006) Microbial communities of deep marine subsurface sediments: molecular and cultivation surveys. *Geomicrobiology journal* **23**: 357-368.

Teske, A., and Sorensen, K.B. (2008) Uncultured archaea in deep marine subsurface sediments: have we caught them all? *Isme Journal* **2**: 3-18.

Teske, A., Hinrichs, K.U., Edgcomb, V., Gomez, A.D., Kysela, D., Sylva, S.P. et al. (2002) Microbial diversity of hydrothermal sediments in the Guaymas Basin: Evidence for anaerobic methanotrophic communities. *Applied and Environmental Microbiology* **68**: 1994-2007.

Thamdrup, B., and Dalsgaard, T. (2002) Production of N_2 through Anaerobic Ammonium Oxidation Coupled to Nitrate Reduction in Marine Sediments. *Applied and Environmental Microbiology* **68**: 1312-1318.

Thamdrup, B., Finster, K., Hansen, W.J., and Bak, F. (1993) Bacterial disproportionation of elemental sulfur coupled to chemical reduction of iron or manganese. *Applied and Environmental Microbiology* **59**: 101-108.

Thauer, R.K. (1998) Biochemistry of methanogenesis: a tribute to Marjory Stephenson. *Microbiology* **144**: 2377-2406.

Thauer, R.K., Jungerman, K., and Decker, K. (1977) Energy conservation in chemotrophic anaerobic bacteria. *Bacteriol. Rev* **41**: 100-180.

Thiele, J.H., and Zeikus, J.G. (1989) Control of interspecies electron transfere during anaerobic digestion: significance of formate transfer versus hydrogen transfer during synthrophic methanogenesis in flocs. *Applied and Environmental Microbiology* **54**: 20-29.

Thompson, J.D., Gibson, T.J., Plewniak, F., Jeanmougin, F., and Higgins, D.G. (1997) The CLUSTAL_X windows interface: flexible strategies for multiple sequence alignment aided by quality analysis tools. *Nucleic Acids Research* **25**: 4876-4882.

Tor, J.M., Kashefi, K., and Lovley, D.R. (2001) Acetate oxidation coupled to Fe(III) reduction in hyperthermophilic microorganisms. *Applied and Environmental Microbiology* **67**: 1363-1365.

Turick, C.E., Tisa, L., and Caccavo, F. (2002) Melanin production and use as a soluble electron shuttle for Fe(III) oxide reduction and as a terminal electron acceptor by *Shewanella algae* BrY. *Applied and Environmental Microbiology* **68**: 2436-2444.

Valentine, D.L. (2002) Biogeochemistry and microbiol ecology of methane oxidation in anoixc environments: A review. *Antonie Van Leeuwenhoek* **81**: 271-282.

Vargas, M., Kashefi, K., Blunt-Harris, E.L., and Lovley, D.R. (1998) Microbiological evidence for Fe (III) reduction on early Earth. *Nature* **395**: 065.

Von Damm, K.L. (1995) Controls on the chemistry and temporal variability of seafloor hydrothermal fluids. In *Seafloor Hydrothermal systems: Physical, Chemical, Biological and Geological Interactions*. Humpris, S.E., Zierenberg, R.A., Mullineaux, L.S., and Thomson, R.E. (eds): American geophysical union, pp. 222-247.

Wakita, H., Nakayama, Y., Kita, I., Fujiii, N., and Notsu, K. (1980) Hydrogen Release: New Indicator of Fault Activity. *Science* **210**: 188-190.

Watson, P.G., Frickers, P.E., and Goodchild, C.M. (1985 a) Spatial and seasonal variations in the chemistry of sediment interstitial waters in the Tamar Estuary. *Est. Coastal. Marine Sci.* **21**: 105-119.

Watson, P.G., Frickers, P.E., and Goodchild, C.M. (1985 b) A comparison of nutrients in the interstitial water of reducing (Tamar) and oxic (Carmarthen Bay) coastal sediments. *Netherlands Journal of Sea Research* **19**: 231-239.

Weber, K.A., Achenbach, L.A., and Coates, J.D. (2006a) Microorganisms pumping iron: anaerobic microbial iron oxidation and reduction. *Nature Reviews Microbiology* **4**: 752-764.

Weber, K.A., Urrutia, M.M., Churchill, P.F., Kukkadapu, R.K., and Roden, E.E. (2006b) Anaerobic redox cycling of iron by freshwater sediment microorganisms. *Environmental Microbiology* **8**: 100-113.

Weber, K.A., Pollock, J., Cole, K.A., O'Connor, S.M., Achenbach, L.A., and Coates, J.D. (2006c) Anaerobic nitrate-dependent iron(II) bio-oxidation by a novel lithoautotrophic betaproteobacterium, strain 2002. *Applied And Environmental Microbiology* **72**: 686-694.

Webster, G., Embley, T.M., and Prosser, J.I. (2002) Grassland management regimens reduce small-scale heterogeneity and species diversity of beta-proteobacterial ammonia oxidizer populations. *Applied and Environmental Microbiology* **68**: 20-30.

Webster, G., Newberry, C.J., Fry, J.C., and Weightman, A.J. (2003) Assessment of bacterial community structure in the deep sub- seafloor biosphere by 16S rDNA-based techniques: a cautionary tale. *Journal of Microbiological Methods* **55**: 155-164.

Webster, G., Parkes, R.J., Fry, J.C., and Weightman, A.J. (2004) Widespread Occurrence of a Novel Division of Bacteria Identified by 16S rRNA Gene Sequences Originally Found in Deep Marine Sediments. *Appl. Environ. Microbiol.*

Webster, G., Embley, T.M., Freitag, T.E., Smith, Z., and Prosser, J.I. (2005) Links between ammonia oxidizer species composition, functional diversity and nitrification kinetics in grassland soils. *Environmental Microbiology* **7**: 676-684.

Webster, G., Parkes, R.J., Cragg, B.A., Newberry, C.J., Weightman, A.J., and Fry, J.C. (2006) Prokaryotic community composition and biogeochemical processes in deep subseafloor sediments from the Peru Margin. *Fems Microbiology Ecology* **58**: 65-85.

Welch, S.A., Barker, W.W., and Banfield, J.F. (1999) Microbial extracellular polysaccharides and plagioclase dissolution. *Geochemica et Cosmochimica Acta* **63**: 1405-1419.

Wellsbury, P., and Parkes, R.J. (1995) Acetate Bioavailability and Turnover in an Estuarine Sediment. *Fems Microbiology Ecology* **17**: 85-94.

Wellsbury, P., Mather, I., and Parkes, R.J. (2002) Geomicrobiology of deep, low organic carbon sediments in the Woodlark Basin, Pacific Ocean. *FEMS Microbiology Ecology* **42**: 59-70.

Wellsbury, P., Goodman, K., Barth, T., Cragg, B.A., Barnes, S.P., and Parkes, R.J. (1997) Deep marine biosphere fuelled by increasing organic matter availability during burial and heating. *Nature* **388**: 573-576.

Wetzel, L.R., and Shock, E.L. (2000) Distinguishing ultramafic-hosted from basalt-hosted submarine hydrothermal systems by comparing calculated vent fluid compositions. *Journal of Geophysical Research* **105**: 8319-8340.

Whiticar, M.J. (1994) Correlation of natural gases with their sources. *In: The petroluem system-from source to trap. AAPG memor 60*: 261-284.

Whiticar, M.J. (1999) Carbon and hydrogen isotope systematics of bacterial formation and oxidation of methane. *Chemical Geology* **161**: 291-314.

Whiticar, M.J., Faber, E., and Schoell, M. (1986) Biogenic methane formation in marine and freshwater environments: CO_2 reduction vs acetate fermentation - isotope evidence. *Geochim. Cosmochim Acta* **50**: 693-709.

Whitman, W.B., Coleman, D.C., and Wiebe, W.J. (1998) Prokaryotes: The unseen majority. *Proceedings of the National Academy of Sciences of the United States* **95**: 6578 -6583.

Widdel, F. (1986) Growth of methanogenic bacteria in pure culture with 2-propanol and other alcohols as hydrogen donors. *Applied and Environmental Microbiology* **51**: 1056-1062.

Widdel, F. (1988) Microbiology and ecology of sulfate and sulfur reducing bacteria. In *Biology of anaerobic Microorganisms*. Zehnder, A.J.B. (ed). New York: John Wiley, pp. 469-585.

Wilhelms, A., Larter, S.R., Head, I., Farrimond, P., di-Primio, R., and Zwach, C. (2001) Biodegradation of oil in uplifted basins prevented by deep- burial sterilization. *Nature* **411**: 1034-1037.

Winfrey, M.R., and Ward, D.M. (1983) Substrates for sulfate reduction and methane production in intertidal sediment. *Applied Environ. Micro.* **45**: 193-199.
Wood, H.G. (1991) Life with CO or CO_2 and H_2 as a soure of carbon and energy. *FASEB. J* **5**: 156-163.

Wood, H.G., and Ljungdahl, L.G. (1991) Autotrophic character of acetogenic bacteria. In *Variations in Autotrophic Life*. Shively, J.M., and Barton, L.L. (eds). San Diego Ca: Academic Press, pp. 202-250.

Yoshida, N., Yagi, K., Sato, D., Watanabe, N., Kuroishi, T., Nishimoto, K. et al. (2005) Bacterial communities in petroleum oil in stockpiles. *J. Biosci. Bioeng.* **99**: 143-149.

Zeikus, J. (1972) Methanobacterium thermoautotrophicus sp. n., an Anaerobic, Autotrophic, Extreme Thermophile. *J Bacteriol.* **109**: 707-713.

Zyakun, A.M. (1992) Isotopes and their possible use as biomarkers of microbial end products. In *Bacterial Gas*. Vially, R. (ed). Paris: Editions Technip, pp. 27-46.

Appendix

Appendix 1. 60 degree magnetite experiment

Type 1 magnetite from Fisher processed

Type 2 magnetite from natural source (Simon Cobb Bristol) no ICP-OES done

Acetate concentrations μmol l^{-1}, 60°C magnetite incubation

Days	Control	No mineral	Type 1 22-63 μm	Type 2 22-63 μm	Type 2 75-105 μm
1	161	787	1052	529	326
7	338	14.9	30.7	198	45
13	9.5	9.6	8.6	4.6	
20	10	34	5.2	8.1	13.4
27	57.5	14.2	67.7	9.9	9.5
34	9.7	8.8	7.1	5.7	8.6
41	15.5		7.1	20.5	
48	45.2	16.919	19.6	25.2	21.5
54	4.6	2.3		2.8	13.2
69	9.6	11.5	11.3	12.7	4.3
76	16.5	15.7	2.2	13.5	17.6
83	17.1	26.8	19.5	37	22.2
90	4.6	14.8	8.6	8.5	9.2
97	14.3	19	14.3	6	12.1
104	6.7	18.3	13.6	17.4	16.5
111	11	40.1	13.1	11.6	23
118	6.3	115.2	12.6	13.2	25.7
124	12.7	192	25	14.9	60.8
131	10.1	325.3	12.6	16.4	195.2
138	1	593	3	6	327
145					
152	1	913	21	9	531
159	3	968	83	29	925
166	2	1526	120	104	1025

Methane concentrations (PPMV) magnetite experiment 60°C

Days	Control	No mineral	Type 1 22-63 μm	Type 2 22-63 μm	Type 2 75-105 μm
1	8.3	37.2	32	18	28
7	134	743	445	384	573
13	209	973	627	638	886
20	275	1032	682	774	1066
27	324	1001	696	827	1184
34	311	1015	660	817	1196

41	354	1013	405	891	1218
48	367	993	460	1031	1231
54	303	717	306	962	966
69	369	790	373	1940	1046
76	327	873	403	1929	1026
83	292	879	358	2689	1041
90	349	901	387	2849	1067
97	362	930	308	2883	1023
104	359	933	356	3746	1115
111	376	919	378	4293	1130
118	302	930	402	5004	1139
124	343	942	377	5459	1144
131	347	951	351	5983	1152
138	348	973	352	6605	934
145	343	989	359	6062	968
152	349	1179	372	6923	1081
159	391	1455	394	7192	1292
166	359	1789	385	7855	1656
173	356	1893	386	8089	1966

Carbon dioxide (PPMV) magnetite 60°C

Days	Control	No mineral	Type 1 22-63 μm	Type 2 22-63 μm	Type 2 75-105 μm
1	8524	2.05E+05	1.42E+05	1.43E+05	1.51E+05
7	51261	3.44E+05	2.52E+05	3.03E+05	2.82E+05
13	68317	3.65E+05	2.95E+05	3.33E+05	2.98E+05
20	87400	3.63E+05	3.11E+05	3.57E+05	3.25E+05
27	1.10E+05	3.45E+05	3.35E+05	3.86E+05	3.62E+05
34	1.06E+05	3.80E+05	3.40E+05	3.92E+05	3.72E+05
41	1.35E+05	4.22E+05	3.68E+05	4.43E+05	4.18E+05
48	1.68E+05	4.44E+05	3.68E+05	4.78E+05	4.40E+05
54	1.42E+05	3.23E+05	2.27E+05	3.70E+05	3.35E+05
69	1.83E+05	3.89E+05	2.69E+05	4.02E+05	3.64E+05
76	1.69E+05	4.28E+05	3.21E+05	3.50E+05	3.60E+05
83	1.54E+05	4.38E+05	3.04E+05	4.30E+05	3.69E+05
90	1.99E+05	4.46E+05	3.56E+05	3.84E+05	3.83E+05
97	2.11E+05	4.77E+05	2.88E+05	3.85E+05	3.73E+05
104	2.13E+05	4.87E+05	3.30E+05	4.31E+05	4.10E+05
111	2.15E+05	4.86E+05	3.45E+05	4.50E+05	4.24E+05
118	1.84E+05	5.06E+05	3.51E+05	4.53E+05	4.37E+05
124	2.18E+05	5.17E+05	3.68E+05	4.63E+05	4.51E+05
131	2.27E+05	5.29E+05	3.41E+05	4.81E+05	4.67E+05
138	2.31E+05	5.37E+05	3.49E+05	4.83E+05	3.82E+05
145	2.42E+05	5.15E+05	3.59E+05	3.93E+05	3.93E+05
152	2.48E+05	5.52E+05	3.73E+05	4.50E+05	4.02E+05
159	2.58E+05	5.35E+05	3.79E+05	4.52E+05	4.16E+05

166	2.67E+05	5.39E+05	3.96E+05	4.68E+05	4.31E+05
173	3.07E+05	4.83E+05	4.52E+05	5.28E+05	4.33E+05

Hydrogen concentrations (PPMV) magnetite 60°C

Days	Control	No mineral	Type 1 22-63 μm	Type 2 22-63 μm	Type 2 75-105 μm
1	0	281	630	304	299
7	610	0	0	0	0
13	0	0	0	0	0
20	0	609	0	0	0
27	133	109	0	0	373
34	122	0	203	0	326
41	163	0	0	235	403
48	0	0	0	234	340
54	0	0	0	219	0
69	0	0	0	0	0
76	0	0	0	0	0
83	0	0	0	0	0
90	0	0	0	0	0
97	0	0	833	359	0
104	0	1483	794	1318	0
111	0	1040	931	632	335
118	0	1079	795	843	0
124	0	1051	821	764	284
131	0	1041	1055	817	975
138	0	1103	1188	886	1465
145	0	1559	1244	1069	0
152	0	1921	1076	767	923
159	0	2168	1395	1288	822
166	0	1983	1311	1463	1398
173	0	910	1745	597	525

Sulphate μmol l^{-1} magnetite 60°C

Days	Control	No mineral	Type 1 22-63 μm	Type 2 22-63 μm	Type 2 75-105 μm
1	17610	15664	15770	15036	6953
7	15317	10880	11063	12349	11019
13	14590	9411	9924	12723	6290
20	13095	14063	8155.9	9215	7960
27	12889	6152	6743	8025	7080
34	12044	5369	6865	7434	6511
41	11992	1191	5632	6557	
48	9479	4665	5190	5655	4930
54	7499	3537		6250	5562
69	7327	2827	3755	4986	4026
76	8409	3088	4049	4492	3215

83	6839	1787	3353	4403	3516
90	7203	1879	3123	3422	2093
97	6983	1050	2564	3124	2135
104	5588	1061	2697	2768	1649
111	5874	790	2447	2183	1238
118	5683	488	2166	2067	1148
124	5526	956	1315	1731	1671
131	5237	509	1463	1495	990

Appendix 2. pH experiment

Magnetite experiment using fisher magnetite at 60° not reground mineral. Different buffers and pH

Methane (PPMV)

Days	pipes 6.5	bicarbonate 7.6
1	12	8
3	9	28
8	49	72
15	120	193
22	190	279
29	256	294
36	153	272
44	164	283
50	172	293
57	179	305
64	187	318
71	195	322
78	204	334
85	214	344
92	217	347
99	229	348
106	220	354

Carbon dioxide(PPMV)

Days	pipes 6.5	bicarbonate 7.6
1	16595	47036
3	25178	69798
8	61563	1.06E+05
15	1.09E+05	1.42E+05
22	1.30E+05	1.87E+05
29	1.43E+05	2.02E+05
36	1.45E+05	2.11E+05

44	1.57E+05	2.09E+05
50	1.59E+05	2.20E+05
57	1.65E+05	2.28E+05
64	1.73E+05	2.27E+05
71	1.78E+05	2.35E+05
78	1.79E+05	2.41E+05
85	1.85E+05	2.50E+05
92	1.85E+05	2.56E+05
99	1.86E+05	2.14E+05
106	1.90E+05	2.18E+05

Hydrogen (PPMV)

Days	pipes 6.5	bicarbonate 7.6
1	347	200
3	0	0
8	0	0
15	0	0
22	0	0
29	0	0
36	0	0
44	0	0
50	0	0
57	0	0
64	0	0
71	0	0
78	0	0
85	0	0

$(\mu mol\ l^{-1})$

Days	pipes 6.5 Acetate	bicarbonate 7.6 Acetate	6.5 sulphate	7.6 sulphate
1	12.5	8.5	17916	15892
4				
9	152.8	161.6	14246	16139
16	21	9.6	10978	13309
23		19.9	8616	11128
30	18	5.7	8642	9461
37				
45	7.1	8.9	9079	7493
51	8.8	8.5	8796	7619
58	8.1	6.7	7813	8026
65	7.8	6.4	7507	8079
72	10.7	6.6	6954	7568
79	18.1	7.3	6195	6888

Appendix

| 86 | 10.8 | 11.6 | 6515 | 6331 |

Appendix .3

Various differing temperature initial experiment Magnetite (fisher) non ground
No hydrogen detected.

1= Days incubation   3=4°C sterile control   5=30°C sterile control   7=60°C sterile control

2= 4°C   4=30°C   6=60°C   8= no mineral additon

acetate μmol l^{-1}

1	2	3	4	5	6	7	8
0	50.5	270	40	390	640	320	1270
7	30.6	240.9	30.9	850.7	240.5	1240.9	230.5
14	20.6	260.5	30.1	810.9	50.2	510	320
21	40.5	260	30.6	930.7	60.3	50	490.5
28	30.7	240.2	30.8	1060.6	80	50.6	600.4
35	20.3	260.9	20.2	980.6	100.4	50.5	700.1
42	20.9	220.9	30.2	990	290.7	60	1170.8
49	20.8	270.9	30.1	990.5	420.5	50.6	1220.5
56	20.9	310.1	40.9	1120.7	720.3	80.9	1200
63	23	160	10.4	824	664	32.2	924.6
70	51	56	4	1608	1376		1301
84	3	163	4	1544	1340	7.6	26.4
98	0	112		1183	768	26	340
105	0	71.7	0	1263.5	436	17.2	226.5
112	7.8	61.3	0	1176.1	169	9	416
147	0	115	379	1262	1360		1024
154	0	94.8	0	1502	1611		369
161	0	95	15	1498	1488		314
168	0	92.3	0	2006	1893.9		158
182	0	209	5.7	1288	1520		89
189	0	184	283	141	1353		101
196	0	213	768	1166	1178		120
231	0	156	2101	934	103		106

Methane (PPMV)

1	2	3	4	5	6	7	8
0	25.16	4.6	1243	17.3	971	49.5	704.8
7	61.14	5.1	1668	29.15	2749	129.7	2643
14	73.6	5.8	1449	31.07	3939	169	10361
21	104	6.3	189	37	5955.7	201	13667
28	144	6.2	151.9	40.1	6219.2	216	15908
35	178	6.7	178.1	40.4	6475	229	17326
42	202	7.2	240	42	7759	236.8	18704
49	220	6.2	296	41.1	10154	235	27976
56	266	6.6	365	40.51	13630	257	56583
63	238	12.7	461.8	40.7	22823	274.8	1.06E+05
70	240	7	749	40	37827	298	676
77	180	6	1159	40	1912	242	7217
84	221	7	3074	47	1.18E+05	289	21671
91	11	3	4257	48	2260	231	29531
98	188	7	6485	54	10032	245	42473
105	184	7	10112	56	19222	253	53221
112	198	7	15041	63	29107	277	63630
119	116	6	16620	55	32026	176	72209
126	174	7	32626	71	48859	300	90643
133	168	5.7	39658	1490			72122
140	158	7	81194	75	51551		1.33E+05
147	133	163	93193	67	57545		1.59E+05
154	164	5.6	1.06E+05	74	66025		1.87E+05
161	182	138	1.04E+05	87	75475		
168	179	6.7	1.17E+05	122	87388		
175	183	6.5	1.28E+05	94	97783		
182	195	9	1.41E+05	848	1.14E+05		

189	185	14	1.48E+05	94	1.31E+05		
196	188	17	1.53E+05	85	1.71E+05		
203	179	11	1.53E+05	66	1.84E+05		2.29E+05
210	176	14	1.57E+05	77	1.88E+05		
217	159	7.09	1.56E+05	67	1.95E+05		2.31E+05

Carbon dioxide (PPMV)

1	2	3	4	5	6	7	8
7	13825	352	65028	2506	2.54E+05	20188	2.56E+05
14	16193	271	90355	4441	3.2395	45018	3.16E+05
21	15749	402	98560	8732	3.40E+05	58026	3.09E+05
28	20493	425	1.40E+05	12408	4.54E+05	92563	4.12E+05
35	21215	133	1.46E+05	16135	4.36E+05	1.04E+05	4.27E+05
42	22057		1.48E+05	19402	4.47E+05	1.14E+05	4.26E+05
49	22530		1.50E+05	16612	4.62E+05	1.16E+05	3.84E+05
56	23775		1.53E+05	22183	4.80E+05	1.18E+05	4.18E+05
63	57585	1205	1.63E+05	25124	4.57E+05	1.33E+05	4.04E+05
70	31296		1.59E+05	2947	4.93E+05	1.39E+05	4.16E+05
77	28045	0	1.59E+05	27467	5.00E+05	1.20E+05	3.94E+05
84	21353		1.24E+05	21109		1.39E+05	1.39E+05
91		7127	1.26E+05	19639	3.48E+05	1.15E+05	1.97E+05
98		3105	1.25E+05	18412	74705	1.16E+05	2.05E+05
105	12034	4362	1.27E+05	9613	1.49E+05	1.24E+05	2.12E+05
112	23187	3407	1.36E+05	19107	1.79E+05	1.31E+05	2.31E+05
119	25706	2081	1.33E+05	19344	1.91E+05		2.36E+05
126	15995	1528	1.22E+05	23775	1.74E+05		2.55E+05
133	29743		1.62E+05	25549	2.35E+05	1.69E+05	2.86E+05
140	29598	1738	1.19E+05	14630	4567		1.89E+05
147	30600	0	1.20E+05	26432	1.63E+05		2.43E+05

154	24734		1.26E+05	25690	1.67E+05		2.56E+05
161	30301		1.31E+05	25376	1.75E+05		2.64E+05
168	36440		1.30E+05	27934	1.78E+05		2.62E+05
175	35218		1.37E+05	26779	1.85E+05		2.73E+05
182	35392		1.41E+05	30902	1.80E+05		2.69E+05
189	41179		1.60E+05	33817	1.94E+05		2.72E+05
196	39649		1.74E+05	38215	2.01E+05		2.74E+05
203	44606		1.73E+05	39065	2.01E+05		2.79E+05
210	43737		1.60E+05	40974	1.98E+05		2.76E+05
217	43948		1.67E+05	41622	2.25E+05		2.79E+05
224	44062	0	1.67E+05	41805	2.33E+05		2.80E+05

SO_4^{2-} µmol l^{-1}

1	2	3	4	5	6	7	8
0	13409	13898	13649	14490	13171	14113	13458
7	12783	13053	11498	14356	7295	12768	5255
14	13142	14095	8846	12227	3604	10455	2282
21	11065	12509	6925	13053	1889	7614	1428
28	12678	11050	6078	11855	1130	6215	366
35	9069	13848	4898	11634	575	6302	
42	12417	10249	4783	12005	342	5987	74
49	9488	12125	4490	11977	350	5008	180
56	9969	10207	4009	12476	233	4171	249
91	12097	12612	1189	13000	267	2781	193
98	11517	12110	796	12748	213	2197	167
105	10385	13214	733	13307	239	2021	176
140	13256	15304	67	13364	192		183
147	12057	14312	475	14847	76		148
154	13307	13753	318	15507	57		193
161	11628	15487	135	18373	112		457

Hornblende XRD

Chart legend:

T= Tremolite $Ca_2Mg_5S_{18}O_{22}(H)_2$

C= Clinochore $(Mg, Al, Fe)_6Si\ Al$

X-axis: 2 Theta (0 to 70)

Y-axis: 0 to 350

Ilmenite

I = Ilmenite
H= Hematite

2 Theta

OLIVINE

F=Fosterite
C=Clinochlore
M= margarite
E=Enstatite

BASALT XRD

A=Anorthite

Q=Quartz

C=Clinochlore

PYRRHOTITE XRD

P= pyrrohotite
S=Sphalerite

M= magnetite

C= Chalcocite

2 THETA

PYRITE

P=PYRITE

2 THETA

LABRADORITE

Poor match close to anorthite

Chart axes: Y-axis labeled from 0 to 1200 (intervals of 200); X-axis labeled "2 THETA" from 0 to 80 (intervals of 10).

Olivine bombs

F= forsterite
E=enstatite

2 Theta

HEMATITE

H=HEMATITE

Q=Quartz